CZECH TECHNICAL
UNIVERSITY
IN PRAGUE

FACULTY
OF ELECTRICAL
ENGINEERING

VISIBLE LIGHT COMMUNICATIONS FOR INDOOR APPLICATIONS

DOCTORAL THESIS BY **PETR CHVOJKA**
NOVEMBER 2017

PH.D. PROGRAMME:
ELECTRICAL ENGINEERING AND INFORMATION
TECHNOLOGY (P2612)

BRANCH OF STUDY:
RADIOELECTRONICS (2601V010)

SUPERVISOR: PROF. STANISLAV ZVANOVEC

written by: Ing. Petr Chvojka
supervised by: Prof. Ing. Stanislav Zvanovec, Ph.D

Declaration of Originality

I, the undersigned, hereby declare that this doctoral thesis is the result of my research in our research team and my contribution corresponds to that specified at the beginning of each research chapter. The thesis was written under the professional supervision of Prof. Stanislav Zvanovec, using the literature and resources listed in the Bibliography and References.

In Prague, November 20th 2017

.....

Ing. Petr Chvojka

Acknowledgement

Firstly, I would like to acknowledge my supervisor Stanislav Zvanovec, who guided me through my whole doctoral studies, for his never-ending support, more or less positive feedback, trust and as well the opportunities he offered me. Thanks to him, I was given a chance to work at foreign universities which became a great experience.

Next, I would like to thank Paul Anthony Haigh and Fary Ghassemlooy whom I met at the beginning of my Ph.D. studies and whose support was crucial for my research. Their opinions and support were always helpful.

During the years of collaboration, we all became more friends than colleagues. Stan, Paul and Fary had a significant impact on the results presented in this thesis.

I would like to acknowledge also my mom, dad, grandmas and grandpas, who all believed that I could finish this important period of my life. Unfortunately, not all of them can read these lines.

Finally, my special thanks must go to my partner Klara and our son Jachym. They can simply make my day as no one else can do. We are a family.

Abstract

The field of visible light communications (VLC) has undergone a rapid development in recent years. The increased utilization of light emitting diodes (LEDs) has opened new possibilities for especially indoor services such as broadband internet connection and positioning. Thus, a research within VLC is the main focus of the thesis and is divided into two main parts. At first, the multiband carrier-less amplitude and phase (m-CAP) modulation, introducing a newly adopted format for spectrally efficient VLC links, is under investigation using both theoretical and experimental approaches. The recommendations for m-CAP transmitter site design are proposed. Next, the channel modeling of indoor VLC is investigated with emphasis on the dynamically changing environments caused by moving people and non-line of sight (NLOS) propagation and new statistical models are derived.

Keywords: channel modeling, multiband carrier-less amplitude and phase, visible light communications

Abstrakt

V oblasti komunikace ve viditelném světle (visible light communications, VLC) došlo za poslední roky k prudkému rozvoji. Zvyšující se využití technologie bílé světlo emitujících LED otevírá nové možnosti zejména v oblasti poskytování nových služeb pokrývajících vnitřní prostory budov, např. vysokorychlostní internet či přesná lokalizace. VLC je proto hlavním tématem dizertační práce, která je dále rozdělena na dvě hlavní části. Nejprve se práce zabývá jak experimentálně tak teoreticky pomocí simulací novým modulačním formátem - vícepásmovou amplitudově fázovou modulací bez nosné, která byla pro využití v oblasti VLC adoptována z vláknových systémů a nabízí vysoce spektrálně účinné datové přenosy. Následně jsou navržena řešení pro implementaci této modulační techniky pro VLC. Ve druhé části je důraz kladen na výzkum modelování komunikačního kanálu VLC pro dynamicky se měnící prostředí uvnitř budov zahrnující pohyb osob, kvůli kterému dochází k částečnému zakrytí detektoru a změně parametrů komunikačního kanálu, zejména při ztrátě přímé viditelnosti mezi vysílačem a přijímačem (tzv. NLOS konfigurace). Na základě výzkumu jsou odvozeny nové statistické modely pro komunikační kanál VLC.

Keywords: komunikace ve viditelném světle, modelování kanálu, vícepásmová amplitudově fázová modulace bez nosné

Contents

Abbreviation List

Abbreviation	Meaning
5G	$5th$ generation
ACO-OFDM	Assymetrically clipped optical orthogonal frequency division multiplexing
ANN	Artificial neural network
APD	Avalanche photodiode
AWGN	Additive white Gaussian noise
BER	Bit error rate
BLW	Baseline wander
C2C	Car-to-car
C2I	Car-to-infrastructure
CAP	Carrier-less amplitude and phase
Ce:YAG	Cerium doped yttrium aluminium garnet
CP	Cyclic prefix
DAS	Distributed antenna system
DC	Direct current
DCO-OFDM	DC biased optical orthogonal frequency division multiplexing
DFE	Decisioin-feedback equalizer
DMT	Discrete multi-tone
EVM	Error vector magnitude
FDE	Frequency domain equalizer
FEC	Forward error correction
FFT	Fast Fourier transform
FIR	Finite impulse response
FOV	Field of view
FPGA	Field progammable gate array
GaN	Gallium nitride
GSSK	Generalized space shift keying
HPF	High-pass filter
ICI	Inter-carrier intereference
IEEE	Institute of Electrical and Electronics Engineers
IFFT	Inverse fast Fourier transform
IM/DD	Intensity modulation/direct detection

Abbreviation	**Meaning**
IoT	Internet of things
IR	Infrared
ISI	Inter-symbol interference
ISO	International Organization for Standardization
ITO	Indium tin oxide
LED	Light emitting diode
LOS	Line of sight
L-PAM	Multilevel pulse amplitude modulation
LPF	Low-pass filter
m-CAP	Multiband carrier-less amplitude and phase modulation
M2M	Machine-to-machine
MIMO	Multiple-input multiple-output
NLOS	Non-line of sight
NRZ	Non-return to zero
OFDM	Orthogonal frequency division multiplexing
OLED	Organic light emitting diode
OOK	On-off keying
OPD	Organic photodiode
OVLC	Organic visible light communications
OWC	Optical wireless communications
P/S	Parallel-to-serial
PAM	Pulse amplitude modulation
PAPR	Peak-to-average power ratio
PD	Photodiode
PIN	Positive-intrincis-negative
PLED	Polymer light emitting diode
PPM	Pulse position modulation
PRBS	Pseudorandom binary sequence
QAM	Quadrature amplitude modulation
RC	Resistor-capacitor
RF	Radio frequency
RGB	Red green blue
RMS	Root mean square

Abbreviation	Meaning
RYGB	Red yellow green blue
S/P	Serial-to-parallel
Si	Silicon
SMOLED	Small molecule organic light emitting diode
SMP	Spatial multiplexing
SNR	Signal-to-noise ratio
SPAM	Superposed pulse amplitude modulation
SRRC	Square root raised cosine
SSK	Space shift keying
SSL	Solid state lighting
U-OFDM	Unipolar orthogonal frequency division multiplexing
UV	Ultra violet
VLC	Visible light communications
VNI	Visual network indexing
WBAN	Wireless body area network
WDM	Wavelength division multiplexing
WLAN	Wireless local area network
WP	White phosphor
WPAN	Wireless personal area network
WPLED	White phosphor light emitting diode
ZFE	Zero-forcing equalizer

1 Introduction

Recent data traffic in telecommunications networks has increased significantly. As the number of smart end-user devices (smart TVs, smartphones, tablets etc.) increases, the demand for high-speed internet connection availability anywhere and anytime grows accordingly. However, due to the naturally limited radio-frequency (RF) spectrum, researchers have been focusing on a development of new communication technologies capable of avoiding spectrum congestion [1]. According to the Cisco Visual Networking Index (VNI) report which forecasts trends in global networks trends, mobile data traffic will increase sevenfold between 2016 and 2021 and the number of mobile devices per capita will reach 1.5 by 2021. This represents 11.6 billion mobile-connected devices all over the world [2]. Such data show the need for high capacity network architectures that will be able to fulfil increasing requirements in next generation communication systems. Optical wireless communications (OWC) is an emerging technology that can overcome the spectrum challenge. OWC utilize infrared (IR), ultraviolet (UV) and visible wavelengths and offer high and unregulated bandwidth (in the order of THz), high security and immunity to electromagnetic interference. The IR and UV bands are mostly used in outdoor applications for line of sight (LOS) and non-LOS (NLOS) links, whereas the visible band has been widely adopted for indoor environments. The idea of using a visible part of the electromagnetic spectrum to provide both data transmission and illumination while simultaneously using white light-emitting diodes (LEDs) is relatively new and known as visible light communications (VLC). The first reports of VLC technology were introduced by Keio University in Japan by a number of conference publications in the beginning of the first decade of this century [3-6]. Following this, VLC have undergone rapid development leading to an ongoing standardization process by the Institute of Electrical and Electronics Engineers (IEEE), namely IEEE 802.15.7 in 2012, introducing the individual layer standards required for industrial implementation [7]. A revision of the standard from 2012 is now in preparation and denoted as 802.15.7.1r. Despite the fact that VLC have been the focus of enormous attention for less than 20 years, transmission systems with a data rate of several Gb/s have already been demonstrated [8-10].

VLC have gained huge attention among researchers and industrial companies due to the rapid development of solid state lighting (SSL) which refers to lighting infrastructures utilizing LEDs, both inorganic and organic (OLEDs) to provide illumination and replace incandescent and fluorescent lamps. LEDs offer several benefits over existing lighting infrastructures, such as lower power consumption, longer lifetimes (up to 50 000 h), high energy conversion efficiency (>260 lm/W compared to 52 lm/W and 90 lm/W for incandescent and fluorescent lighting infrastructures, respectively [8]), reduced maintenance, lower heat generation characteristics and fast switching. Among the advantages resulting from the LED technology itself, visible light utilization comes up with a significant benefit in the available bandwidth. The spectrum allocated for different communication technologies including OWC, microwaves and RF is illustrated in Fig. 1.1 showing a bandwidth of $\sim$400 THz for VLC ($\sim$370 $-$ 780 nm) which is $\sim$10 000 wider than the RF bandwidth. Due to the ability to be switched on and off very rapidly, data transmission is carried out

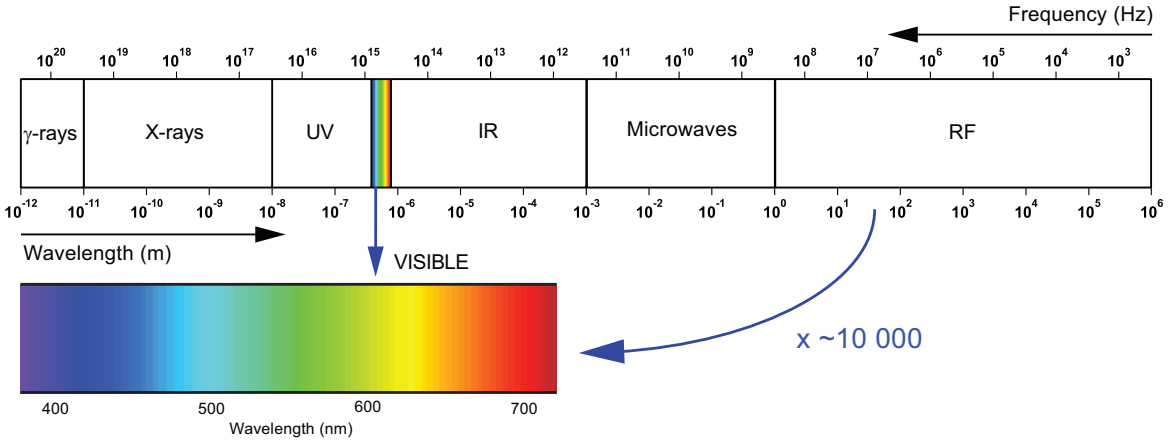

Fig. 1.1: The electromagnetic spectrum with the highlighted visible part utilized by VLC.

Table 1.1: The comparison of VLC and RF systems (adopted from [12])

Property	**VLC**	**RF**
Bandwidth	Unlimited	Regulated and limited
Electromagnetic interference	No	Yes
Distance	Short	Short to long
Security	Good	Poor
Sevices	Illumination, communication, localization	Communication
Noise source	Sun light, other ambient lights	All electrical appliances
Power consumption	Relatively low	Medium
Mobility	Limited	Good
Coverage	Narrow and wide	Mostly wide

by modulating LED intensity directly. Such a method is of relatively lower complexity and cost than modulations in RF systems. Due to these advantages, white LEDs are ideal candidates for future applications providing both illumination and data communication while decreasing the energy consumption at a global level [12]. However, user mobility in VLC can be limited in some cases which is one of the challenging areas within the LED based systems. A comparison of VLC with RF communications is shown in Table 1.1.

Thus, VLC systems can be utilized in a wide range of applications including wireless local area, personal area and body area networks (WLANs, WPANs and WBANs), namely

indoor localization [13-15], car-to-car (C2C) or car-to-infrastructure (C2I) communication [16-19], machine-to-machine (M2M) communication or the internet of things (IoT) [20-22] in addition to toys and the theme park industry [23, 24], underwater communications [25, 26], and electromagnetic interference-sensitive or security-sensitive scenarios [27, 28]. The huge potential of VLC is shown in the effort to include this communication technology in next generation communication networks (5G) which are supposed to be deployed after 2020. 5G networks are expected to meet several challenges which come from mobile data traffic growth, such as high spectral efficiency, efficient energy consumption, lower cost and high capacity broadband links and mobility [29, 30]. 5G will support the concept of cellular architecture while separating indoor and outdoor channels to avoid high penetration loss causing performance degradation. This will be controlled by a distributed antenna system (DAS) and a massive multiple input multiple output (MIMO) network. Considering all the requirements for 5G architectures and networks, VLC may overcome the technical issues and support future communication systems.

The thesis is divided into several sections and is organized as follows. At first, in Section 2, the state of the art of VLC is presented with an emphasis on transmitter and receiver principles, methods for increasing data rates in VLC systems and on the modeling of the optical channel. The objectives of the thesis are given in Section 3. Then, the core of the thesis is provided in Section 4 by the collection of journal and conference papers published during my research with my contributions to the state of research highlighted. Finally, conclusions and future research directions are drawn in Section 5.

2 State of the Art

2.1 Principles of Visible Light Communications

In this chapter, the basic principles of a VLC system will be described based on a typical communication scheme from a transmitter through an optical channel towards a receiver with an emphasis on individual blocks. The transmitter site is discussed in LED terms including also organic sources utilized in VLC, multiplexing techniques, equalizations and modulation schemes. Next, the optical channel follows with a focus on characterizing a VLC channel by essential channel parameters including channel impulse response and coherent bandwidth. Finally, the receiver part is discussed including organic based components as well.

2.1.1 VLC Transmitter

A block diagram of a typical VLC link is illustrated in Fig. 2.1 showing individual parts of the system. First, the data is generated (e.g., in testing cases using pseudorandom binary sequence (PRBS)) and the desired modulation format is applied. There are two typical groups of modulation schemes for optical communications: (i) baseband modulations and (ii) subcarrier modulations. The most popular baseband schemes are on-off keying (OOK), pulse position modulation (PPM) or pulse amplitude modulation (PAM) [1]. The subcarrier modulations include orthogonal frequency division multiplexing (OFDM) and carrierless amplitude and phase (CAP) modulation. A more detailed discussion on modulation techniques in VLC systems is given in Section 2.2.

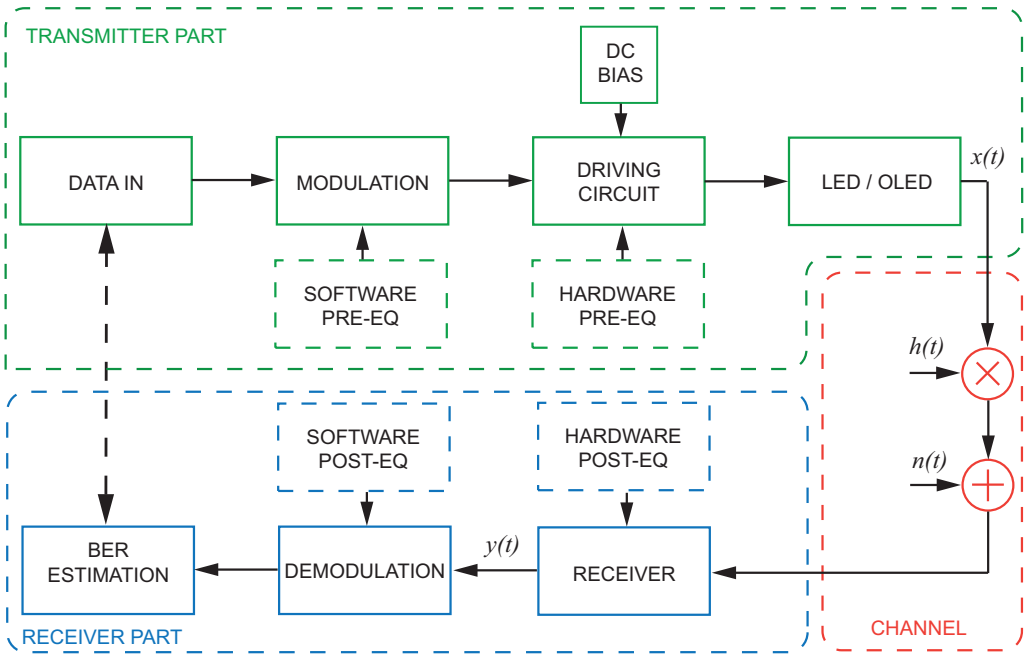

Fig. 2.1: The schematic block diagram of a general VLC system..

Data transmission is based on the intensity modulation and direct detection (IM/DD) technique. The driving circuit is a key component at the transmitter site ensuring overall system performance. Besides other analogue circuits it includes a bias-T, which enables an LED to be driven by (i) passing the high frequency signal modulating an LED intensity and (ii) setting an operating point. An LED is driven by a direct current (DC) bias which is directly modulated by the signal with a desired modulation causing variations of an optical source intensity. Each LED is characterized by a transfer function known as an $L{-}I$ curve, where L stands for optical power and I is the drive current as depicted in Fig. 2.2. An LED must be operated in the proper operating point in the linear region of the $L{-}I$ curve to ensure the high dynamics of a transmitting signal and optimal performance (red circle in Fig. 2.2). The operating point is set via a DC bias. If the drive current is pushed too high, the operating point is shifted to the nonlinear region or beyond which causes signal distortion and even a device degradation.

As mentioned, VLC utilizes the visible part of electromagnetic spectrum (i.e., from $\sim 370 - 780$ nm) employing high-power white LEDs. The recent development of such LEDs has enabled sufficient illumination level as per the International Organization for Standardization (ISO) standard [31], thus existing LED infrastructures in buildings may be used for VLC networks. There are two possibilities of white light generation. The first applies three individual red ($\sim$625 nm), green ($\sim$525 nm) and blue ($\sim$470 nm) emitters (RGB LED, see Fig. 2.3(a)) and white light is emitted by combining these three colors. Alternatively,

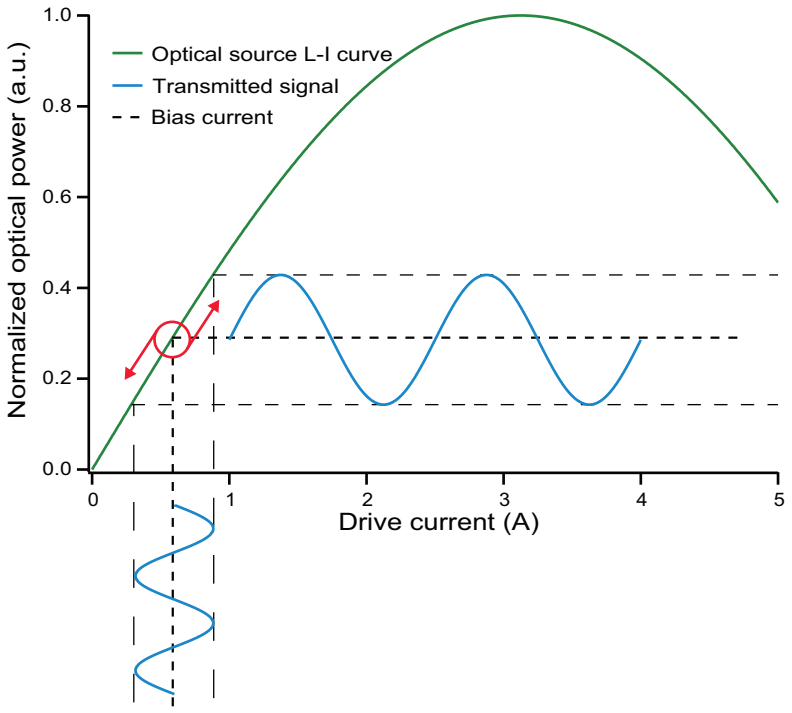

Fig. 2.2: An example of the LED $L{-}I$ curve and the intensity modulation, the red circle denotes the operating point in the linear region of the $L{-}I$ curve.

(a) (b)

Fig. 2.3: White light generation by (a) combining three individual RGB emitters and (b) covering yellow phosphor layer over a blue LED chip. Note, that the emitted colour is indicated in yellow to improve visibility, but in reality the emitted light is white.

yellow color is added to develop RYGB LEDs. Such a multicolor device is attractive for VLC applications due to the possibility of a parallel transmission using wavelength division multiplexing (WDM). The second approach uses a blue LED chip covered by a yellowish phosphor layer known as white phosphor LED (WP LED) as illustrated in Fig. 2.3(b). The latter method is usually preferred due to its lower complexity and cost; moreover, color balancing is not required [1, 11]. Most manufactured LEDs are made of gallium nitride (GaN) coated by a yellowish cerium doped yttrium aluminium garnet (Ce:YAG) phosphor layer. Such an LED is predominantly used in VLC applications. The low modulation bandwidth of LEDs behaving as a first-order low-pass filter (LPF) is a critical challenge towards future high-capacity networks. The blue LED itself offers a bandwidth on the order of tens of MHz, however a color converting phosphor layer reduces it to a few MHz region, typically less than 5 MHz [32, 33]. Thus, achieving high data rates and spectral efficiencies are two of the most challenging areas in VLC. Recently it has been shown that GaN based μLEDs, with a dimension of less than 100 μm, can potentially offer higher modulation bandwidths exceeding 800 MHz [34]. The pixel area is much smaller than conventional LEDs, which enables μLEDs to be driven at much higher current densities. However, a trade-off between the modulation bandwidth and the transmitted optical power (in orders of mW) needs to be taken into consideration when utilizing μLEDs which limits their applications [35]. The vast majority of studies have focused on the implementation of advanced techniques to achieve higher data rates and spectrally efficient VLC systems such as: (i) blue filtering; (ii) equalization (see Fig. 2.1); (iii) utilizing multiple LEDs via WDM and MIMO; (iv) advanced modulation formats. These techniques are frequently combined to achieve the best possible system performance. For further details on increasing data rates in VLC, see Section 2.2.

Alternatively, OLEDs are a possible candidate for VLC applications. They offer a number of benefits when compared to inorganic LEDs, including large, arbitrarily shaped photoactive areas limited only by the size of the printing apparatus, mechanical flexibility, low heat dissipation and long lifetime. There are two basic types of OLEDs: (i) small molecule-based OLEDs (SMOLEDs) and (ii) large molecule polymers (PLEDs); both of which are utilized in organic VLC (OVLC). The main difference between both types of OLEDs is the fabrication method. The production of SMOLEDs is usually done by thermal evaporation

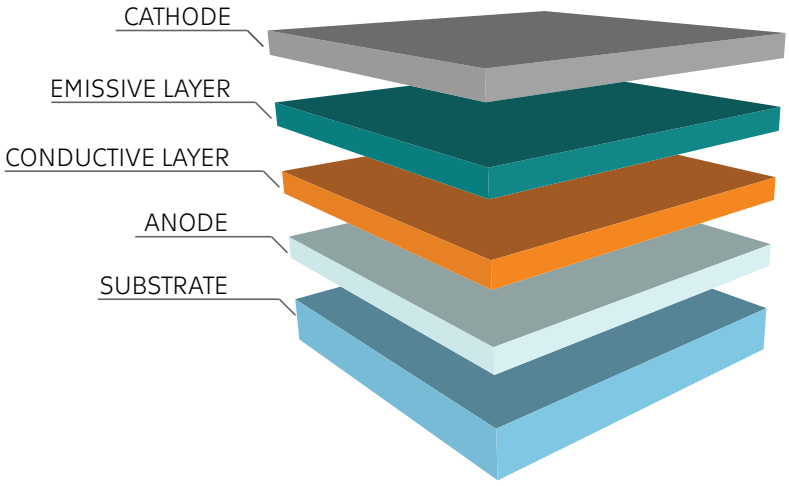

Fig. 2.4: The generic structure of an OLED.

in a vacuum, while PLEDs are processed in a solution which introduces a cheaper method. OLEDs usually consist of one or more thin organic layers placed between two oppositely polarized electrodes − an anode and a cathode (see Fig. 2.4). At least one of the electrodes needs to be transparent or semi-transparent so that light can be emitted from the device. After a recombination of the positive and negative charges, energy is emitted in the form of photons.

The possibility to extend an emission surface of a light source simply and operate an OLED at lower luminous intensity to get the same luminous flux, as with a single LED, makes OLEDs attractive for VLC applications. However, large-area OLED panels suffer from several issues such as short circuits, non-uniform light emission, hot spots, power loss or heat generation [36]. OLEDs exhibit a capacitor-like behavior with a plate capacitance given by $C = Ad^{-1}\epsilon_0\epsilon_r$, where A is an OLED photoactive area, d is an OLED thickness and ϵ_0 and ϵ_r are the permittivity of free space and a relative dielectric constant of the organic layer, respectively. The modulation bandwidth is given by a transfer function with a cut-off frequency given by $f_c = (2\pi RC)^{-1}$, where R is effective resistance. As can be seen from the equations, increasing the device size is proportional to its plate capacitance and, thus, the modulation bandwidth is decreased. Large area panels are being considered for long-distance VLC applications, however one must consider the trade-off between the response speed and the luminous flux on the selection of the panel size. The typical total OLED thickness is usually between 1 and 200 nm which results in high capacitance and low bandwidth, typically in the order of kHz. Thus, modulation bandwidth remains the most challenging factor in OVLC. In [37], OLEDs with bandwidths exceeding 60 MHz were already produced. However, the device emission surface of 0.018 mm^2 is clearly too small to provide sufficient illumination.

The main difficulties for OVLC are inter-symbol interference (ISI), due to bandwidth limitation caused by low transport mobility, and the so-called baseline wander (BLW) phenomenon resulting in bit error rate (BER) performance degradation [38, 39]. Despite

the mentioned impediments, OVLC has attracted great attention among researchers and significant results have already been demonstrated. In [40], the first experimental OVLC link based on an artificial neural network (ANN) equalizer and OOK modulation with an error-free (BER $< 10^{-6}$) data rate of 550 kb/s was reported using an SMOLED with a raw modulation bandwidth of 93 kHz and silicon PIN PD as the transmitter and receiver, respectively. Next, a 1.4 Mb/s OVLC system with discrete multi-tone (DMT) modulation was experimentally demonstrated using an OLED with a modulation bandwidth of less than 100 kHz [41]. An almost two-fold improvement, up to 2.7 Mb/s, using a 93 kHz bandwidth OLED with real time ANN filtering, was reported in [42]. In [43], a breakthrough in OVLC was achieved by demonstrating a 10 Mb/s link based on OOK with real time equalization on a field programmable gate array (FPGA). The transmission speed was achieved using a PLED with a bandwidth of 270 kHz at BER $< 4.6 \cdot 10^{-3}$. This was followed by another 10 Mb/s PLED (bandwidth of 350 kHz) system based on OFDM with pre-emphasis technique [44] and 20 Mb/s OVLC link (350 kHz bandwidth) with multilayer perceptron equalizer, both operating beyond the 7% FEC BER limit [45]. Significant improvements and state of the art transmission capacity were reported in [46]. The WDM technique was applied on three individual RGB pixels of a PLED. The data rates of individual PLED chips were 27.9 Mb/s, 18.6 Mb/s and 8.4 Mb/s for the red, blue and green components, respectively, when using an ANN equalizer and considering a 7% forward error correction (FEC) BER limit. Thus, the aggregate capacity of the link was $\sim$55 Mb/s, which is an almost three-fold gain over the previous state of the art 20 Mb/s, and an approximately ninety-fold improvement over the first reported OVLC system in last three years. Recently, a data rate of 51.6 Mb/s has been experimentally demonstrated using a monochromic OLED fed by an OFDM signal with offset quadrature amplitude modulation (QAM), the bit and power loading technique and the equalization at the receiver [47].

Despite the enormous development of OVLC, it is still questionable whether OLEDs will penetrate the SSL market and other applications in future communication systems. Manufacturing costs are the key factor and still remain a challenge that needs addressing. Inorganic LED costs have been reduced from US$20/lm to US$0.01/lm over the last four decades. In comparison, OLEDs cost about US$10/lm [36]. Another disadvantage of OLEDs is their power efficiency, which is typically between 40 and 60 lm/W [40]. The typical efficiency of inorganic LEDs is about 120 lm/W and LEDs exceeding 200 lm/W were already demonstrated [36]. However, white OLEDs with a power efficiency of 150 lm/W have already been demonstrated in [48], which is a significant step to bringing them into line with white LEDs.

During my Ph.D. research, we also characterized OVLC performance using an OLED with an emission surface of $\sim$100 cm^2 and a very low 3 dB modulation bandwidth at 310 kHz [C6]. Thus, we would like to join our experience from OLED-based measurements and other research in VLC to include OLEDs in our future experimental work.

2.1.2 Optical Channel

In addition to increasing data rates in both inorganic and organic VLC systems, channel modeling represents another challenge being deeply investigated. Modeling of the VLC optical channel is the first step for robust VLC system design. In the current literature, most of the computational algorithms originally developed for IR communications are utilized for VLC purposes, such as recursive-based methods [49, 50] or Monte Carlo ray tracing [51-53]. However, IR communications utilize a monochromatic LED source while VLC uses white LEDs ($\sim$370 $-$ 780 nm). Hence, the wavelength dependency must be taken into account when characterizing a VLC indoor channel. For instance, the reflectance coefficient of materials in the IR band is typically modelled as a constant, in contrast to VLC where the reflectance is dependent on the wavelength. For more details on VLC indoor channel modeling, see Section 2.3.

2.1.3 VLC Receiver

After the incoming signal is captured by a photodetector, the received signal $y(t)$ is given as:

$$y(t) = RGx(t) \otimes h(t) + n(t), \tag{2.1.1}$$

where $h(t)$ is the channel impulse response, R and G are the photodetector's responsivity and gain, respectively, $\otimes$ is the time domain convolution and $n(t)$ is additive white Gaussian noise (AWGN) with a zero mean and variance of $N_0/2$, where N_0 is a power spectral density. After resampling, the signal is then passed through a matched filter, demodulated and processed for obtaining required information such as BER performance, error vector magnitude (EVM) or signal-to-noise (SNR) ratio.

The photodetectors used in VLC are usually silicone-based positive-intrinsic-negative (PIN) photodiode (PD) with no internal gain or alternatively silicone (Si) avalanche PD (APD). APDs provide internal gain which is usually within the range of 50$-$300 [54]. Thus, the responsivity of an APD can be greater than unity in contrast to PIN responsivity which is always below 1. Moreover, APDs offer higher sensitivity than PIN photodetectors. On the other hand, the gain of APDs is associated with additional noise due to the multiplication process which must be taken into account. The noise in a PD is of great importance since it ensures a lower sensitivity limit of a detector. The primary noise sources are the shot noise σ_s^2 and thermal noise σ_t^2 (or Johnson noise) caused by photocurrent fluctuations and by receiver electronics, respectively. The shot noise is caused by the fact that the number of photons impinging on a photodetector per second is not constant and follows a Poisson distribution resulting in photon fluctuations. The photon shot noise for a PIN PD is given by [11]:

$$\sigma_s^2 = 2qI_dB, \tag{2.1.2}$$

where B is the bandwidth of the filter following the photodetector, q is a charge of an electron, and I_d is the dark current. I_d is present even when no light impinges on the

receiver and imposes the device's lower sensitivity limit. The value of I_d is determined by a photodetector material and the size of a photoactive area with typical values of 1-10 and 0.1-1 nA for PIN PD and APD, respectively [11].

Beyond the OLED-based transmitters, the receiver side may also employ an organic component such as an organic PD (OPD) which can substitute silicon photodiodes. OPDs offer superior responsivity when compared to a Si-based PD in the visible part of the electromagnetic spectrum, as illustrated in Fig. 2.5. The material for the fabrication of such an OPD is low cost and its price is reduced to ∼US$0.23/cm^2 [55]. The OPD with a modulation bandwidth of 30 kHz introduced a bottleneck in the system in [40]. The achieved capacity was 750 kb/s using the ANN post-equalizer. However, the light density on the OPD was not maximized. In [56], an OPD with a bandwidth of up to 160 kHz was reported, resulting in a data rate of 3.75 Mb/s using ANN filtering. Thus, the achieved results demonstrate the potential of OPD for VLC systems. However, an organic device was only implemented on the receiver side. To date the only fully organic VLC system was introduced in [57]. The system bandwidth was limited by an OPD up to 135 kHz and a data rate of 1.1 Mb/s was supported at a BER of 10^{-5} using the ANN equalizer.

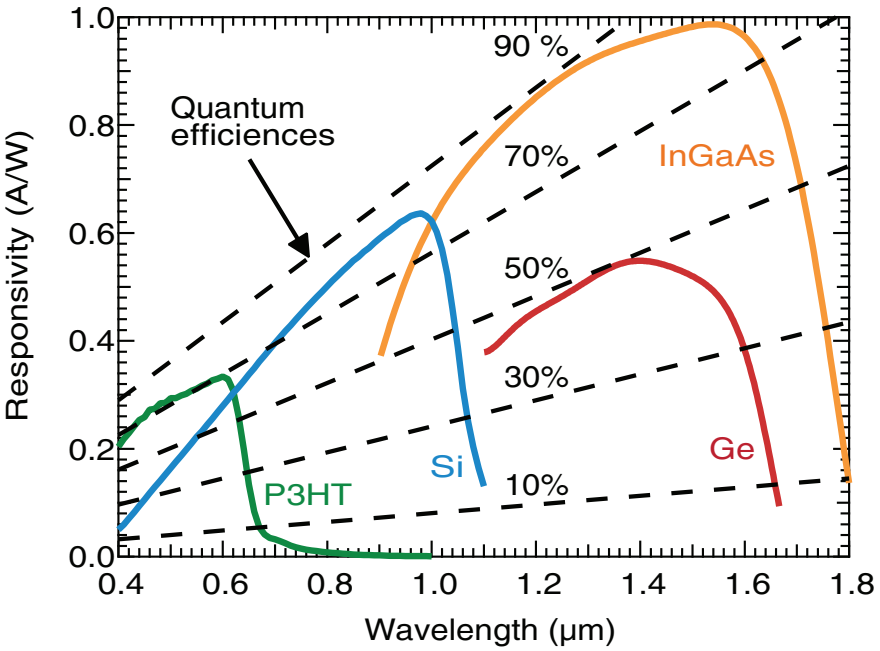

Fig. 2.5: Photodetector material responsivity.

2.2 Methods for Increasing Data Rates in VLC

The progress in VLC systems over the last decade is clearly demonstrated in Fig. 2.6 starting in 2007 with a 100 Mb/s link and DMT modulation and ending with a reported 10 Gb/s OFDM link based on WDM technique in 2016. Such rapid evolution is observed due to the implementation of several key technologies including (i) improved available bandwidth by employing devices with a higher bandwidth; (ii) utilization of spectrally efficient multi-level modulations (PAM, OFDM); (iii) advanced signal processing such as pre- and post-equalization and bit and power loading techniques; (iv) utilization of spatial diversity and multiplexing; (v) implementation of WDM. These techniques will be discussed in greater detail in the following sections.

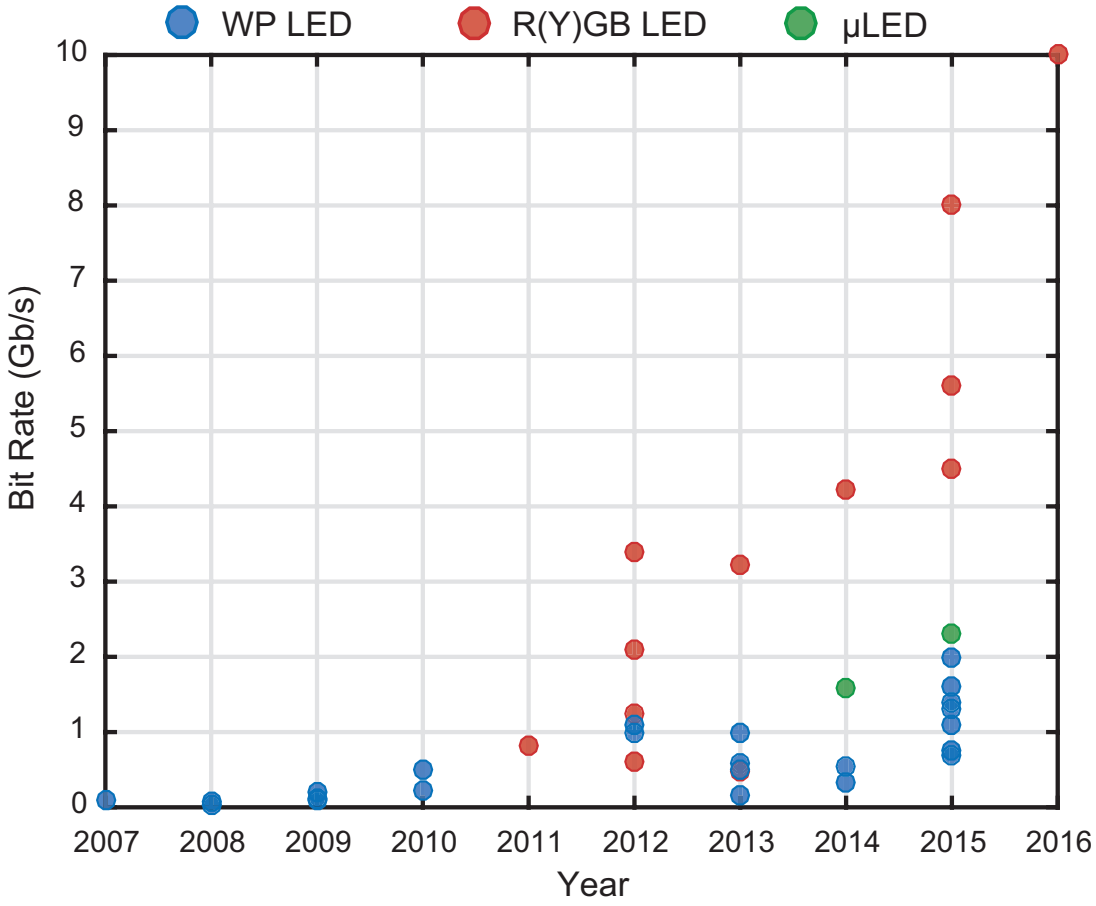

Fig. 2.6: The evolution of the reported data rates in VLC using white LEDs: WP LEDs (blue circle), R(Y)GB LEDs (red circle) and μLEDs (green circle), adopted from [58].

2.2.1 Modulation Schemes for VLC

Baseband Modulation Formats

OOK is one of the most popular schemes due to its simplicity in implementation and power efficiency. OOK scheme has been widely adopted in VLC supporting transmission speeds of hundreds of Mb/s [59-62]. Other baseband modulation formats such as PPM or multilevel PAM (L-PAM) are adopted due to their incredibly high power and spectral efficiency, respectively. PPM format is popular due to dimming support, as reported in [7, 63-65]. PAM has been implemented for VLC systems in a number of reports [66-68]. Next, the error free (i.e., BER $< 10^{-12}$) transmission over 0.6 m distance supporting 2 Gb/s based on 4-PAM was demonstrated in [69]. The spectral efficiency of L-PAM increases with a higher number of amplitude levels, but at the cost of lower power efficiency. However, L-PAM systems are sensitive to the nonlinear electro-optics characteristics of LEDs. To overcome this limitation, a superposed PAM (SPAM) utilizing spatially separated LEDs was introduced in [70]. Signals are transmitted with different amplitudes and combined in a free space resulting in multi-level modulation.

Subcarrier Modulation Formats

Recently, advanced modulation schemes such as OFDM and CAP have been the focus of enormous attention among researchers due to the possibility of supporting high-order modulation formats such as QAM and to be efficiently utilized in bandlimited communication channels enabling throughputs of several Gb/s. Thus, a more detailed discussion on these modulation schemes is given in the following sections.

OFDM is a form of subcarrier modulation that can efficiently utilize the available bandwidth in bandlimited systems using bit- and power-loading algorithms [71]. OFDM transmits the data in parallel over a large number of subcarriers that are orthogonal over a symbol period to reduce the ISI. Moreover, the OFDM scheme can be implemented by simply utilizing an inverse fast Fourier transform (IFFT) and FFT at the transmitter and receiver, respectively. The OFDM schematic block diagram is depicted in Fig. 2.7. Input data is mapped into M-ary QAM (M-QAM) constellation symbols before a serial-to-parallel (S/P) conversion. The signal is then mapped into individual subcarriers by means of IFFT, and a cyclic prefix (CP) is added at the beginning of each symbol to reduce both ISI and inter-carrier interference (ICI). After parallel-to-serial (P/S) conversion, the signal is used to modulate LED intensity. At the receiver, the CP is first removed and S/P conversion is performed. The FFT is applied on the data and demodulation follows. After P/S conversion, the received bits are estimated.

In the RF-based OFDM systems, the output signal is generally complex and bipolar. However, to directly modulate LED optical intensity, a real and unipolar signal is required [72]. Thus, there are several approaches how to ensure the desired signal at the output of an OFDM transmitter. To generate a real signal, Hermitian symmetry is imposed on the complex signal before IFFT is applied. This reduces the spectral efficiency by at least half when compared to conventional OFDM systems [73]. To obtain a positive signal, a

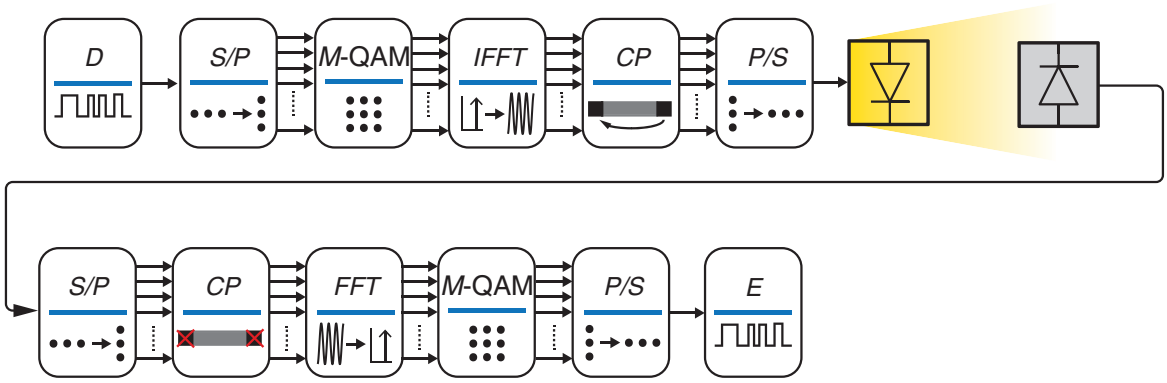

Fig. 2.7: Schematic block diagram of an OFDM system.

DC level is added in a DC-biased optical OFDM (DCO-OFDM) system. Asymmetrically clipped optical OFDM (ACO-OFDM) is another approach. In ACO-OFDM, the bipolar and real signal is clipped at a zero level and the entire negative signal is removed, hence no DC bias is required. In the case of ACO-OFDM, the signal is transmitted only on odd subcarriers. Thus, spectral efficiency is reduced by half compared to DCO-OFDM. On the other hand, power efficiency is increased due to the absence of a DC bias. Other forms of OFDM modulation such as unipolar OFDM (U-OFDM) and flip-OFDM were reported in the literature offering the same system performance as ACO-OFDM in AWGN channels [74-76]. The performance comparison of different OFDM schemes in a bandlimited system, showing that DCO-OFDM outperforms other forms of OFDM, was reported in [77-80]. The performance degradation of the ACO-OFDM scheme is introduced mainly by clipping noise and the BLW phenomenon due to a large DC component [81]. One of the key drawbacks of OFDM is high peak-to-average power ratio (PAPR) due to the summation of a high number of subcarrier signals to high signal peaks, making OFDM systems sensitive to the devices with nonlinear electro-optics characteristics such as LEDs. However, many techniques have been proposed to reduce PAPR, including employing pilot symbols [82], linearization of an LED frequency response [83], or encoding transmit data symbols, including DC biasing [84]. In recent years, the OFDM scheme has been applied to VLC systems to support several Gb/s transmission speeds [9, 10, 85-88].

As an alternative solution, CAP is an optimal candidate for VLC systems supporting high data rates as already reported in the literature [8, 89-91]. The CAP scheme was experimentally shown to outperform OFDM in terms of data rate using the same physical link in VLC [92]. The principle of the CAP system is illustrated in Fig. 2.8(a). Input data is mapped into M-QAM constellation symbols and upsampled by means of zero padding. After splitting the data into real (in-phase) and imaginary (quadrature) parts, the signal is passed through in-phase and quadrature pulse shaping filters, e.g., the square root raised cosine (SRRC). In CAP, carrier frequencies are generated using a pair of finite impulse response (FIR) filters, unlike QAM, which requires a local oscillator. The impulse responses of the CAP transmit filters form a Hilbert pair and are given as the product of the FIR filter impulse response and the sine and cosine wave as given by [93]:

$$f_I(t) = \left(\frac{\sin(\gamma(1-\beta)) + 4\beta\frac{t}{T_s}\cos(\gamma\xi)}{\gamma(1-(4\beta\frac{t}{T_s})^2)} \right) \cdot \cos(\gamma\xi) \tag{2.2.1}$$

for the in-phase filter and

$$f_Q(t) = \left(\frac{\sin(\gamma(1-\beta)) + 4\beta\frac{t}{T_s}\cos(\gamma\xi)}{\gamma(1-(4\beta\frac{t}{T_s})^2)} \right) \cdot \sin(\gamma\xi) \tag{2.2.2}$$

for the quadrature filter, where T_s is symbol duration, $\gamma = \pi t/T_s$ and $\xi = 1+\beta$. The roll-off factor β determines the excess of bandwidth and varies in the range of $0 \leq \beta \leq 1$. A larger β results in a greater bandwidth requirement, which is $(1+\beta)$ times the symbol rate. Values close to 0 should be chosen to use the bandwidth efficiently. The impulse responses of the in-phase and quadrature transmit filters are illustrated in Fig. 2.8(b) and 2.8(c), respectively. Real and imaginary components are added prior to transmission via intensity modulation of an LED. At the receiver, the signal is passed through the time-reversed in-phase and quadrature filters that are matched to the transmit filters as $g_I^m(t) = f_I^m(-t)$ and $g_Q^m(t) = f_Q^m(-t)$. After downsampling and constellation de-mapping, the received bits are estimated.

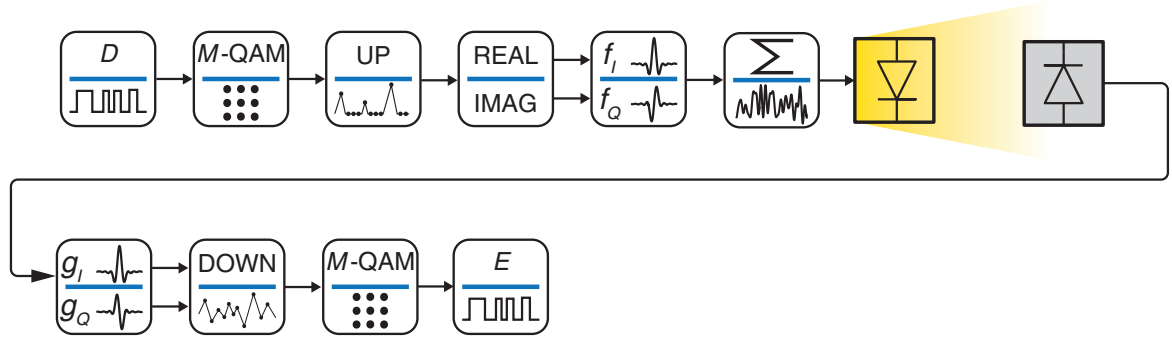

(a)

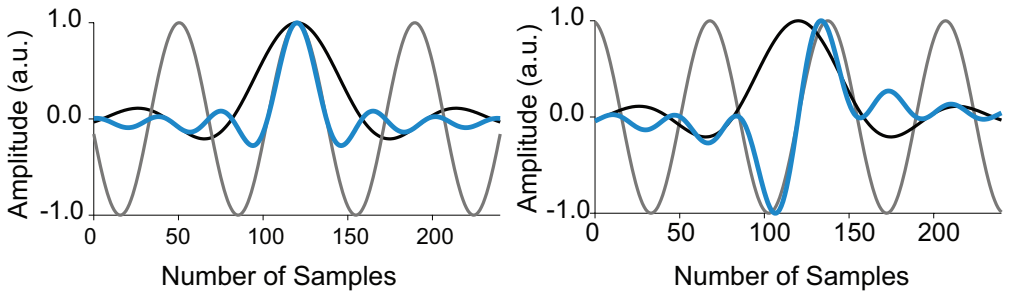

(b)

(c)

Fig. 2.8: (a) The schematic block diagram of the CAP system, (b) and (c) are the impulse responses of the in-phase and quadrature transmit filters, respectively.

When compared to OFDM, the CAP scheme offers a simpler implementation and lower PAPR values [92]. However, the flat frequency response is required in order to effectively implement CAP, which is seldom available in real VLC. Additionally, CAP must have a fixed modulation order cardinality, unlike OFDM that can be tailored to any frequency response using bit- and power-loading algorithms. To increase the link performance of systems with a non-flat frequency response, a complex equalizer is needed [8]. In [93, 94], a solution to overcome the flat band requirement was introduced (for optical fiber links) by splitting the available signal bandwidth into m sub-bands (or subcarriers to remain consistent with OFDM nomenclature) thus resulting in a multiband CAP (m-CAP), see Fig. 2.9. The multiband approach relaxes the flat-band response requirement and allows the utilization of bit- and power-loading algorithms to adapt the number of bits/symbol to every individual subcarrier. By increasing the number of subcarriers m, the subcarrier bandwidth is decreased and a frequency flatness can be easily approximated. This can be a substantial advantage in VLC systems since LEDs exhibit high attenuation outside of the modulation bandwidth. On the other hand, the multiband form significantly increases the computational complexity of the system by requiring $2m$ FIR filters at the transmitter and additional $2m$ FIR filters at the receiver, thus resulting in $4m$ filters in total. Such an issue needs to be taken into account for hardware implementation, e.g., on FPGAs. All aforementioned results considering an m-CAP scheme were reported for fiber optical links. However, based on the aforementioned results reported for fiber optical links, the m-CAP scheme introduces a promising solution for VLC systems.

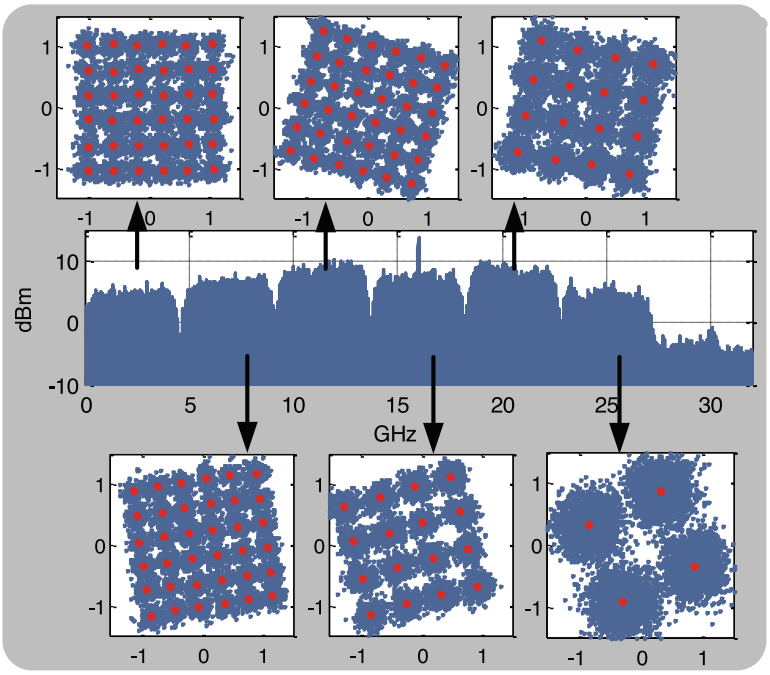

Fig. 2.9: The m-CAP signal spectrum showing the splitting of the signal bandwidth into $m = 6$ subcarriers [94].

2.2.2 Blue Filtering

Using a blue optical band-pass filter before a photodetector at a receiver is the simplest and most straightforward method for increasing LED bandwidth. The slow yellowish component is filtered out resulting in increased modulation bandwidth of up to 20 MHz [59, 95, 96]. However, signal attenuation is not negligible due to the rejection of longer wavelengths resulting in up to a 50% loss of optical power [97]. It was reported that blue filtering has a marginal effect on VLC links with advanced modulation schemes, such as DMT or CAP, and can even degrade system performance (by reducing SNR). On the other hand, the filter application in OOK-based systems can further increase the measured bit rate [98, 99]. Nevertheless, blue filtering remains the simplest way to improve system capacity without increasing the overall complexity of the receiver.

2.2.3 Equalization Techniques

Alternatively, equalization can be applied to increase the system modulation bandwidth by applying a filter that has a frequency response inverse to the system frequency response. Equalizers combat ISI that occurs when the transmitted symbol is spread to adjacent symbols resulting in error performance degradation. Equalization can be analogue or digital and can be implemented at the transmitter (pre-equalization) or at the receiver (post-equalization), see Fig. 2.10.

Analogue equalizers are designed from passive components such as resistors, inductors and capacitors, or active parts, including operational amplifiers. As already mentioned, an LED can be modelled as a first-order LPF introducing attenuation of 20 dB/decade outside the 3 dB modulation bandwidth. To compensate for this, a resistor-capacitor (RC) analogue high-pass filter (HPF) can be applied at the receiver as in [59], where the bandwidth was extended up to 50 MHz resulting in the demonstration of a 100 Mb/s link. In [100], analogue resonant RC circuits equalizing different regions of the system frequency response were utilized at the transmitter (made of 16 LEDs) to increase the bandwidth from ∼2.5 MHz

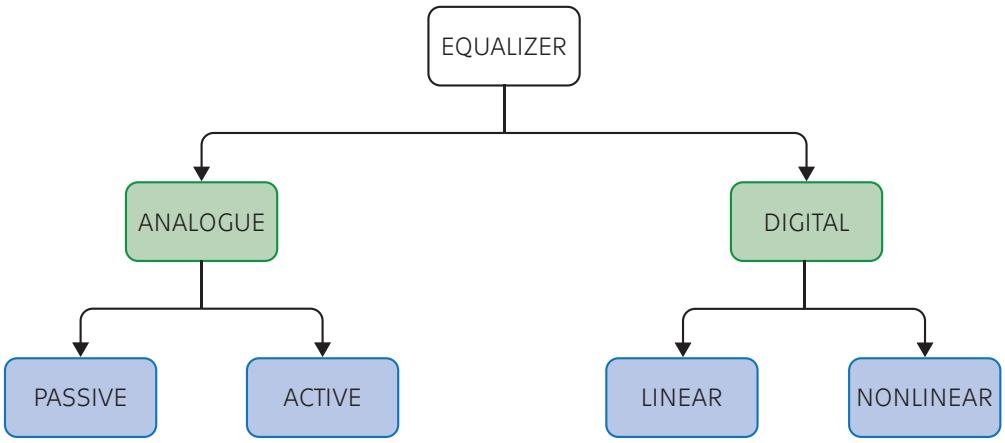

Fig. 2.10: Types of equalizers for VLC.

to 25 MHz and to support a 40 Mb/s data rate. However, using HPF equalizer results in the attenuation of low frequency components introducing the BLW phenomenon, lower modulation index and reduced SNR. An active component-based pre-equalizer was applied in [101]. The bandwidth of a VLC system was enhanced from 3 to 12 MHz by blue filtering and up to 77 MHz using a pre-emphasis circuit to demonstrate a non-return to zero (NRZ) OOK system with a throughput of 200 Mb/s. The system bandwidth was further improved up to 233 MHz using pre- and post-equalization with blue filtering supporting a bit rate of 550 Mb/s based on NRZ OOK [102]. Other reports demonstrating the utilization of analogue equalization to improve the modulation bandwidth in excess of 100 MHz can be found in the literature [103-105]. In VLC, post-equalization is often the preferred option. Pre-equalization circuits need to be adapted to each individual source and operate in currents of hundreds of mA which can be challenging. Also, the nonlinear electro-optic characteristic of LEDs needs to be considered. Post-equalization techniques are not limited by these constraints. However, the noise at the receiver increases when applying post-equalization [58].

Digital equalizers can be categorized into two groups − linear and non-linear, known as a decision-feedback equalizer (DFE). They can be implemented based on FIR digital filters using any signal processing platforms such as an FPGA. DFE offers more enhanced BER performance than linear equalizers at the cost of increased computational complexity. The principle of digital equalizers is based on removing ISI by adapting the estimated filter coefficients (or weights) that are calculated using the known training sequence. A linear zero-forcing equalizer (ZFE) forces zero ISI by applying the flat frequency response as $H(f) = 1/G(f)$, where $H(f)$ is the frequency response of the equalizer and $G(f)$ is the system frequency response. ZFE is based on a transversal filter with a number of adjustable coefficients. The filter coefficients are determined by transmitting the known data sequence over the system. The main drawback of ZFE is sensitivity to noise. Non-linear DFEs remove ISI on the principle of a feedback structure with two filters required − a feedforward and a feedback filter. ISI in a current symbol is reduced, based upon previously detected symbols. DFE offers improved performance over ZFE in very band-limited environments without increased computational complexity [106].Thus, a number of studies on DFE-based VLC systems can be found in the literature [33, 89, 92].

Due to the nonlinear characteristic of an LED, filter-based equalizers are not an optimal solution for VLC systems. ANN filtering was shown to compensate for LED nonlinearity and outperform previously mentioned equalizers [33, 107]. On the other hand, much higher computational complexity is to be expected when implementing ANN. Alternatively, a Volterra-based DFE was introduced as a solution to combat ISI and nonlinear LED response in PAM and CAP VLC systems [90, 108]. Another possibility is the utilization of frequency domain equalization (FDE), which works on the principle of FFT applied on a block of received symbols followed by a single-tap equalizer in the frequency domain. FDE techniques were investigated in [109-111].

2.2.4 Spatial and Wavelength Division Multiplexing

To increase VLC system coverage and fully support the required illumination levels, a large number of LEDs can be deployed in an indoor environment. A highly efficient, reliable and robust VLC system can be designed by adopting multiple LEDs and multi-color devices known as spatial multiplexing (SMP) and WDM, respectively.

Spatial Multiplexing

The following approaches can be applied to drive spatially separated LEDs: (i) a ganging technique and (ii) MIMO. In the ganging approach, individual LEDs are fed with the same data stream and spatially superposed in a free space, see Fig. 2.11(a). Each LED can be driven by the individual driver. The benefits of using multiple LED sources include wider coverage or increased robustness against blocking the signal path between a transmitter and receiver. The transmitter consisting of 16 spatially separated LEDs was demonstrated to increase SNR at the receiver and support link capacity of 40 Mb/s with NRZ OOK in [100]. Spatial multiplexing can be further applied for angle diversity schemes by utilizing a number of LEDs with a limited divergence angle or by arranging LEDs in a semi-spherical base [112, 113].

The MIMO scheme is based on the parallel transmission of individual data streams using multiple LEDs to increase system capacity as illustrated in Fig. 2.11(b). Several MIMO techniques can be implemented in VLC systems such as (i) spatially superposed modulation; (ii) SMP; (iii) space shift keying (SSK). In the spatially superposed scheme, the desired signal at the receiver plane is achieved by superposing optical intensities from multiple LEDs in a free space. The SPAM scheme for VLC can be implemented by driving LEDs either independently with a different driving voltage [70], or, together with equal driving currents [114]. Moreover, the spatially superposed modulation can be utilized in OFDM systems to reduce PAPR and the effect of an LED nonlinear characteristic. This is achieved by splitting the OFDM signal into several narrowband OFDM signals that are transmitted by different LEDs [115, 116].

The last of the MIMO techniques, SSK, also known as optical spatial modulation, utilizes multiple spatially separated LEDs [117-119]. During the transmission, only one

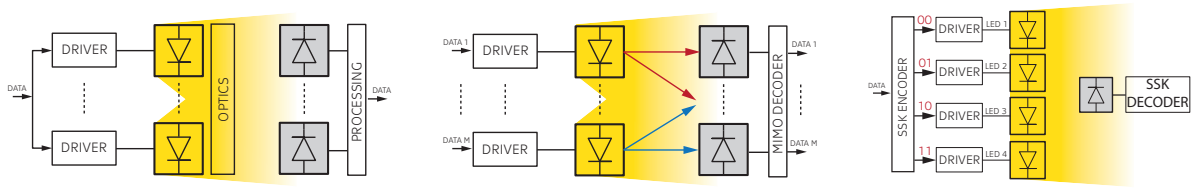

(a) (b) (c)

Fig. 2.11: Spatial multiplexing techniques: (a) ganging approach, (b) MIMO approach, (c) space shift keying.

LED at a time is active and the rest are in the 'OFF' state. The LED is activated by the incoming data sequence, e.g., LED1 is active for input bit stream '00', LED2 for bit stream '01' and so on, see Fig. 2.11(c). Data decoding is based on light intensities that depend on the relative transmitter position. The effect of ICI is removed due to the only one active LED at a time. Moreover, SSK was reported to improve OFDM-based VLC link capacity supporting 1.34 Gb/s [120, 121]. Spectral efficiency is enhanced by a factor of $log_2(T_M)$, where T_M is the number of transmitters. To further increase bandwidth efficiency, a generalized SSK (GSSK) can be adopted. In GSSK, multiple LEDs transmit the information at a given time [97, 122].

The SMP technique is based on the principle of multiple transmitters fed by independent data streams resulting in increased spectral efficiency by up to a number of transmitters. Regarding the aforementioned MIMO techniques, SMP is the most spectrally efficient, at the price of high computational complexity, and its performance is dependent upon the channels correlation. The investigation of SMP in VLC systems has attracted great attention over the last decade resulting in multi Gb/s transmission speeds [35, 109, 123-125]. SMP was also investigated in OVLC utilizing 4×4 MIMO [126].

Wavelength Division Multiplexing

The system capacity can be increased using the WDM technique that utilizes multiple different wavelengths to transmit individual data streams. In VLC, white light is generated by combining three (RGB LED) or alternatively four colors by adding yellow (RYGB LED). The signals carried on different wavelengths are superposed in a free space and optical bandpass filters, with the appropriate central wavelength, are applied at the receiver to separate individual channels. WDM has been successfully demonstrated in a number of research works. For instance, the data rate of 803 Mb/s using RGB LED and DMT modulation was reported in [127]. A number of reports on multi-Gb/s VLC systems were experimentally demonstrated using RGB LED [85, 90] and RYGB LED [8, 9]. To date, the highest achieved bit rate of 10 Gb/s was reported in [86].

2.3 Channel Modeling

In addition to increasing transmission throughputs in both inorganic and organic VLC systems, channel modeling and characterization remain an open issue. There are number of possible link configurations for VLC systems as illustrated in Fig. 2.12. The directed LOS method is used in the vast majority of experimental studies due to maximized SNR and, hence, a link capacity. The non-directed LOS increases user mobility at the cost of decreased SNR. However, the LOS system is sensitive to shadowing and blocking. The NLOS (also called diffuse) configurations are another possible solution. The data transmission is based on the signal reflected from the walls, floor and ceiling, and other objects within a room. Such a scenario offers high mobility and signal coverage. On the other hand, low values of optical received power and multipath distortion should be expected resulting in limited achievable data rates. Both LOS and NLOS have to be considered to design a robust VLC properly.

In VLC, computationally-based channel models such as the recursive method [6, 49, 50, 128, 139], Monte Carlo ray tracing [51-53, 130-132] or the ceiling bounce model [133, 134] have been commonly adopted from IR communications. The benefit of the recursive method is in its simplicity of implementation. On the other hand, it suffers from increased computational complexity, especially for the high number of reflections added to the calculation. The iterative side-based model, which is much faster than a recursive algorithm, was

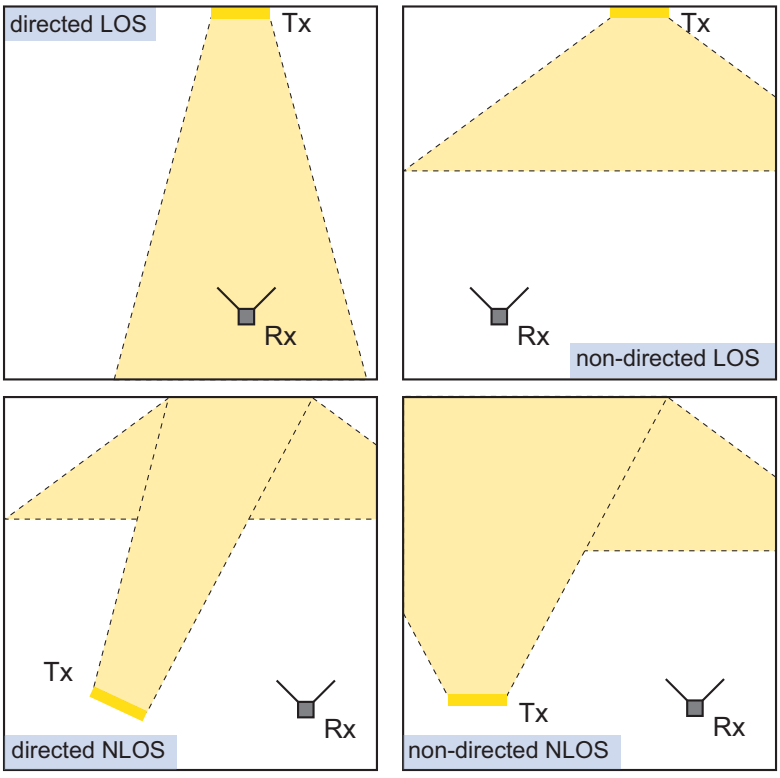

Fig. 2.12: Possible VLC link configurations, adopted from [135].

proposed in [136]. The Monte Carlo ray tracing algorithm is based on transmitting a large number of photons with randomly generated direction according to the source emission pattern. The final channel impulse response is calculated using the trajectories of the emitted photons. In [137], a new ray tracing method was proposed to decrease the complexity of the model.

Contrary to the IR band, where the reflections from walls are independent of the wavelength due to the monochromatic source, wavelength dependency should be taken into consideration when calculating VLC channel parameters such as channel bandwidth, channel impulse response or delay spread to provide accurate results. The channel impulse response is the essential parameter that fully characterizes the propagation channel. In VLC, the modeling of reflections from walls and objects within a room is crucial for achieving accurate results. Several types of reflections can be observed that are dependent on the surface material, wavelength or angle of incidence − the purely diffuse, specular and a mix of both [138]. However, most reflections can be approximated by the Lambertian model as having a typical diffusive pattern [11]. The example of the measured reflection coefficients of different indoor materials is given in Fig. 2.13. The most extensive comparison between IR and VLC channel parameters was published in [132] confirming the improvement in coherence bandwidth and the root mean square (RMS) delay spread in VLC while diffuse, specular and mixed specular-diffuse wavelength dependent reflections were considered to attain a realistic channel impulse response.

In the next sections, the modeling of individual VLC system parts will be discussed with a focus on the recursive algorithm since such a method was applied in publications related to this doctoral thesis.

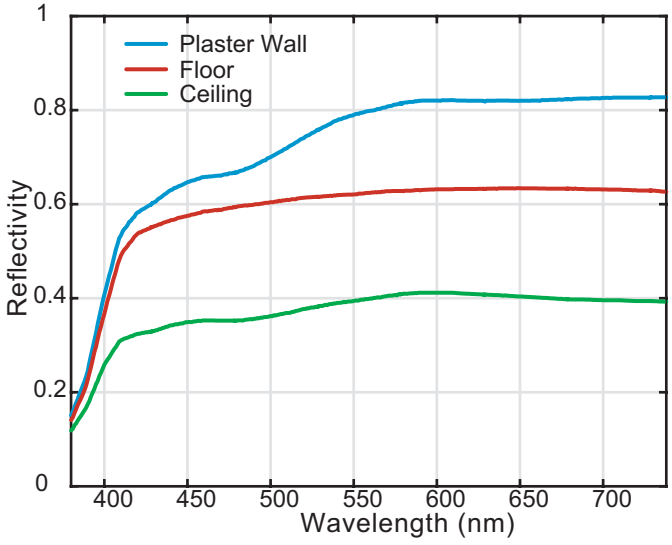

Fig. 2.13: Measured reflectivity for different indoor materials, adopted from [50].

2.3.1 Transmitter Model

Transmitted optical power (or the channel input) is nonnegative and satisfies the following condition:

$$x(t) \geq 0. \tag{2.3.1}$$

The average transmitted optical power of an LED source is given as:

$$P_t = \lim_{T\to\infty} \frac{1}{2T} \int_{-T}^{T} x(t)dt. \tag{2.3.2}$$

The emission from an optical light source (both LED and OLED) can be modelled by Lambert's cosine law using luminous intensity R_0 as [49, 129]:

$$R_0(\theta) = \frac{m_l + 1}{2\pi} \cos^{m_l}(\theta), \tag{2.3.3}$$

where θ is the angle of emission and m_l is the Lambertian order defined as [49, 129]:

$$m_l = -\frac{ln(2)}{ln(\cos(\vartheta_{1/2}))}, \tag{2.3.4}$$

where $\vartheta_{1/2}$ is the semiangle at half illuminance of an LED. The Lambertian emitter is a source with $m_l = 1$ (i.e. $\vartheta_{1/2} = 60°$). The directivity of the source is increased with higher m_l as illustrated in Fig. 2.14. The LED transmitters with $m_l = 1$ are assumed in most research works. However, Lambertian order optimization can further enhance VLC system performance in terms of received power and channel bandwidth as reported in [139].

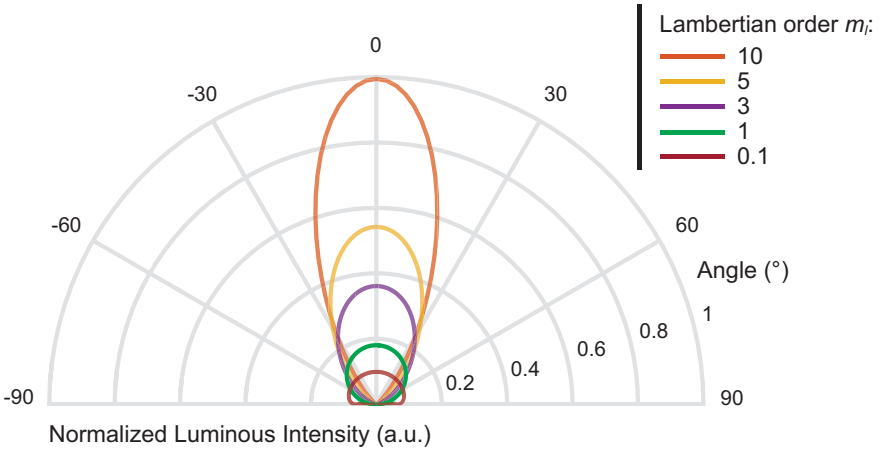

Fig. 2.14: Luminous intensity profiles for sources with different Lambertian order.

2.3.2 Receiver Model

At the receiver, the optical signal impinging on the detector active area is collected and converted into an electrical domain. The main parameters of photodetectors included in channel models are the surface area of a photodetector A_{det} and the receiver's field of view (FOV). To further increase system performance, components, such as an optical concentrator, lenses and optical filters, can be utilized. The gain of an optical concentrator at the receiver is given as:

$$g_{oc}(\phi) = \begin{cases} \frac{n^2}{\sin^2 \omega_{FOV}} & 0 \leq \phi \leq \omega_{FOV} \\ 0 & \phi > \omega_{FOV} \end{cases} \tag{2.3.5}$$

where n is the refractive index of an optical concentrator, ϕ is the incident angle of the optical signal and ω_{FOV} is the receiver FOV. The typical values of the receiver parameters used in the literature are listed in Table 2.1 [5, 6, 132, 139].

Table 2.1: Typical parameters of the receiver components set in the simulations.

Parameters	**Symbol**	**Value**
Receiver FOV	ω_{FOV}	$\leq 90°$
Optical filter gain	g_{of}	1
Refractive index	n	1.5
Photodetector area	A_{det}	1 cm^2

2.3.3 Optical Channel

The essential parameter characterizing an optical propagation channel is the channel impulse response, which is given as a superposition of LOS and NLOS (diffuse) signal components at the detector as:

$$h(t) = h_{LOS}(t) + h_{NLOS}(t). \tag{2.3.6}$$

The LOS impulse response $h_{LOS}(t)$, from source S to receiver R, can be expressed according to a geometrical model illustrated in Fig. 2.15 as [49, 129]:

$$h_{LOS}(t, S, R) = \frac{A_{det}(m_l + 1)}{2\pi d^2} \cos^{m_l}(\theta) g_{of}(\theta) g_{oc}(\theta) \cos(\theta) \delta\left(t - \frac{d}{c}\right), \tag{2.3.7}$$

where d is the distance between S and R, c is the speed of the light in free space and $\delta(\cdot)$ is the Dirac function representing the signal propagation delay. The expression assumes that $\theta < 90°$, $\phi < FOV$ and $d \gg \sqrt{A_{det}}$. The diffuse part of the impulse response is given as an infinite sum of multipath components propagating within a room. In [49], the multipath propagation model was proposed to calculate $h_{NLOS}(t)$. The room surface was divided into

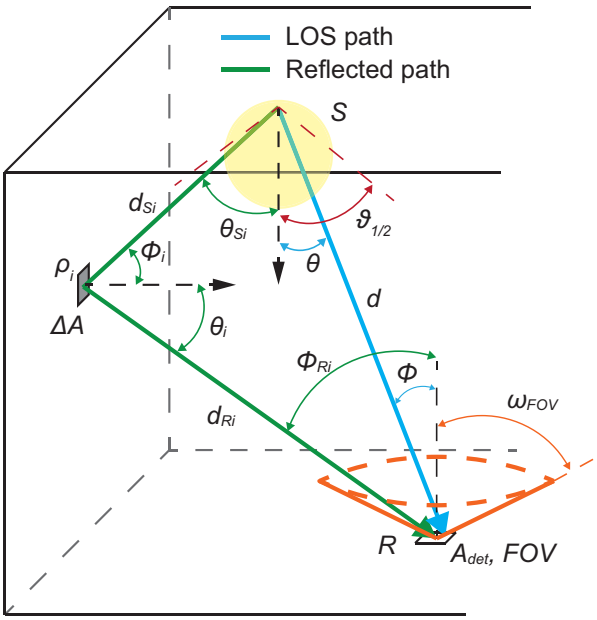

Fig. 2.15: The geometry for calculating channel impulse response.

N reflecting elements E with an area ΔA behaving both like a detector and an emitter that re-transmits the incident signal as a point source. The impulse response after k reflections is calculated using a recursive algorithm as [49, 129]:

$$h_{NLOS}(t,S,R) = \frac{m+1}{2\pi}\sum_{i=1}^{N}\rho_i \cos^m(\theta_i)\frac{\cos(\theta_i)}{d_{Si}^2} rect\left(\frac{2\theta_i}{\pi}\right)\cdot \\ \cdot h_{NLOS}^{k-1}\left(t-\frac{d_{Si}}{c}, E_i, R\right)\Delta A, \tag{2.3.8}$$

where ρ_i is the reflection coefficient of E_i, θ_i and ϕ_i are the emitting and incident angles of E_i, d_{Si} is the distance between S and E_i, $h_{NLOS}^{k-1}(t, E_i, R)$ is the impulse response of order $k-1$ between reflector E_i and R, and $rect(x)$ is the rectangular function equal to 1 for $|x| \leq 1$ and 0 for $|x| > 1$.

From the known channel impulse response, two important parameters, such as the DC channel gain $H(0)$ and RMS, delay spread τ_{RMS} which estimates how susceptible the optical channel is to ISI, can be calculated as [1]:

$$H(0) = \int_{-\infty}^{\infty} h(t)dt, \tag{2.3.9}$$

$$\tau_{RMS} = \sqrt{\left(\frac{\int (t-\mu)^2 h^2(t)dt}{\int h^2(t)dt}\right)}, \tag{2.3.10}$$

where t is propagation time and μ is mean excess delay defined by [1]:

$$\mu = \frac{\int t h^2(t) dt}{\int h^2(t) dt}, \tag{2.3.11}$$

Obviously, the channel parameters are dependent on the geometrical configuration of the system, i.e., the size of a room, positions and rotations of the transmitter and receiver and other objects within the room.

The LOS-based links, in principle, have infinite channel bandwidth and are beneficial due to the maximized SNR and achievable data rates. However, any obstacle between the transmitter and receiver can cause the degradation of the quality of services or even service failure. Most of the research works focuses on the LOS VLC scenarios as reported in [50, 53, 132, 133, 139]. However, NLOS-based communication is of great importance towards implementing robust VLC systems. NLOS (diffuse) indoor IR optical wireless systems have been extensively investigated, both theoretically and experimentally [134, 140-143]. The NLOS VLC scenarios were investigated in several publications. For instance, the undesirable impact of the NLOS environment on the accuracy of VLC-based indoor localization, with the highest errors near the edge of the room, was reported in [144]. In [145] the effect of multipath reflections on the signal-to-interference plus noise ratio (SINR) was investigated, showing that higher order reflections have a stronger adverse impact on the SINR than the 1^{st} order reflection when utilizing narrow FOV receivers. A new analytical method with low computational complexity to determine the NLOS channel impulse response was presented in [146]. However, the number of publications on NLOS channel modeling in VLC is limited and, therefore, this scheme needs further research.

3 Objectives of the Thesis

The thesis is based on two main research directions in VLC with the given goals as follows:

G1: To propose, implement and experimentally verify a new modulation scheme suitable for VLC.

G2: To propose new analytical and experimental models for VLC channel parameters with an emphasis on dynamically changing the indoor environment including movement of people and NLOS reception.

The following tasks have to be addressed to attain goal **G1**:

T1: To develop a theoretical model of the VLC-based m-CAP system and evaluate the system performance through numerical simulations.

T2: To verify experimentally the results from numerical simulations.

T3: To analyze the trade-off between the parameters of pulse-shaping filters at the transmitter and receiver and m-CAP VLC system performance.

T4: To propose recommendations for m-CAP system design based on the measurement campaign.

The following tasks have to be addressed to attain goal **G2**:

T5: To evaluate the algorithms for VLC channel modeling and optimize them for the investigation of channel model parameters in a dynamic indoor environment.

T6: To investigate the effect of movement of people within a room on the VLC channel parameters for different indoor scenarios.

T7: To investigate the NLOS VLC system channel model for different receiver orientations and through an experimental campaign.

4 Achieved Results

The core of the thesis is based on published research articles, including five papers in peer-reviewed journals with impact factor [J1-J5] and one paper in conference proceedings listed in the *Web of Knowledge* [C1]. The full and original papers with bibliographic citations and individual paper contributions to the thesis are given in the next sections.

Section 4.1, *Multi-band Carrier-less Amplitude and Phase Modulation for Bandlimited Visible Light Communications Systems*, is focused on the numerical simulations of the m-CAP scheme, which is newly adopted for VLC systems from the field of optical fiber networks. The concept, principles, benefits and drawbacks of m-CAP VLC are discussed and show the suitability of newly adopted modulation scheme for VLC links. The effect of the bandlimited system, caused by a real limitation of LED frequency response, on the received signal is described in detail. It is shown that the m-CAP scheme outperforms a traditional 1-CAP modulation.

After theoretical analyses, the m-CAP VLC link is experimentally tested in Section 4.2 *A Multi-CAP Visible-Light Communications System with 4.85 b/s/Hz Spectral Efficiency*. The relationship between the measured data rate, spectral efficiency and the number of subcarriers is investigated. It is demonstrated that an increase in the number of subcarriers can enhance VLC system performance up to 31.53 Mb/s (i.e., spectral efficiency up to 4.85 b/s/Hz) utilizing an LED with only a 4.5 MHz bandwidth.

Based on the results achieved in Sections 4.1 and 4.2, m-CAP VLC system complexity is the main focus of next research steps highlighted in Section 4.3 *Evaluation of Multi-band Carrier-less Amplitude and Phase Modulation Performance for VLC under Various Pulse Shaping Filter Parameters*. It is shown how the performance of the system is strongly dependent on the parameters (i.e., filter length and roll-off factor) of the pulse shaping filters utilized at both the transmitter and receiver. Based on the numerical simulations, we illustrate that increasing both parameters improves BER performance of the system substantially. From the reported results, it is shown that utilizing filters with filter length higher than 12 symbols is impractical due to minimal performance improvement.

In Section 4.4 *On m-CAP Performance with Different Pulse Shaping Filters Parameters for Visible Light Communications*, we verify and extend the analytical work reported in Section 4.3. We experimentally investigate the performance of the m-CAP VLC system for a range of transmit/receiver filter conditions. The trade-off between system complexity and performance in terms of transmission rates and spectral efficiencies is discussed in detail and recommendations towards the hardware implementation of m-CAP are proposed. We show that lower order m-CAP can offer the same system performance as a higher order system while offering much lower system computational complexity. We show that m-CAP VLC link with $m \geq 6$ can be designed with the same filter parameters to demonstrate a link with both the highest data rate and spectral efficiency simultaneously in contrast to lower order m-CAP systems.

In the next Section 4.5 *Channel Characteristics of Visible Light Communications within a Dynamic Environment*, we focus on the second goal of the thesis. Channel characterization of a VLC system affected by movement of people within a room is investigated

for the first time in a VLC domain. Both analytical and experimental results are given for different indoor conditions (i.e., furnished office room, empty hall and corridor). The impact of shadowing and blocking on user mobility and link performance is discussed using a newly determined cumulative distribution function of received power distributions and delay profiles. Based on the measured data, we derive the scale parameters of Rayleigh distribution of the normalized received power for different densities of people.

Following the previous research in channel modeling, the last Section 4.6 *Analyses of non-line of sight visible light communications* is focused on the characterization of the NLOS VLC system. The paper is focused on a comparison of the pure NLOS- and LOS-based VLC systems in terms of channel bandwidth and received optical power while considering an arbitrary position both in azimuth and the elevation of the receiver. A typical ceiling-to-device and device-to-device (D2D) VLC are considered. We show that pure NLOS path can offer a higher bandwidth (up to 14 MHz) compared to the link with LOS and NLOS components for a particular transmitter configuration. The model from numerical simulations is extended by statistics of shadowing due to people's movement which are derived from the measurement campaign. The received optical power drop can be observed due to the effect of shadowing.

4.1 Multi-band Carrier-less Amplitude and Phase Modulation for Bandlimited Visible Light Communications Systems

This chapter is a version of the published manuscript:

P. A. Haigh, S. T. Le, S. Zvanovec, Z. Ghassemlooy, P. Luo, T. Xu, **P. Chvojka**, T. Kanesan, E. Giacoumidis, P. Canyelles-Pericas, H. Le Minh, W. Popoola, S. Rajbhandari, I. Papakonstantinou and I. Darwazeh, "Multi-band carrier-less amplitude and phase modulation for bandlimited visible light communications systems," in *IEEE Wireless Communications*, vol. 22, no. 2, pp. 46-53, 2015.

Connection with my Ph.D. thesis:

Most high-speed VLC systems are based on an OFDM or CAP scheme. However, CAP requires flat band system response which is barely available in VLC. In this paper, we adopt, for the first time, an m-CAP scheme for VLC and evaluate its performance using numerical simulations. The results indicate that a multiband approach outperforms a traditional single CAP system, relaxes the flat band requirement and enables the use of bit- and power-loading algorithms. Thus, m-CAP modulation is verified to be suitable for bandlimited VLC systems. The theoretical analysis demonstrates that spectral efficiency can approach slightly short of 10 b/s/Hz when the number of subcarriers is higher than 10. Here, we set the basis for the next piece of research and complete task **T1**.

MULTI-BAND CARRIER-LESS AMPLITUDE AND PHASE MODULATION FOR BANDLIMITED VISIBLE LIGHT COMMUNICATIONS SYSTEMS

PAUL ANTHONY HAIGH, SON THAI LE, STANISLAV ZVANOVEC, ZABIH GHASSEMLOOY, PENGFEI LUO, TONGYANG XU, PETR CHVOJKA, THAVAMARAN KANESAN, ELIAS GIACOUMIDIS, PEP CANYELLES-PERICAS, HOA LE MINH, WASIU POPOOLA, SUJAN RAJBHANDARI, IOANNIS PAPAKONSTANTINOU, AND IZZAT DARWAZEH

Paul A. Haigh is with the University of Bristol.

Son Thai Le and Elias Giacoumidis are with Aston University.

Petr Chvojka and Stanislav Zvanovec are with Czech Technical University in Prague.

Zabih Ghassemlooy, Pengfei Luo, Pep Canyelles-Pericas, and Hoa Le Minh are with Northumbria University.

Tongyang Xu, Ioannis Papakonstantinou, and Izzat Darwazeh are with the University College London.

Thavamaran Kanesan is with Telekom Research & Development (TM R&D).

Wasiu O. Popoola is with the University of Edinburg.

Sujan Rajbhandari is with the University of Oxford.

ABSTRACT

Visible light communications is a technology with enormous potential for a wide range of applications within next generation transmission and broadcasting technologies. VLC offers simultaneous illumination and data communications by intensity modulating the optical power emitted by LEDs operating in the visible range of the electromagnetic spectrum (~370–780 nm). The major challenge in VLC systems to date has been in improving transmission speeds, considering the low bandwidths available with commercial LED devices. Thus, to improve the spectral usage, the research community has increasingly turned to advanced modulation formats such as orthogonal frequency-division multiplexing. In this article we introduce a new modulation scheme into the VLC domain; multi-band carrier-less amplitude and phase modulation (m-CAP) and describe in detail its performance within the context of bandlimited systems.

INTRODUCTION

Advanced modulation formats are becoming increasingly important in visible light communications (VLC) systems [1, 2] utilizing light-emitting diode (LED)-based lighting infrastructure. One of the primary aims of VLC is to provide high-capacity broadcasting networks to next generation smart homes and offices, while simultaneously providing full room illumination. Therefore, one of the key challenges associated with VLC concerns the bandwidth limitation associated with commercial white LEDs, which behave as first order low-pass filters [3, 4]. White light is produced using blue LEDs coated in yellow color converting phosphor. Even though blue LEDs offer bandwidths on the order of tens of megahertz, the color converting phosphor substantially reduces this to just a few megahertz, thus creating a large impediment to achieving high-speed networks. A straightforward method to combat the bandwidth limitation of LEDs is to employ appropriate power pre-emphasis techniques [2]. However, using power equalization will introduce additional signal distortion due to the nonlinear effects of the LEDs [5], thus limiting the achievable performance gain. As a result, achieving high capacities has been a major challenge for researchers working in this field.

In recent years, orthogonal frequency-division multiplexing (OFDM) has been the focus of enormous attention due to its ability to support spectrally efficient and high order modulation formats such as quadrature amplitude modulation (QAM) and efficiently overcome the distortion imposed by bandwidth limitation or non-flat fading. This enables an improvement in power and spectral usage over more traditional formats such as on-off keying (OOK), thus resulting in increased transmission speeds. For instance, transmission speeds in the region of 1 Gb/s/wavelength have been reported in [1] by optimizing the OFDM modulation format using adaptive bit and power loading, while speeds on the order of hundreds of megabits per second have been achieved using OOK [4]. Adaptive loading techniques operate by adjusting the number of bits per symbol and power per subcarrier according to the measured error vector magnitude (EVM) at the receiver.

Regardless of the increased popularity of OFDM, researchers are searching for alternative modulation formats. New multi-carrier techniques have been considered recently to save system bandwidth in optical communications by compressing the subcarrier spacing. Fast OFDM [6], spectrally efficient frequency-division multiplexing [7], and faster than Nyquist [8] have all been studied and demonstrated for use in optical

1536-1284/15/$25.00 © 2015 IEEE

communications, resulting in up to 50 percent bandwidth savings. However, complexity remains an issue that has to be resolved before these systems can be adapted to VLC. The other important issue that needs to be addressed is power efficiency, since OFDM VLC systems exhibit an inherent high peak-to-average power ratio (PAPR) and suffer from nonlinear distortions due to the limited dynamic range of optical sources. Several authors proposed more power-efficient schemes like low PAPR single-carrier frequency-domain equalization (SC-FDE) [9]. Here, the inverse fast Fourier transform (IFFT) block was moved from the transmitter to the receiver side, avoiding the generation of complicated waveforms and consequently reducing PAPR. Further improvement of spectral efficiency has been reached by novel OFDM SC-FDE signal formats — polar OFDM and polar SC-FDE in [10].

Currently, one of the most novel and popular modulation formats is carrier-less amplitude and phase (CAP) modulation, which has been experimentally shown to offer improved transmission speeds in comparison to OFDM when utilizing the same physical link, but with potentially high implementation cost using existing digital signal processing (DSP) hardware [1]. This is significant, as CAP modulation is relatively simple to implement in real time. In CAP the carrier frequencies are generated using finite impulse response (FIR) filters, where most of the complexity is introduced depending on the filter length, while the most computationally complex component is the digital-to-analog converter module. On the other hand, OFDM requires the use of inverse and forward fast Fourier FFT, which can also be computationally costly depending on the required number of subcarriers.

Unfortunately, to the authors' knowledge, CAP has only been tested in the case of flat-band magnitude responses, which is a phenomenon that is seldom available in VLC due to the low modulation bandwidths available from LEDs [11, Fig. 4b]. Despite CAPs advantages, its candidacy as a promising format for generic VLC systems is questionable. OFDM can be tailored to any frequency response using bit loading algorithms, unlike CAP, which must have a fixed modulation order cardinality. In [12] a solution to this problem was proposed for optical fiber links. The gross transmission bandwidth was divided into six subbands (or subcarriers, for consistency with OFDM nomenclature), relaxing the condition for a flat-band response and allowing the number of bits per symbol to be adjusted for each subcarrier.

Based on this, it follows that additional performance can be gained by increasing the number of subcarriers towards m, thus the concept of m-CAP, as the decreasing subcarrier bandwidth approximate toward flat bands. This is a substantial advantage for VLC systems, which rarely exhibit flat-band responses, as found in the literature (i.e., [11, Fig. 4b], which shows high attenuation outside of the modulation bandwidth. Having an approximately flat-band response means the frequency-dependent attenuation is minimized, and hence an increasing order of m should offer continuous improvements in terms of power penalty and bit error rate (BER) performance. On the other hand, by increasing to m subcarriers, the FIR filter requirement scales up to $2m$, and consequently the relative computational complexity is increased accordingly. Simultaneously, [12] showed that with increasing m, the required sampling frequency approaches the Nyquist rate, which is a significant and unexpected advantage.

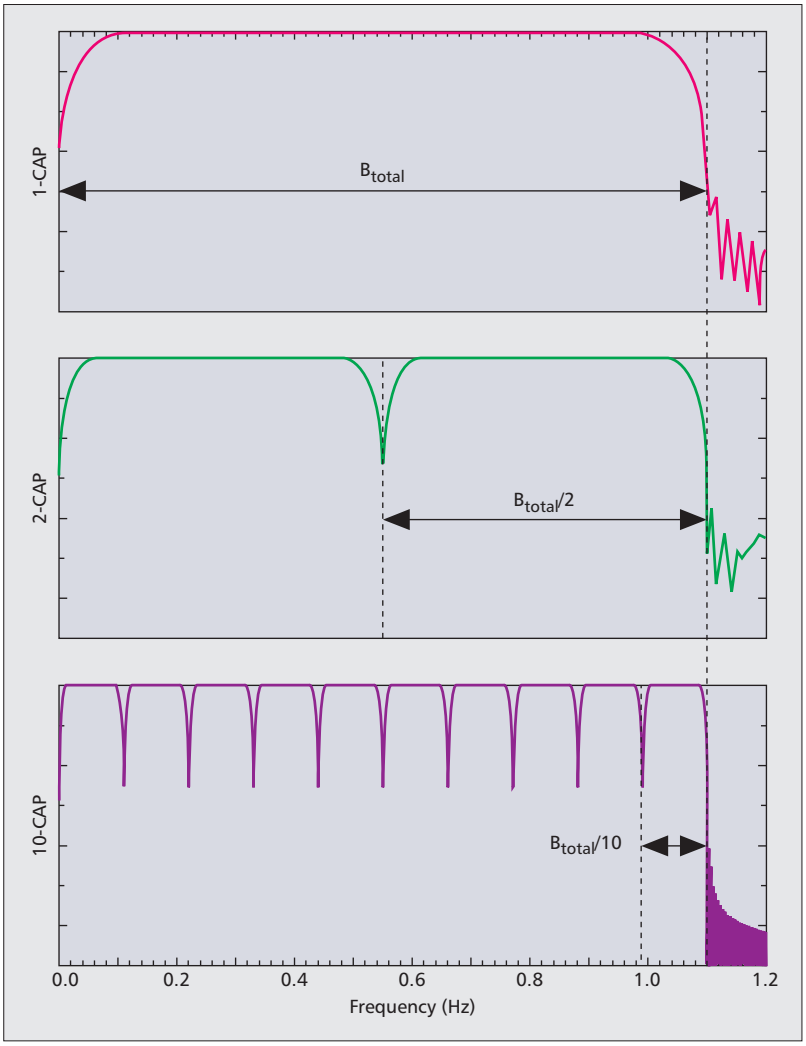

Figure 1. The concept of m-CAP illustrated in terms of the frequency response for several values of m. It should be noted that B_{total} indicates the system bandwidth to be discussed.

In Fig. 1 the concept of m-CAP is illustrated for m = 1, 2, and 10. By increasing m, the subcarrier bandwidth is reduced, thus offering additional protection to attenuation caused by the low-pass LEDs in comparison to the high bandwidth subcarriers (i.e., low m). Therefore, there is a trade-off between complexity and performance as in OFDM systems. The objective of this article is not to analyze the relative computational complexities between OFDM and m-CAP; hence, this discussion is left open for research. In this article, we propose m-CAP as a standalone modulation format for VLC and consider its performance for a bandlimited LED system. The proposed system is studied using realistic system and device models, and verified through numerical simulations.

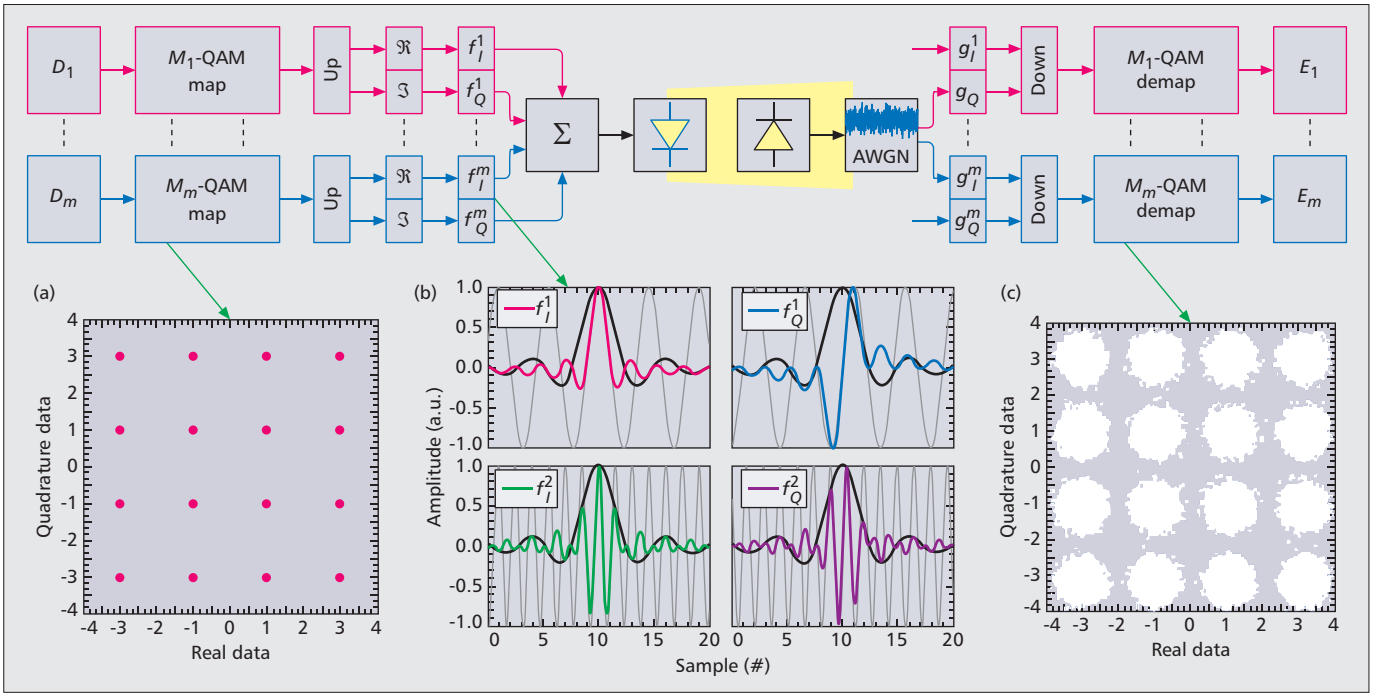

Figure 2. The schematic block diagram of the proposed system. It should be noted that in b) the impulse responses displayed are for $m = 1$ and 2 at the minimum carrier frequencies and variations on these pulse shapes are likely, depending on the desired carrier frequency.

M-CAP Modulation for VLC

A block diagram for an *m*-CAP VLC system is illustrated in Fig. 2.

M-CAP Generation

In this section a description on *m*-CAP generation is provided. First, *m* independent data streams, D_m, are generated and mapped into the QAM constellation (Fig. 2a). Here 16-QAM will be considered to illustrate the concept. The choice of constellation cardinality is insignificant as without any loss of generality, the ensuing discussion is valid across every order of QAM. The data is up-sampled by means of zero padding by a number of samples per symbol, N_{ss}, in order to match the system sampling frequency before the real $\Re$ and imaginary $\Im$ components of the modulated data are isolated. The components are passed through real and imaginary transmit filters with impulse responses that form a Hilbert pair [12]. The impulses are found as the product of a cosine or sine (real or imaginary, respectively) with a root-raised cosine filter (RRCF) as shown in Fig. 2b, while the analysis can be found in [13]. The minimum carrier frequency must be at least twice the RRCF pulse width. Clearly, the carrier frequency of the subcarrier is controlled by the frequency of the (co)sine wave and hence is introduced by the FIR filters, unlike QAM, which requires a local oscillator. This is the main difference between the two formats and is a significant advantage of CAP, since incoherent time-reversed matched filters can be deployed at the receiver, eliminating the use of a complex phase locking circuit. The real and imaginary components are added prior to transmission via intensity modulation of the LED.

The required sampling frequency and number of samples per symbol can be referred to mathematically in the literature and hence are not shown here [12]. Considering the use of an RRCF, the minimum subcarrier bandwidth is controlled by the rolloff factor, β, as expected, which varies between $0 \le \beta \le 1$. A larger β means a $1 + \beta$ greater bandwidth requirement as illustrated in Fig. 3 for a normalized signal bandwidth. In this work we have set $\beta = 0.1$ due to consistency with recent literature [12] and the fact that a lower β means a higher spectral efficiency can be achieved due to more effective spectral usage.

Further parameters adopted in this article are as follows. The overall system baud rate is set to unity, meaning that each subcarrier has a baud rate of $1/m$. This condition ensures that the bandwidth remains constant regardless of *m*, which is important when considering a bandlimited link, described in the following sentences. In order to examine the performance of *m*-CAP in terms of a bandlimited VLC system, two approaches can be adopted:

- Maintaining a constant –3 dB modulation bandwidth and increasing the overall baud rate
- Maintaining a constant overall unity baud rate and varying the LED low-pass cut-off frequency

In this article we adopt the latter approach for simplicity; thus, the overall baud rate is selected as unity throughout. Therefore, recalling the selection of $\beta = 0.1$, the total bandwidth requirement is calculated as 1.1 Hz, as shown in Fig. 4.

In general, LEDs exhibit a nonlinear electro-optic response (i.e., current to optical power) [5]; however, this varies from device to device and from one model to the next [5]. For instance,

polymer LEDs can display excellent linearity [11], while conventional devices can heavily distort the transmit signal [5], so a generalized solution is impossible to consider at this stage. As a result we select a perfectly linear electro-optic response in this article as it is not our intention to discuss this type of signal distortion concurrently with bandwidth distortion at this point. If the nonlinear properties were taken into account, the *m*-CAP system would still work, but may require customization to the specific LED chosen. The signal propagates over the line-of-sight indoor channel (reported mathematically in [11]), excluding multi-path components, and is detected by an ideal positive-intrinsic-negative (p-i-n) photodiode.

Modulation Bandwidths

As reported in [4], the major impediment to achieving high transmission speeds in VLC is the slow temporal response of the yellow phosphor, limiting bandwidths to a few megahertz. This means that achieving high transmission speeds is a considerable challenge facing the VLC research community. It is well known that the frequency response of LEDs can be modeled, as a good first approximation, by a first order low-pass filter [4], as the parasitic components will vary from device to device. For example, polymer LEDs have substantially more parasitics (i.e., capacitance) than conventional inorganic devices. The LED bandwidths f_c under test are selected as a fraction of the overall 1.1 Hz signal bandwidth as follows: $f_c = \{0.1, 0.25, 0.5, 0.75, 0.9\}$. As an example, this means that when $f_c = 0.5$, the cutoff frequency of the LED is given by the ratio of the signal bandwidth to the LED bandwidth (i.e., 1.1/0.5 = 0.55 Hz), as illustrated in Fig. 4 for 5-CAP, 10-CAP, and 20-CAP.

It is clear from Fig. 4 that as the order of m increases (i.e., a higher number of subcarriers); each subcarrier suffers reduced distortion due to the attenuation as a result of the low-pass filter in spite of the fact that the envelopes of all signals possess the same shape. The reason for this is that each subcarrier has a lower bandwidth requirement for higher orders of m-CAP and hence is less prone to attenuation induced distortion. It should be noted that there will be no improvement in the noise performance since the total signal power for every value of m is equal. Thus, it would be expected that additional transmission speed performance will be obtained when using higher values of m in band-limited systems, at the cost of additional hardware complexity because of the increased requirement for FIR filters.

Receiver

At the receiver, the sampling frequency should be equal to that at the transmitter, and hence needs to be set as described in [12], which shows that with an increasing value of m, the sampling frequency approaches the Nyquist limit. The implication of this is that when using m-CAP, available transmission speeds will at least equal those available in conventional 1-CAP while using a lower sampling frequency that approaches the Nyquist limit. Thus, the conditions for high-speed digital-to-analog converters are relaxed, leading to reduced cost and complexity.

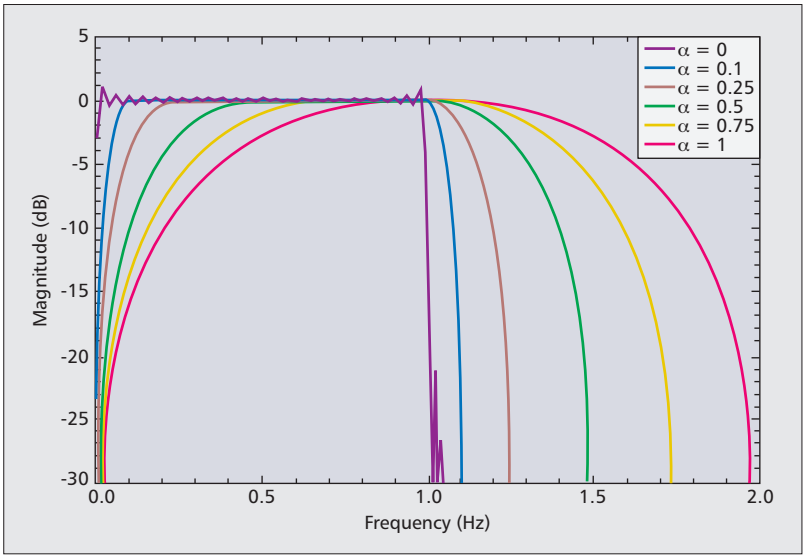

Figure 3. 1-CAP pulse shapes considering a range of β.

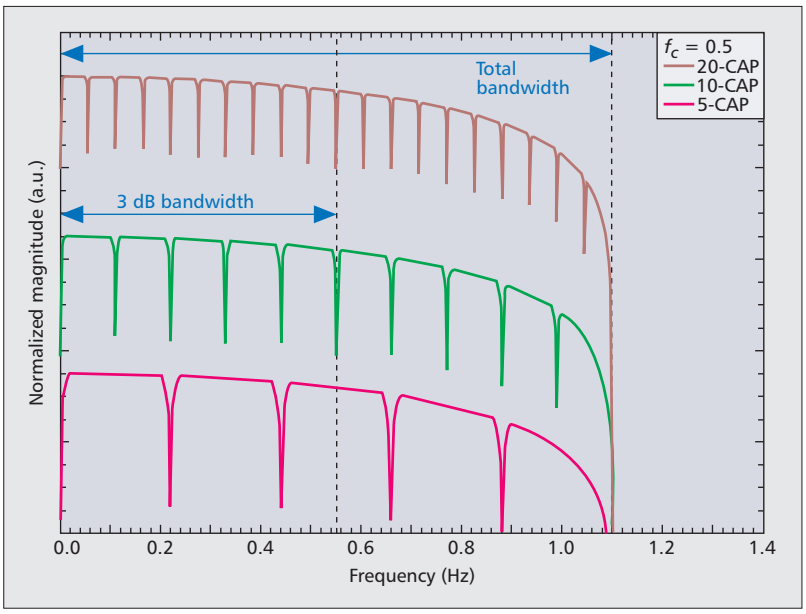

Figure 4. Example frequency responses considering $f_c = 0.5$; note that the distortion on each subcarrier for high values of m is less than that for lower values of m.

The dominant noise source present in the system is introduced by the receiver electronics and is modeled as additive white Gaussian noise (AWGN). Once more referring to Fig. 2, the received signal is split into $2m$ branches (real and imaginary for each m) and passed through reverse-time real and imaginary receiver filters matched to the transmit filters before down-sampling and constellation de-mapping (Fig. 2c) in order to provide an estimate of the symbols E_m for comparison with D_m in a symbol-by-symbol BER measurement.

FIR Filters

Several advantages can be gained by dividing the desired transmission bandwidth into m subcarriers. The most important of these is that the attenuation observed over the signal frequencies

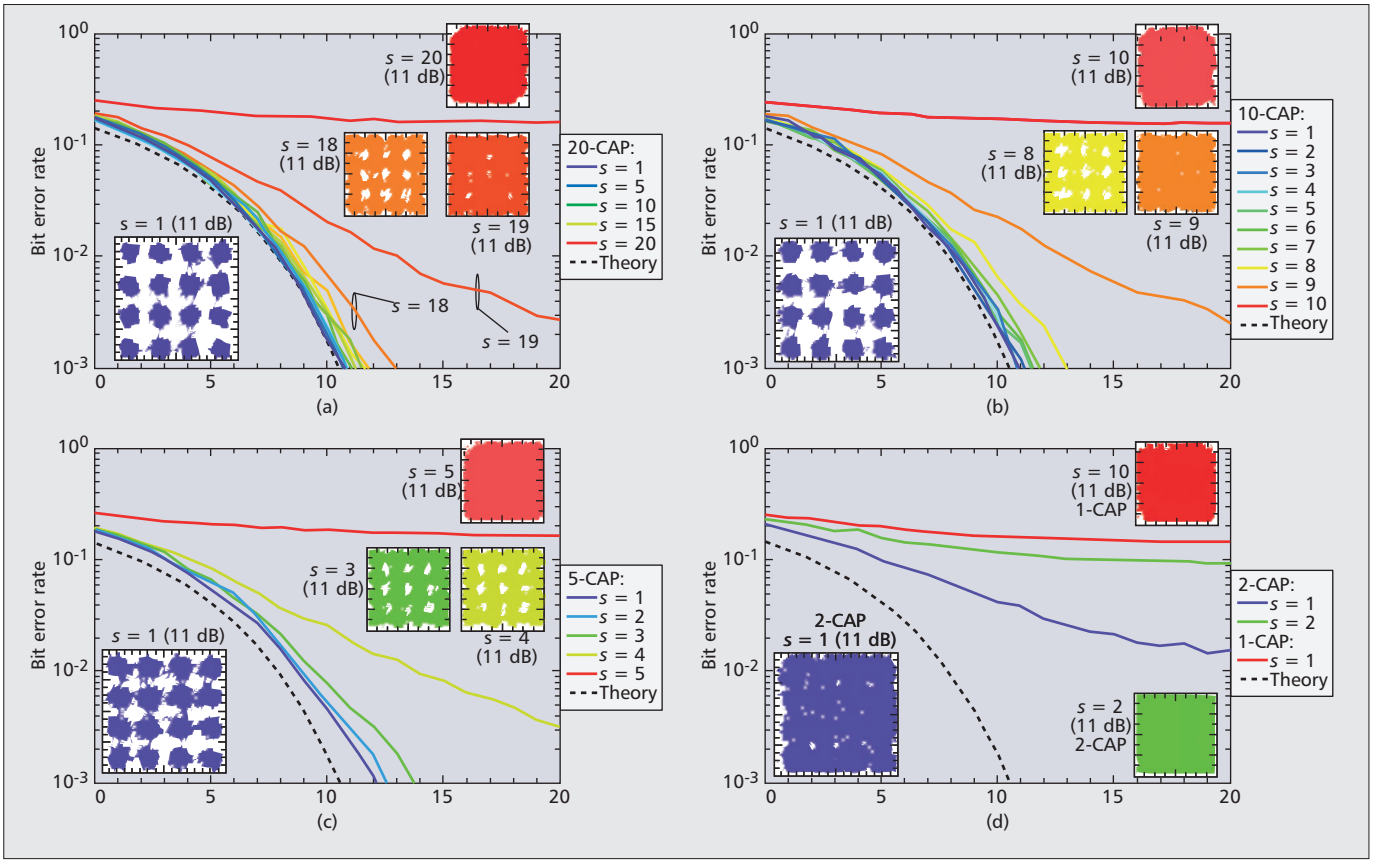

Figure 5. BER performance as a function of SNR for m = a) 20; b) 10; c) 5; d) {2, 1}. Clearly, the BER performance improves with increasing m as reflected in the constellation diagrams, all of which consider a signal-to-noise ratio (SNR) of 11 dB.

due to the low-pass filter is severely reduced due to the smaller subcarrier bandwidth requirements, as mentioned in the previous section. Therefore, here we examine the error performance across five different values of m (i.e., m = {1, 2, 5, 10, 20}), chosen to allow a large window of observation into any improvement. It should be noted that m = 20 corresponds to 40 FIR filters in the transmitter alone and a further 40 in the receiver, among other resources. Therefore, the length of the filters is crucial; hence, studies have been performed that investigated the effect on varying lengths [14] and demonstrated improved BER performance with longer filter lengths. Depending on system requirements such as the target bit rate, BER, or application, among others, 40 FIR filters could be considered excessive, depending on the available resources. Therefore, it is essential to keep in mind the trade-off between performance improvement and implementation complexity in m-CAP systems.

M-CAP Bit Error Rate Performance

Simple Bandlimited M-CAP

The BER performance of the proposed bandlimited m-CAP systems are shown for f_c = 0.5 in Figs. 5a–d, which show the performance of each subcarrier (denoted as s in Fig. 5) starting with 20-CAP in Fig. 5a, 10-CAP in Fig. 5b, 5-CAP in Fig. 5c, and finally 2-CAP and 1-CAP, both in Fig. 5d. The BER is presented as a function of the energy-per-bit to noise power spectral density ratio E_b/N_0. The BER target is selected to be 10^{-3}, which is slightly lower than the International Telecommunication Union's (ITU's) recommended error floor (3.8×10^{-3}) when using forward error correction (FEC) with an overhead of 7 percent.

Figure 5a illustrates that the BER performance of the vast majority of subcarriers approaches the theoretical BER limit for 16-QAM systems, with only a few subcarriers (s = {19, 20}) failing to converge to the theoretical limit. This is attributed to the following reasons:

- The limited frequency response of the LED means the first half of the subcarriers, s = 1:10, are not affected by the attenuation introduced by the LED low-pass filter; they are within the modulation bandwidth and hence have a maximum signal attenuation of 3 dB at s = 10.
- The second half of the subcarriers, s = 11:20, incur an additional E_b/N_0 power penalty of several dB (approximately ~1–3 dB) in the best case, and failure in the worst cases, as can be seen for s = 19 and 20.
- In the worst case this is because an ideal low-pass filter is used, and hence a rolloff of 20 dB per decade is expected. Thus, between s = 10 and s = 20, the attenuation should be roughly 20 dB, so hence significantly degraded performance is shown at s = 20. This is also reflected in the constellation diagrams inset at E_b/N_0 dB for cases s = 1, 18, 19, and 20, showing continual degradation.

Figure 5b illustrates the BER performance of

a 10-CAP link under the same operating conditions of f_c = 0.5. A very similar profile to 20-CAP can be observed; however, some very discrete differences between the two cases can be found. The most important is a slight power penalty for the best performing subcarriers s = 1, 2, …, 8 of 0.5 to 2.5 dB in comparison to the theoretical performance of 16-QAM. Recalling that the 10-CAP subcarrier bandwidth requirement is twice that of 20-CAP, this slight power penalty is because of the attenuation of the low-pass filter, since a larger attenuation acts on the subcarriers due to the additional bandwidth requirements. This is reflected in the constellation diagrams shown inset for s = 1, 8, 9, and 10 for E_b/N_0 = 11 dB.

Next, in Fig. 5c, the same effect as the previous cases can be observed for 5-CAP with an exaggerated power penalty in comparison to the 16-QAM theory, which has increased to ~1.5 dB in the best case (s = 1) and 3.5 dB in the worst (s = 3). Larger subcarrier values fail due to the large attenuation observed, as expected, and once more this is reflected in the constellation diagrams inset. Finally, the results are essentially confirmed in Fig. 5d, where both 2-CAP and 1-CAP fail to meet the BER target in the E_b/N_0 range considered. It should be noted that the remaining f_c values do follow the same trend but are not reported here due to space considerations.

Adaptive Bit Loading within Bandlimited *m*-CAP

One advantage of m-CAP that has not been explored so far in this article is the possibility to change adaptively the order of the modulation format to suit a given system based on the measured SNR values at the receiver. This technique is called adaptive bit loading and is well known and widely reported for OFDM-based systems [1]. To provide a brief overview, the same block diagram as proposed in Fig. 2 can be implemented, but the process starts with the lowest modulation constellation/format of binary phase shift keying (BPSK). The principles of transmission are exactly the same as described previously; however, at the receiver a BER measurement is not made in a symbol-by-symbol manner as has been done so far in this work. Instead, the root mean square error vector magnitude (EVM) of the received BPSK constellation is measured, and the SNR is extracted. The measured SNR values are compared to the known SNR values, considering a target BER, for every order of M-QAM, and the maximum possible number of bits per symbol are loaded into each subcarrier in order to improve the spectral efficiency of the system and avoid errors in subcarriers where the SNR is insufficient. As always; this comes as a trade-off with hardware complexity as the adaptive algorithms will require resources within both the transmitter and receiver.

We implemented such an adaptive m-CAP system based on the adaptive bit loading technique for E_b/N_0 = 10, 20, and 30 dB for every value of f_c, and the results are illustrated in Fig. 6. For the system exhibiting higher E_b/N_0 of 30 dB, we found that spectral efficiencies (b/s/Hz) can approach slightly short of 10 b/s/Hz in the case of f_c =0.9, as the vast majority of subcarriers can be loaded with higher order values of M-QAM, thus allowing a high throughput link to be supported. As expected, the spectral efficiencies decrease for decreasing values of f_c. The decrease is approximately linear across the range of m. It is clearly indicated in the 30 dB case that high spectral efficiencies between ~8–10 b/s/Hz can be achieved when using $m \to 20$. However, the improvement shown for lower values of m could be considered marginal when reflecting on the additional hardware complexity that arises from high values of m. For example, m = 10 can achieve spectral efficiencies within the range of ~9–6 b/s/Hz for f_c = 0.9–0.1, respectively, and it appears that an asymptotic level can be found in each case where limited improvement is available, even as m tends to a very large number. This is supported by the 20 dB case, which shows a similar trend. The spectral efficiency is much more consistent with less variation over a wider range of m, implying that the asymptote is reached earlier. For the 10 dB case due to noise restrictions no improvement in spectral efficiency can be found for any value of m.

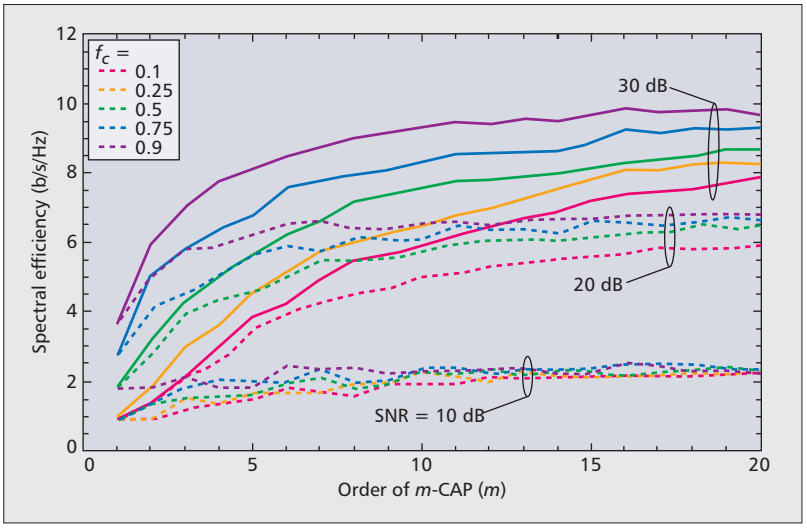

Figure 6. Spectral efficiencies of m-CAP systems considering five degrees of band limitation; spectral efficiencies up to ~ 10 b/s/Hz can be achieved with sufficient SNR at a BER of 10^{-3} in this case.

Finally, in comparison to the literature, the predicted spectral efficiency of ~10 b/s/Hz is significantly higher than that already achieved experimentally, with the maximum state-of-the-art efficiency reported at 6.25 b/s/Hz in [15], to the best of our knowledge. Thus, m-CAP theoretically offers significant improvements in the transmission speeds available.

Future Outlook and Conclusions

Here we have shown the considerable potential for m-CAP systems in a bandlimited VLC environment, where higher spectral efficiencies can be achieved. However, the only way to achieve this performance is to use the adaptive bit loading techniques outlined here.

Here we have provided the first deep insight into this advanced modulation format and illus-

There is currently no evidence in the literature that reports an experimental *m*-CAP VLC link. It would be of the upmost importance in the next step to examine the performance of 1-CAP and *m*-CAP in terms of BER performance for a series of experimental measurements.

trated the potential improvement attainable with this scheme. If *m*-CAP were to be adopted in VLC systems, further investigation is required. The next stage in the theoretical work is to examine the impact on the link considering the LED nonlinearity. In parallel to the enormous potential outlined here by simulations, we are finalizing an experimental testbed to support our simulations. There is currently no evidence in the literature that reports an experimental *m*-CAP VLC link. It would be of the upmost importance in the next step to examine the performance of 1-CAP and *m*-CAP in terms of BER performance for a series of experimental measurements.

References

[1] F. M. Wu *et al.*, "Performance Comparison of OFDM Signal and CAP Signal over High Capacity RGB-LED-Based WDM Visible Light Communication," *IEEE Photonics J.*, vol. 5, 2013, pp. 7901507–7901507.

[2] S. T. Le *et al.*, "10-Mb/s Visible Light Transmission System using a Polymer Light-Emitting Diode with Orthogonal Frequency Division Multiplexing," *Opt. Lett.*, vol. 39, 2014, pp. 3876–79.

[3] P. A. Haigh *et al.*, "Visible Light Communications: 170 Mb/s Using an Artificial Neural Network Equalizer in a Low Bandwidth White Light Configuration," *J. Lightwave Tech.*, vol. 32, 2014, pp. 1807–13.

[4] H. Le Minh *et al.*, "100-Mb/s NRZ Visible Light Communications Using a Postequalized White LED," *IEEE Photonics Tech. Lett.*, vol. 21, 2009, pp. 1063–65.

[5] H. Elgala, R. Mesleh, and H. Haas, "An LED Model for Intensity-Modulated Optical Communication Systems," *IEEE Photonics Tech. Lett.*, vol. 22, 2010, pp. 835–37.

[6] J. Zhao and A. D. Ellis, "A Novel Optical Fast OFDM with Reduced Channel Spacing Equal to Half of the Symbol Rate per Carrier," *2010 OFC/NFOEC*, 2010, pp. 1–3.

[7] I. Darwazeh *et al.*, "Optical Spectrally Efficient FDM System for Electrical and Optical Bandwidth Saving," *IEEE ICC*, 2014, pp. 3432–37.

[8] M. I. Anis *et al.*, "Field Trial Demonstration of Spectrum Defragmentation and Grooming in Elastic Optical Node," *J. Lightwave Tech.*, vol. 31, 2013, pp. 1845–55.

[9] V. S. C. Teichmann *et al.*, "SC-FDE for MMF Short Reach Optical Interconnects using Directly Modulated 850 nm VCSELs," *Opt. Express*, vol. 20, 2012, pp. 25,369–77.

[10] H. Elgala and T. D. C. Little, "Polar-Based OFDM and SC-FDE Links Toward Energy-Efficient Gbps Transmission under IM-DD Optical System Constraints [Invited]," *IEEE J. Opt. Commun. Net.*, vol. 7, 2015, pp. A277–A284.

[11] P. A. Haigh *et al.*, "Visible Light Communications: Real Time 10 Mb/s Link with a Low Bandwidth Polymer Light-Emitting Diode," *Opt. Express*, vol. 22, 2014, pp. 2830–38.

[12] M. I. Olmedo *et al.*, "Multiband Carrierless Amplitude Phase Modulation for High Capacity Optical Data Links," *J. Lightwave Tech.*, vol. 32, 2014, pp. 798–804.

[13] J. Zhang *et al.*, "11× 5× 9.3 Gb/s WDM-CAP-PON Based on Optical Single-side Band Multi-level Multi-band Carrierless Amplitude and Phase Modulation with Direct Detection," *Opt. Express*, vol. 21, 2013, pp. 18,842–48.

[14] R. Rodes *et al.*, "Carrierless Amplitude Phase Modulation of VCSEL with 4 bit/s/Hz Spectral Efficiency for Use in WDM-PON," *Opt. Express*, vol. 19, 2011, pp. 26,551–56.

[15] D. Tsonev *et al.*, "A 3-Gb/s Single-LED OFDM-Based Wireless VLC Link Using a Gallium Nitride μLED," *IEEE Photonics Tech. Lett.*, vol. 26, 2014, pp. 637–40.

Biographies

PAUL ANTHONY HAIGH (paul.anthony.haigh@bristol.ac.uk) received his Ph.D. degree in the area of organic visible light communications from Northumbria University, United Kingdom, in 2014, publishing over 20 scholarly articles including 13 articles in high ranking journals such as *IEEE Journal on Selected Areas in Communications*, *Optics Express*, *IEEE Communications Magazine*, and *IEEE/OSA Journal of Lightwave Technology*. In 2010–2011 he held the prestigious Marie Curie Fellowship at the European Organization for Nuclear Research (CERN), where he worked on the optoelectronic links in large hadron collider experiments. In 2010 he received his B.Eng. (Hons) degree in communications engineering from Northumbria University. Currently, he is a research associate within the High Performance Networks group at the University of Bristol working on the EPSRC TOUCAN project. His research is focused on real-time seamless, transparent, and adaptive and programmable interfaces between wireless and wired multi-technology networks.

SON THAI LE received his M.E. degree with highest distinction from Southern Federal University of Russia in 2012. He joined Aston Institute of Photonic Technologies as a Ph.D. student in January 2013. His research mainly focuses on coherent optical orthogonal frequency-division multiplexing (CO-OFDM), fiber nonlinearity mitigation techniques, and visible light communication.

STANISLAV ZVANOVEC received his M.Sc. in 2002 and his Ph.D. in 2006, both from the Czech Technical University (CTU) in Prague. Now he is a full professor and vice-head of the Department of Electromagnetic Field, Faculty of Electrical Engineering, CTU. He leads the free-space and fiber optics team at CTU and is vice-chair of WG1 of EU COST project IC1101 OPTICWISE — Optical Wireless Communications — An Emerging Technology. His current research interests include wireless optical communications, visible light communications, remote sensing, and optical fiber sensors.

ZABIH GHASSEMLOOY received his B.Sc. (Hons) degree (1981) in electrical and electronics engineering from Manchester Metropolitan University, and his M.Sc. (1984) and Ph.D. (1997) in optical communications from the University of Manchester Institute of Science and Technology (UMIST). From 1987 to 1988 he was a post-doctoral research fellow at City University, London. In 1988–2004 he joined Sheffield Hallam University. From 2004 to 2014 he was Associate Dean for Research, Faculty of Engineering and Environment, Northumbria University. Currently he heads the Optical Communications Research Group. His research interests are in optical wireless and wired communications, visible light communications, and mobile communications. He is currently involved as co-Principal Investigator with three EU projects: cLINK (GN. 372242-1-2012-1-UKERA; 2002-16, 2.5m), FUSION (GN: 2013-545774, 3M), and COST ActionIC1101 (over 600k, on OWCs, 2012-2015). He is a co-author of a book, *Optical Wireless Communications Systems and Channel Modelling with MATLAB* (CRC, 2012). From 2004 to 2006 he was the IEEE UK/IR Communications Chapter Secretary, and Vice-Chairman (2004-2008), Chairman (2008–2011, Oct. 2011–present) of the IET Northumbria Network.

PENGFEI LUO received his B.Eng. degree in communication engineering from Beihua University, China, in 2007, and his joint M.Sc./Ph.D. in optical communications engineering from Beijing University of Posts and Telecommunications, China, in 2013. He is a research fellow at the Department of Physics and Electrical Engineering, Northumbria University. His research interests include optical wireless communications and vehicle communications.

TONGYANG XU received his M.Sc. degree (with distinction) in telecommunications from University College London (UCL), United Kingdom, in 2012. He is currently working toward his Ph.D. degree at UCL. His research interests include 5G communications technology, spectral efficiency, and FPGA design. His current research project is to implement a 5G spectrally efficient technique on a real-time experimental platform.

PETR CHVOJKA received his M.Sc. degree in 2013 at CTU. Now he is a postgraduate student and Ph.D. researcher at the Department of Electromagnetic Fields, CTU, where he is a member of the free-space and fiber optics team. His research area includes visible light communications, OLED technologies and wireless optical communications.

THAVAMARAN KANESAN received his B.Eng. (Hons) in electrical and electronic engineering from Northumbria University in 2009. He was then awarded the Northumbria Ph.D. Studentship in 2010 to work on radio-over-fiber (RoF) system design for 4G Long Term Evolution (LTE) technology and completed his degree in under three years (2013) with numerous IEEE publications. He then worked at the Aston Institute of Photonic Technologies (AIPT), Birmingham, United Kingdom, as a postdoctoral research associate, a position funded by the European Union (EU) FP7 FOX-C project, focusing on all-optical OFDM (AO-OFDM) and add-drop multiplexers. In January 2014, he joined Telekom Research & Development as a senior researcher,

where he currently leads a project on multiservice wireless access networks based on a radio-over-fiber platform. In his four years of research, he has published over 20 papers, mostly in IEEE and OSA journals and conference proceedings, and has filed two patents. His research interests are in radio-over-fiber systems, LTE, and 5G mobile communications.

ELIAS GIACOUMIDIS is currently with the Aston University Institute of Photonics Technologies group (previously with Telecom Paris-Tech and Athens Information Technology). His research focuses on key modern DSP algorithmic techniques, such as OFDM/Fast-OFDM, Nyquist-WDM, and fiber nonlinearity DSP compensation techniques, such as Volterra-based nonlinear equalizers (NLEs), digital back-propagation, artificial-neural-networks-based , and adaptive loading algorithms, for next-generation data centers, radio-over-fiber systems, and core/passive optical networks. His research work has resulted in > 60 papers (380 citations) that have appeared in high-quality peer reviewed journals and top international conference proceedings.

PEP CANYELLES-PERICAS received his electrical engineering degree from the Barcelona College of Industrial Engineering EUETIB — Technical University of Catalonia UPC — BarcelonaTech, Spain, in 2006. He also obtained a B.Eng. degree in electrical and electronic engineering (Hons) in 2006 from Northumbria University through a student exchange program. He continued his work, obtaining an M.Sc. in engineering management (Distinction) from the University of Sunderland in 2008. After finishing this he worked as a project engineer for an SME in Newcastle, United Kingdom, for one year. In 2009 he joined the Institute of Cross Disciplinary Physics and Complex Systems IFISC at the University of the Balearic Islands, Spain, as a research engineer, specializing in electronic prototyping and PCB design, where he stayed until September 2012. Then he joined Northumbria University as a Ph.D. student, working in the field of nonlinear control and chaos synchronization applications. His research interests are observer design and chaos communications.

HOA LE MINH [M] received his B.Eng. degree in telecommunications from Ho Chi Minh University of Technology, Vietnam, in 1999, his M.Sc. in communications engineering from Munich University of Technology, Germany, in 2003, and his Ph.D. from Northumbria University in 2007. Previously he worked at R&D Siemens AG, Munich, Germany (2002–2004) as a research assistant in DWDM networks. He was a research fellow with the Department of Engineering Science, University of Oxford, United Kingdom, during 2007–2010 before becoming a senior lecturer at Northumbria University. His research is in visible light communications, photonics networks, and smartphone technology. He is currently Secretary of the IEEE UK and Ireland Communications Chapter.

WASIU POPOOLA received his first class (Hons) degree in electronic and electrical engineering from Obafemi Awolowo University, Ife, Nigeria, his M.Sc. degree with distinction in optoelectronic and communication systems from Northumbria University, where he also received his Ph.D. degree in free-space optical communications. He was awarded the Xcel Best Engineering and Technology Student of the Year 2009. He is currently with the Li-Fi R&D Centre University of Edinburgh, United Kingdom. Previously, between March 2010 and July 2012, he worked at the University of Edinburgh as a research fellow on visible light communications. He has published more than 40 conference and journal papers and two book chapters, one of which has over 8000 downloads since its publication in 2010. He is also a co-author of the book *Optical Wireless Communications: System and Channel Modelling with MATLAB* (Taylor & Francis, 2012). His research interests include optical (wireless and fiber) communications, digital communications, and signal processing. He is a member of the Institute of Physics.

SUJAN RAJBHANDARI [M] obtained his Bachelor's degree in electronics and communication engineering from the Institute of Engineering, Pulchowk Campus, Tribhuvan University, Nepal, in 2004. He obtained an M.Sc. in optoelectronic and communication systems with Distinction in 2006 and was awarded the P O Byrne Prize for most innovative project. He then joined the Optical Communications Research Lab at Northumbria University and was awarded a Ph.D. degree in 2010. His Ph.D. thesis was on mitigating channel effect on indoor optical wireless communications using wavelet transform and neural networks. He worked at Northumbria University as senior research assistant (December 2009–August 2012) and research fellow (September 2012–December 2012). He joined the University of Oxford as a postdoctoral research fellow in December 2012 and is working on the EPSRC Ultra Parallel VLC project. He has published more than 80 scholarly articles in the area of optical wireless communications. He is a co-author of a book, *Optical Wireless Communications Systems and Channel Modelling with MATLAB* (CRC, 2012). He has served as a reviewer for several leading publications including the *IEEE/OSA Journal of Lightwave Technology*, *IEEE Selected Areas of Communications*, *Photonics Technology Letters*, and *Optics Express*. His research interests lie in optical wireless communications, modulation techniques, equalization, artificial intelligence, and wavelet transforms. He is an associate member of the Institute of Physics.

IOANNIS PAPAKONSTANTINOU is currently a lecturer in the Electronic and Electrical Engineering Department at UCL, where he leads a team of six Ph.D. students as principal and second supervisor. His research interests lie in the areas of nano-photonics for renewable energy, medical equipment, and ICT applications. He has almost 10 years of experience in optical components made of polymers. He was awarded his Ph.D. in polymer optical interconnects from UCL in 2008. He then joined Sharp Laboratories of Europe as research associate in 2008. While at Sharp, he received training in nano-imprint lithography, the subject of his proposed work in this proposal, and specialized in sub-wavelength structures to improve the energy efficiency, uniformity, and brightness of liquid crystal displays. Together with his colleagues at Sharp, he filed and was awarded five patents on the design and fabrication of antireflection coatings, non-absorbing polarizers, color separating gratings, and light in-coupling and out-coupling structures for backlights, all made by NIL. Prior to joining UCL, he worked for the Physics Department at CERN-European Organization for Nuclear Research in 2009–2011 where he developed optical network topologies for the distribution of time, trigger, and control signals in the Large Hadron Collider.

IZZAT DARWAZEH received his M.Sc. and Ph.D. degrees in electronic engineering from UMIST) in 1986 and 1991, respectively. He holds the University of London Chair of Communications Engineering and leads the 60-strong Communications and Information Systems Group in the Department of Electronic and Electrical Engineering of UCL. His research interests are in the areas of wireless and mobile communication circuits and systems, high-speed optical communication, microwave circuits, and III-V MMICs for high-bit-rate and high-frequency applications. He has authored/co-authored more than 200 papers in the areas of optical and cellular communications and MMICs and high-speed/frequency circuits. He is a co-editor of the 1995 book *Analogue Optical Fibre Communications* (IEE, 1995) and a co-author of *Linear Circuit Analysis and Modelling* (Elsevier, 2005). He is a Chartered Engineer and a Fellow of the IET.

4.2 A Multi-CAP Visible Light Communication System with 4.85 b/s/Hz Spectral Efficiency

This chapter is a version of the published manuscript:

P. A. Haigh, A. Burton, K. Werfli, H. Le Minh, E. Bentley, **P. Chvojka**, W. O. Popoola, I. Papakonstantinou and S. Zvanovec, "A Multi-CAP Visible-Light Communications System With 4.85-b/s/Hz Spectral Efficiency," in *IEEE Journal on Selected Areas in Communications*, vol. 33, no. 9, pp. 1771-1779, 2015.

Connection with my Ph.D. thesis:

In the next paper, we evaluate the m-CAP scheme performance using an experimental setup. We investigate the trade-off between measured data rate/spectral efficiency and the number of subcarriers. We achieve a data rate of 31.53 Mb/s (i.e., spectral efficiency of 4.85 b/s/Hz) over a transmission span of 1 m using the 10-CAP system. At the time of publication, we reported the highest spectral efficiency in any VLC system over a distance of 1 m. Based on the achieved results, we verify our conclusions from the previous work in Section 4.1 and task **T2** is met.

A Multi-CAP Visible-Light Communications System With 4.85-b/s/Hz Spectral Efficiency

Paul Anthony Haigh, Andrew Burton, Khald Werfli, Hoa Le Minh, Edward Bentley, Petr Chvojka, Wasiu O. Popoola, Ioannis Papakonstantinou, and Stanislav Zvanovec

***Abstract*—In this paper, we experimentally demonstrate a multiband carrierless amplitude and phase modulation format for the first time in VLC. We split a conventional carrierless amplitude and phase modulated signal into m subcarriers in order to protect from the attenuation experienced at high frequencies in low-pass VLC systems. We investigate the relationship between throughput/spectral efficiency and m, where $m = \{10, 8, 6, 4, 2, 1\}$ subcarriers over a fixed total signal bandwidth of 6.5 MHz. We show that transmission speeds (spectral efficiencies) of 31.53 (4.85), 30.88 (4.75), 25.40 (3.90), 23.65 (3.60), 15.78 (2.40), and 9.04 (1.40) Mb/s (b/s/Hz) can be achieved for the listed values of m, respectively.**

***Index Terms*—Bit error rate, equalizers, light emitting diodes, visible light communications.**

I. Introduction

SEVERE bandwidth limitation introduced by light-emitting diodes (LEDs) is the major bottleneck to high capacity visible light communications (VLC) systems. The vast majority of VLC links employ blue gallium nitride (GaN) LEDs with cerium-doped yttrium aluminum garnet (Ce:YAG) yellowish phosphor wavelength converters to achieve white light [1]–[3]. This is an inexpensive and simple solution to providing a high level of illumination and also data communications simultaneously. On the other hand, the major problem is that optimized GaN LEDs can have bandwidths in the GHz region [4], while the Ce:YAG phosphor is limited to the low MHz region, with values reported in the literature ranging up to 3 MHz [5], [6]. To overcome this bandwidth limitation there have been suggestions to use optical bandpass filters to isolate the fast blue component and reject the slow yellowish component, with remarkable gains up to 26 MHz [5], [6]. Using optical filters is a suboptimal solution because they introduce a severe reduction in the signal power (up to 50% [7]), and hence a hugely reduced signal-to-noise ratio (SNR). Furthermore, in [3] it was reported that with the appropriate digital signal processing and equalization at the receiver, a higher transmission speed could be supported with the whole spectra of white light (170 Mb/s) in comparison to the blue filter (150 Mb/s) due to the reduction in SNR. Thus it is desirable to avoid the use of the blue filter, where possible. Aside from using equalizers at the receiver, the most commonly proposed technique to improve the transmission speed of white phosphor based VLC systems is the use of modulation formats that offer high spectral efficiency, such as orthogonal frequency division multiplexing (OFDM), which has shown remarkable capacity gains in the literature up to $\sim$1.5 Gb/s using a single Ce:YAG phosphor converted GaN LED [8]. In order to achieve such a transmission speed, additional signal processing techniques such as the adaptive bit- and power-loading were introduced [9] to compensate for the attenuation of the high frequencies.

In recent times, OFDM is beginning to decline in popularity in VLC systems with the re-emergence of carrier-less amplitude and phase modulation (CAP), which has been experimentally shown to outperform OFDM in terms of transmission speed when using the same link [10], offering a lower bit error rate (BER) and higher throughput of 1.32 Gb/s using CAP and 1.08 Gb/s using OFDM in the best case. Thus CAP is deserving of further attention for research in VLC systems both for this reason and also because it has several other advantages over OFDM. Considering that CAP is a passband modulation format just as in OFDM, one must consider the generation of the carrier frequencies and the complexity it introduces to the system. The most important advantage of CAP over OFDM is that there is no (inverse) fast Fourier transform, while OFDM requires one at the transmitter and one at the receiver. This means that the computational complexity is significantly reduced and real time implementation is more straightforward. It should be noted that in comparison to the simplest scheme; an unequalized on-off keying (OOK) link, the computational complexity is generally increased. The carrier frequencies in CAP are generated by carefully designing the impulse responses of finite impulse response (FIR) filters, which can either be analogue or digital

Manuscript received May 28, 2014; revised November 3, 2014; accepted April 10, 2015. Date of publication May 25, 2015; date of current version August 17, 2015. The work of P. A. Haigh and A. Burton was supported by Northumbria University.

P. A. Haigh is with the Faculty of Engineering, University of Bristol, Bristol BS8 1TR, U.K. (e-mail: paul.anthony.haigh@ieee.org).

A. Burton, K. Werfli, H. Le Minh, and E. Bentley are with the Faculty of Engineering and Environment, Northumbria University, Newcastle upon Tyne NE1 8ST, U.K. (e-mail: andrew.burton@northumbria.ac.uk; khald.werfli@northumbria.ac.uk; hoa.le-minh@northumbria.ac.uk; edward.bentley@northumbria.ac.uk).

P. Chvojka and S. Zvanovec are with the Department of Electromagnetic Field, Czech Technical University in Prague, 16 627 Prague, Czech Republic (e-mail: chvojpe8@fel.cvut.cz; xzvanove@fel.cvut.cz).

W. O. Popoola is with the Institute for Digital Communications, School of Engineering, University of Edinburgh, Edinburgh EH9 3JL, U.K. (e-mail: w.popoola@ed.ac.uk)

I. Papakonstatniou is with the Department of Electrical and Electronic Engineering, University College London, London WC1E 6BT, U.K. (e-mail: i.papakonstantinou@ucl.ac.uk)

Color versions of one or more of the figures in this paper are available online at http://ieeexplore.ieee.org.

Digital Object Identifier 10.1109/JSAC.2015.2433053

[11]. Digital FIR filters are proposed as the preferred type, being generally cheap, easily reconfigurable, integrated and simple to program.

CAP also provides an advantage over single carrier modulation formats such as quadrature amplitude modulation (QAM) which requires a local oscillator at both the transmitter and receiver. The dominant noise source present in CAP VLC systems is additive white Gaussian noise (AWGN) introduced by the receiver electronics, consistent with other VLC systems [12].

VLC systems are highly bandlimited, as mentioned and can be modelled as a first order low pass filter [1]. Therefore frequencies outside the 3 dB modulation bandwidth will experience an attenuation of 20 dB/decade, and thus to gain any sufficient gain from a wideband modulation format such as CAP (or OFDM/QAM) frequency domain equalizers such as analogue high pass filters [1], [13] have generally been considered, with post-equalizers at the receiver consistently showing the best performance in the literature [1], [14]. Much as with optical filters, high pass filters in the receiver electronics introduce a significant power penalty due to power dissipation in the discrete components, causing the overall SNR to drop at low frequencies inside the modulation bandwidth. This is a substantial disadvantage when considering multi-carrier systems, where a high number of bits-per-symbol can be selected at these frequencies, thus improving the spectral efficiency. However, traditional CAP is not a multi-carrier system and this technique cannot be applied. In [15] a multi-carrier CAP system is proposed for short-haul optical fiber links. The proposed multi-CAP system (m-CAP, where m is the number of subcarriers) is compared with a traditional single carrier CAP system over 15 km of standard single mode fiber with a 25 GHz externally modulated as the transmitter. The multi-CAP system is split into $m = 6$ subcarriers, each of 4.26 GHz bandwidth while the single CAP system occupies 25 GHz bandwidth. It was found that a transmission speeds of 102.4 Gb/s and 100 Gb/s could be achieved for multi-CAP and CAP, respectively. This is not a significant gain in transmission speed; however a substantial improvement in dispersion and SNR performance, as well as a substantial reduction in computation complexity due to a reduction in sampling frequency per carrier, was also reported. In terms of computational complexity, as the order of m increases, the number of FIR filters increases by $2m$ in both the transmitter and receiver. If m is selected excessively high this can introduce additional computational complexity, which is undesirable. On the other hand, the literature has shown that increasing m results in a reduction of overall sampling frequency requirements, causing them to approach the Nyquist rate, meaning lower clock speeds can be used in the digital signal processors. Finally, although the pulse shaping filter required for m-CAP is more involved than that of OFDM, the IFFT/FFT required by OFDM is still a more complex operation than designing a pulse shaping filter for m-CAP. Moreover, such an m-CAP pulse shaping filter is physically realizable as demonstrated in the experiments presented in this paper.

Provided the system design process as described in this paper is followed and the pulse shaping filter correctly realized (having matched pulse shaping filters at the transmitter and receiver), we do not expect it to have any adverse effect on the system performance.

We believe that the proposed m-CAP system is an effective method for improving the bandwidth usage in VLC systems. However there have been no experimental or theoretical demonstrations of its suitability to date. Therefore in this work we propose to investigate a number of m-CAP systems with increasing number of subcarriers belonging to the set $m = \{2, 4, 6, 8, 10\}$, in comparison to the traditional, single-carrier CAP format. First we load every subcarrier in every system with binary phase-shift keying (BPSK) before transmission in order to establish the SNR/subcarrier before increasing the number of bits/symbol to the maximum allowed by our experimental system. We demonstrate that transmission speeds (spectral efficiencies) of 31.53 (4.85), 30.88 (4.75), 25.40 (3.90), 23.65 (3.60), 15.78 (2.40), 9.04 (1.40) Mb/s (b/s/Hz) can be achieved for $m = \{10, 8, 6, 4, 2, 1\}$, respectively.

This paper is organized as follows. In Section II the communications test setup and theoretical description of the m-CAP modulation format is discussed. Finally in Sections III and IV the results are discussed and the conclusions are drawn, respectively.

II. m-CAP Test Setup

The test setup for our link is shown in Fig. 1 in the form of a schematic block diagram and picture of the experimental setup inset. A $2^{11} - 1$ pseudorandom binary sequence is generated for each subcarrier D_m where m is the subcarrier, before being mapped into the M_m-QAM modulation format, where $M = 2^k$ and k is the number of bits/symbol. In the first instance $k = 1$, as mentioned. The signal is upsampled before being split into the real and imaginary parts before filtering. The I_m and Q_m filters form a Hilbert pair. The impulse response of the filters are given as the product of a square root raised cosine (SRRC) filter and a cosine (real) or sine (imaginary) wave with frequency at least twice that of the pulse width of the SRRC filter. The roll-off factor of the SRRC is set to $\beta = 0.15$, as is consistent with the literature [15], [16]. The concept of impulse response generation is illustrated in Fig. 2 where the top half shows the filter impulse response for the real-valued upsampled QAM data (blue), SRRC impulse (red) and cosine (black); the bottom half shows the imaginary-valued upsampled QAM data filter impulse response (green), SRRC impulse (red) and sine (black). For higher subcarriers the frequency of the (co)sine wave is simply increased appropriately.

The output of each filter is real-valued and summed to form the time domain signal for transmission. The output signal $s(t)$ is given by [17]:

$$s(t) = \sum_{n=1}^{m} \left[A_I^n(t) \otimes f_I^n(t) - A_Q^n(t) \otimes f_Q^n(t) \right] \tag{1}$$

where $\otimes$ denotes time-domain convolution, A_I^n and A_Q^n are the in-phase and quadrature M_m-QAM mapped symbols on the n^{th} subcarrier and f_I^n and f_Q^n are the in-phase and quadrature

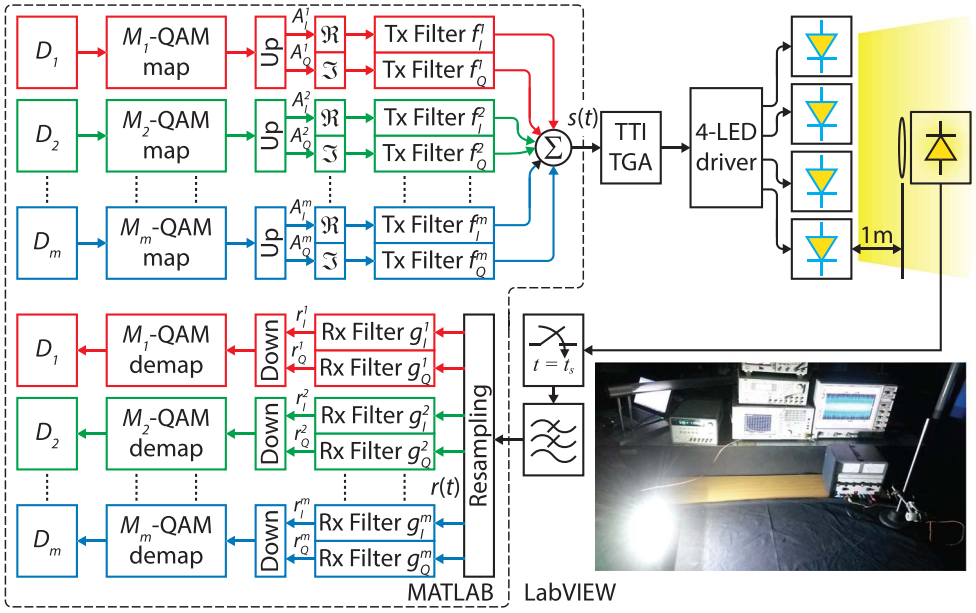

Fig. 1. Schematic block diagram of the system under test including a photograph inset; it should be noted that the "Up" block indicates up-sampling and the "Down" block indicates down-sampling.

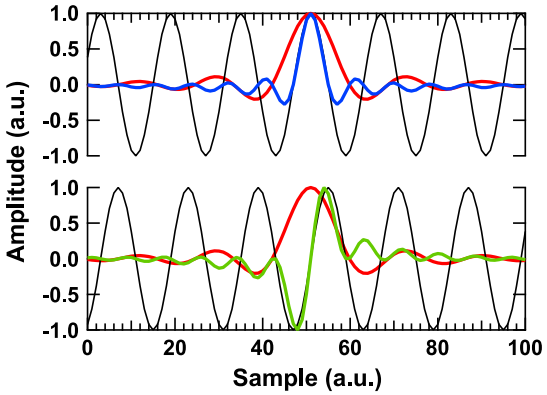

Fig. 2. (Top) shows the cosine carrier (black), SRRC impulse response (red) and overall in-phase filter impulse response (blue) for the first subcarrier of an m-CAP system; (bottom) shows the sine carrier (black), SRRC impulse (red) and quadrature filter impulse (green) for the same subcarrier.

transmit filters of the n^{th} subcarrier, respectively. The impulse responses of the transmit filters are given by [17]:

$$f_I^m(t) = \left[\frac{\sin\left(\xi[1-\beta]\right) + 4\beta\frac{t}{T_s}\cos\left(\xi[1+\beta]\right)}{\xi\left[1-\left(4\beta\frac{t}{T_s}\right)^2\right]}\right] \cdot \sin\left(\pi\frac{t}{T_s}(2m-1)(1+\beta)\right) \quad (2)$$

for the in-phase filter and the following for the quadrature filter, where T_s is the symbol duration and $\xi = \pi\frac{t}{T_s}$ [17]:

$$f_I^m(t) = \left[\frac{\sin\left(\xi[1-\beta]\right) + 4\beta\frac{t}{T_s}\cos\left(\xi[1+\beta]\right)}{\xi\left[1-\left(4\beta\frac{t}{T_s}\right)^2\right]}\right] \cdot \cos\left(\pi\frac{t}{T_s}(2m-1)(1+\beta)\right) \quad (3)$$

A TTI TGA12104 arbitrary waveform generator is selected due to it's deep memory (up to 1 Mpoints) and high arbitrary clock frequency (up to 100 MHz). The signal frequency is given as the ratio of the length of the data sequence to the desired transmission frequency. Therefore in this work, due to the high length of the transmission sequences, the transmission bandwidth is limited to 6.5 MHz. On the other hand, the bandwidth of our Ce:YAG/GaN LEDs is 4.5 MHz, meaning an additional 2 MHz is required for communications and hence there is an out of band transmission, where high attenuation can be expected.

Thus with the 6.5 MHz bandwidth limitation imposed, the m-CAP system must be designed appropriately. The baud rates are set as follows; 6.50, 3.25, 1.625, 1.083, 0.8125 and 0.65 Mbaud for $m = \{1, 2, 4, 6, 8, 10\}$, respectively and this is illustrated in Fig. 3.

The arbitrary waveform generator is controlled by LabVIEW and feeds a custom transmission circuit that is detailed in [18]. The circuit is a current mirror with four arms that intensity modulates four individual Ce:YAG/GaN LEDs with the same signal. The LEDs are biased at 350 mA to ensure operation in the linear region (see Fig. 4 for the measured L-I-V curve).

This allows us to set the transmission distance at ~1 m, which is substantially larger than in the majority of the experimentally tested VLC systems published in literature [1], [8], [19]. The light is focused onto the photodetector (OSD15-5T) using a 25 mm bi-convex lens with a focal distance of 25 mm. The photocurrent is passed through an Analog Devices AD8015 differential transimpedance amplifier before both of the differential channels are digitized by an Agilent DSO9254A real time oscilloscope.

After capture, the signal is processed offline in MATLAB starting with a 4^{th} order low pass filter with cut-off frequency set to 6.5 MHz to remove out of band noise. The dominant noise source in this system is expected to be the shot and thermal noise introduced by the receiver electronics which can

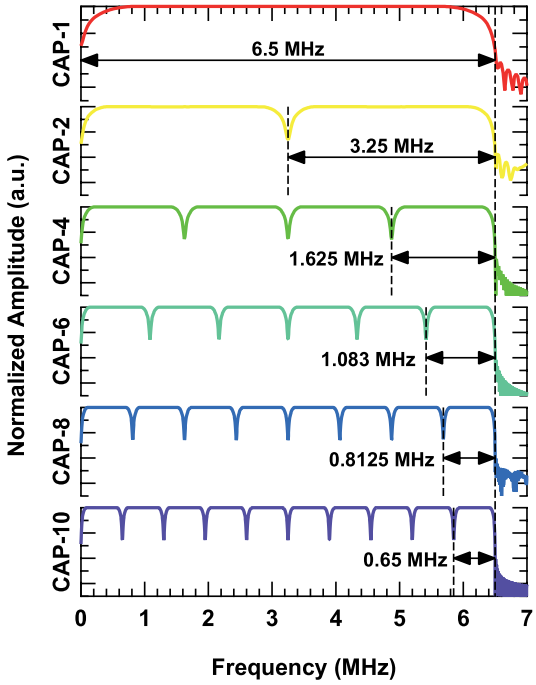

Fig. 3. Ideal frequency responses and bandwidth requirements for different orders of m.

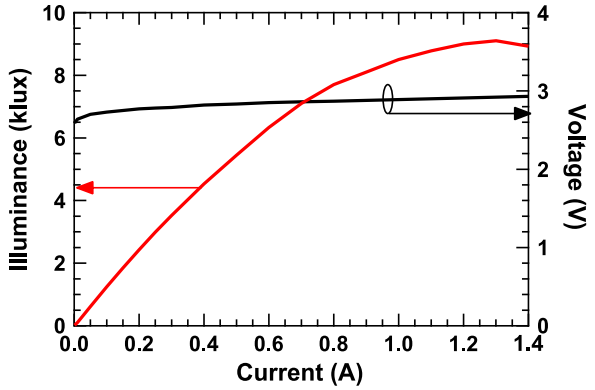

Fig. 4. Measured L-I-V curves of a single Ce:YAG/GaN LED used in this work.

be modelled as additive white Gaussian noise sources [12], as opposed to ambient noise or noise induced by clipping from the LED L-I-V response. After low pass filtering, the signal is resampled to match that of a reference version of the transmitted signal and passed through the time-reversed in-phase and quadrature receiver filters g_I and g_Q, which are matched to the corresponding transmit filter so that $g_I^m(t) = f_I^m(-t)$ and $g_Q^m(t) = f_Q^m(-t)$. The received in-phase and quadrature signals are given as follows [17]:

$$r_I^m(t) = r(t) \otimes g_I^m(t) \tag{4}$$

for the in-phase receiver matched filter and

$$r_Q^m(t) = r(t) \otimes g_Q^m(t) \tag{5}$$

for the quadrature receiver matched filter, where $r(t)$ is the discrete time digitized signal after resampling.

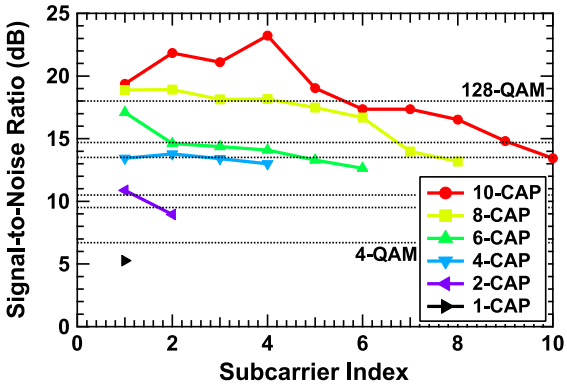

Fig. 5. Measured SNR from the BPSK tests for each m-CAP system tested; also shown are the SNR thresholds.

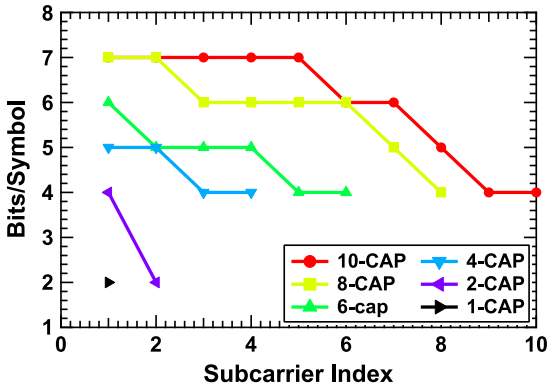

Fig. 6. The assigned number of bits-per-symbol for each value of m-CAP.

In the first instance, BPSK is transmitted in order to gain an estimate of the SNR available in each subcarrier as in [19]. The SNR is estimated as the square of the root mean square error vector magnitude (EVM) measured from the received BPSK constellation as follows [20]:

$$\text{SNR} = \frac{1}{\text{EVM}^2} \tag{6}$$

The received and measured SNR values and assigned M_m-QAM modulation orders are illustrated in Figs. 5 and 6, respectively. Although at least 10^5 bits are captured during the measurements, the BER target was set at 10^{-3}, in order to provide a small error allowance in consideration of the forward error correction (FEC) 7% and 20% BER limits of 3.8×10^{-3} and 2×10^{-2}, respectively [21]. Thus, several theoretical SNR thresholds emerge that dictate the maximum number of bits-per-symbol-per-subcarrier, which are shown as dashed lines in Fig. 5. The exact values can easily be found in the literature [21] as follows; $\text{SNR}_{threshold} = \{6.7, 9.5, 10.5, 13.5, 14.7, 18\}$ dB for $k = \{2, 3, 4, 5, 6, 7\}$ bits/symbol, respectively at a BER of 10^{-3}. From Fig. 5 it is inferrable that for $m > 1$ the number of bits-per-symbol can be optimized from the measured SNRs as shown in Fig. 6, which states the allocation for each m-CAP system. The maximum SNR value measured is 23.22 dB for the 4$^{\text{th}}$ subcarrier of 10-CAP. On the other hand, for $m = 1$ the threshold for 4-QAM is not met. Instead of selected BPSK

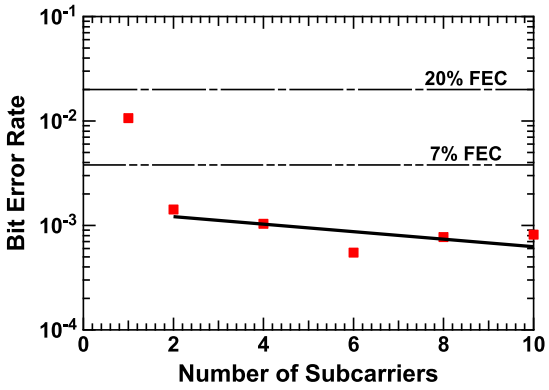

Fig. 7. The measured BER performance for every value of m-CAP; showing the BER for $m = 1$ ($\sim 10^{-2}$) and for $m > 1$ ($\sim 10^{-3}$) as expected.

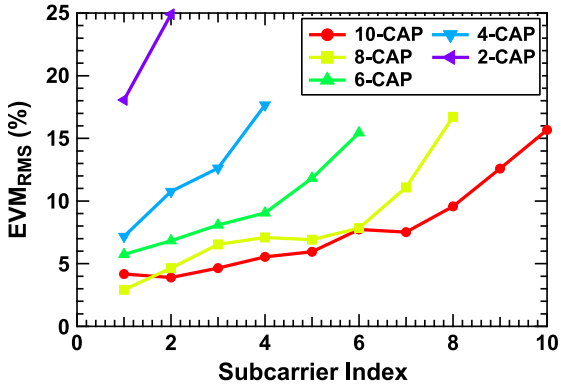

Fig. 8. The measured EVM for each subcarrier for every version of m-CAP tested; showing a clear improvement with increasing m.

for the 1-CAP modulation format we decided that it was advantageous to persist with 4-QAM at the cost of a higher BER ($\sim 10^{-2}$), which is still beneath the 20% FEC limit.

The m-CAP signals optimized with the appropriate number of bits-per-symbol-per-subcarrier are subsequently loaded into the TTI TGA12104 and the same routine occurs. There have been reports of equalization in the literature before de-mapping from the M_m-QAM constellation, including the use of analogue [10] and digital [22] frequency domain equalizers, the constant multi-modulus [17], [23], least mean squares [24] and k-means [15] algorithms and decision feedback equalization [25], [26]. In this work we do not consider an equalizer because we would like to demonstrate the raw improvement in spectral efficiency with increasing order of m. Further, in an m-CAP system with a high m, an individual equalizer would be required for every subcarrier, drastically increasing the computational complexity and surrendering some of the advantages of CAP over OFDM and single-carrier QAM systems.

The received signal is then downsampled and de-mapped from the M_m-QAM constellation to give an estimate of the transmitted symbols. The estimates are compared with the actual transmitted symbols to provide a symbol-by-symbol BER performance characterization for each value of m.

III. Results

The results will be discussed as follows. The BER performance of each m-CAP system is shown in Fig. 7, which also highlights the FEC limits of 3.8×10^{-3} (7%) and 2×10^{-2} (20%). Following a discussion of the overall BER performance for each system and considering the 6.5 MHz bandwidth occupancy, the available transmission speed and spectral efficiency will be discussed for every m-CAP system in descending order. The BER is calculated by aggregating the individual BERs from each subcarrier in the same manner as the overall transmission speed is calculated as the sum of the total capacity from each subcarrier.

Overall, for $m > 1$ the 7% FEC limit is comfortably met as expected due to the BER targets set, shown with a linear fit in Fig. 7, excluding $m = 1$. The aggregated BER for each m-CAP system is approximately 10^{-3} as expected, indicating the correct functionality of the system. For higher orders of m (i.e. $m = 10$) it can be seen that the measured SNR is comfortably above the threshold for 128-QAM, yet the BER performance is close to the 10^{-3} threshold (exact BER $= 8.17 \times 10^{-4}$). The reason is because a high number of bit errors are introduced by the high subcarriers, which are very close to the threshold limits for the target BER. Further, it is clear that the worst performance occurs for the 1-CAP system, which offers a BER of $\sim 10^{-2}$, failing to meet the 7% FEC limit as expected but comfortably within the 20% FEC limit. This is not a fatal problem for 1-CAP; however it does mean a significantly larger overhead of redundant symbols and a further reduction in spectral efficiency in comparison to the other systems, especially considering that 4-QAM is used as the modulation order.

Further insight into the system performance can be gained by analyzing the EVM-per-subcarrier for each m-CAP system as is illustrated in Fig. 8, which does not include the EVM_{RMS} result for 1-CAP. The reason for this is because 1-CAP achieved an EVM result of 43.32% and caused a severe reduction in resolution of the y-axis, distorting the remaining data. Clearly the EVM results follow a similar trend of a reduction in EVM with an increasing order of m. Recalling that the high-index subcarriers are carried at higher frequencies than the low-index subcarriers, the increased EVM is heavily dependent on the modulation bandwidth of the system (4.5 MHz). Subcarriers outside of the bandwidth experience a higher level of attenuation due to the characteristic low pass frequency response and thus the EVM increases substantially due to the reduced signal power.

A discussion of the individual m-CAP performances will commence in the next subsections.

A. 10-CAP

The received and normalized electrical spectra for 10-CAP is shown in Fig. 9 with constellations for the 1st (red), 6th (blue) and 10th (green) subcarriers inset as highlighted in their respective colors. The EVM_{RMS} values for the three constellations shown are 4.1741%, 7.7326% and 15.666% for the 1st, 6th and 10th subcarriers, respectively.

The gross transmission speed that can be achieved using the 10-CAP system at a BER of 10^{-3} is 33.9 Mb/s. After removal of the 7% FEC overhead, this corresponds to a net

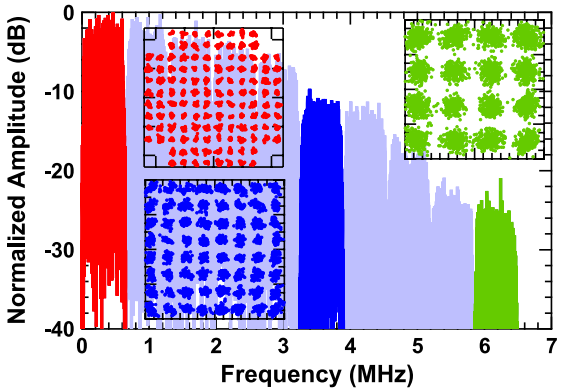

Fig. 9. The measured electrical spectrum of the 10-CAP system with 6.5 MHz bandwidth showing clear and increasing attenuation with every additional subcarrier; inset are the constellations for the highlighted subcarriers.

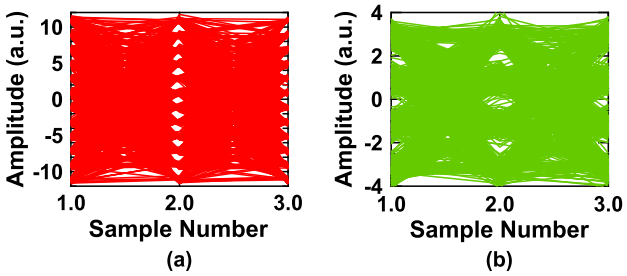

Fig. 10. Eye diagram of 10-CAP down-sampled data for (a) subcarrier 1 and (b) subcarrier 10; clearly subcarrier 1 shows a significantly improved SNR over subcarrier 10 due to the clean eye opening (note the different y-axis scales).

transmission speed of 31.53 Mb/s. It should be noted that the point of this paper is not to set a world record transmission speed but to demonstrate the gain that can be achieved using the proposed *m*-CAP system. Recalling that the maximum bandwidth allowed by the TGA12104 is 6.5 MHz, this was adopted as the transmission bandwidth, corresponding to a spectral efficiency of 4.85 b/s/Hz; the highest reported in this work. To the best of the authors' collective knowledge, this is the highest spectral efficiency reported in any VLC system at the 1 m distance considered. Other systems have reported higher spectral efficiencies; for example 6.25 b/s/Hz was demonstrated in [19], however the link distance had to be severely reduced to just 0.05 m in order to do achieve this, a reduction of twenty-fold in comparison to this work. We anticipate with a smaller distance the spectral efficiency we report could be improved beyond 6.25 b/s/Hz; due to the additional optical power that would be absorbed by the photodetector. This would benefit not only the low-index subcarriers but also more importantly the high-index subcarriers where the number of bits-per-symbol was severely limited by noise. This is best demonstrated by examining the eye diagrams of the 1st and 10th subcarriers at the receiver.

Only the in-phase signals are shown (equally we could have shown the quadrature) after being down-sampled. The two eye diagrams are shown in Fig. 10(a) and (b), respectively, where the difference in SNR is clear. With a shorter distance the SNR of both would improve and thus more bits-per-symbol could be added and a higher spectral efficiency achieved.

B. 8-CAP

The gross transmission speed that can be supported using the 8-CAP system is slightly reduced to 33.2 Mb/s in comparison to the 33.9 Mb/s available in 10-CAP; a reduction of 0.7 Mb/s. After removal of the overhead the net transmission speed available is 30.88 Mb/s, ∼0.65 Mb/s less than for 10-CAP and therefore a slight reduction in spectral efficiency to 4.75 b/s/Hz, or a 0.1 b/s/Hz reduction, which could be considered negligible for the current system. We suggest this because if the transmission speed is approximately equal, the system complexity can be reduced by omitting the 9th and 10th subcarriers at the transmitter and receiver at the cost of 0.65 Mb/s. Recalling that the most expensive filters computationally are the ones that require the highest sampling frequencies this could be classed as a significant advantage.

C. 6-CAP

For 6-CAP the overall transmission speed is 27.3 Mb/s before overhead removal; a large reduction over 8-CAP and 10-CAP of at least 5.9 Mb/s. After overhead removal the data rate drops to 25.4 Mb/s with a spectral efficiency of 3.9 b/s/Hz. The severe reduction in capacity for 6-CAP in comparison to the previous two systems is attributed to the wider subcarrier bandwidth of 1.083 MHz, which is more prone to attenuation that the previous bands, which were both ≤ 0.8125 MHz. This causes a significant reduction in SNR (as can be referred to in Fig. 5), meaning a lower allocation of bits-per-symbol (Fig. 6) and a higher EVM (Fig. 8). It can be noted from Figs. 5 and 7 that both the profiles of 8-CAP and 10-CAP are very similar, when considering a frequency normalized case, thus explaining their very similar performances and their additional performance over 6-CAP.

D. 4-CAP and 2-CAP

4-CAP offers a gross (net) throughput of 25.40 (23.65) Mb/s, a further drop of 1.90 (1.75) Mb/s in comparison to 6-CAP and a large drop of 8.50 (7.88) Mb/s in comparison to 10-CAP and the spectral efficiency is reduced to 3.6 b/s/Hz. For the 2-CAP system, there is a substantial drop in gross (net) throughput to ∼17 (15.78) Mb/s. This is a substantial drop in comparison to 4-CAP and a drop of around 50% when considering the transmission speeds of 10-CAP and 8-CAP are slightly over 30 Mb/s. This can be attributed once more to the bandwidth of the subcarriers; for $m = \{4, 6, 8, 10\}$ the bandwidth sizes vary by a fraction of a single MHz, meaning that the baud rate for each constellation must increase in order to maintain the overall transmission speed and hence there is a slight dip with decreasing m. However for $m = 2$, the bandwidth doubles in comparison to $m = 4$ indicating a substantially larger attenuation. This is reflected in the electrical spectrum of the 2-CAP signal (Fig. 11), which, for the first subcarrier, shows attenuation of ∼8–10 dB and, for the second subcarrier, ∼10–12 dB.

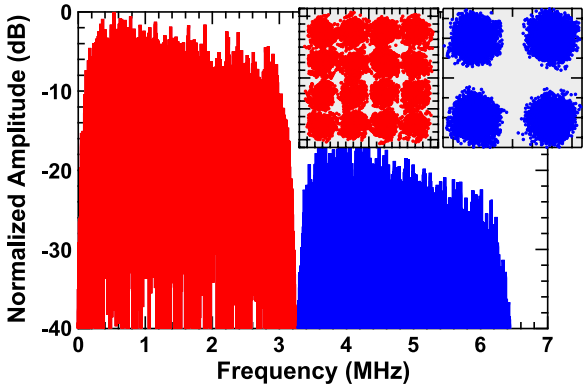

Fig. 11. Measured electrical spectrum of 2-CAP, showing much higher attenuation per subcarrier than previous spectra; thus the EVM of the inset subcarriers is severely reduced.

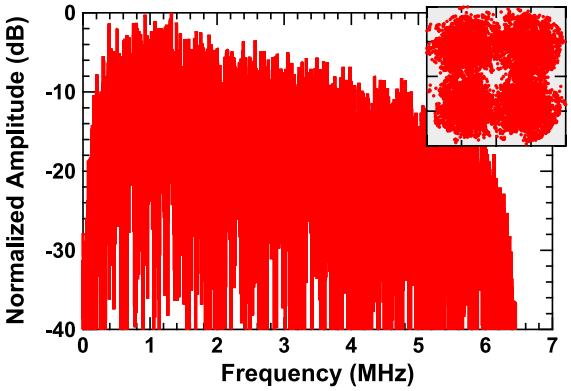

Fig. 12. Measured electrical spectrum for 1-CAP with 4-QAM constellation inset.

When comparing with 10-CAP (Fig. 9), there is no obvious attenuation in any of the subcarriers until the 9th and 10th subcarriers, which show ∼1 dB each. The spectral efficiency of 2-CAP is 2.4 b/s/Hz, confirming the substantial drop in efficiency.

E. 1-CAP

The conventional 1-CAP system can support a gross data rate of 11.3 Mb/s. Recalling that the BER of the 1-CAP system is $\sim 10^{-2}$ it is not possible to use a 7% FEC in this case. Thus, the 20% FEC must be used here, reducing the overall transmission speed to 9.04 Mb/s, thus dropping beneath 10 Mb/s for the first time. In comparison to 10-CAP this is a drop of $>$ 20 Mb/s, while in comparison to 2-CAP a drop of ∼6 Mb/s is reported. The spectral efficiency drops to 1.4 b/s/Hz; the lowest efficiency reported here and a massive ∼3.5 times smaller than 10-CAP and 8-CAP. Just as reported with 2-CAP, this is attributed to the large attenuation suffered due to out-of-band transmission, refer to the electrical spectrum in Fig. 12 which shows 10–20 dB attenuation.

Finally, in Fig. 13 we summarize the reported results into a graph that shows the net transmission speed and spectral efficiency simultaneously. The data corresponds to both axes. It is possible to notice that the data follows an exponential trend

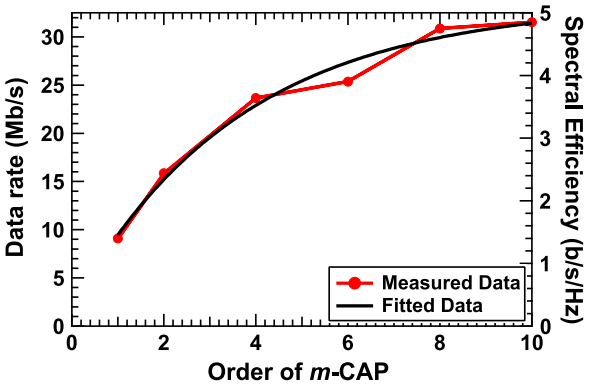

Fig. 13. Measured throughput and spectral efficiency for each order of m-CAP with exponential fitting curve implying an eventual asymptotic behavior.

and hence we fitted the curve to the available net transmission speed with the following equation:

$$R_b = 33.486 - 24.026 \exp\left(\frac{1-m}{3.6615}\right) \tag{7}$$

where R_b is the net transmission speed (Mb/s). As an exponential fit is required and not a linear fit, this implies asymptotic behavior where at a certain point, increasing the number of subcarriers will not provide any improvement but will introduce additional computational complexity. We propose to theoretically investigate this in our future work in order to derive the upper bounds for the capacity of the m-CAP modulation format for VLC systems.

IV. Conclusion

In this paper we have experimentally demonstrated an m-CAP system for VLC for the first time considering a fixed bandwidth of 6.5 MHz, where m is the number of subcarriers under consideration and belongs to the set $m = \{10, 8, 6, 4, 2, 1\}$. We observed that for a higher number of subcarriers, a higher throughput could be supported, up to ∼31.5 Mb/s with a spectral efficiency of 4.85 b/s/Hz. Reducing the number of subcarriers results in a lower throughput and spectral efficiency due to the wider bandwidths of the subcarriers, which are more prone to high frequency attenuation in the first order low-pass VLC systems.

Acknowledgment

P. A. Haigh also acknowledges James Thomas Steven Savage, University of Bristol, for providing the platform to perform several of the measurements.

References

[1] H. Le Minh *et al.*, "100-Mb/s NRZ visible light communications using a postequalized white LED," *IEEE Photon. Technol. Lett.*, vol. 21, no. 15, pp. 1063–1065, Aug. 2009.

[2] L. Grobe *et al.*, "High-speed visible light communication systems," *IEEE Commun. Mag.*, vol. 51, no. 12, pp. 60–66, Dec. 2013.

[3] P. A. Haigh, Z. Ghassemlooy, S. Rajbhandari, I. Papakonstantinou, and W. Popoola, "Visible light communications: 170 Mb/s using an artificial neural network equalizer in a low bandwidth white light configuration," *J. Lightw. Technol.*, vol. 32, no. 9, pp. 1807–1813, May 2014.

[4] D. S. Lee *et al.*, "300-GHz InAlN/GaN HEMTs with InGaN back barrier," *IEEE Electron Device Lett.*, vol. 32, no. 11, pp. 1525–1527, Nov. 2011.
[5] J. Grubor, S. C. J. Lee, K.-D. Langer, T. Koonen, and J. W. Walewski, "Wireless high-speed data transmission with phosphorescent white-light LEDs," in *Proc. ECOC*, 2007, pp. 1–2.
[6] Z. Ghassemlooy, W. Popoola, and S. Rajbhandari, *Optical Wireless Communications: System and Channel Modelling*. Boca Raton, FL, USA: CRC Press, 2012.
[7] W. O. Popoola and H. Haas, "Demonstration of the merit and limitation of generalised space shift keying for indoor visible light communications," *J. Lightw. Technol.*, vol. 32, no. 10, pp. 1960–1965, May 2014.
[8] G. Cossu, A. M. Khalid, P. Choudhury, R. Corsini, and E. Ciaramella, "3.4 Gbit/s visible optical wireless transmission based on RGB LED," *Opt Express*, vol. 20, no. 26, p. B501-6, Dec. 2012.
[9] D. Bykhovsky and S. Arnon, "An experimental comparison of different bit-and-power-allocation algorithms for DCO-OFDM," *J. Lightw. Technol.*, vol. 32, no. 8, pp. 1559–1564, Apr. 2014.
[10] F. M. Wu *et al.*, "Performance comparison of OFDM signal and CAP signal over high capacity RGB-LED-based WDM visible light communication," *IEEE Photon. J.*, vol. 5, no. 4, Aug. 2013, Art. ID. 7901507.
[11] A. F. Shalash and K. K. Parhi, "Multidimensional carrierless AM/PM systems for digital subscriber loops," *IEEE Trans. Commun.*, vol. 47, no. 11, pp. 1655–1667, Nov. 1999.
[12] J. Kahn and J. Barry, "Wireless infrared communications," *Proc. IEEE*, vol. 85, no. 2, pp. 265–298, Feb. 1997.
[13] H. Le Minh *et al.*, "80 Mbit/s visible light communications using pre-equalized white LED," in *Proc. IEEE 34th Eur. Conf. Opt. Commun.*, 2008, pp. 1–2.
[14] P. A. Haigh *et al.*, "Exploiting equalization techniques for improving data rates in organic optoelectronic devices for visible light communications," *J. Lightw. Technol.*, vol. 30, no. 19, pp. 3081–3088, Oct. 2012.
[15] M. I. Olmedo *et al.*, "Multiband carrierless amplitude phase modulation for high capacity optical data links," *J. Lightw. Technol.*, vol. 32, no. 4, pp. 798–804, Feb. 2014.
[16] M. Wieckowski, J. B. Jensen, I. Tafur Monroy, J. Siuzdak, and J. Turkiewicz, "300 Mbps transmission with 4. 6 bit/s/Hz spectral efficiency over 50 m PMMA POF link using RC-LED and multi-level carrierless amplitude phase modulation," in *Proc. Nat. Fiber Optic Eng. Conf.*, 2011, pp. 1–3.
[17] J. Zhang *et al.*, "$11 \times 5 \times 9.3$ gb/s WDM-CAP-PON based on optical single-side band multi-level multi-band carrier-less amplitude and phase modulation with direct detection," *Opt. Exp.*, vol. 21, no. 16, pp. 18 842–18 848, Aug. 2013.
[18] A. Burton *et al.*, "Experimental demonstration of a 10BASE-T ethernet visible light communications system using white phosphor light-emitting diodes," *IET Circuits, Devices Syst.*, vol. 8, no. 4, pp. 322–330, Jul. 2014.
[19] D. Tsonev *et al.*, "A 3-Gb/s Single-LED OFDM-based wireless VLC link using a gallium nitride μled," *IEEE Photon. Technol. Lett.*, vol. 26, no. 7, pp. 637–640, Apr. 2014.
[20] R. A. Shafik, S. Rahman, and R. Islam, "On the extended relationships among EVM, BER and SNR as performance metrics," in *Proc. Int. Conf. Elect. Comput. Eng.*, 2006, pp. 408–411.
[21] J. Proakis, *Digital Communications*. New York, NY, USA: McGraw-Hill, 2004.
[22] R. Rodes *et al.*, "Carrierless amplitude phase modulation of VCSEL with 4 bit/s/hz spectral efficiency for use in WDM-PON," *Opt. Exp.*, vol. 19, no. 27, pp. 26 551–26 556, Dec. 2011.
[23] L. Tao *et al.*, "Experimental demonstration of 10 Gb/s multi-level carrier-less amplitude and phase modulation for short range optical communication systems," *Opt. Exp.*, vol. 21, no. 5, pp. 6459–6465, Mar. 2013.
[24] L. Tao *et al.*, "40 Gb/s CAP32 system with DD-LMS equalizer for short reach optical transmissions," *IEEE Photon. Technol. Lett.*, vol. 25, no. 23, pp. 2346–2349, Dec. 2013.
[25] J. Wei, D. Cunningham, R. Penty, and I. White, "Study of 100 gigabit ethernet using carrierless amplitude/phase modulation and optical OFDM," *J. Lightw. Technol.*, vol. 31, no. 9, pp. 1367–1373, May 2013.
[26] J. Wei, L. Geng, D. G. Cunningham, R. V. Penty, and I. White, "100 gigabit ethernet transmission enabled by carrierless amplitude and phase modulation using QAM receivers," in *Proc. Opt. Fiber Commun. Conf.*, 2013, pp. 1–3.

Paul Anthony Haigh received the B.Eng.(Hons.) degree in communications engineering and the Ph.D. degree in organic visible-light communications from Northumbria University in 2010 and 2014, respectively. He is currently a Research Associate within the High Performance Networks Group, University of Bristol, working on the EPSRC TOUCAN project. He is the author of over 30 scholarly articles, including more than 16 articles in high ranking journals such as IEEE JOURNAL ON SELECTED AREAS IN COMMUNICATIONS, *IEEE Wireless Communications Magazine*, *Optics Express*, *IEEE Communications Magazine*, and IEEE/OSA JOURNAL OF LIGHTWAVE TECHNOLOGY. His research interests include real-time, seamless, transparent, and programmable interfaces between wired and wireless multitechnology networks. Between 2010 and 2011, he held the prestigious Marie Curie Fellowship at the European Organization for Nuclear Research (CERN), where he worked on the optoelectronic links in Large Hadron Collider experiments.

Andrew Burton received the B.Eng.(Hons.) and M.Sc. degrees (with distinction) and the Ph.D. degree in visible-light communications from Northumbria University, U.K. He is currently an Associate Lecturer with Northumbria University. Starting July 2015, he will be involved in collaboration between Northumbria University and the European Space Agency to develop a simulation package for ground-to-space and space-to-ground free-space optical communications. His research interests include electronics, optical communications and visible-light communications, in which he has 19 journal/conference publications.

Khald Werfli received the B.Sc. degree in telecommunications from The High Institute of Electronic Professions, Tripoli, Libya, in 2002 and the M.Sc. degree (with first class honors) in communications and signal processing from the University of Newcastle in 2010. He is currently working toward the Ph.D. degree with the Department of Physics and Electrical Engineering, Northumbria University. He is currently a member of the Optical Communications Research Group, Northumbria University. His research interests include optical wireless communications and visible-light communications.

Hoa Le Minh was a Researcher with Siemens AG, Munich, Germany, in 2002 and with the University of Oxford, U.K., in 2010. Since 2010, he has been with the Northumbria University, U.K., where he served as a Senior Lecturer (in 2010) and then as a Program Leader of electrical and electronics engineering (in 2013). He is the author of over 100 papers published in referred journals and conferences. His research interests include optical communications, visible-light communications, and smartphone technology.

He currently serves as the Vice-Chair for IEEE Communications Chapter of U.K. and Ireland, and serves as a Guest Editor for IET and ETT journals.

Edward Bentley received the B.Eng. and Ph.D. degrees from the Northumbria University, U.K. He is currently a Lecturer of power engineering and analog electronics with the Faculty of Engineering and Environment, Northumbria University. His research interests include electric vehicles, smart grids, artificial neural networks, and optical wireless communications.

Petr Chvojka was born in 1987. He received the M.Sc. degree from the Czech Technical University in Prague, Prague, Czech Republic, in 2013. He is currently working toward the Ph.D. degree with the Department of Electromagnetic Fields, Czech Technical University in Prague, where he is also a Ph.D. Researcher and a member of the free-space and fiber optics team. His research interests include visible-light communications, OLED technologies, and wireless optical communications.

Wasiu O. Popoola received the first class (Hons.) degree in electronic and electrical engineering from Obafemi Awolowo University, Nigeria, and the M.Sc. and Ph.D. degrees from Northumbria University. From March 2010 to June 2012, he was a Research Fellow in visible light communications with the Institute for Digital Communications, University of Edinburgh. Between August 2012 and December 2014, he was a Lecturer of electronic engineering with Glasgow Caledonian University. He is currently a Chancellor's Fellow with the Institute for Digital Communications, University of Edinburgh. He is the author of over 60 journal articles/conference papers/patent, and about six of those are invited papers. He is a coauthor of the book *Optical Wireless Communications: System and Channel Modelling with MATLAB* (CRC Press, 2012). He received the Xcel Best Engineering and Technology Student of the Year in 2009 for his Ph.D. studies.

Ioannis Papakonstantinou received the Ph.D. degree in polymer optical interconnects from UCL in 2008. In 2008, he joined Sharp Laboratories of Europe as a Research Associate. While at Sharp, he received training on nanoimprint lithography, the subject of his proposed work in this proposal, and specialized in subwavelength structures to improve the energy efficiency, uniformity, and brightness of liquid crystal displays. He has almost ten years of experience in optical components made of polymers. Together with his colleagues at Sharp, he filed and was awarded 5 patents on the design and fabrication of antireflection coatings, nonabsorbing polarizers, color separating gratings, and light in-coupling and out-coupling structures for backlights, all made by NIL. From 2009 to 2011, he was with the Physics Department, European Organization for Nuclear Research (CERN), where he developed optical network topologies for the distribution of time, trigger, and control signals in the Large Hadron Collider. He is currently a Lecturer with the Department of Electronic and Electrical Engineering, UCL, where he leads a team of six Ph.D. students as Principal and Second Supervisor. His research interests include nanophotonics for renewable energy, medical equipment, and ICT applications.

Stanislav Zvanovec received the M.Sc. and Ph.D. degrees from Czech Technical University (CTU) in Prague in 2002 and 2006, respectively. He is a Full Professor and the Vice Head of the Department of Electromagnetic Field, Faculty of Electrical Engineering, CTU. He leads the Free-Space and Fiber Optics Team at CTU and is the Vice Chair of WG1 of EU COST project IC1101 OPTICWISE-Optical Wireless Communications-An Emerging Technology. His current research interests include wireless optical communications, visible-light communications, remote sensing, and optical fiber sensors.

4.3 Evaluation of Multi-band Carrier-less Amplitude and Phase Modulation Performance for VLC under Various Pulse Shaping Filter Parameters

This chapter is a version of the published manuscript:

P. Chvojka, P. A. Haigh, S. Zvanovec, P. Pesek and Z. Ghassemlooy, "Evaluation of Multi-band Carrier-less Amplitude and Phase Modulation Performance for VLC under Various Pulse Shaping Filter Parameters", *Proceedings of the 13th International Joint Conference on e-Business and Telecommunications - Volume 3: OPTICS (ICETE 2016)*, Lisbon, 2016, pp. 25-31.

Connection with my Ph.D. thesis:

We show how m-CAP system performance is dependent on transmitter and receiver filter parameters, such as the roll-off factor and number of taps. Using numerical simulations, we demonstrate that increasing both parameters can enhance the BER system performance significantly. However, the setting of the roll-off factor is more critical. We also derive the limit for the filter length which should not exceed 12 symbols/filter due to no additional significant performance improvement. Task **T3** is fulfilled and a direction for further research is given. Please note, the conference paper received the prize for the *Best Student Paper award*.

Evaluation of Multi-band Carrier-less Amplitude and Phase Modulation Performance for VLC under Various Pulse Shaping Filter Parameters

Petr Chvojka[1], Paul Anthony Haigh[2], Stanislav Zvanovec[1], Petr Pesek[1] and Zabih Ghassemlooy[3]
[1]*Department of Electromagnetic Field, Faculty of Electrical Engineering, Czech Technical University in Prague, Technicka 2, 16627, Prague, Czech Republic*
[2]*High Performance Research Group, Faculty of Engineering, University of Bristol, BS8 1TH, Bristol, U.K.*
[3]*Optical Communications Research Group, NCRLab, Faculty of Engineering and Environment, Northumbria University, NE1 8ST, Newcastle upon Tyne, U.K.*

Keywords: Carrier-less Am4plitude and Phase Modulation, Roll-off Factor, Filters, Visible Light Communications.

Abstract: In multi-band carrier-less amplitude and phase modulation (*m*-CAP), the transmitter and receiver pulse shaping filters have a significant impact on the signal performance. Since *m*-CAP is an emerging and promising modulation format for visible light communications (VLC), it is necessary to balance the system performance and the filter length, due to limited integration density in field programmable gate arrays (FPGAs). In this paper we investigate the *m*-CAP VLC system performance for different number of sub-bands $m = \{2, 5, 10\}$ under varying finite impulse response (FIR) filter parameters, such as the filter length L_f and the roll-off factor β. We show that increasing both β and L_f improves the bit error rate (BER) performance of the system substantially. We demonstrate that a BER target of 10^{-4} is achieved using $L_f \leq 12$ symbols for $m = 5$ and 10 for low order subcarriers. Moreover, the BER limit is attained for $\beta = 0.2$ by all subcarriers, except the last two for $m = 5$ and 10, which is a significant improvement, even considering the slightly increased excess bandwidth in comparison to the literature.

1 INTRODUCTION

As the number of end user devices connected to the internet will increase, the demand for high speed internet connection and the transmission capacity required will grow exponentially (Zvanovec et al., 2015). Thus, the next generation networks (5G) face several challenges such as high spectral and energy efficiency and high capacity. Visible light communications (VLC) is an emerging technology, which is able to meet the mentioned requirements by utilizing existing solid state lighting (SSL) structures based on light-emitting diodes (LEDs). VLC provides users with both illumination and data transmission at the same time and could be used for localization as well (Armstrong et al., 2013).

Despite the advantage in using existing SSL infrastructures, the bottleneck of the VLC system is introduced by LEDs behaving as a first order low pass filter (LPF), with a 3 dB cut-off frequency in the MHz region (Haigh et al., 2014). Thus, spectrally efficient modulation formats such as orthogonal frequency division multiplexing (OFDM) are frequently proposed due to such bandwidth limitations in conjunction with high capacity requirements. OFDM supports bit- and power-allocation algorithms that assign bits and electrical power to each subcarrier (Bykhovsky et al., 2014). However, OFDM suffers from a high peak-to-average power ratio (PAPR) that can lead to signal clipping, due to the LED nonlinear electro-optic characteristic resulting in the link performance degradation (Mesleh et al., 2012).

Recently, the research community has turned attention to carrier-less amplitude and phase (CAP) modulation format as an alternative to OFDM (Wu et al., 2012; Wei et al., 2012; Wu et al., 2013). CAP is similar to quadrature amplitude modulation (QAM). The main difference is that CAP uses finite impulse response (FIR) filters to generate carrier frequencies unlike QAM, which utilizes a local oscillator. This results in a simpler solution for CAP receivers, since time-reversed matched filters are deployed. In previous research it was experimentally shown that CAP outperforms OFDM in VLC when using the sa-

Chvojka, P., Haigh, P., Zvanovec, S., Pesek, P. and Ghassemlooy, Z.
Evaluation of Multi-band Carrier-less Amplitude and Phase Modulation Performance for VLC under Various Pulse Shaping Filter Parameters.
DOI: 10.5220/0005956900250031
In *Proceedings of the 13th International Joint Conference on e-Business and Telecommunications (ICETE 2016) - Volume 3: OPTICS*, pages 25-31
ISBN: 978-989-758-196-0

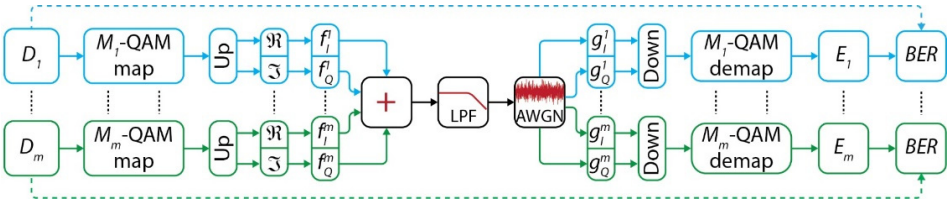

Figure 1: Schematic diagram of the VLC system. Note, that 'UP' and 'DOWN' block represent upsampling and downsampling, respectively.

me experimental setup. The improvement in achieved transmission speed was ~ 22%, which is significant (Wu et al., 2013). Nevertheless, CAP requires a flat channel frequency response, which is a rare commodity in VLC networks, due to the LEDs LPF behaviour. To overcome this, a new approach called multi-band CAP (*m*-CAP) was proposed for short range optical fibre links (Olmedo et al., 2014). The available bandwidth was split into 6 sub-bands (or subcarriers for compatibility with OFDM nomenclature) and a 6-CAP system was compared to the traditional single CAP (1-CAP) system. Splitting the bandwidth into *m* sub-bands has two key advantages over 1-CAP: *i)* relaxing the flat frequency response requirement and *ii)* allowing to adjust number of bits-per-symbol for each sub-band. Only a slight improvement in data rate (100 Gb/s and 102.4 Gb/s for 1-CAP and 6-CAP, respectively) was shown in (Olmedo et al., 2014), however *m*-CAP outperformed the conventional 1-CAP system in bandwidth efficiency and dispersion.

Thus, we adopted *m*-CAP modulation for VLC systems in our previous work both experimentally (Haigh et al., 2015; Haigh et al., 2015) and theoretically using numerical simulations (Haigh et al., 2015; Werfli et al., 2015; Haigh et al., 2015). For instance, in (Haigh et al., 2015) we showed that for a higher number of sub-bands, a higher transmission capacity can be supported. The highest data rate we achieved was ~ 31.5 Mb/s in the 10-CAP system, using an LED with a low 4.5 MHz modulation bandwidth. Increasing the number of sub-bands results in a lower bandwidth occupied by each subcarrier. Thus, they are less prone to the frequency dependent attenuation caused by the first order LPF behaviour of an LED and hence can support higher throughput, as mentioned. A highly bandlimited VLC link was investigated in (Haigh et al., 2015). The LPF cut-off frequency was set to 0.1 of the signal bandwidth and it was shown, that 10-CAP system can support up to 40% improvement in the bit rate compared to the traditional 1-CAP for the same bit error rate (BER) target.

As mentioned before, the carrier frequencies are generated by FIR filters, which are crucial in determining the system performance and complexity. Thus, in this paper we investigate performance of the *m*-CAP system using different filter parameters such as filter length L_f and roll-off factor β through numerical simulations. We show that a 2-CAP system does not meet the BER target for any filter length, while usage of filter lengths in the range of $8 < L_f < 12$ is sufficient for the most of the subcarriers except two highest for $m = 5$ and 10. Moreover, just a slight increment of the roll-off factor β results in significant improvement in BER performance when a higher number of sub-bands is deployed. The rest of the paper is organized as follows: in Section 2 the main principles of *m*-CAP and filter parameters are discussed. In Section 3 and 4 the results from *m*-CAP filter analyses are given and the conclusions are drawn, respectively.

2 SYSTEM DESCRIPTION

2.1 Multi-band CAP Principle

The schematic block diagram of the tested system is illustrated in Fig. 1. Firstly, *m* independent data streams of the length of 10^6 are generated. The data is mapped into *M*-QAM constellation symbols, upsampled by means of zero padding and split into the real (in-phase) and imaginary (quadrature) branches. The order of QAM modulation *M* is set to 16 to stay in consistency with recent literature (Haigh et al., 2015). The upsampling factor is given as (Olmedo et al., 2014):

$$n_s = \lceil 2m(1+\beta) \rceil \quad (1)$$

where $\lceil \cdot \rceil$ is the ceiling function and β is the roll-off factor of a square root raised cosine (SRRC) filter. The real and imaginary parts of the signal are then passed through the in-phase and quadrature SRRC filters, respectively. The setting of FIR filters will be discussed in detail later with respect to particular parameters under investigation. Finally, the filter outputs are summed up and modulate the LED intensity. The output signal is described by (Haigh et al., 2015; Junwen et al., 2013):

$$s(t) = \sum_{n=1}^{m} \left(s_I^n(t) \otimes f_I^n(t) - s_Q^n(t) \otimes f_Q^n(t) \right) \quad (2)$$

where s_I and s_Q are the real and imaginary QAM symbols for the n^{th} subcarrier and f_I and f_Q are the in-phase and quadrature transmit filter impulse responses, respectively, and $\otimes$ denotes time-domain convolution.

The output signal is passed through an ideal analogue LPF channel and the signal bandwidth is set to B = 1 Hz without any loss of generality. Thus, we can expect the same results for any signal bandwidth. The cut-off frequency of the LED is set as f_c = 0.5 Hz as in (Haigh et al., 2015), which results in an out of band transmission, where the signal attenuation of 20 dB/decade is assumed. After passing the zero-mean additive white Gaussian noise (AWGN) channel, the signal is passed through time reversed real and imaginary receiver filters, which are matched to the transmit filters. Next, both the real and imaginary parts of the signal are downsampled according to n_s and de-mapped for QAM constellation symbols estimation. Finally, the transmitted bits are compared with the received bits for BER estimation.

As in our previous work we set the BER target limit to 10^{-4} (Haigh et al., 2015), which is below the International Telecommunication Union's (ITU's) recommendation error floor (3.8×10^{-3}) for forward error correction (FEC) with an overhead of 7%.

2.2 FIR Filters

The FIR filters at both the transmitter and receiver are critical for the final m-CAP VLC system performance, since their number is scaled by a factor of $2m$ (two filters for each sub-band placed at both transmitter and receiver). Thus, one must consider the trade-off between performance and system complexity when implementing m-CAP in e.g. field programmable gate array (FPGA). However, to the best of author's knowledge filter parameters for m-CAP VLC systems have never been tested. There is a strong requirement to test such filter performance, as the computational complexity of the FIR filters increases with $2L_f$/symbol.

The pulse shaping SRRC filters have two key parameters: *i)* roll-off factor β and *ii)* filter length L_f. The value of β varies in the range of $0 \leq \beta \leq 1$ and determines the excess of bandwidth. A larger β results in the greater bandwidth requirements (see Fig. 2(a)), which is $(1 + \beta)$ times the symbol rate. Clearly, using $\beta = 0$ means ideal spectrum utilization. The impulse responses of the SRRC filters are orthogonal in the time domain with a 90° phase shift forming a Hilbert pair. They are generated as the product of a cosine and sine wave with SRRC filter impulse response for the real and imaginary parts of the signal, respectively. Obviously, the cosine/sine wave frequency gives the carrier frequency of each sub-band. The impulse responses of the transmit filters are given by (Haigh et al., 2015; Junwen et al., 2013):

$$f_I^m(t) = \left[\frac{\sin[\gamma(1-\beta)] + 4\beta \frac{t}{T_s} \cos[\gamma\delta]}{\gamma \left[1 - \left(4\beta \frac{t}{T_s} \right)^2 \right]} \right] \cdot \cos[\gamma(2m-1)\delta] \quad (3)$$

for the in-phase filter and

$$f_Q^m(t) = \left[\frac{\sin[\gamma(1-\beta)] + 4\beta \frac{t}{T_s} \cos[\gamma\delta]}{\gamma \left[1 - \left(4\beta \frac{t}{T_s} \right)^2 \right]} \right] \cdot \sin[\gamma(2m-1)\delta] \quad (4)$$

for the quadrature filter, where T_s is the symbol duration, $\gamma = \pi t/T_s$ and $\delta = 1+\beta$.

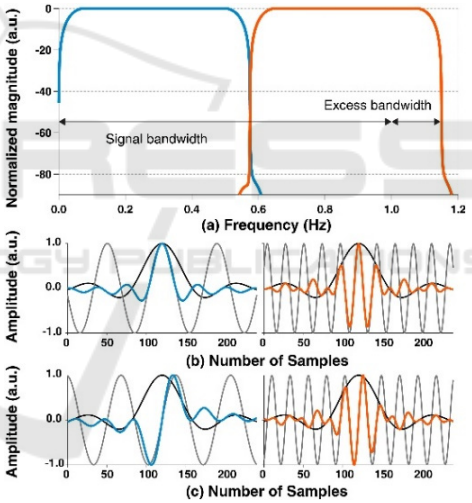

Figure 2: (a) shows frequency responses of the SRRC filters for m = 2. The impulse responses for each sub-band for the real and imaginary part of the signal are in Fig. 2(b) and 2(c), respectively. Note the excess bandwidth for β = 0.15.

Fig. 2(a) illustrates filters' frequency responses for 2-CAP system for each sub-band, the time domain equivalents for the real and imaginary signal are depicted in their respective colours in Fig. 2(b) and 2(c), respectively.

3 RESULTS

In this paper, we investigate the m-CAP VLC system

performance under various filters parameters for the first time. The order of QAM modulation format is set to M = 16, while the number of sub-bands is m = {2, 5, 10}. As mentioned before, the signal bandwidth B and the LED 3-dB modulation bandwidth f_c are 1 Hz and 0.5 Hz, respectively.

We adopted two different approaches and set the parameters to stay in consistency with recent literature (Olmedo et al., 2014; Haigh et al., 2015; Werfli et al., 2015):

- Fixing the roll-off factor $\beta = 0.15$ and varying the filters length in the range of $2 \leq L_f \leq 16$ symbols
- Fixing the filter length L_f = 10 symbols and varying the roll-off factor in the range of $0 \leq \beta \leq 1$

3.1 Fixed Roll-off Factor

The number of filter taps is crucial for the system performance, since the implementation of the m-CAP modulation on a digital signal processor (DSP) such as an FPGA is limited by the available hardware resources. Dividing the signal bandwidth into m = 10 sub-bands requires 20 FIR filters at the transmitter part and a further 20 at the receiver. Thus, we investigate the BER performance of the system (see Fig. 1) for a range of L_f. The results are illustrated in Fig. 3(a)-(c) for E_b/N_0 = 10 dB (solid line, unfilled markers) and 20 dB (dashed line, filled markers) for each subcarrier (denoted as s) while β is fixed to 0.15. It can be seen that increasing L_f for low values of E_b/N_0 improves the BER performance by one order of magnitude in the best case for m = 5 and 10, while for m = 2 the improvement in BER is almost negligible. With higher order subcarriers such a performance enhancement due to the increased filter lengths is considerably reduced. This is caused by the attenuation outside of the modulation bandwidth. On the other hand, when higher E_b/N_0 is employed, the BER target is easily met for low order subcarriers for m = 5 (s = 1, 2, 3) and 10 (s = 1, 2, …, 8). However, note: the 2-CAP system completely fails to meet the BER limit in the whole considered range of L_f due to a wider bandwidth requirement, which is five times higher that of 10-CAP. The performance improvement is further illustrated in Fig. 3(d), where

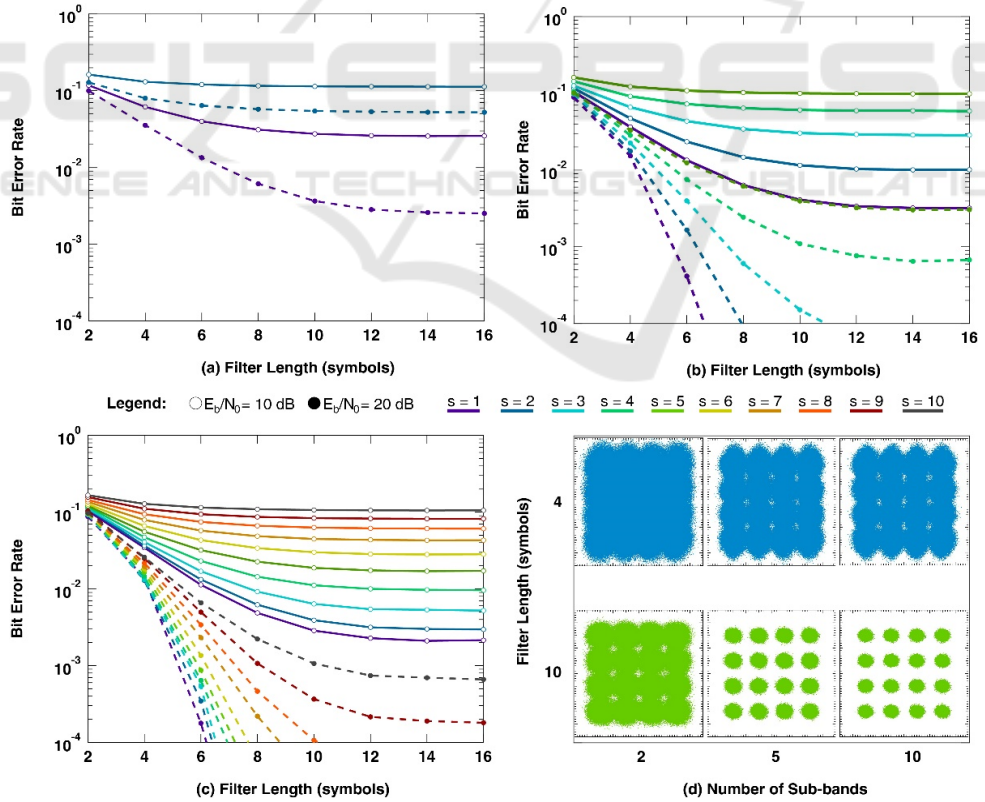

Figure 3: BER performance for a range of L_f for different values of m is shown in (a)-(c). Two different values of E_b/N_0 = 10 and 20 dB were considered. The performance improvement is most significant for low order subcarriers for m = 5 and 10. When employing m = 2, BER target is never met. Received constellation diagrams are shown in Fig. 3(d) for each m for the subcarrier s = 1 and two filter lengths L_f = 4 and 10 at E_b/N_0 = 20 dB.

constellation diagrams for the subcarrier s = 1 for each value of m and filter lengths L_f = 4 and 10 are illustrated.

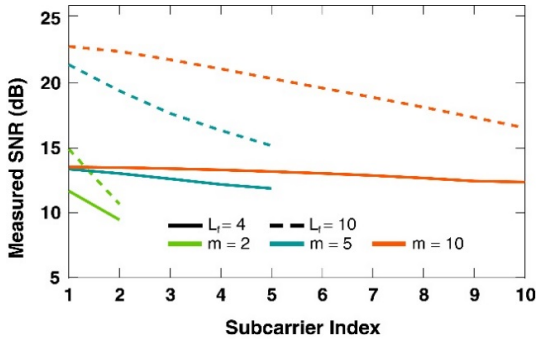

Figure 4: The measured SNR for each subcarrier for a range of m and L_f = 4 and 10 at E_b/N_0 = 20 dB. Increasing the number of subcarriers increases the differences between measured SNR when using short (4 symbols) and long (10 symbols) filter.

The highest value of L_f to attain the BER target is 12, which is reflected in Fig. 3(b) and 3(c) for s = 3 and 8, respectively. This introduces an important result: utilization of longer filters (i.e., L_f > 12) for higher order subcarriers is impractical since no additional BER improvement is achieved. Fig. 4 illustrates the measured signal-to-noise (SNR) ratio for the range of m = {2, 5, 10} for L_f = 4 (solid line) and 10 (dashed line) at E_b/N_0 = 20 dB. By utilization of higher order m-CAP system we can experience increasing SNR gain when compared short and long filter. The SNR gain for the last subcarrier is then ~ 1.2 dB, ~ 3.3 dB and ~ 4.1 dB for m = 2, 5 and 10, respectively.

3.2 Fixed Filter Length

The roll-off factor β determines the excess of bandwidth, as mentioned. Thus, using lower values of β is appropriate to save the bandwidth employed in the system. In contrast, it is also possible to increase the system BER performance at the cost of the bandwidth.

Fig. 5(a)-(c) illustrate the BER performance of the system for a range of β for all values of m under E_b/N_0 of 10 dB (solid line, unfilled markers) and 20 dB (dashed line, filled markers) and for L_f = 10.

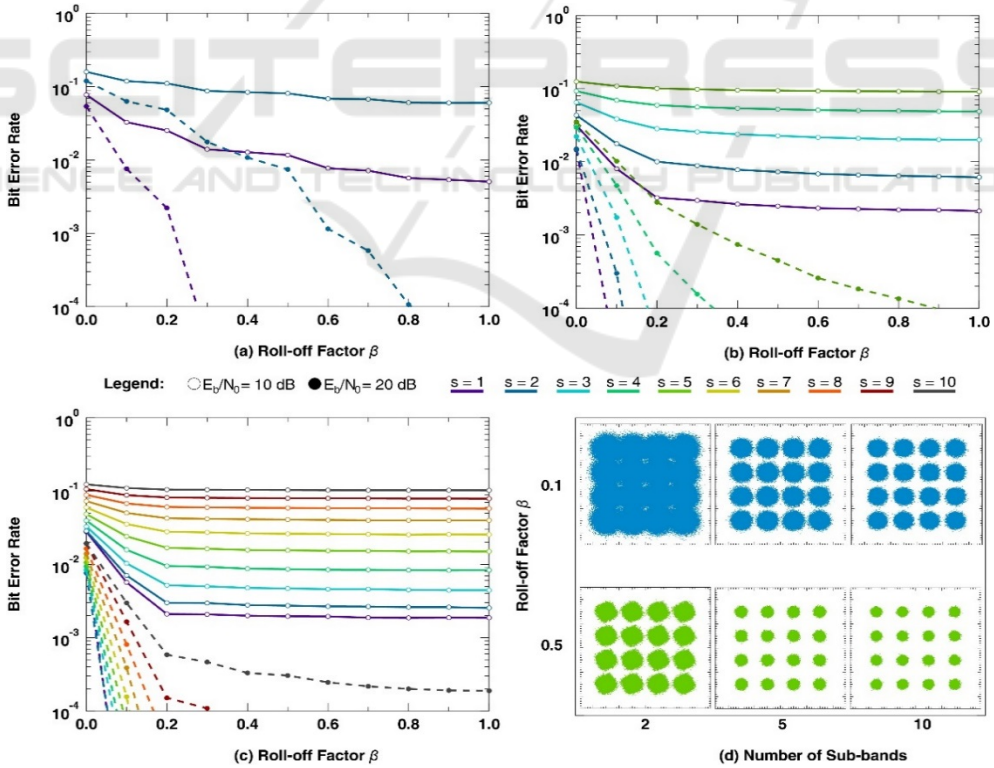

Figure 5: BER performance for a range of β for each m is shown in (a)-(c). Two different values of E_b/N_0 = 10 and 20 dB were considered. Only slight increment of β improves the BER performance for low order subcarriers for m = 5 and 10. When employing m = 2, BER target is met for β = 0.3 and 0.8 for the subcarriers s = 1 and s = 2, respectively. Received constellation diagrams are shown in Fig. 5(d) for each m for the subcarrier s = 1 and two values of β = 0.1 and 0.5 at E_b/N_0 = 20 dB showing improved performance while increasing β.

The results show that the performance enhancement of each subcarrier is negligible with increasing β at E_b/N_0 = 10 dB (maximum one order of magnitude for low order subcarriers for m = 5 and 10). Surprisingly, setting β > 0.2 does not bring any additional improvement and BER curves have almost constant character for m = 5 and 10.

On the other hand, only a slight increment of β improves the BER performance significantly for lower order subcarriers at higher E_b/N_0 (i.e., 20 dB). The BER target is achieved by almost all subcarriers, except the last subcarriers, i.e., s = 4, 5 and for m = 5 and s = 8, 9 for m = 10, respectively, for β = 0.2. This is remarkable improvement when compared to E_b/N_0 of 10 dB even in the cost of a slightly increased bandwidth excess. Moreover, both subcarriers in the 2-CAP system attain to meet the BER target when using β = 0.3 and 0.8 for s = 1 and 2, respectively. This is in contrast with Fig. 3(a) where both subcarriers failed to achieve the BER target even for longer FIR filters. Fig. 5(d) illustrates received constellation diagrams for s = 1 for each value of m = {2, 5, 10} and β = 0.1 and 0.5 showing the performance improvement while increasing β.

The measured SNR for each subcarrier for the range of m for β = 0.1 (dashed line) and 0.5 (solid line) at E_b/N_0 = 20 dB is illustrated in Fig. 6. It is clear that the SNR gain for β = 0.5 is decreased when the higher order subcarriers are deployed. For instance, the SNR gain for the last subcarrier is ~ 4.5 dB, ~ 3.5 dB and ~ 2 dB for m = 2, 5 and 10, respectively, which is in contrast with previous measurements in Fig. 4. This is caused by the higher bandwidth requirements for β = 0.5, which results in larger attenuation acting on the individual subcarriers.

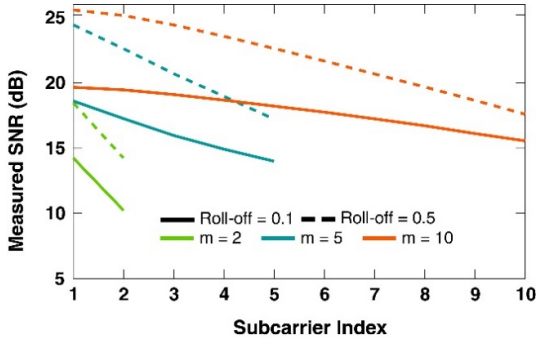

Figure 6: The measured SNR for each subcarrier for a range of m and β = 0.1 and 0.5 at E_b/N_0 = 20 dB. Increasing the number of sub-bands reduces the SNR gain for higher order subcarriers when employing a higher roll-off factor β.

4 CONCLUSIONS

In this paper we investigated the m-CAP performance under varying filter parameters such as filter length and roll-off factor. Increasing both parameters considerably improves the BER performance of the system. The main result for this analyses towards real implementation is that deploying L_f > 12 symbols is impractical, since no more performance improvement can be achieved for m = 5 and 10. The 2-CAP system utilization is not recommended since it failed to attain BER target for any value of L_f. The roll-off factor β has significant impact on the system performance especially at higher E_b/N_0. The BER target was achieved for the range of values of β for all the subcarriers in the tested system except the highest subcarrier of m = 10.

For future work, we will implement m-CAP system in FPGA for further investigation of filters' impact on the system performance for the cases of limited hardware resources.

ACKNOWLEDGEMENTS

This work was supported by CTU grant SGS14/190/OHK3/3T/13.

REFERENCES

Zvanovec, S., Chvojka, P., Haigh, P.A., Ghasemlooy, Z., Visible light communications towards 5G, *Radioengineering,* vol. 24, April 2015.

Armstrong, J.; Sekercioglu, Y.; Neild, A., Visible light positioning: a roadmap for international standardization, in *Communications Magazine, IEEE*, vol.51, no.12, pp.68-73, December 2013.

Haigh, P. A., Ghassemlooy, Z., Rajbhandari, S., Papakonstantinou, I., Popoola W., Visible Light Communications: 170 Mb/s Using an Artificial Neural Network Equalizer in a Low Bandwidth White Light Configuration, *Lightwave Technology, Journal of,* vol. 32, pp. 1807-1813, 2014.

Bykhovsky, D., Arnon S., An Experimental Comparison of Different Bit-and-Power-Allocation Algorithms for DCO-OFDM, *Lightwave Technology, Journal of,* vol., vol. 32, pp. 1559-1564, Apr 15 2014.

Mesleh, R.; Elgala, H.; Haas, H., LED nonlinearity mitigation techniques in optical wireless OFDM communication systems, in *Optical Communications and Networking, IEEE/OSA Journal of* , vol.4, no.11, pp.865-875, Nov. 2012.

Wu, F.M., Lin, C.T., Wei. C.C., Chen, C.W., Huang, H.T., Ho, C.H., 1.1-Gb/s White-LED-Based Visible Light Communication Employing Carrier-Less Amplitude

and Phase Modulation, in *Photonics Technology Letters, IEEE* , vol.24, no.19, pp.1730-1732, Oct.1, 2012.

Wei, J.L., Ingham, J.D., Cunningham, D.G., Penty, R.V., White, I.H., Performance and Power Dissipation Comparisons Between 28 Gb/s NRZ, PAM, CAP and Optical OFDM Systems for Data Communication Applications, in *Lightwave Technology, Journal of* , vol.30, no.20, pp.3273-3280, Oct.15, 2012.

Wu, F.M., Lin, C.T., Wei, C.C., Chen, C.W., Chen, Z.Y., Huang, H.T., Sien Chi, Performance Comparison of OFDM Signal and CAP Signal Over High Capacity RGB-LED-Based WDM Visible Light Communication, in *Photonics Journal, IEEE* , vol.5, no.4, pp.7901507-7901507, Aug. 2013.

Olmedo, M.I., Tianjian, Z., Jensen, J.B., Qiwen, Z.,Xiaogeng X., Popov, S., Monroy, I.T., Multiband Carrierless Amplitude Phase Modulation for High Capacity Optical Data Links, in *Lightwave Technology, Journal of* , vol.32, no.4, pp.798-804, Feb.15, 2014.

Haigh, P.A., Burton, A., Werfli, K., Le Minh, H., Bentley, E., Chvojka, P., Popoola, W.O., Papakonstantinou, I., Zvanovec, S., A Multi-CAP Visible-Light Communications System With 4.85-b/s/Hz Spectral Efficiency, in *Selected Areas in Communications, IEEE Journal on* , vol.33, no.9, pp.1771-1779, Sept. 2015.

Haigh, P.A., Chvojka, P., Zvanovec, S., Ghassemlooy, Z., Son T.L., Kanesan, T., Giacoumidis, E., Doran, N.J., Papakonstantinou, I., Darwazeh, I., "Experimental verification of visible light communications based on multi-band CAP modulation," in *Optical Fiber Communications Conference and Exhibition (OFC), 2015* , vol., no., pp.1-3, 22-26 March 2015.

Haigh, P.A., Thai Le. S., Zvanovec, S., Ghassemlooy, Z., Pengfei L., Tongyang X., Chvojka, P., Kanesan, T., Giacoumidis, E., Canyelles-Pericas, P., Minh H.L., Popoola, W., Rajbhandari, S., Papakonstantinou, I., Darwazeh, I., Multi-band carrier-less amplitude and phase modulation for bandlimited visible light communications systems, in *Wireless Communications, IEEE* , vol.22, no.2, pp.46-53, April 2015.

Werfli, K., Haigh, P.A., Ghassemlooy, Z., Chvojka, P., Zvanovec, S., Rajbhandari, S., Long, S., Multi-band carrier-less amplitude and phase modulation with decision feedback equalization for bandlimited VLC systems, in *Optical Wireless Communications (IWOW), 2015 4th International Workshop on* , vol., no., pp.6-10, 7-8 Sept. 2015.

Haigh, P.A., Aguado, A., Ghassemlooy, Z., Chvojka, P., Werfli, K., Zvanovec, S., Ertunc, E., Kanesan, T., Multi-band carrier-less amplitude and phase modulation for highly bandlimited visible light communications — Invited paper, in *Wireless Communications & Signal Processing (WCSP), 2015 International Conference on* , vol., no., pp.1-5, 15-17 Oct. 2015.

Junwen Z., Jianjun Y., Fan L., Nan C., Ze D., Xinying L., 11 × 5 × 9.3Gb/s WDM-CAP-PON based on optical single-side band multi-level multi-band carrier-less amplitude and phase modulation with direct detection, Opt. Express 21, 18842-18848 (2013).

4.4 On m-CAP Performance with Differente Pulse Shaping Filter Parameters for Visible Light Communications

This chapter is a version of the published manuscript:

P. Chvojka, K. Werfli, S. Zvanovec, P. A. Haigh, V. Hubata Vacek, P. Dvorak, P. Pesek and Z. Ghassemlooy, "On m-CAP Performance with Different Pulse Shaping Filters Parameters for Visible Light Communications," in *IEEE Photonics Journal*, vol. 9, no. 5, pp. 1-12, 2017.

Connection with my Ph.D. thesis:

Building on the previous work reported in Section 4.3, we experimentally investigate the trade-off between the m-CAP scheme performance, measured data rates and computational complexity which is given especially by the filters utilized at the transmitter and receiver. We demonstrate the benefits of low order m-CAP systems having much lower complexity than higher order schemes. However, to design a VLC link supporting the highest spectral efficiency and data rate simultaneously, m-CAP links with $m \geq 6$ are recommended. The measured spectral efficiency of the experimental can attain nearly 6 b/s/Hz. The reported results meet task **T4** and finalize goal **G1**.

IEEE Photonics Journal
An IEEE Photonics Society Publication

Open Access

On the *m*-CAP Performance with Different Pulse Shaping Filters Parameters for Visible Light Communications

Volume 9, Number 5, October 2017

Petr Chvojka
Khald Werfli
Stanislav Zvanovec
Paul Anthony Haigh
Vaclav Hubata Vacek
Petr Dvorak
Petr Pesek
Zabih Ghassemlooy

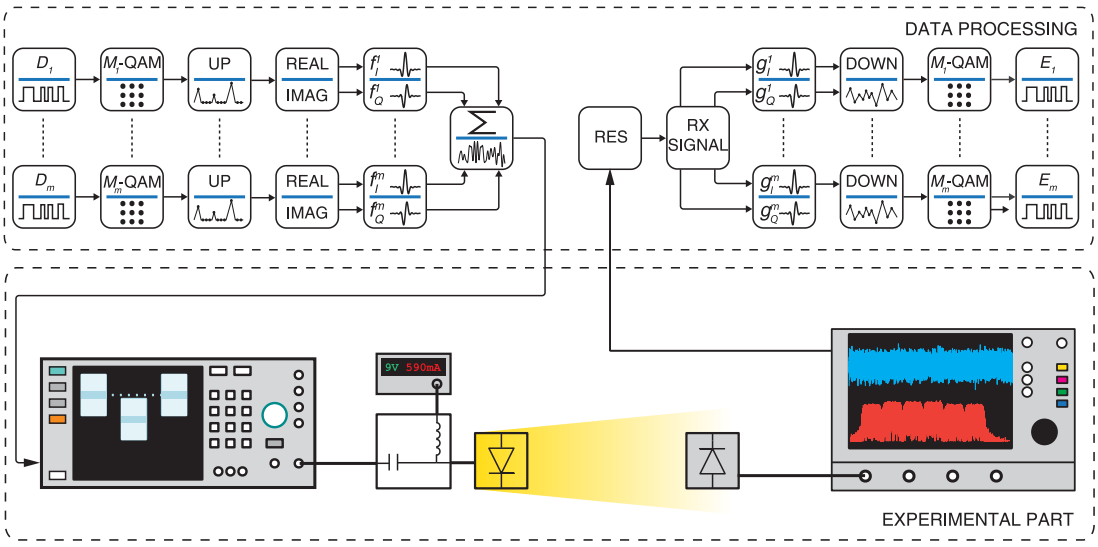

DOI: 10.1109/JPHOT.2017.2749203
1943-0655

On the *m*-CAP Performance with Different Pulse Shaping Filters Parameters for Visible Light Communications

Petr Chvojka,[1] Khald Werfli,[2] Stanislav Zvanovec,[1] Paul Anthony Haigh,[3] Vaclav Hubata Vacek,[1] Petr Dvorak,[1] Petr Pesek,[1] and Zabih Ghassemlooy[2,4]

[1]Department of Electromagnetic Field, Faculty of Electrical Engineering, Czech Technical University in Prague, Prague 16627, Czech Republic
[2]Optical Communications Research Group, Northumbria University, Newcastle upon Tyne NE1 8ST, U.K.
[3]Department of Electronic and Electrical Engineering, University College London, London WC1E 6BT, U.K.
[4]QIEM, Chinese Academy of Sciences, Fujian 350002, China

DOI:10.1109/JPHOT.2017.2749203

Manuscript received August 11, 2017; revised August 31, 2017; accepted August 31, 2017. Date of publication September 4, 2017; date of current version September 27, 2017. This work was supported in part by GACR 17-17538S, in part by CTU Grant SGS17/182/OHK3/3T/13, and in part by the U.K. ESPRC Grant EP/P006280/1: Multifunctional Polymer Light-Emitting Diodes with Visible Light Communications (MARVEL). Corresponding author: Petr Chvojka (e-mail: chvojpe8@fel.cvut.cz).

Abstract: In pulse shaping filters, parameters such as the roll-off factor and the symbol span, which determine the overall performance, are of great importance when implementing a real-time system due to limited hardware resources. In this paper, we experimentally investigate a multiband carrier-less amplitude and phase (*m*-CAP) visible light communications (VLC) system employing such filters and assess the link performance for a range of filter lengths and show the relationship between the system data rate (or spectral efficiency) and computational complexity. We show that lower order *m*-CAP can offer the same system performance as higher order systems while offering much lower computational complexity. By optimizing the filter parameters and the order m of an *m*-CAP VLC link, we achieve the largest improvement in the data rate and bandwidth efficiency of 9.69% and 40.43%, respectively, when compared with 2- and 8-CAP. We also show that the *m*-CAP VLC link with $m \geq 6$ can be designed with the same filter parameters to demonstrate a link with both the highest data rate and spectral efficiency simultaneously in contrast to lower order systems.

Index Terms: Multiband carrier-less amplitude and phase modulation, pulse shaping filters, visible light communications.

1. Introduction

Recently, radio frequency (RF) based wireless spectrum has become a valuable commodity due to the exponentially increasing demand for very high-speed internet access [1]. As a result, spectrum congestion, which affects the availability of high-speed internet services, has become an issue that needs to be addressed [2]. Optical wireless communications (OWC), which is most suitable for indoor environments, is an alternative and complementary technology to RF, appropriate to overcome spectral challenges offering unregulated and high bandwidth (in the orders of THz). Over the last decade, visible light communications (VLC), as a part of OWC, has undergone rapid

development, exploiting advantages from solid-state lighting (SSL) technologies with high-speed switching capabilities [2]. VLC utilizes white light-emitting diodes (LEDs) to provide illumination and high-speed data transmission simultaneously for a range of applications including broadcasting, indoor positioning, and vehicular or underwater communications [2]. Despite the benefits of LEDs (i.e., energy efficiency and longer lifetime), they introduce a major system drawback due to the very low modulation bandwidths available, in the order of few MHz [2]. This impediment is caused by the long recombination times of cerium-doped yttrium aluminium garnet (Ce:YAG) phosphors used for colour conversion to create a white light.

The vast majority of studies have focused on implementation of advanced techniques to achieve higher data rates and spectrally efficient communication links such as: *i*) blue filtering that suppresses the slow phosphor layer; thus increasing the LED bandwidth up to 20 MHz [3], *ii*) pre- and post-equalization [4], [5]; *iii*) utilizing multiple LEDs via wavelength-division multiplexing (WDM) and spatial-multiplexing known as multiple-input multiple-output (MIMO) [6]; *iv*) advanced modulation schemes such as carrier-less amplitude and phase modulation (CAP) [7] and orthogonal frequency division multiplexing (OFDM) [8], [9].

The modulation formats outlined above provide a straightforward approach for increasing the link capacity, especially in bandlimited environments. Recently, optical OFDM VLC links with data rates $>$ 5 Gb/s based on a single blue μLED and WDM technique have been reported in [10] and [11], respectively. The key advantage of OFDM lies in the possibility to optimise the system performance based on the channel parameters by means of bit- and power-loading algorithms [12]. On the other hand, the main drawback of OFDM is the high peak-to-average power ratio (PAPR) due to the summation of a high number of subcarrier signals to high signal peaks [13], making OFDM systems sensitive to the devices with the nonlinear electro-optics characteristics such as amplifiers and LEDs. Many techniques have been proposed to reduce PAPR including employing pilot symbols (PS) [14], linearization of the LED response [15], or encoding transmit data symbols including DC biasing [16].

As an alternative solution, CAP is conceptually simpler and has lower PAPR compared with OFDM [17]. However, the CAP modulation scheme requires a flat frequency response, which is seldom available in VLC, in order to effectively implement it. To increase the link performance of systems with a non-flat frequency response, a complex equalizer is needed [18]. In [19] a solution to overcome the flat band requirement was introduced by the way of splitting the available signal bandwidth into *m* sub-bands (or subcarriers) thus resulting in multiband CAP (*m*-CAP). Such an approach enables to relax the flat-band response requirement by allocating a narrow bandwidth to individual subcarriers, thus the frequency flatness can be easily achieved. Moreover, it enables bit- and power-loading by adjusting the number of bits-per-symbol or the power level of individual subcarriers. Note that, increasing *m* leads to improvement of the transmission speed due to the lower attenuation of each subcarrier induced by an LED frequency response as was shown in [20]. In *m*-CAP schemes finite impulse response (FIR) pulse shaping filters are utilized to generate carrier frequencies introducing most of the complexity. Thus, the multiband approach can significantly increase the computational complexity of the system by requiring 2*m* FIR filters at the transmitter and additional 2*m* FIR filters at the receiver, thus resulting in 4*m* filters in total.

In our previous works, we investigated *m*-CAP VLC performance in VLC via numerical simulations [21], [22] and experimental measurements [20], [23]. Firstly, in [19] we showed an experimental VLC link over a 1 m distance with a high spectral efficiency 4.85 b/s/Hz, demonstrating promising results for the following research. In our most recent works, *m*-CAP was tested using MATLAB simulations. For instance, a new concept of *m*-CAP utilizing unequally distributed subcarriers was introduced showing both reduced computational complexity and higher achievable data rates [24], [25]. However, such a scheme has greater requirements for a flat-band response due to the high bandwidth allocated to the first subcarrier, which is set within passband region of an LED. The system performance in a highly bandlimited environment was investigated in [26], and it was shown that *m*-CAP could significantly outperform a traditional 1-CAP scheme in terms of the achievable data rate (by up to 40%). Nevertheless, none of these reports did consider the length of the pulse shaping filters. This is because filters were not a crucial in the investigation, and since they

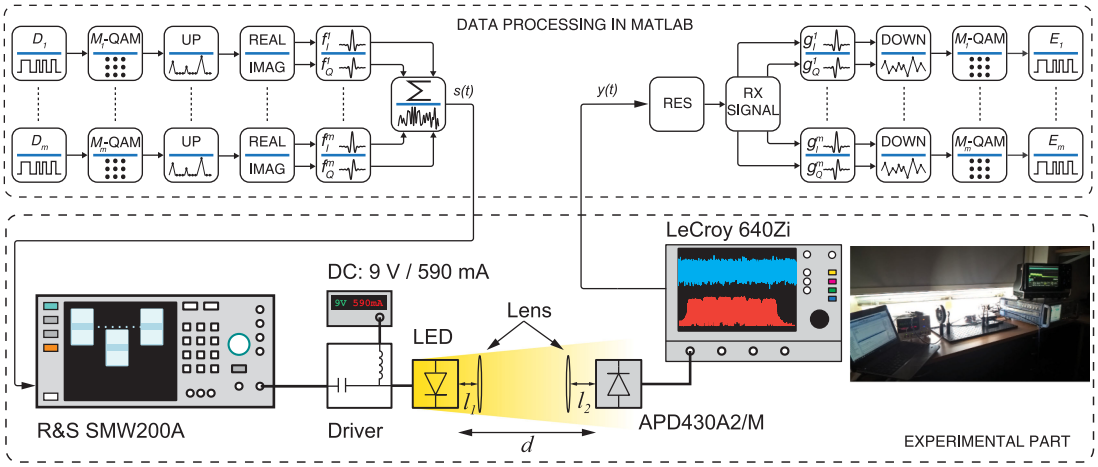

Fig. 1. The schematic block diagram of the *m*-CAP VLC system. Inset is a photo of the experimental link. Note that, 'UP', 'RES' and 'DOWN' blocks refers to up-sampling, resampling and down-sampling, respectively.

were offline systems with no practical limits on the number of filter taps that could be used, which is an issue in real time systems. However, in a real implementation, the filter parameters such as the roll-off factor and the symbol span significantly impact the system performance [27]. Increasing both parameters leads to a lower bit error rate (BER) performance at the cost of increased computational complexity, which is a major issue in the implementation of *m*-CAP on field programmable gate arrays (FPGAs) due to the limited hardware resources.

Therefore, in this paper, we build on our previous work in [27] and experimentally investigate in considerable detail, the performance of the *m*-CAP VLC system for a range of FIR filter conditions to understand the physical performance of the system. We set the filter parameters within given ranges in terms of the roll-off factor β, symbol span L_s for the set of subcarriers m, and demonstrate how these parameters influence both the measured bit rates and spectral efficiencies. We focus on the dependence of data rate and spectral efficiency on the filter parameters and system complexity, then show how these parameters trade-off enables to achieve an optimum *m*-CAP VLC hardware implementation. The paper focuses on the *m*-CAP VLC link performance with no equalisation schemes, although further performance gains could be expected with equalization.

2. System Setup

The schematic block diagram of the system under test is illustrated in Fig. 1, showing both the *m*-CAP generation in MATLAB and, the experimental set-up with a photo from the experiment inset. Firstly, a $2^{15} - 1$ pseudorandom binary sequence (PRBS) D_m is generated for each subcarrier and the bits are then mapped onto an *M*-ary quadrature amplitude modulation (*M*-QAM) constellation, where $M = 2^k$ is the order of QAM and k is the number of bits/symbol. The data is up-sampled using the normal zero-padding method with the following number of zeros-per-symbol, according to [19], [20]:

$$n_s = 2 \cdot \lceil 2m(1+\beta) \rceil \tag{1}$$

where $\lceil \cdot \rceil$ is the ceiling function. Next, the data is split into the real (in-phase *I*) and imaginary (quadrature *Q*) parts prior to being passed through the pulse shaping square-root-raised cosine (SRRC) filters. The impulse responses of the transmit filters are given as a product of the SRRC filter impulse responses and sine (*Q*) and cosine (*I*) waves forming a Hilbert pair for the *I* and *Q*

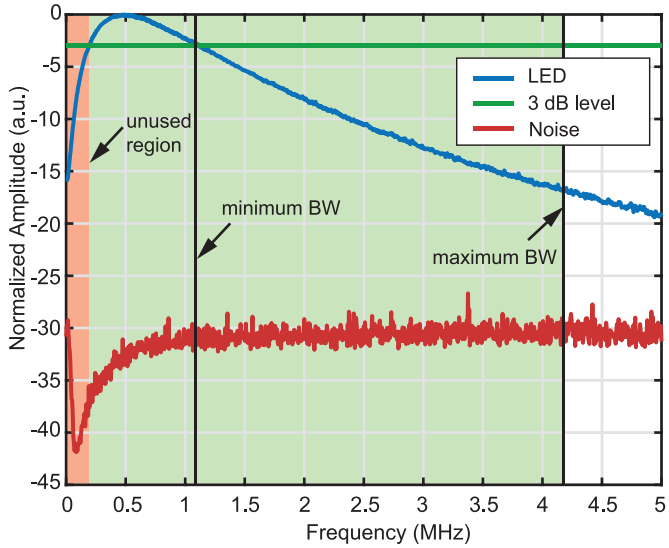

Fig. 2. The measured LED frequency response showing the unused low frequencies and minimum and maximum available signal bandwidths. Also shown the noise spectrum.

filters, respectively as given by [20], [27]:

$$f_I^m(t) = \frac{\sin(\gamma(1-\beta)) + 4\beta\frac{t}{T_s}\cos(\gamma\delta)}{\gamma[1-(4\beta\frac{t}{T_s})^2]}\cos[\gamma(2m-1)\delta] \tag{2}$$

for the *I* filter and

$$f_Q^m(t) = \frac{\sin(\gamma(1-\beta)) + 4\beta\frac{t}{T_s}\cos(\gamma\delta)}{\gamma[1-(4\beta\frac{t}{T_s})^2]}\sin[\gamma(2m-1)\delta] \tag{3}$$

for the *Q* filter, where T_s is the symbol duration, $\gamma = \pi t/T_s$ and $\delta = 1+\beta$. The output signal of the *m*-CAP transmitter is given by [20], [27]:

$$s(t) = \sqrt{2}\sum_{n=1}^{m}(s_I^n(t)\otimes f_I^n(t) - s_Q^n(t)\otimes f_Q^n(t)), \tag{4}$$

where $s_I^n(t)$ and $s_Q^n(t)$ are *I* and *Q* *M*-QAM symbols for the n^{th} subcarrier and $\otimes$ represents the time domain convolution.

The output signal $s(t)$ is loaded into a Rohde & Schwarz SMW200A vector signal generator (with the maximum sampling rate 200 MSa/s) and passed through the custom-built LED driving circuit for intensity modulation of the LED. We used the commercially available LED (OSRAM Golden Dragon) biased at $\sim$ 590 mA to ensure the operation in its most linear region. The measured LED frequency response is illustrated in Fig. 2 showing the 3 dB modulation bandwidth at 1.2 MHz (with a cut-on frequency of 0.2 MHz). For the experiment, we shifted the signal in the frequency domain by 0.2 MHz due to the significant signal distortion caused by the non-flat frequency response of the LED (denoted by the red region in Fig. 2). By varying β from 0.1 to 1, the signal bandwidth requirements are changed according to $B_{tot} = B_{sig}(1+\beta)$, where B_{sig} is the signal bandwidth set in this work to $\{1, 2\}$ MHz. Thus, the minimum and maximum total signal bandwidth B_{tot} were 1.1 MHz and 4.2 MHz, respectively, as highlighted in Fig. 2. The reason for choosing such a low B_{sig} is to ensure the optimal system performance during the measurement even for the maximum B_{tot}, which is $\sim$ 4 times higher than minimum B_{tot}.

The transmission distance d between the LED and the avalanche photodetector (PD) (Thorlabs APD430A2/M) based receiver was set to 1 m. Two 25.4 mm biconvex lenses were placed at distances of $l_1 = 0.25$ m and $l_2 = 0.35$ m from the LED and the PD, respectively, for beam collimation

TABLE 1
SNR Thresholds for BER Target 10^{-3}

k	**1**	**2**	**3**	**4**	**5**
SNR (dB)	6.8	9.8	14.4	16.5	20.6
k	**6**	**7**	**8**	**9**	
SNR (dB)	22.6	26.5	28.4	32.3	

and focusing, see Fig. 1. At the receiver, the regenerated electrical signal was captured using real time oscilloscope (LeCroy WaveRunner Z640i with 2 GSa/s sampling rate) for further offline data processing in MATLAB.

The received signal is given as:

$$y(t) = \Re G\, s(t) \otimes h(t) + n(t), \tag{5}$$

where $h(t)$ is the channel impulse response, $\Re$ and G are the PD's responsivity and gain, respectively and $n(t)$ is the additive white Gaussian noise (AWGN) with zero mean and variance of $N_0/2$, where N_0 is power spectral density. The received signal $y(t)$ was resampled to have the same sampling frequency as $s(t)$ and passed through time-reversed receive filters g_I (in-phase) and g_Q (quadrature) matched to the transmit filters as $g_I^m(t) = f_I^m(-t)$ and $g_Q^m(t) = f_Q^m(-t)$. Following down-sampling and demodulation, the *M*-QAM symbols are recovered and the received bits are compared with the transmitted data and the link BER is determined by aggregating BER values from every subcarrier. To maximize system performance, a bit-loading technique was applied as follows. A binary phase shift keying (BPSK) pilot signal was transmitted to measure the root-mean-square error vector magnitude (EVM_{RMS}) for individual subcarriers. Based on the signal to noise ratio (SNR), defined as $SNR = 20\log_{10}(EVM_{RMS})$, the appropriate number of bits/symbol $k = \{1, 2, 3, 4, 5, 6, 7, 8, 9\}$ was loaded into each subcarrier based on the SNR threshold levels listed in Table 1 for a target BER of 10^{-3}, which is slightly below the forward error correction (FEC) limit with an overhead of 7%, and in consistency with our previous works [20], [21], [23]. The SNR thresholds can be found in the literature [28]. The example of the measured SNR against the subcarrier index for $L_s = 10$, $\beta = 0.2$ and $m = \{2, 4, 6, 8, 10\}$ for a range of *M*-QAM is illustrated in Fig. 3. Also depicted are SNR threshold levels for *M*-QAM modulations.

3. Results and Discussion

As previously outlined, the goal of this paper is to show the relationship between the FIR filter parameters and the VLC system performance. The length (number of taps) of the filters, which introduces major system complexity, is given by three main parameters: *(i)* $L_s = \{2, 4, 6, 8, 10\}$; *(ii)* $\beta = \{0.1, 0.2, 0.3, 0.4, 0.5, 0.6, 0.7, 0.8, 0.9, 1\}$; and *(iii)* $m = \{2, 4, 6, 8, 10\}$. The reason for setting a value of L_s up to 10 is based on our previous research [27]. We showed that utilizing $L_s > 12$ is impractical due to no additional performance improvement. However, increasing L_s from 10 to 12 brings only slight enhancement in the system performance while system complexity is increased substantially. Thus, here we set $L_s = 10$ as a maximum analysed value. In the experiments described below, B_{sig} is set to 1 MHz unless otherwise stated. The achieved results are discussed in terms of the measured bit rate R_b, spectral efficiency η_{se} and filter length L_f (taps/filter) over the entire range of L_s and β. We will focus particularly on $m = \{2, 6, 8, 10\}$, detailed discussion on $m = 4$ will be limited due to their similar performances. The comparison with a 1-CAP system is not included here, since we have already shown in our previous reports that *m*-CAP significantly

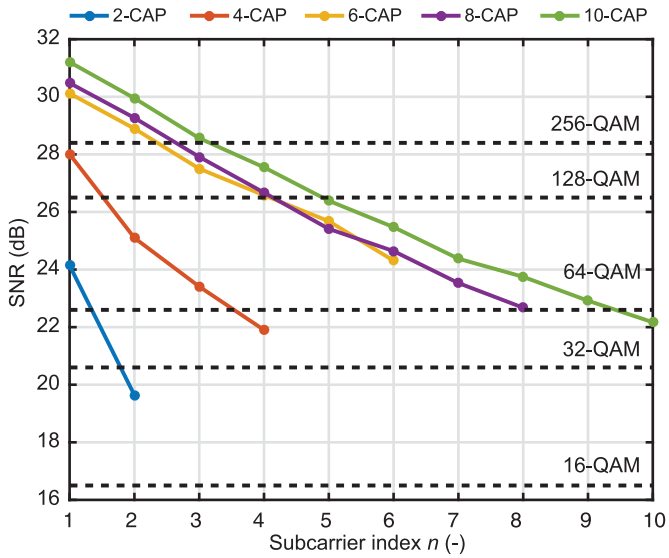

Fig. 3. The measured SNR against the subcarrier index using a BPSK pilot signal for $L_s = 10$, $\beta = 0.2$, $m = \{2, 4, 6, 8, 10\}$ and a range of *M*-QAM. Also depicted are SNR thresholds for different *M*-QAM signals (dashed line).

outperforms a 1-CAP scheme [20], [21], [26]. The achieved R_b was determined in the same manner as BER, i.e., as the sum of the transmission speeds from individual subcarriers.

3.1 2-CAP

The measured R_b, η_{se} and corresponding L_f are illustrated in Fig. 4(a), (b), and (c), respectively. Increasing both filter parameters L_s and β improves the measured R_b significantly from 1 Mb/s to 6.5 Mb/s (the highest R_b for 2-CAP in this work), thus having approximately the same impact on the measured R_b and η_{se}, see Fig. 4(a). However, the effect on η_{se} is different as can be seen from Fig. 4(b). For low values of $L_s = 4$ and $L_s = 2$, η_{se} is increased slowly or remains almost constant over the range of β, respectively. The effect of β is much more significant for $L_s > 4$ showing at first a rapid improvement in η_{se} up to 4.23 b/s/Hz in case of $\beta = 0.3$ and $L_s = 10$ (the highest η_{se} in 2-CAP) due to the higher bandwidth allocated to individual subcarriers, which are however not significantly attenuated by the LED response. Nevertheless, for $\beta > 0.3$ and > 0.5 and for $L_s = 10$ and 8, we notice degradation in the measured η_{se}. The performance degradation in η_{se} is caused by the increasing bandwidth requirement of the subcarriers, which are more prone to the frequency dependent attenuation caused by the LED frequency response. Moreover, the higher the bandwidth is the flat-band response approximation is decreased. It is clear from Fig. 4(a) and (b) that 2-CAP system can be designed either for the highest R_b or η_{se}, which introduces a substantial drawback in comparison to higher order *m*-CAP systems.

Fig. 4(c) illustrates the corresponding length of filters L_f as a function of β and for a range of L_s. Also shown are the received constellation diagrams for subcarriers n_1 and n_2 for the case of the most bandwidth efficient 2-CAP (i.e., $\beta = 0.3$, $L_s = 10$) with L_f of 120 taps/filter requirement. Note that, higher values of β and L_s will lead to increasing system complexity. As can be seen, L_f is increased more rapidly with L_s for a fixed value of β reaching up to ~ 5 times higher number of taps (for $\beta = 1$), in contrast to the case of a fixed L_s and increasing β where complexity raises up to ~ 1.6 times (for $L_s = 10$). Note, some parts of the individual curves remain constant over the range of β (e.g., from 0.3 to 0.5 for all values of L_s), which means that increasing β does not necessarily lead to longer filters. Therefore, higher computational complexity can be avoided, which is desirable in real time implementation of the link. This introduces an unexpected advantage over the higher order *m*-CAP systems. As will be seen later, the higher order *m*-CAP links (in this work

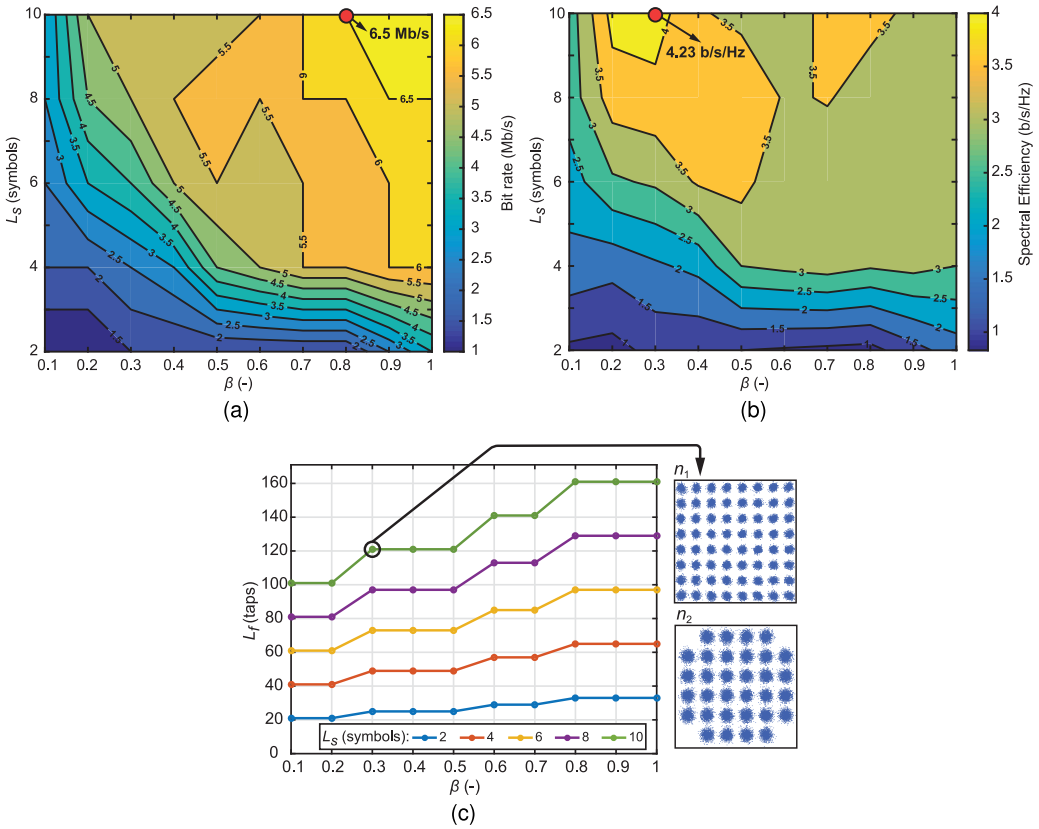

Fig. 4. Experimentally measured: (a) data rates, (b) spectral efficiencies and (c) corresponding filter lengths for 2-CAP with the received constellation diagrams for subcarriers n_1 and n_2 for $L_s = 10$ and $\beta = 0.3$. Note that a red dot in (a) and (b) denotes the highest measured data rate and spectral efficiency.

$m \geq 6$) can be optimized for both the highest bit rate and spectral efficiency using the same FIR filter parameters, i.e. the given value of L_s and β.

3.2 6-CAP

The measured R_b and η_{se} and appropriate L_f for 6-CAP against a range of β are depicted in Fig. 5(a), (b), and (c), respectively. As expected, both filter parameters have the same impact on the measured R_b as in the previous case, see Fig. 4(a). However, to achieve the optimal R_b (i.e., $>$ 6.5 Mb/s in this case) the values of $L_s \geq 4$ and $\beta \geq 0.6$ should be set, thus allowing a far greater degree of freedom in a system design compared to the 2-CAP system. For 6-CAP, the highest measured R_b is 7 Mb/s for $\beta = 0.3$ and $L_s = 10$. Note that, the impact of β is more distinctive for $L_s \geq 4$. At first, R_b is rapidly increasing to $>$ 6.5 Mb/s for $L_s = \{4, 6, 8, 10\}$ and corresponding $\beta = \{0.6, 0.4, 0.3, 0.2\}$. Further increase of β does not improve the link capacity significantly since the transmission speed is within the range of 6.5 to 7 Mb/s. However, we notice a slight decrease in R_b for $L_s = 4$ and $\beta > 0.6$.

The measured η_{se} as a function of β is illustrated in Fig. 5(b), showing similar behaviour to the 2-CAP system. Nevertheless, increasing both L_s and β have a higher impact on the system as higher improvement in η_{se} can be expected. The highest η_{se} of 5.83 b/s/Hz was measured for $\beta = 0.2$ and $L_s = 10$. For $L_s > 4$, increasing β beyond a certain value (e.g., $L_s = 6$ and $\beta > 0.5$) leads to a system performance degradation in terms of η_{se} as the individual subcarriers with higher bandwidth requirement are more prone to higher frequency attenuation. Fig. 5(c) depicts L_f as a function of β, for a range of L_s. The insets show the received constellation diagrams for the first n_1 and third n_3 subcarriers with $L_f = 300$ taps/filter for the most bandwidth efficient configuration of 6-CAP (i.e., with $\beta = 0.2$ and $L_s = 10$). Clearly, L_f increases with L_s for a given value of β. For instance, for

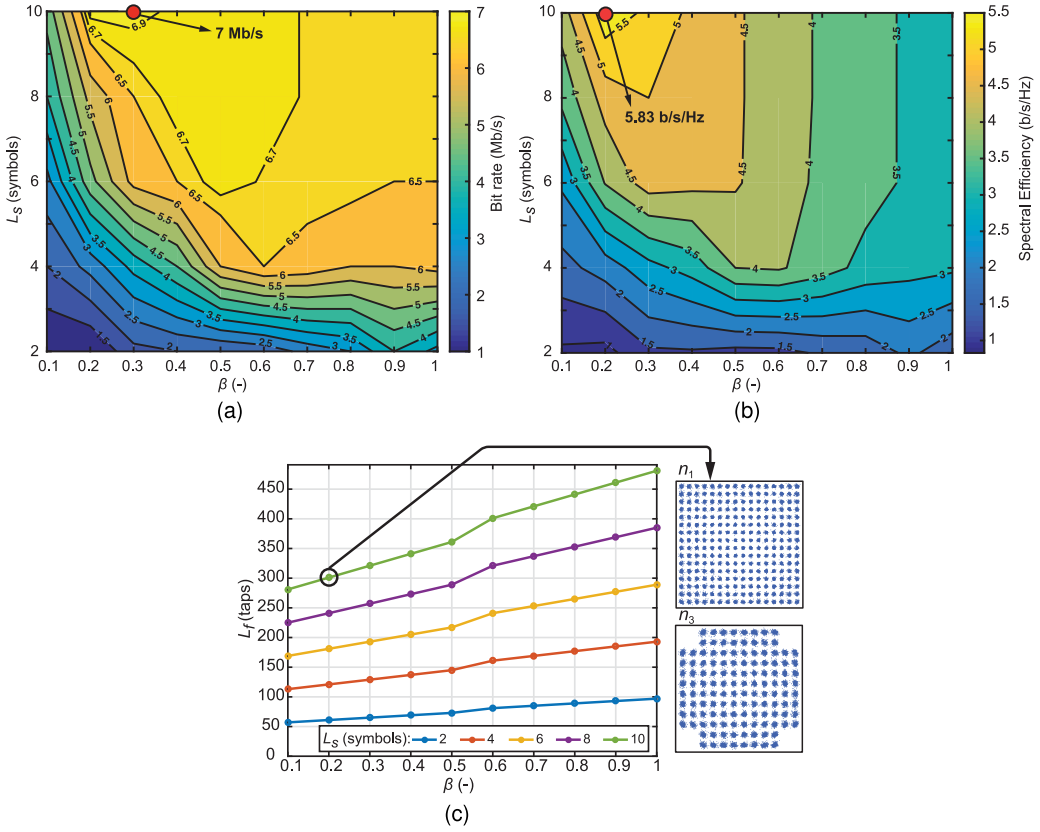

Fig. 5. Experimentally measured: (a) data rates, (b) spectral efficiencies and (c) corresponding filter lengths for 6-CAP with the received constellation diagrams for subcarriers n_1 and n_3 for $L_s = 10$ and $\beta = 0.2$. Note that a red dot in (a) and (b) denotes the highest measured data rate and spectral efficiency.

$\beta = 1$ the value of L_f is increased by over 4 times when L_s is changed from 2 to 10. In contrast to 2-CAP, where we can reach either R_b or η_{se} to be maximal, here a link with both the highest R_b and η_{se} can be can be designed for a single system setup, i.e. $\beta = 0.2$ and $L_s = 10$.

To illustrate further the performance of the system, B_{sig} was increased to 2 MHz and the measured R_b and η_{se} for 6-CAP are depicted in Fig. 6(a) and (b), respectively. As can be seen, the optimum R_b and η_{se} are observed within $0.3 < \beta < 0.6$ and $0.2 < \beta < 0.4$, respectively. Note that, the highest measured R_b and η_{se} are 11.33 Mb/s ($L_s = 10$ and $\beta = 0.4$) and 4.31 b/s/Hz ($L_s = 10$ and $\beta = 0.2$), respectively. By increasing B_{sig} we achieved $\sim$ 62% improvement in maximum measured R_b in 6-CAP system but the highest η_{se} decreased by $\sim$ 26%. This is due to the higher bandwidth of individual subcarriers, which are more prone to the attenuation outside the LED modulation bandwidth.

3.3 8-CAP

Fig. 7(a) and (b) illustrate the measured R_b and η_{se} for the 8-CAP system, respectively, showing a similar profile to the previous 6-CAP case. The optimal $R_b > 6.5$ Mb/s was measured in two separate regions. The ripple is caused by optimal subcarrier allocation within the LED frequency response. However, the significant performance degradation in η_{se} should be expected for the region where $\beta = \{0.7, 0.8, 0.9\}$, compared to lower β values, see Fig. 7(b). The highest $R_b = 7.14$ Mb/s and $\eta_{se} = 5.94$ b/s/Hz in 8-CAP (both are the highest measured values in this work for $B_{sig} = 1$ MHz) were measured for $L_s = 10$ and $\beta = 0.2$.

The corresponding filter tap requirement L_f as a function of L_s and β is illustrated in Fig. 7(c) with the received constellation diagrams for the first n_1 and fourth n_4 subcarriers inset. For the best performing filter setup, i.e. $L_s = 10$ and $\beta = 0.2$, a single filter requires $L_f = 401$ taps/filter, which

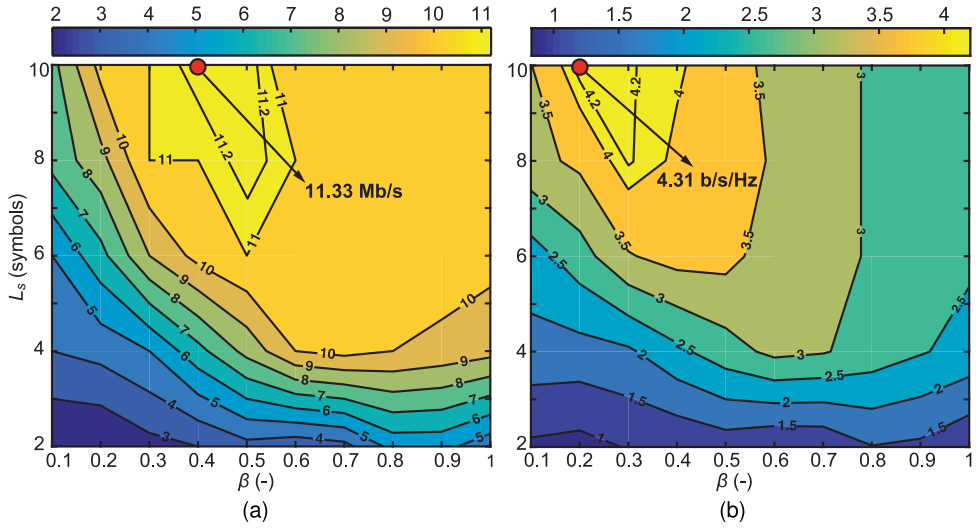

Fig. 6. The measured: (a) bit rate and (b) spectral efficiency for 6-CAP link for $B_{sig} = 2$ MHZ. Compared to $B_{sig} = 1$ MHz, higher data rate and lower bandwidth efficiency were measured. Note that a red dot in (a) and (b) denotes the highest measured data rate and spectral efficiency.

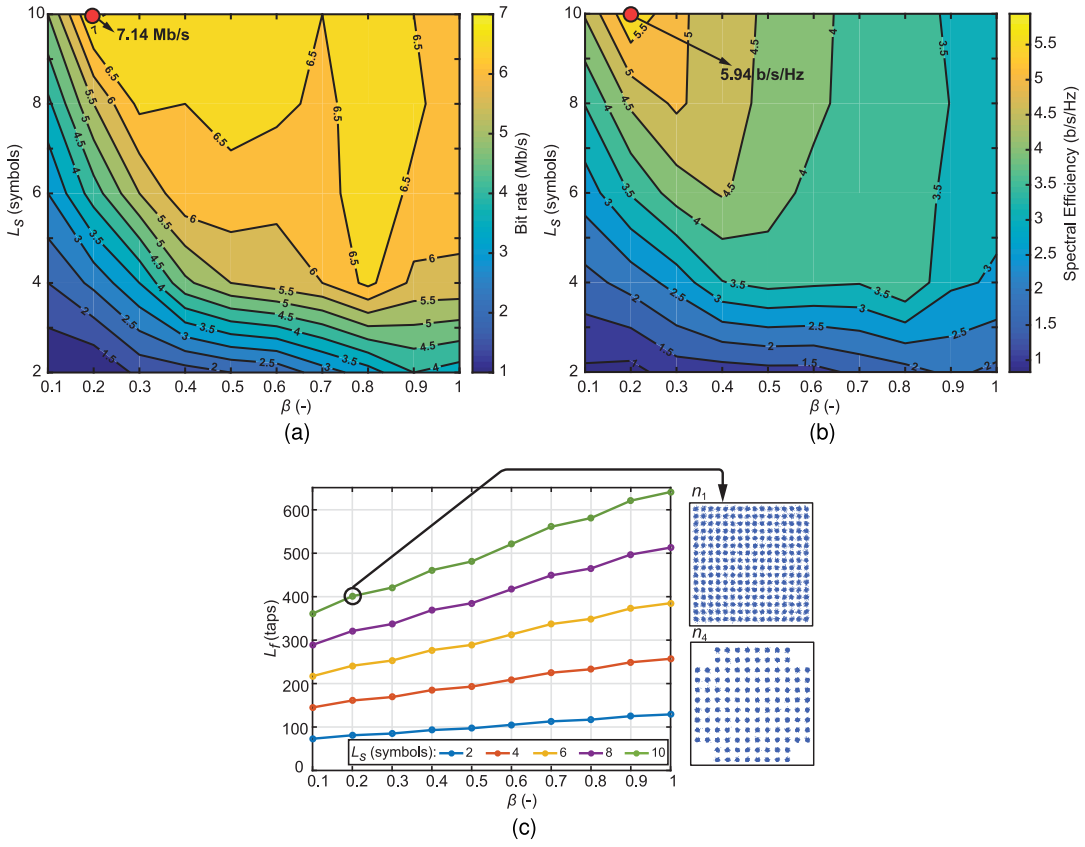

Fig. 7. Experimentally measured: (a) data rates, (b) spectral efficiencies and (c) filter lengths for 8-CAP with the received constellation diagrams for subcarriers n_1 and n_4 for $L_s = 10$ and $\beta = 0.2$. Note that a red dot in (a) and (b) denotes the highest measured data rate and spectral efficiency.

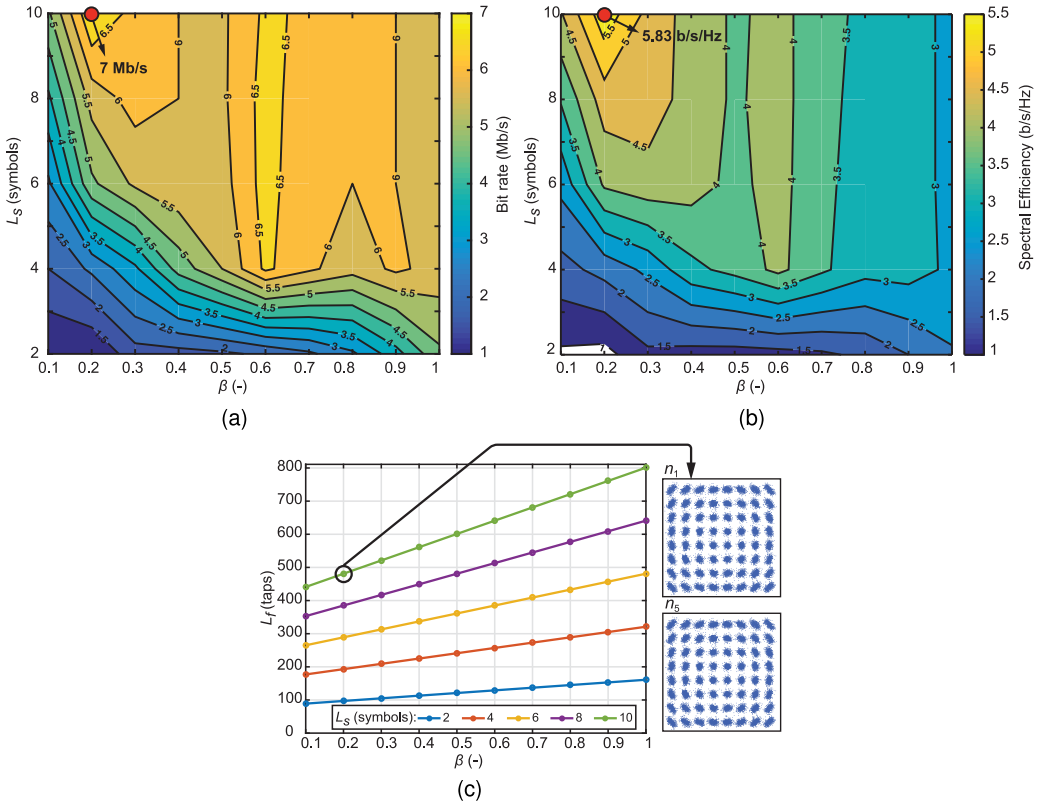

Fig. 8. Experimentally measured: (a) data rates, (b) spectral efficiencies and (c) filter lengths for 10-CAP with the received constellation diagrams for subcarriers n_1 and n_5 for $L_s = 10$ and $\beta = 0.2$. Note that a red dot in (a) and (b) denotes the highest measured data rate and spectral efficiency.

substantially increases the overall system complexity. On the other hand, to keep the optimal value of $R_b > 6.5$ Mb/s, the computational complexity can be reduced by $\sim 31\%$, i.e. from $L_f = 337$ taps/filter ($L_s = 8$ and $\beta = 0.3$) to $L_f = 233$ taps/filter ($L_s = 4$ and $\beta = 0.8$). The corresponding measured η_{se} is then reduced by 30% from 5 b/s/Hz to 3.5 b/s/Hz, see Fig. 7(a) and (b).

3.4 10-CAP

For 10-CAP the measured R_b and η_{se} are illustrated in Fig. 8(a) and (b), respectively showing similar profiles to 2- and 6-CAP systems. However, R_b is $>$ 6.5 Mb/s was measured for two separated maxima for $\beta = 0.2$ and 0.6, which is because of optimal subcarrier allocation within to the LED frequency response. Note that, the loss of η_{se} should be expected around $\beta = 0.6$ when compared to the $\beta = 0.2$ case. The maximum measured R_b and η_{se} are 7 Mb/s and 5.83 b/s/Hz for $L_s = 10$ and $\beta = 0.2$, which is the same as in 6-CAP link but higher than 2-CAP. Therefore, we observe no additional improvement in both R_b and η_{se} when a high number of subcarriers (i.e., $m \geq 6$) is used in *m*-CAP system because of low B_{sig}. The value of $L_f = 481$ taps/filter for such a 10-CAP system introduces a redundant increase of the system complexity. Fig. 8(c) illustrates the filter taps requirement for a range of β and L_s (inset are examples of the received constellation diagrams for the subcarriers n_1 and n_5 for $L_s = 10$ and $\beta = 0.2$) showing the significant increment in the system complexity in comparison with 2- and 6-CAP links.

Finally, the summary of the highest measured R_b and η_{se} as well as corresponding L_s and L_f for $m = \{2, 4, 6, 8, 10\}$ for $B_{sig} = 1$ MHz and 2 MHz are given in Tables 2 and 3, respectively. Note that, the results for 4-CAP are given as well, although we did not discussed them since they display similar performance to the other *m*-CAP systems. For $B_{sig} = 1$ MHz the highest improvement in

TABLE 2
The Highest Measured Bit Rates and Spectral Efficiencies for the Signal Bandwidth 1 MHz

m	**2**	**4**	**6**	**8**	**10**
R_b (Mb/s)	6.50	7	7	7.13	7
L_s (symbols) / β	10 / 0.8	10 / 0.8	10 / 0.2	10 / 0.2	10 / 0.2
L_f (taps/filter)	161	301	301	401	481
η_{se} (b/s/Hz)	4.23	5	5.83	5.94	5.83
L_s (symbols) / β	10 / 0.3	10 / 0.2	10 / 0.2	10 / 0.2	10 / 0.2
L_f (taps/filter)	121	201	301	401	481

TABLE 3
The Highest Measured Bit Rates and Spectral Efficiencies for the Signal Bandwidth 2 MHz

m	**2**	**4**	**6**	**8**	**10**
R_b (Mb/s)	9.8	10.5	11.33	12.25	11.6
L_s (symbols) / β	10 / 0.8	10 / 0.8	10 / 0.4	10 / 0.2	10 / 0.2
L_f (taps/filter)	161	301	341	401	481
η_{se} (b/s/Hz)	3.7	4	4.31	5.1	4.83
L_s (symbols) / β	10 / 0.3	10 / 0.2	10 / 0.2	10 / 0.2	10 / 0.2
L_f (taps/filter)	121	201	301	401	481

R_b is 9.69%, i.e. from 6.50 Mb/s (2-CAP) to 7.13 Mb/s (8-CAP). For $m > 4$ the improvement in measured R_b is negligible, which is attributed to the fact that increasing m (i.e., decreasing the bandwidth requirement of individual subcarriers) does not lead to further improvement in the flat-band approximation of the LED frequency response, and hence higher SNR values cannot be achieved. Note that, η_{se} is improved by 40.43% from 4.23 b/s/Hz (2-CAP) to 5.94 b/s/Hz (8-CAP), which is significant. However, this improvement comes at the cost of increased number of filter taps (i.e., system complexity). Improvement in R_b can be showed when considering higher $B_{sig} = 2$ MHz but at the cost of reduced η_{se} as given in Table 3. For higher order systems with $m \geq 6$ the same filter parameters can be adopted in order to optimize the system design to achieve both maximum R_b and η_{se}. To increase further both R_b and η_{se} in a point-to-point VLC system, pre- and post-equalization schemes (hardware or software) should be adopted.

4. Conclusion

In this work, we experimentally tested *m*-CAP system performance for different parameters of the FIR filters that introduce major complexity in a VLC system. We showed that both filter parameters L_s and β have a significant impact on the measured R_b and η_{se}. We achieved an improvement of 9.69% and 40.43% in the measured R_b and η_{se}, respectively, when compared 2-CAP and 8-CAP systems. The low order *m*-CAP schemes can be utilized providing the similar link R_b and η_{se} as higher

order systems and having much lower filter taps requirement (e.g., $L_f = 201$ and 401 taps/filter for $m = 4$ and 8, respectively). Contrary, the higher order systems with $m \geq 6$ can be designed to offer both the highest transmission speed and spectral efficiency using the same filter parameters (e.g., 8-CAP with $L_s = 10$ and $\beta = 0.2$).

References

[1] Cisco, San Jose, CA, USA, "Cisco visual networking index: Global mobile data traffic forecast update, 2016–2021 white paper," 2017.

[2] Z. Ghassemlooy, L. N. Alves, S. Zvanovec, and M. A. Khalighi, *Visible Light Communications Theory and Applications*. Boca Raton, FL, USA: CRC Press, 2017.

[3] J. Grubor, S. C. J. Lee, K. D. Langer, T. Koonen, and J. W. Walewski, "Wireless high-speed data transmission with phosphorescent white-light LEDs," in *Proc. 33rd Eur. Conf. Exhib. Opt. Commun.*, Berlin, Germany, 2007, pp. 1–2.

[4] X. Li *et al.*, "Wireless visible light communications employing feed-forward pre-equalization and PAM-4 modulation," *J. Lightw. Technol.*, vol. 34, no. 8, pp. 2049–2055, Apr. 2016.

[5] H. Le Minh *et al.*, "100-Mb/s NRZ visible light communications using a postequalized white LED," *IEEE Photon. Technol. Lett.*, vol. 21, no. 15, pp. 1063–1065, Aug. 2009.

[6] S. Rajbhandari, "Spatial and wavelength division multiplexing for high-speed VLC systems: An overview," in *Proc. 10th Int. Symp. Commun. Syst., Netw. Digital Signal Process.*, Prague, Czech Republic, 2016, pp. 1–6.

[7] F.-M. Wu, C.-T. Lin, C.-C. Wei, C.-W. Chen, Z.-Y. Chen, and H.-T. Huang, "3.22-Gb/s WDM visible light communication of a single RGB LED employing carrier-less amplitude and phase modulation," in *Proc. Opt. Fiber Commun. Conf. Expo. Nat. Fiber Opt. Eng. Conf.*, Anaheim, CA, USA, 2013, pp. 1–3.

[8] S. D. Dissanayake and J. Armstrong, "Comparison of ACO-OFDM, DCO-OFDM and ADO-OFDM in IM/DD systems," *J. Lightw. Technol.*, vol. 31, no. 7, pp. 1063–1072, Apr. 2013.

[9] J. Armstrong, "OFDM for optical communications," *J. Lightw. Technol.*, vol. 27, no. 3, pp. 189–204, Feb. 2009.

[10] R. X. G. Ferreira *et al.*, "High bandwidth GaN-based micro-LEDs for multi-Gb/s visible light communications," *IEEE Photon. Technol. Lett.*, vol. 28, no. 19, pp. 2023–2026, Oct. 2016.

[11] G. Cossu, W. Ali, R. Corsini, and E. Ciaramella, "Gigabit-class optical wireless communication system at indoor distances (1.5–4 m)," *Opt. Exp.*, vol. 23, pp. 15700–15705, 2015.

[12] D. Bykhovsky and S. Arnon, "An experimental comparison of different bit-and-power-allocation algorithms for DCO-OFDM," *J. Lightw. Technol.*, vol. 32, no. 8, pp. 1559–1564, Apr. 2014.

[13] H. Elgala, R. Mesleh, and H. Haas, "Nonlinearity effects and predistortion in optical OFDM wireless transmission using LEDs," *Int. J. Ultra Wideband Commun. Syst.*, vol. 1, no. 2, pp. 143–150, 2009.

[14] W. O. Popoola, Z. Ghassemlooy, and B. G. Stewart, "Pilot-assisted PAPR reduction technique for optical OFDM communication systems," *J. Lightw. Technol.*, vol. 32, no. 7, pp. 1374–1382, Apr. 2014.

[15] V. Guerra, C. Suarez-Rodriguez, O. El-Asmar, J. Rabadan, and R. Perez-Jimenez, "Pulse width modulated optical OFDM," in *Proc. IEEE Int. Conf. Commun. Workshop*, 2015, pp. 1333–1337.

[16] K. Weiwei and S. Hranilovic, "Power reduction techniques for multiple-subcarrier modulated diffuse wireless optical channels," *IEEE Trans. Commun.*, vol. 56, no. 2, pp. 279–288, Feb. 2008.

[17] F. M. Wu *et al.*, "Performance comparison of OFDM signal and CAP signal over high capacity RGB-LED-based WDM visible light communication," *IEEE Photon. J.*, vol. 5, no. 4, Aug. 2013, Art. no. 7901507.

[18] Y. Wang, L. Tao, X. Huang, J. Shi, and N. Chi, "8-Gb/s RGBY LED-based WDM VLC system employing high-order CAP modulation and hybrid post equalizer," *IEEE Photon. J.*, vol. 7, no. 6, Dec. 2015, Art. no. 7904507.

[19] M. I. Olmedo *et al.*, "Multiband carrierless amplitude phase modulation for high capacity optical data links," *J. Lightw. Technol.*, vol. 32, no. 4, pp. 798–804, Feb. 2014.

[20] P. A. Haigh *et al.*, "A multi-CAP visible-light communications system with 4.85-b/s/Hz spectral efficiency," *IEEE J. Sel. Areas Commun.*, vol. 33, no. 9, pp. 1771–1779, Sep. 2015.

[21] P. A. Haigh *et al.*, "Multi-band carrier-less amplitude and phase modulation for bandlimited visible light communications systems," *IEEE Wireless Commun.*, vol. 22, no. 2, pp. 46–53, Apr. 2015.

[22] K. Werfli *et al.*, "Multi-band carrier-less amplitude and phase modulation with decision feedback equalization for bandlimited VLC systems," in *Proc. 4th Int. Workshop Opt. Wireless Commun.*, Istanbul, Turkey, 2015, pp. 6–10.

[23] P. A. Haigh *et al.*, "Experimental verification of visible light communications based on multi-band CAP modulation," in *Proc. 2015 Opt. Fiber Commun. Conf. Exhib.*, Los Angeles, CA, USA, 2015, pp. 1–3.

[24] P. Chvojka, S. Zvanovec, K. Werfli, P. A. Haigh, and Z. Ghassemlooy, "Variable *m*-CAP for bandlimited visible light communications," in *Proc. IEEE Int. Conf. Commun. Workshops*, Paris, France, 2017, pp. 1–5.

[25] K. Werfli, P. A. Haigh, Z. Ghassemlooy, N. B. Hassan, and S. Zvanovec, "A new concept of multi-band carrier-less amplitude and phase modulation for bandlimited visible light communications," in *Proc. 10th Int. Symp. Commun. Syst., Netw. Digital Signal Process.*, Prague, Czech Republic, 2016, pp. 1–5.

[26] P. A. Haigh *et al.*, "Multi-band carrier-less amplitude and phase modulation for highly bandlimited visible light communications—Invited paper," in *Proc. Int. Conf. Wireless Commun. Signal Process.*, Nanjing, China, 2015, pp. 1–5.

[27] P. Chvojka, P. A. Haigh, S. Zvanovec, P. Pesek, and Z. Ghassemlooy, "Evaluation of multi-band carrier-less amplitude and phase modulation performance for VLC under various pulse shaping filter parameters," in *Proc. 13th Int. Joint Conf. e-Bus. Telecommun. Vol. 3, OPTICS*, Lisbon, Portugal, 2016, pp. 25–31.

[28] J. G. Proakis, *Digital Communications*. New York, NY, USA: McGraw-Hill, 2004.

4.5 Channel Characteristics of Visible Light Communications within a Dynamic Environment

This chapter is a version of the published manuscript:

P. Chvojka, S. Zvanovec, P. A. Haigh and Z. Ghassemlooy, "Channel Characteristics of Visible Light Communications Within Dynamic Indoor Environment," in *Journal of Lightwave Technology*, vol. 33, no. 9, pp. 1719-1725, 2015.

Connection with my Ph.D. thesis:

Within the field of VLC channel modeling, there had been a lack of papers studying the effect of shadowing on channel parameters. In this paper, for the first time, we investigate VLC system performance considering the movement of people within a room. We provide novel experimental results in terms of the cumulative distribution functions of the received power and delay spread for three different indoor scenarios (i.e., a corridor, empty hall and furnished office room). The Rayleigh distribution profiles of the received power are derived based on the measured data. We show the robustness of the VLC technology employed as an indoor communication system. Tasks **T5** and **T6** are fulfilled.

Channel Characteristics of Visible Light Communications Within Dynamic Indoor Environment

Petr Chvojka, Stanislav Zvanovec, *Senior Member, IEEE*, Paul Anthony Haigh, *Member, IEEE*, and Zabih Ghassemlooy, *Senior Member, IEEE*

***Abstract*—Visible light communications (VLC) is a new emerging technology, which provides both data transmission and illumination by utilizing the visible range (370–780 nm) of the electromagnetic spectrum. In order to maximize the available data rate and enhance the users mobility within an indoor environment, it is essential to characterize the communication channel. In this paper, we present both analytical and experimental results for a VLC system affected by movement of people for different indoor conditions (i.e., furnished office room, empty hall, and corridor). VLC systems utilize multiple light-emitting diodes mounted in the ceiling and the configuration is based on the nondirected line of sight. We consider random movement of people within the room, focusing on the impacts of shadowing and blocking on mobility and link system performance by investigating changes in the channel characteristics using the cumulative distribution function of the received power distribution and the delay profile. We demonstrate the behaviour of communication channels for different scenarios from corridor, the most robust against people movement induced fading, to the office rooms and halls, the most vulnerable to the received power fluctuation.**

***Index Terms*—Channel characterization, mobile indoor optics, visible light communications.**

I. Introduction

THE energy consumption at a global level in recent years has led to a new way of thinking in how we should use technologies (including the telecommunications and lighting) and come up with more ecologically and economically friendly solutions. Replacing incandescent light bulbs with more compact light-emitting diode (LED) based light sources is a simple and cost-effective way to reduce carbon emissions and increase the energy utilization efficiency on a global scale. LEDs have several advantages over incandescent and fluorescent lamps including multitude of colours, compactness, longer life expectancy, lower power consumption and higher energy conversion efficiency [1]. Moreover, they can be modulated at high-speed to provide data communications and illumination simultaneously - thus the name visible light communications (VLC) a unique trait that will have a major impact in the way we will use light in future [1]. In recent years we have seen a growing interest in research and development in VLC at a global level [2]–[4]. Achieving higher data rate transmission is one of the key research challenges in VLC [5], [6]. Concurrently, new technologies has emerged for indoor VLC applications like organic LEDs representing an alternative light source to Ce:YAG/GaN LEDs, offering lower cost, a range of flat panel shapes and sizes with much smoother lighting effects due to the solution based processing technology [7], [8].

VLC systems are expected to mainly be utilized for the indoor environment. However they can also be used in outdoor environment to provide internet hot spots using street lighting and mobile access as part of the 5G technology in highly congested areas. In indoor applications with a static environment, which are the most common cases, VLC does offer high quality services. The analysis of the static optical wireless channel is presented in [9], which investigates the effects of multiple order reflections in a rectangular room using Lambertian reflectors. The simulation was carried out for several scenarios (different room dimensions, source and receiver positions and receiver parameters) and it was shown that higher order reflections can be a significant source of intersymbol interference, thus resulting in a decreased bandwidth of the channel from 35 to 9 MHz. However, in dynamic environments (e.g., movement of people or obstacles) the communications link may experience temporarily blockage or shadowing, which must be addressed. The typical example of shadowing and blocking of the signal path for an office room used in the simulation is depicted in Fig. 1(a), while Fig. 1(b) illustrates all the necessary dimensions for the obstacles. Such situation results in reduced total received power and temporal degradation of the channel parameters.

In [10] the vulnerability of a cellular and multi-spot diffusing multiple-input multiple-output architecture to shadowing was investigated. The influence on the received signal by people either sitting or standing was analysed and it was found that the probability of shadowing was less than 2% in a typical office environment (3 m height). The power penalty due to shadowing was insignificant in 99% of the simulated cases. In [11] the effect of shadowing on a VLC link utilizing several LEDs for downlink transmission based on the time division multiple access was studied. In contrast to the static behaviour

Manuscript received August 14, 2014; revised January 13, 2015; accepted January 20, 2015. Date of publication February 1, 2015; date of current version March 13, 2015. This work was supported by the EU COST ICT Action IC1101 Optical Wireless Communications: An Emerging Technology (OPTICWISE) and by the Grant Agency of the Czech Technical University in Prague under Grant SGS14/190/OHK3/3T/13.

P. Chvojka and S. Zvanovec are with the Department of Electromagnetic Field, Faculty of Electrical Engineering, Czech Technical University, Prague 16627, Czech Republic (e-mail: chvojpe8@fel.cvut.cz; xzvanove@fel.cvut.cz).

P. A. Haigh and Z. Ghassemlooy are with the Faculty of Engineering and Environment, Northumbria University, Newcastle upon Tyne NE1 8ST, U.K. (e-mail: paul.anthony.haigh@ieee.org; z.ghassemlooy@northumbria.ac.uk).

Color versions of one or more of the figures in this paper are available online at http://ieeexplore.ieee.org.

Digital Object Identifier 10.1109/JLT.2015.2398894

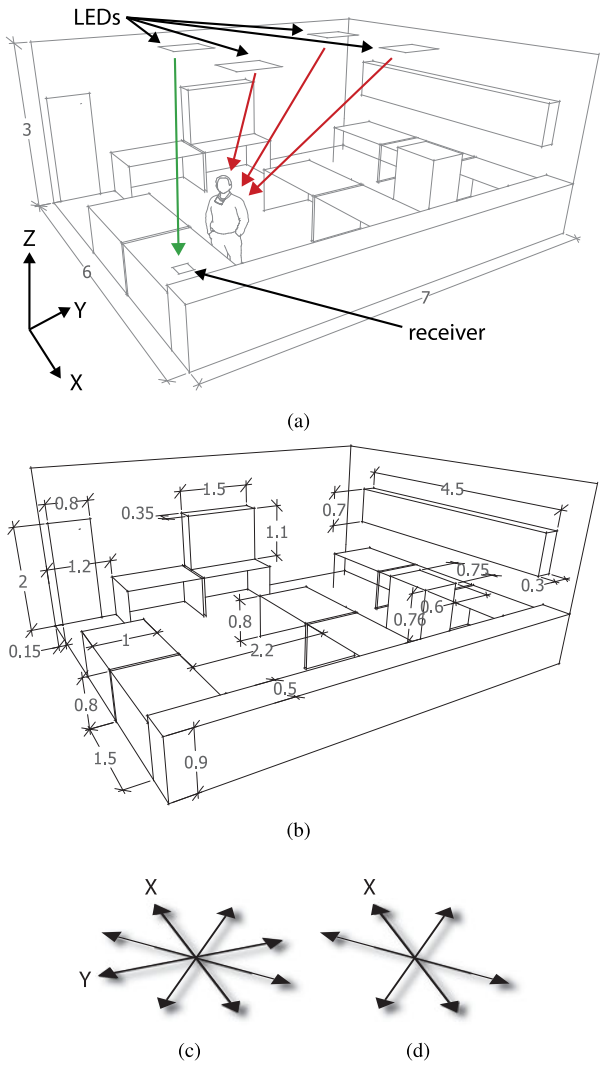

Fig. 1. (a) Example of blocking/shadowing of the signal path, (b) dimensions of all obstacles within the office room and possible directions of the movement: (c) the office room and the empty hall room, and (d) the corridor.

as in [10], it was found that the performance of the link did improve using 3 LEDs, which were identified as the optimal number of LED fittings, when considering movement of people inside the room. Such a system was found to be quite robust against the shadowing.

The channel characteristics are changed due to movement of people and thus when the link is temporarily blocked or shadowed the link experiences a much reduced signal to noise ratio at the receiver. To address the shadowing problem and to enhance the users mobility, the concept of a smart receiver was presented in [12] and [13], based on the introduction of additional photodetectors all with different viewing angles. Each detector receives a version of the transmitted signal and the one with the maximum strength is selected, while the others are discarded. The performance of the receiver in [12] was analysed for a small room with dimensions 2 m $\times$ 1.5 m $\times$ 1.2 m. Using such a receiver, the theoretical maximum channel capacity up to 666 Mb/s with no equalization was reported. Another approach adopted in [14] used an adaptive receiver to improve the data rate (up to 140 Mb/s) for both LOS and NLOS configurations at a bit error rate (BER) of 10^{-9}.

In order to enhance the user's mobility one must investigate the illumination level or the received power uniformity. For instance, in [15] the focus was on LEDs being located in the ceiling with a varying receiver field of view (FOV). It was shown that uniform illumination can be achieved at the cost of illuminance power. The FOV was the key parameter, since increasing it beyond the limit would not result in any further gain in mobility. A second approach proposed in [16] used the evolutionary algorithm to drive the LEDs in order to optimize the power coverage within the room. In this scheme the dynamic signal power range was reduced by up to 26.5% while keeping the BER $< 10^{-6}$. A physical model for a wireless indoor infrared system was analysed in [17] based on simulation and measurement to predict the path loss and the channel bandwidth. It was shown that employing moderate directivity (i.e., a reduced FOV at the receiver and a narrow beam at the transmitter) is sufficient even for data rates beyond 100 Mb/s.

In this paper we extend parameterization of the VLC channel parameters by considering the influence of the movement of people in three indoor scenarios; (*i*) a furniture equipped office room; (*ii*) an empty hall and (*iii*) a corridor. In addition we perform several laboratory measurements to support the analysis carried out. For all scenarios we have adopted the non-directed LOS link configuration with multiple LEDs. We analyse changes in the power distribution and the delay profiles to address the particularly shadowing due to people and mobility issues.

The rest of the paper is organized as follow: Section II describes the analytical system model, model for movement of people and the results from the simulation, in Section III the measurement campaign is given and finally the summary and conclusions are given in the Section IV.

II. System Model

Based on the measurements we carry out theoretical analysis for the VLC channel model. We introduce the theoretical background for the VLC channel model and the key parameters for data evaluation. The parameters of movement of people adopted in the simulation will be subsequently described.

A. VLC Channel Model

In a static optical channel the total received power at the receiver is given by [1]:

$$P_r = P_t H_d(0) + \int P_t H_{\mathrm{ref}}(0) \tag{1}$$

where $H_d(0)$ and $H_{\mathrm{ref}}(0)$ are the DC channel gain of the direct and reflected paths, respectively and P_t is total optical power transmitted by LEDs.

The DC channel gain of the direct path is given as [13]:

$$H_d(0) = \begin{cases} \dfrac{(m+1)}{2\pi d^2} A_{\mathrm{det}} \cos^m(\theta_r) T_s(\vartheta) g(\vartheta) \cos(\vartheta), \\ \qquad \text{for } 0 \le \vartheta \le \vartheta_{\mathrm{FOV}} \\ 0, \qquad \text{for } \vartheta > \vartheta_{\mathrm{FOV}} \end{cases} \tag{2}$$

where m is the order of the Lambertian radiant, d is the distance between transmitter and receiver, θ_r is the angle of irradiance, ϑ is the angle of incidence, $T_s(\vartheta)$ is the optical filter gain, $g(\vartheta)$ is the optical concentrator gain and ϑ_{FOV} is the FOV of the receiver.

The DC gain of the reflected path can be written as [13]:

$$H_d(0) = \begin{cases} \dfrac{(m+1)}{2(\pi d_1 d_2)^2} \rho A_{\mathrm{det}} dA_w \cos^m(\theta_r) \cos(\alpha) \times \\ \qquad \cos(\beta) T_s(\vartheta) g(\vartheta) \cos(\vartheta), \\ \qquad \text{for } 0 \le \vartheta \le \vartheta_{\mathrm{FOV}} \\ 0, \qquad \text{for } \vartheta > \vartheta_{\mathrm{FOV}} \end{cases} \tag{3}$$

where d_1 is the distance between transmitter and reflective point, d_2 is the distance between reflected point and receiver, ρ is the reflectance coefficient, dA_w is a small reflective area on the wall, α is the angle of incidence from the transmitter and β is the angle of irradiance from a reflected point.

The multipath character of the optical link can be described by the delay profile of the channel [18]. The delay spread estimates the upper bound of the maximum channel capacity without the need for equalization [1]. The RMS delay spread can be calculated from the channel impulse response as [12]:

$$\tau_{\mathrm{RMS}} = \sqrt{\frac{\int_{-\infty}^{\infty} (\tau - \tau_0)^2 h^2(t) dt}{\int_{-\infty}^{\infty} h^2(t) dt}} \tag{4}$$

where τ is the time and the mean delay τ_0 is given by [12]

$$\tau_0 = \frac{\int_{-\infty}^{\infty} t h^2(t) dt}{\int_{-\infty}^{\infty} h^2(t) dt}. \tag{5}$$

B. Mobility of People

Since the VLC technology is mostly used for indoor application, the movement of people within a room will certainly affect the channel characteristics and hence the link performance. In our simulation we have modelled the human body in the form of a rectangular shape object with the height, width and depth of 1.8, 0.4 and 0.2 m, respectively. The mobility in terms of speed is chosen for each person randomly within the range of 2 and 5 km/h (0.56−1.39 m/s). The body rotation is also considered to be either 90° (back to the source, worst case) or 0° (sideways to the source, best case).

We assume that people are randomly distributed within the room at the start of our simulation. The number of people is chosen to follow approximately the same people density for different cases, i.e., 0.16 people/m^2 and 0.17 people/m^2. The limitation was set by the maximum number of people in a given office (in this case 7). The position of each person is chosen to be different and people are randomly moved for 30 s. The movement duration is split into one second intervals, where each person is moved by the distance according to its speed (i.e., 0.56 m for the shortest movement). Once a person is moved, all the parameters such as the received optical power and the RMS delay spread are calculated and the positions of all people are saved. Next we randomly selected the direction of next movement (see Fig. 1) and then moved around the people. The whole process was repeated until the movement duration is completed. The direction probabilities are 1/8 for the office and the hall and 1/6 for the corridor, respectively. Note that for the case of the corridor only 6 directions (in contrast to the case of an empty hall and an office room) were assumed in order to represent a more realistic scenario. The simulation was carried out for 3 different cases of corridor, furnished office room and empty hall room, and assumed the same process of peoples movement as described. The only different is in the office room environment where the movement is limited by the location of furniture (see Fig. 1(a) and (b)). The NLOS link configuration is adopted for all VLC channels with multiple LED sources, and the important parameters used are listed in Table I. The parameters are chosen to be consistent with the data given in [1], [11], [12], [14], and [19]. Note that all the reflections are assumed to have a Lambertian pattern [20].

TABLE I
PARAMETERS FOR THE SIMULATION

Parameter	Symbol	Value
Transmitted power per LED	–	10 mW
Size of LED array	–	100 × 100 LEDs
Semiangle at half power	$\varphi_{1/2}$	80°
FOV of the receiver	ϑ_{FOV}	90°
Optical filter gain	T_s	1
Optical concentrator gain	g	1
Photodetector area	A_{det}	1 cm^2
Reflectivity of walls	ρ	0.8
Receiver plane height (hall, office / corridor)	–	0.8 / 1.3
Room size	Corridor	20 × 3 × 3 m
	Office	6 × 7 × 3 m
	Hall	12 × 8 × 3 m
Position of LEDs	Corridor	(2.5, 1.5), (7.5, 1.5) (12.5, 1.5), (17.5, 1.5)
	Office	(2, 2), (4, 2) (2, 5), (4, 5)
	Hall	(4, 2), (8, 2) (4, 6), (8, 6)

In the simulation we only consider a single reflection, beyond which the computation time is rather long. The reason for this is that the contribution from second order reflection is ∼0.7 dB. This is ∼2% decrease in the received power, which is not significant for the practical systems point of view, and is in a good agreement with result outlined in [2].

The power distribution and the RMS delay spread are expressed in the form of CDF to provide a statistical data. All the CDF functions and numerical results are obtained assuming the worst case, i.e., during the movement of people. All the parameters were determined as outlined above, and following

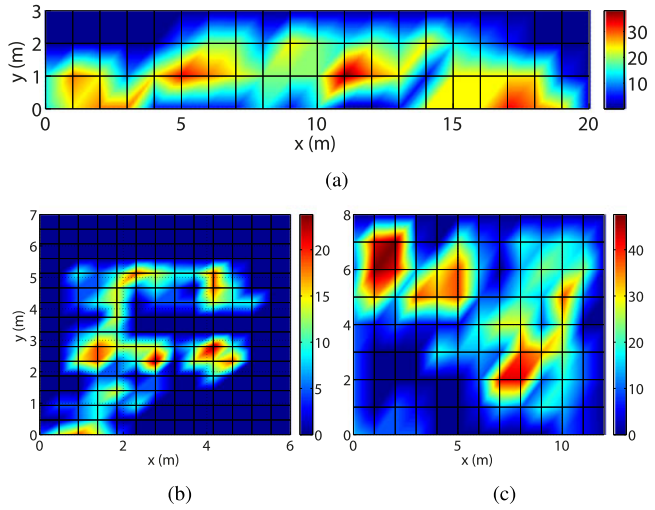

Fig. 2. Movement map of people (percentage of the time when at least one person is situated inside the small area of size 1 m × 1 m): (a) corridor, (b) furnished office room, and (c) empty hall.

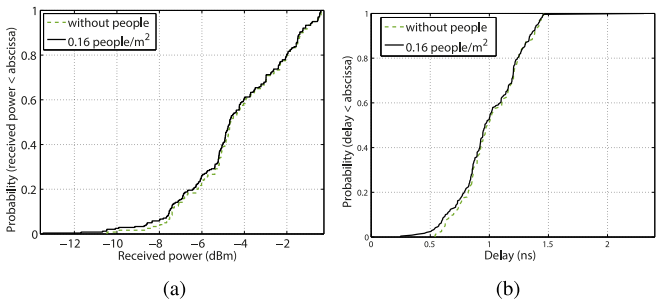

Fig. 3. Resulting CDF for the case of corridor with and without people against: (a) the received power, and (b) the RMS delay spread.

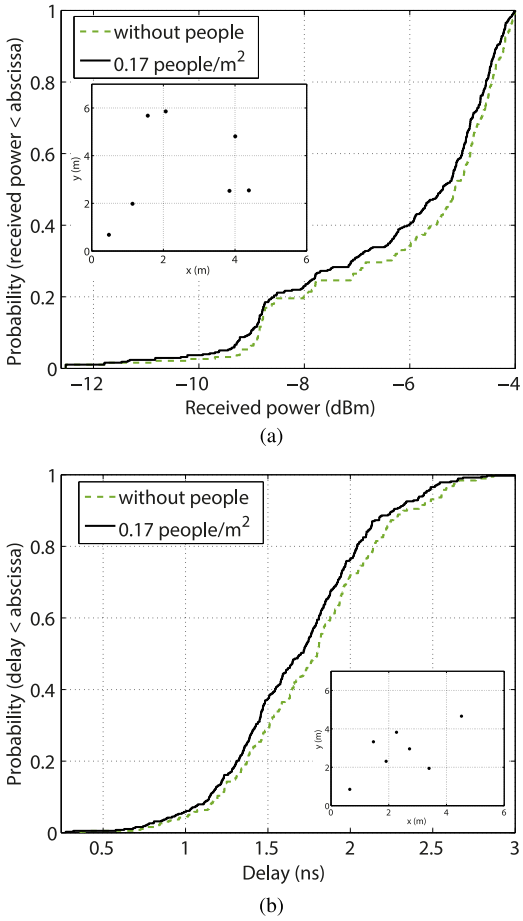

Fig. 4. Resulting CDF for the case of office room with and without people against: (a) the received power, and (b) the RMS delay spread.

the simulation the worst possible case was chosen to represent a given scenario.

To illustrate the movement of the people within the room we have used the movement map for all three scenarios (see Fig. 2). The room is divided into small areas of size 1 m × 1 m and every half a second the position of each person is recorded. The generated map shows the percentage of movement time when at least one person is situated within the small area. Equations (1)–(3) and (4), (5) were used in the simulations for the calculation of the received power and RMS delay spread, respectively.

C. Corridor

The movement map for ten people within the corridor is depicted in Fig. 2(a). The CDFs of the received power and the RMS delay spread are illustrated in Fig. 3(a) and (b), respectively comparing cases without and with people. The two cases are almost equivalent with a minor difference at lower received power levels and the RMS delay spread.

The differences are caused by the specific orientation of the corridor (long and narrow) and the distribution of LED lightings where there is a LOS path from at least one source for most of the time during the movement. With the so-called people density the CDF of the RMS delay spread is marginally shifted to the left (i.e., smaller delays). The reason is that not all signal components reflected from walls are received by the receiver since some are blocked by the people. Of course as people move around within the corridor the delay spread will vary.

D. Furnished Office Room

The movement map considering seven people in an office room with furniture (see Fig. 1) is depicted in Fig. 2(b). The CDFs of the received power and the RMS delay spread are illustrated in Fig. 4(a) and (b), respectively. In comparison to the previous case, a larger difference is observed with no people and with seven people (i.e., people density > 0.17 people/m^2). The cumulative probability of the received power differs by up to 7%, whereas the cumulative probability of the delay spread differs by up to 10%. Both values are higher in comparison to the corridor case. The insets in both figures illustrates the arrangement of people.

E. Empty Hall

Fig. 2(c) illustrates the movement map when considering 15 people inside an empty hall. The cumulative distribution functions of the analysed received power and the RMS delay spread are depicted in Fig. 5(a) and (b), respectively. It can be seen that the cumulative probabilities of the received power and

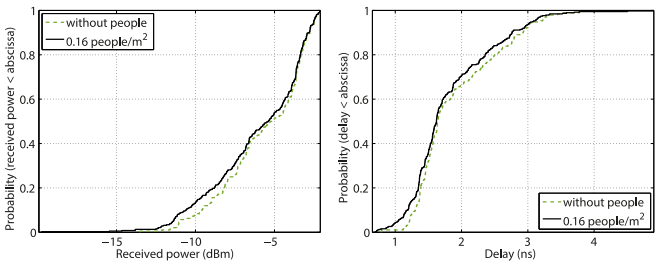

Fig. 5. Resulting CDF for the case of empty hall with and without people against: (a) the eceived power; (b) RMS delay spread.

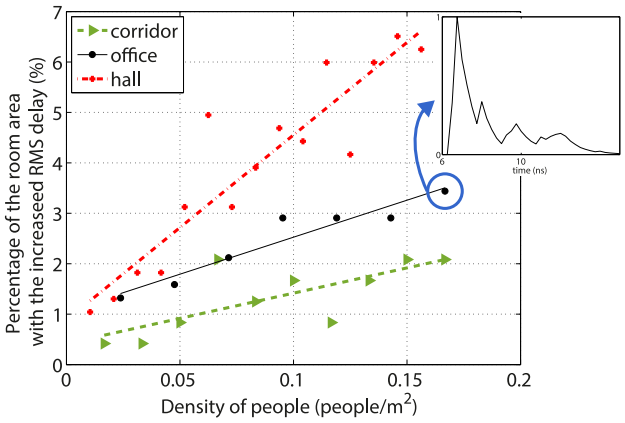

Fig. 6. Comparison of the maximum percentage of the room area with the increased RMS delay against the people density for corridor, office and hall environments.

the RMS delay spread differ by up to 5% for both cases, which is lower when compared to the furnished office room.

As people move within a room, the RMS delay spread changes becoming high compared to an empty room with no people. To illustrate this, we have selected the worst case after the movement of people and the area of the room, where the RMS delay spread is high, is determined and compared to the empty room. Fig. 6 illustrates the measured maximum percentage of area with increased values of RMS delay for three cases of corridor, office and hall with and without peoples movement. For all three cases the plots display a positive linear trend, with the people density in the hall environment displaying the highest profile with a maximum of 6.51% at the people density ~0.16 people/m^2 compared to 2% and 3.4% for the corridor and office environments, respectively. The inset in Fig. 6 illustrates example of the impulse response for the office room as denoted. The channel bandwidth is also affected by the movement of people. Considering the highest people density in our simulation, the bandwidth reduced from 31 to 27 MHz, 25 to 19 MHz and 17 to 11 MHz for the corridor, office room and hall, respectively, which corresponds to those in [9].

III. Measurement

An experimental system in the form of an optical room was devised to demonstrate and evaluate the VLC with shadowing and mobility issues. The optical room has dimensions of 1.75 m × 1.55 m × 1.95 m and was fitted with 16 LEDs (Philips

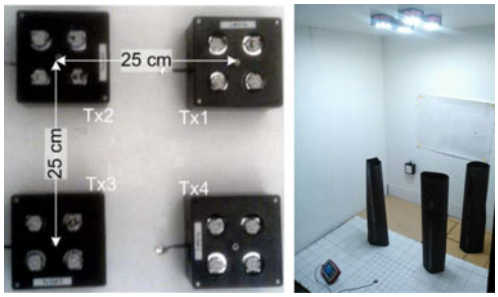

Fig. 7. The optical room: (a) an array of LED transmitters, and (b) the floor plan and obstacles.

Luxeon Rebel white phosphor LEDs) arranged into four independent clusters consisting of a 2 × 2 LED array acting as a single source (see Fig. 7(a)). The optical transmit power of each individual LED was 175 mW at a bias current of 350 mA. The received power was measured using the Thorlabs digital power meter PM100D with the photodiode power sensor S120VC. The receiving plane was divided into a 0.10 m × 0.10 m grid, 1.95 m below the transmitters. The centre point of the grid was aligned directly over the centre of the four transmitters (with Cartesian coordinates of [0, 0]). The optical power was measured in each square of the grid. We randomly placed obstacles representing people (with the width and height of 0.2 and 0.8 m, respectively, see Fig. 7(b)) into several schemes within the room and used different walls coverings (reflective or absorptive) and measured the optical power distributions. The entire experiment was carried out based on a series of static measurements. The positions of obstacles were changed accordingly to the people's movement process. The sizes of objects were chosen to maintain the same ratio of the room height to the human height to the receiver plane height as in the simulation.

Fig. 8 shows the normalized received optical power distribution along the receiver plan with no shadowing or blocking and with one, two and three obstacles. The results demonstrate and confirm a lighting footprint spanning over 1 m^2 for satisfying the ISO standard requirement of 400 lux for illumination within an office environment when there is no shadowing [21]. With shadowing as expected the luminance level drops by 10 dB. The measured power distributions were used to clarify the simulation model adopted the results achieved. For scenarios shown in Fig. 8 the deviations between measured and simulated data are (a) 0.08−0.4 dB, (b) 0.3−1.1 dB, (c) 0.33−1.15 dB, (d) 0.5−1.25 dB. The deviations are due to irregular shape of the obstacles and the limited number of reflections considered in the simulation. Such differences are acceptable and in a good agreement with the model used in the simulation.

The cumulative probability as a function of the normalized received power is illustrated in Fig. 9(a) with and without obstacles. In order to maintain a reference case, all walls were covered with an absorptive black material. The cumulative probability shows an exponential profile for all cases. At the normalized received power level of −2 dBm the cumulative probability increases by 35% for the people density of 1.11 people/m^2 when compared to the case without people.

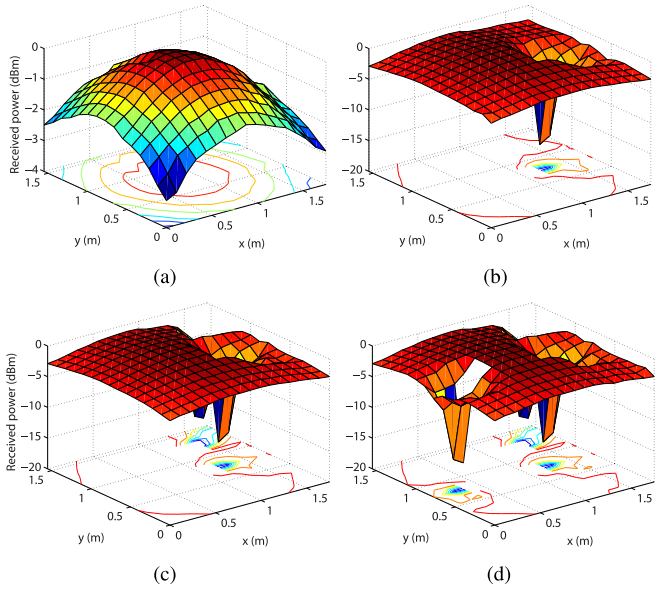

Fig. 8. Normalized received optical power distribution measured in the optical room: (a) no shadowing, (b) one obstacle, (c) two obstacles, and (d) three obstacles. Note the z-axis in the top left figure is not constant with the remaining figures to give the maximum possible resolution.

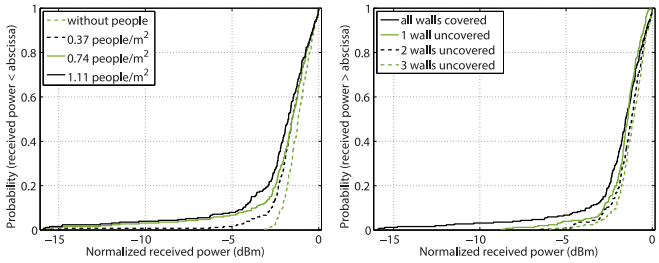

Fig. 9. Resulting CDF against: (a) the normalized received power for a range of peoples density. Note, that all walls were covered with a black material, and (b) the normalized received power for people density 0.74 people/m^2 and covered and uncovered walls.

Fig. 9(b) illustrates the cumulative probability vs. the normalized received power for the people density of 0.74 people/m^2 and with walls being covered and then uncovered. The cumulative probability increases by 23% at the normalized received power level of -2 dBm for the case of three walls uncovered when compared to the covered walls. In the case where all walls are covered, the received power in the optical room varies over 16 dB, which is approximately 10 dB higher than the case with all walls uncovered. The measured results are in a good agreement with the simulation (standard deviation up to approximately 1.3 dB). All the curves follow same trend as expected. Note, that people density was higher than in the simulation model.

The measured probability density function of the normalized received power is depicted in Fig. 10 with and without people, which follows Rayleigh distribution given by [22]:

$$p(x) = \frac{x}{\sigma^2}\exp\left(-\frac{x^2}{2\sigma^2}\right) \tag{6}$$

TABLE II
SCALE PARAMETER FOR DIFFERENT DENSITY OF PEOPLE

People density (people/m^2)	Scale parameter σ
Empty room	0.98
0.37	1.33
0.74	1.57
1.11	1.77

where σ represents the scale parameter. With higher people density of 1.11 people/m^2 the probability density has significantly decreased showing a Rayleigh distribution profile with the scale parameter σ of 1.77. Note that for the case of an empty room the distribution corresponds to the Rayleigh distribution with σ of 0.98. Table II summarised evolution of the scale parameter with increasing people density in the room.

IV. CONCLUSION

In this paper, for the first time we have investigated the VLC system performance considering peoples movement and have provided experimental results for the CDF of the received power and the RMS delay spread for three different indoor scenarios (i.e., corridor, the furniture office room and the empty hall). We showed that in the furniture office environment (people density > 0.16 people/m^2) the CDF of the received power differs in the worst case by up to 7%. On the other hand the highest RMS delay spread of 6.5% in comparison to the case with no people was observed for the empty hall. The results showed that the corridor with the maximum RMS delay of 2% at the people density > 0.16 people/m^2 is the most robust against the people's movement compared to other two where the problem of shadowing or blockage could be readily avoided. The measurement results presented correspond well with the simulated data, the differences in the received power can be reduced significantly by using more reflective wall surfaces. Based on the measurement we plotted the PDF as a function of the normalized received power showing similar profile to Rayleigh distribution with the scale parameter varying from 0.98 to 1.79 from an empty to a crowded room. Our paper therefore has shown that the VLC system is robust as an indoor communications technology, offering excellent mobility even under high people's density.

The measurement results correspond well with the simulated results and the differences in the received power can be reduced significantly by using more reflective wall surfaces.

Our paper shows that VLC technology is robust as an indoor communications technology, offering excellent mobility even when considering a room with high people density.

REFERENCES

[1] Z. Ghassemlooy, W. Popoola, and S. Rajbhandari, *Optical Wireless Communications*. Boca Raton, FL, USA: Taylor & Francis, 2012.
[2] T. Komine and M. Nakagawa, "Fundamental analysis for visible-light communication system using LED lights," *IEEE Trans. Consum. Electron.*, vol. 50, no. 1, pp. 100–107, Feb. 2004.
[3] J. Boyd, "Let there be (a new kind of) light [NEWS]," *IEEE Spectr.*, vol. 44, no. 7, pp. 12–14, Jul. 2007.

[4] J. Armstrong, Y. Sekercioglu, and A. Neild, "Visible light positioning: A roadmap for international standardization," *IEEE Commun. Mag.*, vol. 51, no. 12, pp. 68–73, Dec. 2013.
[5] D. Tsonev, S. Hyunchae Chun, J. J. D. Rajbhandari, S. McKendry, E. Videv, M. Gu, S. Haji, A. E. Watson, G. Kelly, M. D. Faulkner, H. Dawson, D. Haas, and O'Brien, "A 3-Gb/s single-LED OFDM-based wireless VLC link using a Gallium nitride LED," *IEEE Photon. Technol. Lett.*, vol. 26, no. 7, pp. 637–640, Apr. 1, 2014.
[6] G. Cossu, A. Khalid, P. Choudhury, R. Corsini, and E. Ciaramella, "3.4 Gbit/s visible optical wireless transmission based on RGB LED," *Opt. Exp.*, vol. 20, pp. B501–B506, 2012.
[7] P. A. Haigh, F. Bausi, Z. Ghassemlooy, I. Papakonstantinou, and H. L. Minh, "Visible light communications: Real time 10 Mb/s link with a low bandwidth polymer light-emitting diode," *Opt. Exp.*, vol. 22 no. 3, pp. 2830–2838, 2014.
[8] P. A. Haigh, F. Bausi, T. Kanesan, S. T. Le, S. Rajbhandari, Z. Ghassemlooy, I. Papakonstantinou, W. Popoola, A. Burton, H. Le Minh, W. P. Ng, A. D. Ellis, and F. Cacialli, "A 20 Mb/s VLC Link with a polymer LED and a multi-layer perceptron equalizer," *IEEE Photon. Technol. Lett.*, vol. 26, no. 19, pp. 1975–1978, Oct. 2014.
[9] J. R. Barry, J. M. Kahn, W. J. Krause, E. A. Lee, and D. G. Messerschmitt, "Simulation of multipath impulse response for indoor wireless optical channels," *IEEE Sel. Areas Commun.*, vol. 11, no. 3, pp. 367–379, Apr. 1993.
[10] S. Jivkova, Kavehrad, Mohsen, "Shadowing and blockage in indoor optical wireless communications," in *Proc. IEEE Global Telecommun. Conf.*, Dec. 1–5, 2003, vol. 6, pp. 3269–3273.
[11] T. Komine and M. Nakagawa, "A study of shadowing on indoor visible-light wireless communication utilizing plural white LED lightings," in *Proc. 1st Int. Symp. Wireless Commun. Syst.*, Sep. 20–22, 2004, pp. 36–40.
[12] A. Burton, H. Le-Minh, Z. Ghassemlooy, S. Rajbhandari, and P. A. Haigh, "Smart receiver for visible light communications: Design and analysis," in *Proc. 8th Int. Symp. Commun. Syst., Netw. Digit. Signal Process.,* Jul. 18–20, 2012, pp. 1–5.
[13] A. Burton, H. Le-Minh, Z. Ghassemlooy, S. Rajbhandari, and P. A. Haigh, "Performance analysis for 180 receiver in visible light communications," in *Proc. 4th Int. Conf. Commun. Electron.*, Aug. 1–3, 2012, pp. 48–53.
[14] M. Biagi, T. Borogovac, and T. D. C. Little, "Adaptive receiver for indoor visible light communications," *J. Lightw. Technol.*, vol. 31, no. 23, pp. 3676–3686, Dec. 1, 2013.
[15] A. Burton, H. Le Minh, Z. Ghasemlooy, and S. Rajbhandari, "A study of LED lumination uniformity with mobility for visible light communications," in *Proc. Int. Workshop Opt. Wireless Commun.,* Oct. 22–22, 2012, pp. 1–3.
[16] J. Ding, Z. Huang, and Y. Ji, "Evolutionary algorithm based power coverage optimization for visible light communications," *IEEE Commun. Lett.*, vol. 16, no. 4, pp. 439–441, Apr. 2012.
[17] V. Jungnickel, V. Pohl, S. Nonnig, and C. Von Helmolt, "A physical model of the wireless infrared communication channel," *IEEE Sel. Areas Commun..*, vol. 20, no. 3, pp. 631–640, Apr. 2002.
[18] J. M. Kahn and J. R. Barry, "Wireless infrared communications," *Proc. IEEE*, vol. 85, no. 2, pp. 265–298, Feb. 1997.
[19] C. R. Lomba, R.T. Valadas, and A. M. Duarte, "Efficient simulation of the impulse response of the indoor wireless optical channel," *Int. J. Commun. Syst.*, vol. 13, pp. 537–549, 2000.
[20] N. Hayasaka and T. Ito, "Channel modeling of nondirected wireless infrared indoor diffuse link," *Electron. Commun. Jpn.*, vol. 90, pp. 9–19, 2007.
[21] D. Dilaura, K. Houser, R. Mistrick, and G. Steffy, IES lighting handbook: Illumination engineering, 2011.
[22] C. Forbes, M. Evans, N. Hastings, and B. Peacock, *Statistical Distributions*, 4th ed. Hoboken, NJ, USA: Wiley, pp. 173–175.

Petr Chvojka was born in 1987. He received the M.Sc. degree from the Czech Technical University, Prague, Czech Republic, in 2013, where he is currently working toward the Postgraduation degree. He is currently a Researcher at the Department of Electromagnetic Fields, Czech Technical University, where he is a Member of a Free-Space and Fiber Optics Team. His research interests include visible light communications, OLED technologies, and wireless optical communications.

Stanislav Zvanovec received the M.Sc. and Ph.D. degrees from the Czech Technical University, Prague, Czech Republic, in 2002 and 2006, respectively. He is currently a Full Professor and a Vice-Head at the Department of Electromagnetic Field, Faculty of Electrical Engineering, Czech Technical University, where he leads a Free-Space and Fiber Optics Team, Faculty of Electrical Engineering, and several research projects. His current research interests include wireless optical communications, visible light communications, remote sensing, and optical fiber sensors.

Paul Anthony Haigh (M'10–S'11-14–M'15) received the Ph.D. degree in the area of optical wireless communications from Northumbria University, Newcastle upon Tyne, U.K., in 2014.

He is currently a Research Associate with the High Performance Networks Group, University of Bristol, Bristol, U.K., working on the EPSRC TOUCAN Project. His research interests include adaptive and programmable real-time seamless interfaces between wireless and wired multitechnology networks. He has published more than 20 scholarly articles including 13 articles in high ranking journals. In 2010, he received the prestigious Marie Curie Fellowship at the European Organization for Nuclear Research (CERN), where he worked on the optoelectronic links in large hadron collider experiments.

Zabih Ghassemlooy CEng. received the B.Sc.(Hons) degree in electrical and electronics engineering from the Manchester Metropolitan University, Manchester, U.K., in 1981, and the M.Sc. and Ph.D. degrees in optical communications from the University of Manchester Institute of Science and Technology (UMIST), Manchester, in 1984 and 1987, respectively. From 1986 to 1987, he was with UMIST, and from 1987 to 1988, he was a Postdoctoral Research Fellow at the City University, London, U.K. In 1988, he joined Sheffield Hallam University as a Lecturer, become a Professor in optical communications in 1997. From 2004 to 2012, he was an Associate Dean for Research (ADR) in the School of Computing, Engineering, and from 2012 to 2014, ADR for Research and Innovation with the Faculty of Engineering and Environment, Northumbria University, Newcastle, U.K. He has been a Visiting Professor at a number of institutions and he is currently at the University Tun Hussein Onn Malaysia. He is currently the Head of the Northumbria Communications Research Laboratories within the Faculty. His research interests include optical wireless communications, visible light communications, and radio over fibre/free-space optics, supported by research grants from various funding bodies. He has supervised a large number of Ph.D. students, less than 49, and published more than 560 papers, 195 in journals and four books, and presented more than 60 keynote and invited talks. He is a Coauthor of "*Optical Wireless Communications Systems and Channel Modelling With Matlab* (Boca Raton, FL, USA: CRC Press, 2012); a Coeditor the "*Analogue Optical Fibre Communications* "(London, U.K.: IET, 1995). He is the Editor-in-Chief of the *International Journal of Optics and Applications*, and *British Journal of Applied Science and Technology*. From 2004-06, he was the IEEE U.K./IR Communications Chapter Secretary, the Vice-Chairman from 2004 to 2008, the Chairman from 2008 to 2011, and Chairman of the IET Northumbria Network from Oct 2011. He is a Fellow of the IET.

4.6 Analyses of Non-line of Sight Visible Light Communications

This chapter is a version of the published manuscript:

P. Chvojka, S. Vitek, S. Zvanovec, Z. Ghassemlooy and S. Rajbhandari, "Analyses of non-line of sight visible light communications," in *Optical Engineering*, *submitted*.

Connection with my Ph.D. thesis:

Based on the results reported in Section 4.5, we focus on an NLOS VLC system and analyze its performance in terms of channel bandwidth and received optical power using numerical simulations. We show the benefits of an NLOS channel over LOS-based communication and the effect of arbitrary receiver position on user mobility for two schemes – a ceiling placed transmitter and, for the first time, a published D2D scenario. The experimental campaign provides unique data on the shadowing caused by people resulting in reduced optical power received by the detector. The reported results meet task **T7** and complete goal **G2**.

Analysis of non-line of sight visible light communications

Petr Chvojka,[a,*] Stanislav Vitek,[a] Stanislav Zvanovec,[a] Zabih Ghassemlooy,[b,c] Sujan Rajbhandari[d]

[a]Czech Technical University in Prague, Faculty of Electrical Engineering, Department of Electromagnetic Field, Technicka 2, Prague, Czech Republic, 16627

[b]Northumbria University, Faculty of Engineering and Environment, Newcastle Upon Tyne, U.K., NE1 8ST

[c]QIEM, Haixi Institutes, Chinese Academy of Sciences, Quanzhou, China

[d]Coventry University, Centre for Mobility & Transport and School of Computing, Engineering and Mathematics, Coventry, U.K., CV1 5FB

Abstract. In this paper, we analyze the channel properties of a non-line-of-sight (NLOS) ceiling-to-device and device-to-device visible light communications (VLC) systems by considering various receiver's orientation and variable field of views (FOVs). The analyses based on the recursive indoor channel model show that for a particular transmitter configuration, the pure NLOS path can offer higher 3 dB channel bandwidth (up to 14 MHz) compared to the link with LOS and NLOS components. We also show how the receiver rotation (orientation) influences the probability of receiving signals via the NLOS path compared to the LOS and NLOS paths. Moreover, based on the experimental campaign, we demonstrate that shadowing observed at the receiver due people's movement results in decreased received power level (up to 1.8 dB), thus resulting in reshaping of the probability density function of received power.

Keywords: channel modeling; non-line-of-sight link; shadowing; visible light communications.

***First Author**, E-mail: chvojpe8@fel.cvut.cz

1 Introduction

Recent development in highly energy efficient solid state lighting (SSL) devices has opened new possibilities for their use in visible light communications (VLC)[1]. VLC based on visible light emitting diodes (LEDs) has multiple features including illumination, data communications, localization and sensing[2]. VLC can be adopted in a multitude of applications including indoor high-speed wireless connectivity with speeds of hundreds of Mb/s to Gb/s over a typical transmission span of 1-2 meters[1,3]. Most research works reported on VLC have focused on the proof-of-concept demonstration at higher data rates over a very short transmission range (i.e., < 0.5 m at a few Gb/s). However, in typical indoor environments, both the LEDs and the channel introduce bandwidth bottleneck, which limits the achievable data rates. Most commercial white LEDs have a typical modulation bandwidth B_{LED} of a few MHz. However, Gallium Nitride (GaN) micro-LEDs with a dimension of less than 100 μm can potentially offer higher B_{LED} (i.e.,

hundreds of MHz)[4]. However, these small micro-LEDs offer a trade-off between B_{LED} and the transmit optical power P_t[5], and hence limited applications due to low level of P_t (i.e., orders of mW). However, to be able to fully exploit the channel bandwidth B_{ch} of an indoor environment particularly for the non-line-of-sight (NLOS) configuration, channel modelling and characterization remain an open issue and therefore needs a fresh look[6].

In VLC, the computationally based channel models such as the recursive method, Monte Carlo ray tracing or the ceiling bounce model have been commonly adopted from infrared (IR) communications. Contrary to the visible band, in the IR band the reflections from walls are independent of the wavelength[7-10]. The extensive comparison between IR and VLC channel parameters was published in Ref. 10 confirming the improvement in the coherence bandwidth and the root-mean-square (RMS) delay spread in VLC while diffuse, specular and mixed specular–diffuse wavelength dependent reflections were considered to attain a realistic channel impulse response. Moreover, in most VLC channel modelling, the receiver (Rx) is considered to be pointing towards the transmitter (Tx) mounted on the ceiling. To improve the channel DC gain and the signal-to-noise ratio (SNR), Rxs with tilting angles of 45° and 90° with respect to the Tx were investigated in Ref. 10. In Ref. 11, a detailed analysis of the Rx orientation and its impact on the received optical power level as well as the inter-symbol interference (ISI) was reported. However, LOS VLC links can temporarily experience blocking due to shadowing, thus resulting in the link failure and performance degradation[12]. The undesirable impact of the NLOS environment on the accuracy of VLC based indoor localization, with the highest errors near the edge of the room, was reported in Ref. 13. A new analytical method with low computational complexity to determine the NLOS channel impulse response was presented in Ref. 14. In Ref. 15 the effect of multipath reflections on the signal to interference plus noise ratio (SINR) was

investigated, showing that higher order reflections have a stronger adverse impact on the SINR than the 1st order reflection when utilizing narrow field of view (FOV) Rxs.

The NLOS (diffuse) indoor optical wireless systems have been extensively investigated both theoretically and experimentally[16-18]. In Ref. 19 a simple analytical model for LOS and diffuse IR channels for indoor environments for approximate prediction of the path loss and bandwidth was investigate showing that moderate directivity would be sufficient at data rates > 100 Mbit/s. The shadowing effects on LOS and diffuse channels were analyzed in Ref. 20, where it was illustrated that the shadowed LOS configuration exhibited higher path loss, RMS delay spread and power penalty compared to the un-shadowed LOS. To overcome shadowing and to improve the link availability and performance, a NLOS scheme based on the multi-spot diffuse configuration and Rxs with multiple narrow FOV receiving elements employing angle diversity was introduced in Refs. 21 and 22, respectively.

In this paper, we investigate the NLOS VLC channel considering a range of Rx's orientations with arbitrary positions both in azimuth and elevation, and provide the essential channel statistics. In contrast to Ref. 11, in this paper we (*i*) outline detailed analysis with the emphasis being on B_{ch}; (*ii*) consider Rxs with different FOVs and show how the VLC link performance is prone to the Rx's rotation; (*iii*) further extend our work to the device-to-device (D2D) communications and show that NLOS VLC can in specific scenarios outperform LOS VLC in terms of B_{ch} by up to 14 MHz; and finally (*iv*) extend our work to provide statistics on shadowing due to people's movement by means of extensive measurement campaign using a fish-eye camera based Rx. The paper is organized as follows. In Section II the system model and experimental setup are briefly outlined, whereas in Section III the results from simulations and camera-based measurements are shown. Finally, the conclusions are given in Section IV.

2 System Description

2.1 VLC Channel Model

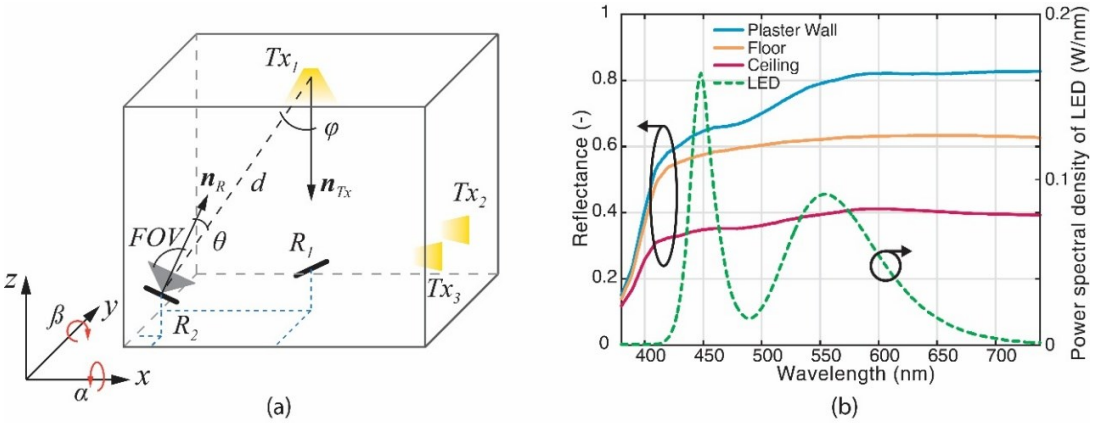

Fig. 1 (a) a geometry of the Tx and Rx in a room for the LOS scenario including the vector rotation, and (b) optical spectrum of a white LED (dashed line) and reflectance of the indoor materials, adapted from Ref. 7 (solid lines).

In NLOS VLC, the channel impulse response can be obtained using the recursive method, which will be described here only briefly due to space constraint. Here both the Tx (i.e., point source emitting a unit pulse of optical intensity) and the Rx elements are given as:

$$Tx = \{\boldsymbol{r}_{Tx}, \boldsymbol{n}_{Tx}, m\}, \tag{1}$$

and

$$R = \{\boldsymbol{r}_{\boldsymbol{R}}, \boldsymbol{n}_{\boldsymbol{R}}, A_R, FOV\}, \tag{2}$$

where $\boldsymbol{r}_{Tx}$ represents a source position, $\boldsymbol{n}_{Tx}$ and $\boldsymbol{n}_R$ are a Tx and a Rx orientation vectors normal to the surfaces of *Tx* and *R*, respectively, $\boldsymbol{r}_R$ is the Rx position, and A_R is photodetector surface area (see Fig. 1(a)). Lambertian order of the source radiation pattern is given as $m = -1/\ln(\vartheta_{1/2})$, where $\vartheta_{1/2}$ is the semi-angle at half power of an LED. To capture a rotation of the Rx, $\boldsymbol{n}_R$ is calculated according to[23]:

$$\boldsymbol{n}_R = \boldsymbol{M}_z(\gamma)\boldsymbol{M}_x(\alpha)\boldsymbol{M}_y(\beta)\boldsymbol{n}_n, \tag{3}$$

where $\boldsymbol{n}_n$ = (0, 0, 1) is the orientation vector for the Rx facing up towards the ceiling. $\boldsymbol{M}_z$, $\boldsymbol{M}_x$ and

$\boldsymbol{M}_y$ are the rotation matrices of $\boldsymbol{n}_n$ rotated around *z*-, *x*- and *y*-axes by angles of γ, α and β, respectively, in a counterclockwise direction using a right-handed coordinate system, see Fig. 1(a). Thus, for the Rx facing up towards the ceiling (i.e., $\alpha = \beta = 0$) the rotation matrices are given as[23]:

$$\boldsymbol{M}_x(\alpha) = \begin{bmatrix} 1 & 0 & 0 \\ 0 & \cos(\alpha) & -\sin(\alpha) \\ 0 & \sin(\alpha) & \cos(\alpha) \end{bmatrix}, \tag{4}$$

$$\boldsymbol{M}_y(\beta) = \begin{bmatrix} \cos(\beta) & 0 & \sin(\beta) \\ 0 & 1 & 0 \\ -\sin(\beta) & 0 & \cos(\beta) \end{bmatrix}, \tag{5}$$

$$\boldsymbol{M}_z(\gamma) = \begin{bmatrix} \cos(\gamma) & -\sin(\gamma) & 0 \\ \sin(\gamma) & \cos(\gamma) & 0 \\ 0 & 0 & 1 \end{bmatrix}. \tag{6}$$

To determine channel impulse response for the *k*-th reflection between *Tx* and *R*, a wall surface was discretized into *N* reflecting elements each having Lambertian intensity profiles. Based on the recursive algorithm, which is the sum of power contributions from each element, the channel impulse response is given as[7]:

$$h^{(k)}(t; Tx, R) = \frac{m+1}{2\pi} \sum_{i=1}^{N} \frac{\rho_{avg,i} \cos^m(\varphi_i) \cos(\theta)}{d_i^2}$$

$$\cdot \operatorname{rect}(2\theta/\pi) h^{(k-1)}(t - d_i/c\,; \{\boldsymbol{r}_{Tx}, \boldsymbol{n}_{Tx}, 1\}, R) dA, \tag{7}$$

where $\rho_{avg,i}$ is the average reflectance of the *i*-th element, θ is the angle between $\boldsymbol{n}_R$ and $(\boldsymbol{r}_{Tx} - \boldsymbol{r}_R)$, φ_i is the angle between $\boldsymbol{n}_{Tx}$ and $(\boldsymbol{r}_R - \boldsymbol{r}_{Tx})$, d_i represents the distance between the *Tx* and *R*, $h^{(k\text{-}1)}$ stands for the impulse response of order (*k*-1) between *i*-th element and *R*, dA is the reflecting element area, *c* is the speed of light and rect(*x*) is the rectangular function equal to 1 for $|x| \leq 1$ and 0 for $|x| > 1$. The average reflectance approximation was used to simulate the wavelength dependency of the reflecting surfaces, which is given as[7]:

$$\rho_{avg,i} = \frac{1}{P_t} \int_{\lambda} \theta(\lambda) \rho(\lambda) d\lambda\,, \tag{8}$$

where $P_t = \int_\lambda \theta(\lambda) d\lambda$ represents the total radiant power from the LED, $\theta(\lambda)$ is the LED power spectral density (PSD), $\rho(\lambda)$ is the spectral reflectance and λ is the wavelength. Fig. 1(b) illustrates a typical LED PSD and the wavelength dependent reflectance from plaster, floor and ceiling adopted from Ref. 7. The Fourier transform on the received channel impulse response was applied and B_{ch} was determined according to $|H(B_{ch})|^2 = 1/2\,|H(0)|^2$. Note that, the effect of Rx's spectral responsivity is not included in the channel model on assumption that a white light LEDs with broad optical spectrum and silicon photodiode are used, and hence will have a limited influence on the results presented here. Since majority of research on the VLC channel modeling has not included the wavelength response of the Rx, we would like to ensure a like-to-like comparison with already reported data[7-15].

2.2 Experimental Setup

The NLOS VLC link performance may be affected by shadowing due to the user's mobility or objects within a room, but not as much as the LOS VLC systems. Here, we experimentally investigate shadowing using a fish-eye camera (Moonglow ASC-N1B) based Rx with a semi-angle FOV ~90°. The Rx was located in the center of a room with dimensions of ~5 m × ~5 m × ~3 m (width × length × height) at the location $(2.5, 2.5, 0.8)$ facing up towards the ceiling (no rotation was considered). Here we considered three people randomly moving around within the room, see Fig. 2(a). A five-minute-long video was recorded using the fish-eye camera and 5 samples per second were consequently extracted for further data processing in order to determine the shadowing probability P_{sh} of the individual elevation angles. A sample from the recorded video is illustrated in Fig. 2(b). Note that, we considered only samples with at least one person captured in the video in order to determine the statistics. Therefore, samples without people were not considered in the image processing.

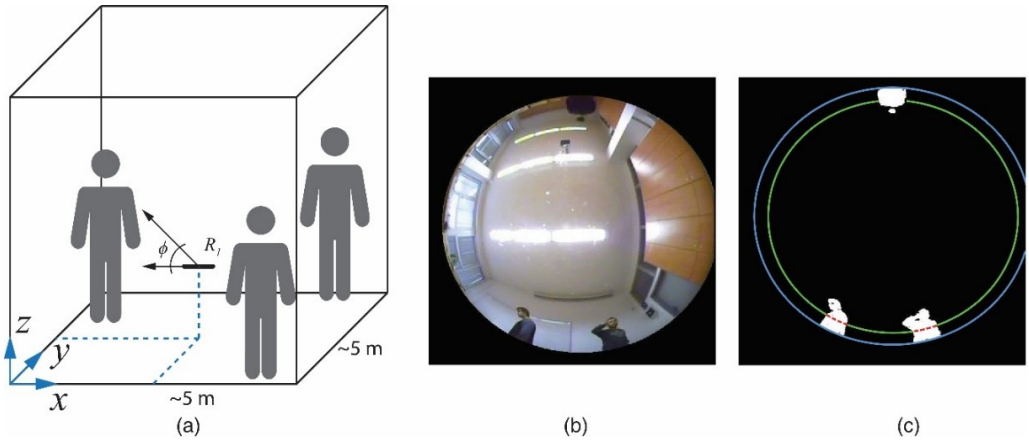

Fig. 2 (a) The experimental setup for VLC with shadowing, (b) a captured video sample, and (c) a processed image with a highlighted elevation angle of 7°. The calculated P_{sh} is ~10%. Note that, the elevation angle and its shadowed part are illustrated by green and red colors, respectively.

The individual samples were processed as follows: The distortion introduced by the lens was corrected by adopting the calibration procedure as in Ref. 24, which allowed us to back-project any pixel point into the 3D space and then estimated the elevation of the shadowed region. For the foreground object segmentation (i.e., people induced shadowing at the Rx), adaptive Gaussian mixture model (GMM) background subtraction method was employed[25]. Finally, the processed images, see Fig. 2(c), were used to determine P_{sh} of the individual elevation angles ϕ measured from the horizontal plane as the ratio between white N_w and black N_b pixels, which is given by:

$$P_{sh} = N_w/N_b. \tag{9}$$

3 Results and Discussions

For numerical simulations in Matlab, we have considered a rectangular room with the dimensions of 5 m × 5 m × 3 m (width × length × height) as illustrated in Fig. 1(a). An LED light source with P_t of 1 W was utilized as in line with the recent literature[7, 10]. We have considered three locations for the Tx and two for the Rx: Tx_1 is located at the center of the ceiling with

$\boldsymbol{r}_{Tx1} = (2.5, 2.5, 3)$ with m = 1 (i.e., $\vartheta_{1/2} = 60°$), Tx_2 and Tx_3 are mounted on the wall with $\boldsymbol{r}_{Tx2} = (5, 2.5, 1)$ and $\boldsymbol{r}_{Tx3} = (5, 1, 1)$, respectively for D2D communications with m = 20 (i.e. $\vartheta_{1/2} = \sim 15°$) with a narrow radiation pattern, and R_1 and R_2 positioned at the center (as in the experimental part) and in the corner of the room with $\boldsymbol{r}_{R1} = (2.5, 2.5, 0.8)$ and $\boldsymbol{r}_{R2} = (0.5, 1, 0.8)$, respectively for the worst case scenario. Note that, we have adopted the following parameters of A_R = 1 cm^2, and FOV = {60°, 70°, 80° and 90°}. As in Ref. 19, we considered k = 3 reflections modelled as purely diffuse, which can be approximated by the interior of an integrating sphere.

The focus of the paper is on the determining the system bandwidth, which is independent of modulation schemes[7,10]. Adopting multicarrier schemes such as orthogonal frequency division multiplexing (OFDM) and multiband carrier-less amplitude and phase (m-CAP) modulation, equalization or error control code techniques can significantly enhance the system performance by eliminating the ripples in the frequency response or by adapting the transmitted signal to the system frequency response. However, a knowledge of the system performance (without any additional advanced technique) in terms of bandwidth, received power and other parameters is essential for an efficient VLC system design. Thus, we focused in this paper on the channel characterization without any additional technique that can improve the system performance, which makes the results of the paper more general and allows the results to be compared with the most of the existing research.

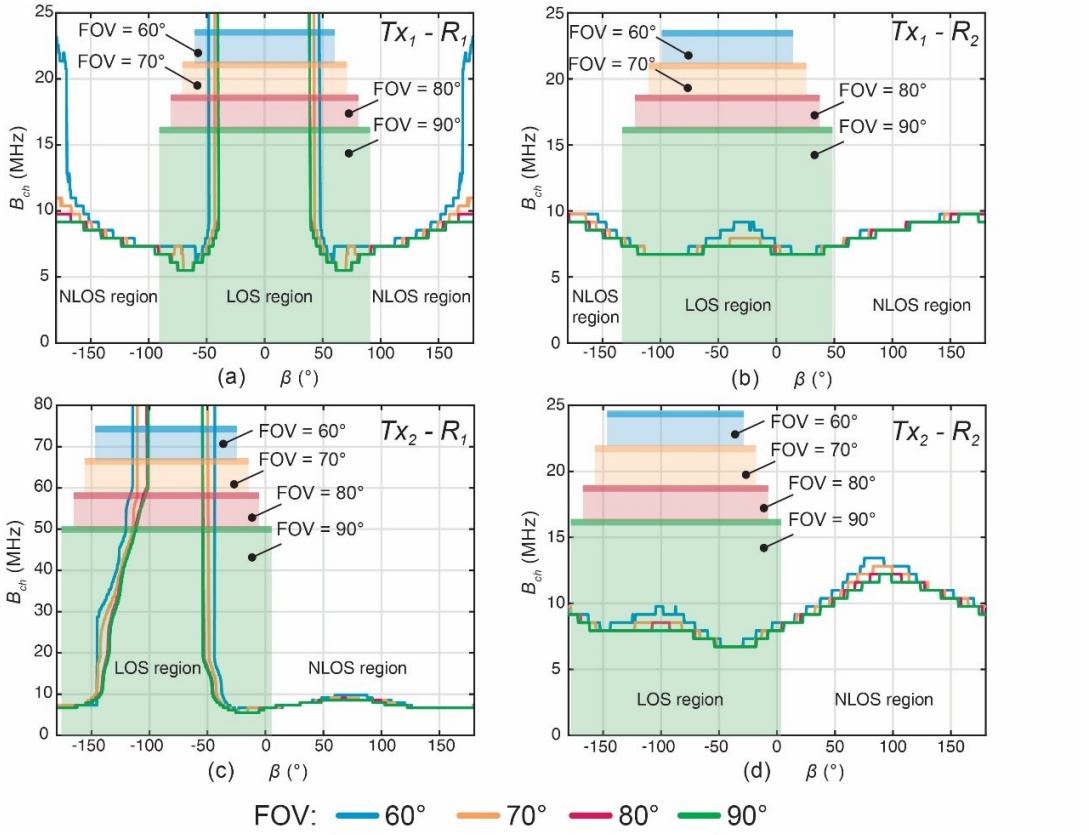

Fig. 3 The channel bandwidth as a function of the rotation angle β around y-axis for Tx placed *i*) on the ceiling (upper row) and Rx's positions: (a) in the middle (R_1), and (b) in the corner of the room (R_2); and *ii*) on the wall for D2D communications (bottom row) and Rx's position: (c) R_1, and (d) R_2. Note, color regions denote the presence of LOS path for particular FOVs.

3.1 Channel Bandwidth

Figs. 3(a) and (b) illustrate B_{ch} against the Rx's rotation angle β (i.e., rotation around the y-axis) for a range of FOVs for Tx_1 placed at the center of the ceiling and for R_1 and R_2 located in the middle and corner of the room, respectively. This provides a NLOS configuration for the typical case of indoor VLC. The color regions in each figure denote the range of rotation angles for FOV values, where the received optical signal also includes LOS component. For example, for a detector with a FOV of 80° for the link $Tx_1 - R_2$, see Fig. 3(b), the rotation angle β is within the

range of -120° to 40°. Note that, the Rx is rotated around the *y*-axis in a counterclockwise direction as depicted in Fig. 1(a). We can see from Fig. 3(a) that B_{ch} is almost the same over the wide range of β independent of the FOV. However, for the Rx with a FOV of 60° (blue curve) and for $|\beta| > \sim 165°$ (i.e., the Rx is facing towards the floor) we notice a significant improvement in B_{ch} by up to 14 MHz when only NLOS path is considered. This is because the received power from the 1st reflection from the floor is considerably higher than signal power from higher order reflections from other surfaces within the room.

The unlimited B_{ch} is achieved for the LOS case, i.e., for $|\beta| < 50°$ for a FOV of 60°. Note that, this range of β decreases with increasing values of FOV, see Fig. 3(a), thus contributing to the limitation of user's mobility. However, the pure NLOS link can still support adequate B_{ch} of > 7 MHz. Note, in the NLOS scenario higher $|\beta|$ leads to higher B_{ch}. Fig. 3(b) illustrates B_{ch} for the worst scenario where the source is located on the ceiling. With R_2 placed in the corner of the room, we observe similar profiles for both LOS and NLOS scenarios for a range of FOVs. However, the pure NLOS offers slightly higher (up to ~3 MHz) B_{ch} compared with the LOS for the FOV = {70°, 80° and 90°} because of lower received power levels of the LOS path.

Figs. 3(c) and (d) show B_{ch} for both the Rx's positions and for the Tx_2 placed on the wall for D2D communications. With the Rx tilted towards the Tx (i.e., see the LOS regions of individual Rxs), we observe a significant improvement in B_{ch} compared to the case where the source is placed on the ceiling, see Fig. 3(a). This is because of the presence of a strong LOS component. In the best case scenario, B_{ch} is ~62 MHz for all values of FOV. Note that, the NLOS case does not outperform the LOS link in D2D as was observed in the previous cases. For the Rx placed in the corner of the room (i.e., R_2) as in Fig. 3(d), the measured B_{ch} of the signal with LOS component is lower (up to ~8 MHz) for all values of FOV for $\beta > \sim 25°$ compared to the NLOS

case. This is attributed to two main reasons: (*i*) lower power contributions from the LOS path compared to the higher order reflections, since the Tx and the Rx are not pointing to each other as is the case in most D2D communications; and (*ii*) higher power contributions from the 1st reflection than from the higher order reflections, thus resulting in slightly increased B_{ch} compared to LOS. Moreover, compared to Fig. 3(c), we observe an improvement up to 4 MHz in B_{ch} for $\beta > \sim 50°$ for the pure NLOS channel, which is caused by stronger NLOS components received by the detector placed in the corner of the room.

To further illustrate the importance of the research findings for the D2D communications, we have evaluated the system performance for the Tx_3 placed off the central position on the wall and R_1 rotated around the *y*-axis. The measured B_{ch} against the rotation angle β is shown in Fig. 4. Compared to the results shown in Fig. 3(a) and Fig. 3(c), the system with NLOS path outperforms the LOS in B_{ch} up to ~4 MHz. Note that, for the LOS path B_{ch} is only ~6 MHz for the range of $-180° < \beta < 5°$. This is significantly lower compared to Figs. 3(a) and (c) due to the lower intensity of the LOS component arrived at the photodetector.

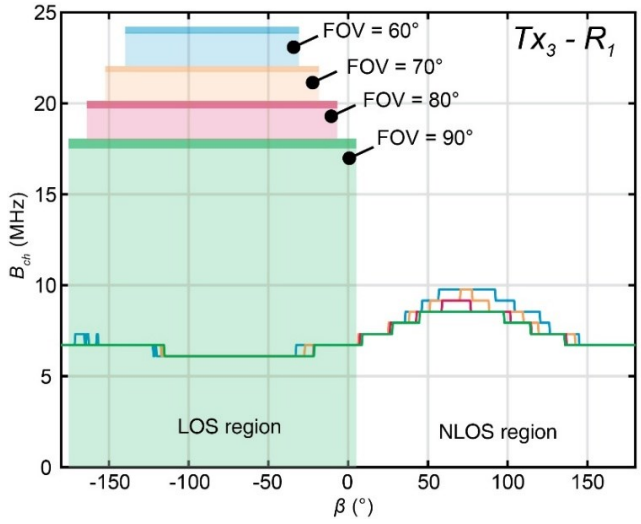

Fig. 4 The channel bandwidth as a function of the rotation angle β around *y*-axis for the Tx_3 and the R_1 for D2D communications. Note, color regions denote the presence of LOS path for particular FOVs.

Next, we considered the effect of the rotation of the Rx by the angle α around the x-axis on B_{ch} for NLOS D2D communications. The results for both R_1 and R_2 are shown in Figs. 5(a) and (b), respectively. B_{ch} is almost flat for all values of FOV and α, i.e., independent of user's mobility. However, for $\alpha < -10°$ the B_{ch} of NLOS is slightly (by ~2.5 MHz) higher compared to the LOS as shown in Fig. 5(b). Note that, for detectors with FOV = {60°, 70° and 80°} and FOV = {60° and 70°} no LOS component was received for any value of α as illustrated for R_1 and R_2 in Figs. 5(a) and (b), respectively.

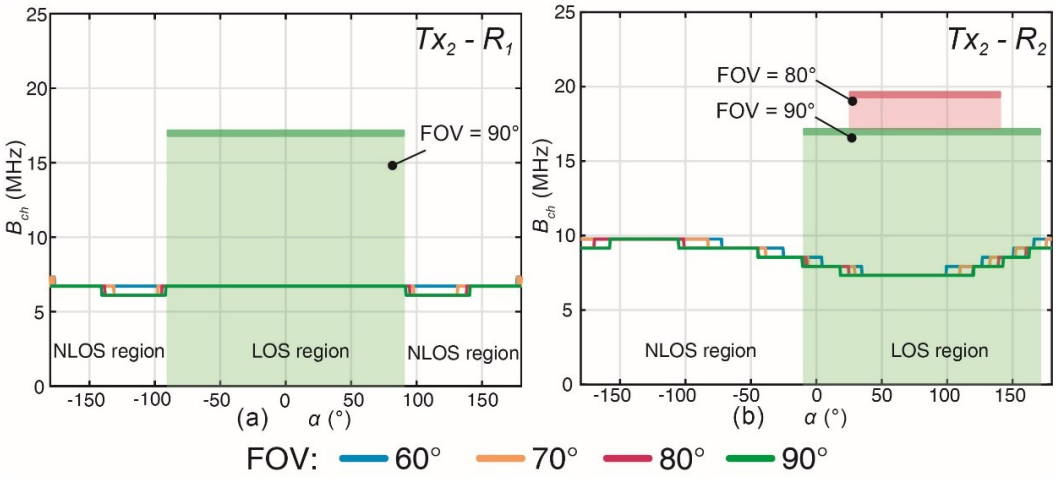

Fig. 5 The channel bandwidth against the rotation angle α around the x-axis for the Rx's position: (a) in the center (R_1), and (b) in the corner of the room (R_2) for D2D communications. Note, the color regions denote the presence of LOS component for particular Rx's FOVs (otherwise NLOS is observed).

3.2 LOS and NLOS Probability

Considering the rotation of the Rx, the numerical simulations show that for a Rx with a narrow FOV (i.e., 60°) the probability density function of receiving a signal including the LOS path is approximately half that of the pure NLOS. As shown in Fig. 6(a) for the case of $Tx_1 - R_1$ link and a Rx with a FOV of 60°, ~69% of transmission is established via the pure NLOS paths at the cost of reduced optical power levels compared to the LOS. However, user's mobility is enhanced.

Increasing the Rx's FOV to 90° resulted in equal transmission via LOS and NLOS paths, see Fig. 6(b).

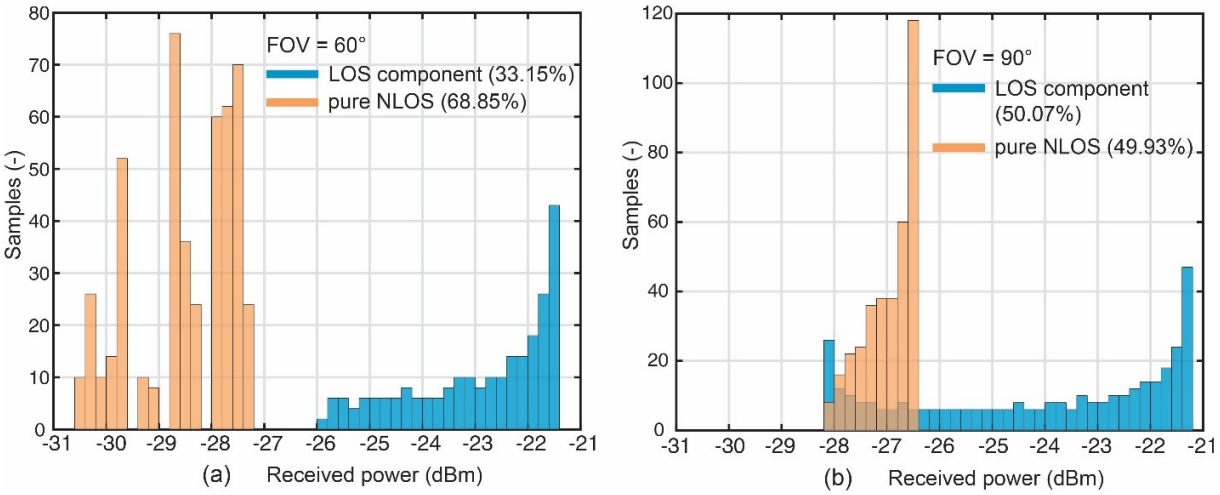

Fig. 6 The histograms of the received power for the configuration $Tx_1 - R_1$ and full rotation around y-axis for a Rx: (a) FOV = 60°, and (b) FOV = 90° with separated signals with LOS and pure NLOS received power components.

3.3 Shadowing

Using the set-up shown in Fig. 2(a) we carried out measurements for the maximum shadowing probabilities P_{sh} for a range of elevation angles ϕ as well as histograms of the received power for the pure NLOS for the FOVs of 60° and 90°, see Fig. 7. Note that, the highest measured P_{sh} of ~35.6% is observed at ϕ of 67°. Clearly, higher ϕ are affected more by people moving around the Rx. However, shadowing at these elevation angles occurs rarely in comparison to low elevation angles. Based on the measured data the received power level for the $Tx_1 - R_1$ configuration was consequently calculated. The same system model as in Section II was adopted in the simulation and only pure NLOS and shadowing (i.e., the measured P_{sh} values from Fig. 7(a)) due to people's movement around the Rx were considered. The total optical received power is dropped by 1.8 dB for the Rx with a FOV of 60°. For the Rx with a wider FOV of 90° the received power is decreased only by 1.3 dB (i.e., such a Rx is less sensitive to shadowing, since signals are

captured over a much wider range of elevation angles). Note that, shadowing also affect the histograms of received optical power for pure NLOS as illustrated in Figs. 7(b) and (c) for the FOVs of 60° and 90°, respectively.

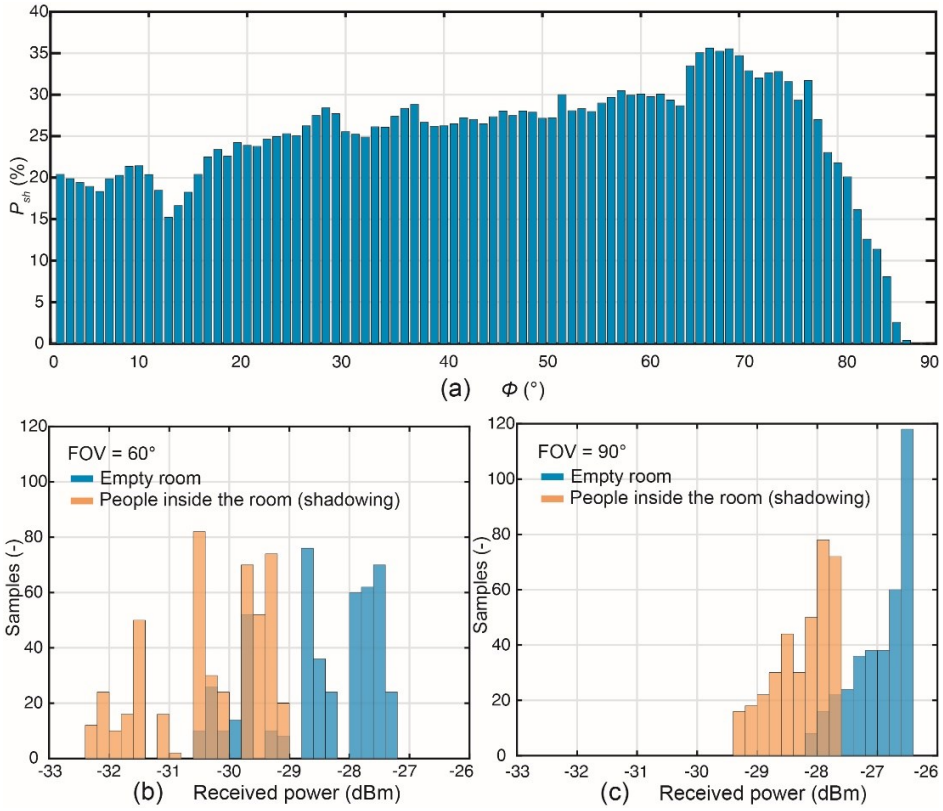

Fig. 7 Configuration $Tx_1 - R_1$ with shadowing caused by people: (a) the measured maximum shadowing probabilities for the range of elevation angles; and histograms of the pure NLOS received power for, and (b) FOV = 60° and (c) FOV = 90°.

4 Conclusion

In this work, we outlined the analysis of the NLOS VLC based on numerical simulations by including the receiver's orientation and a variable field of views. We considered a typical ceiling mounted transmitter for the case of D2D communications and showed that the pure NLOS channel in specific cases offered superior performance compared with the link with both LOS

and NLOS paths resulting in the increased channel bandwidth up to 14 MHz. Moreover, the receiver's rotation increased the probability of transmission via the pure NLOS channel compared to the case with the LOS path for narrow FOV receiver. Based on the experimental campaign we showed that higher elevation angles and receivers with a narrow FOV are more prone to the shadowing caused by people's movement within a room resulting in the received power level drop of 1.8 dB and 1.3 dB for the receiver with the FOV of 60° and 90°, respectively.

Acknowledgments

The work was supported by GACR 17-17538S.

References

1. Z. Ghassemlooy, L. N. Alves, S. Zvanovec, and M. A. Khalighi, *Visible Light Communications Theory and Applications.* CRC Press, Boca Raton (2017).
2. H. Chun, *et al.*, "LED based wavelength division multiplexed 10 Gb/s visible light communications," in *J. Lightw. Techn.*, **34** (13), pp. 3047-3052 (2016).
3. K.-D. Langer, *et al.,* "Rate-adaptive visible light communication at 500Mb/s arrives at plug and play," *Optoelectronics & Communications, SPIE Newsroom* (2013).
4. R. X. G. Ferreira, *et al.*, "High bandwidth GaN-based micro-LEDs for multi-Gb/s visible light communications," *IEEE Photonics Technol. Lett.*, **28** (19), pp. 2023–2026 (2016).
5. S. Rajbhandari, *et al.*, "High-speed integrated visible light communication system: Device constraints and design considerations," *IEEE J. Sel. areas Commun.*, **33** (9), pp. 1750–1757 (2015).
6. Z. Ghassemlooy, S. Arnon, M. Uysal, Z. Xu and J. Cheng, "Emerging optical wireless communications-advances and challenges," *IEEE J. Sel. Area. Comm.*, **33** (9), pp. 1738-1749 (2015).

7. K. Lee, H. Park, and J. R. Barry, "Indoor channel characteristics for visible light communications," *IEEE Commun. Lett.,* **15** (2), pp. 217-219 (2011).
8. S. Long, M. A. Khalighi, M. Wolf, S. Bourennane, and Z. Ghassemlooy, "Investigating channel frequency selectivity in indoor visible-light communication systems," *IET Optoelectron.*, **10** (3), pp. 80-88 (2016).
9. Y. Qiu, H.-H. Chen, and W.-X.Meng, "Channel modeling for visible light communications-a survey". *Wireless Comm. and Mob. Comp.*, **16**, pp. 2016-2034 (2016).
10. F. Miramirkhani and M. Uysal, "Channel modeling and characterization for visible light communications", *IEEE Photonics J.*, **7** (6), 1-16 (2015).
11. C. Le Bas, *et al.,* "Impact of receiver orientation and position on visible light communication link performance," in *Proc. International Workshop on Optical Wireless Communications*, pp. 1-5 (2015).
12. P. Chvojka, S. Zvanovec, P. A. Haigh and Z. Ghassemlooy, "Channel characteristics of visible light communications within dynamic indoor environment," *J. Lightw. Technol.*, **33** (9), pp. 1719-1725 (2015).
13. W. Gu, M. Aminikashani, P. Deng and M. Kavehrad, "Impact of multipath reflections on the performance of indoor visible light positioning systems," *J. Lightw. Technol.*, **34** (10), pp. 2578-2587 (2016).
14. C. Chen, D. Basnayaka and H. Haas, "Non-line-of-sight channel impulse response characterisation in visible light communications," *2016 IEEE International Conference on Communications (ICC)*, pp. 1-6., Kuala Lumpur (2016).
15. Z. Chen, D. Tsonev and H. Haas, "Improving SINR in indoor cellular visible light communication networks," *2014 IEEE International Conference on Communications (ICC)*, pp. 3383-3388, Sydney (2014).
16. J. B. Carruthers and J. M. Kahn, "Modeling of nondirected wireless infrared channels," in *IEEE Transactions on Communications*, **45** (10), pp. 1260-1268 (1997).

17. H. Hashemi, Gang Yun, M. Kavehrad, F. Behbahani and P. A. Galko, "Indoor propagation measurements at infrared frequencies for wireless local area networks applications," in *IEEE Transactions on Vehicular Technology*, **43** (3), pp. 562-576 (1994).
18. F. R. Gfeller and U. Bapst, "Wireless in-house data communication via diffuse infrared radiation," in *Proceedings of the IEEE*, **67** (11), pp. 1474-1486 (1979).
19. V. Jungnickel, V. Pohl, S. Nonnig and C. von Helmolt, "A physical model of the wireless infrared communication channel," *IEEE J. Sel. Area Comm.*, **20** (3), pp. 631-640 (2002).
20. J. M. Kahn, W. J. Krause and J. B. Carruthers, "Experimental characterization of non-directed indoor infrared channels," in *IEEE Transactions on Communications*, **43** (2/3/4), pp. 1613-1623 (1995).
21. S. T. Jovkova and M. Kavehard, "Multispot diffusing configuration for wireless infrared access," in *IEEE Transactions on Communications*, **48** (6), pp. 970-978 (2000).
22. J. B. Carruther and J. M. Kahn, "Angle diversity for nondirected wireless infrared communication," in *IEEE Transactions on Communications*, **48** (6), pp. 960-969 (2000).
23. H. Goldstein, C. Poole, and J. Safko, *Classical Mechanics*, Addison Wesley, Essex (2002).
24. D. Scaramuzza, A. Martinelli and R. Siegwart, "A toolbox for easily calibrating omnidirectional cameras," *in Proc. IEEE/RSJ International Conference on Intelligent Robots and Systems*, pp. 5695-5701, Beijing (2006).
25. Z. Zivkovic, "Improved adaptive Gaussian mixture model for background subtraction," in *Proc. 17th International Conference on Pattern Recognition,* pp. 28-31, Cambridge (2004).

5 Conclusions and Future Work

In this thesis, the state of art of the VLC technology is given at first providing a detailed description of the entire VLC system with an emphasis on techniques for increasing data rates and the characterization of the optical channel. The modulation scheme, called m-CAP, has been newly adopted for bandlimited VLC systems and investigates and verifies via numerical simulations and experimental campaigns. The results reported in [J1-J4] show the m-CAP scheme to be an ideal candidate for VLC systems. By splitting the signal bandwidth into several subcarriers, the attenuation caused by an LED frequency response is decreased and VLC links with high spectral efficiency can be supported. The highest measured spectral efficiency was around 6 b/s/Hz in [J4]. This is significant in VLC as it approaches the theoretically predicted values of achievable spectral efficiency reported in [J1]. The trade-off between m-CAP VLC system performance, in terms of data rates and computational complexity, was also investigated and recommendations for m-CAP scheme design were proposed [J3, J4].

The second part of the thesis, VLC channel modeling, is based on publications [J5, J6] detailing how the novel results were derived. Due to the lack of literature on the effect of shadowing in OWC systems, the VLC channel model considering movement of people was investigated for the first time in a VLC domain and provided both statistical and experimental results [J5]. The focus of the next research was NLOS-based VLC, as reported in [J6], to fulfill channel characterization in a dynamic environment. The results from numerical simulations were extended by a measurement campaign including the shadowing of the receiver. We demonstrated the benefits of NLOS-based communication over an LOS-based system and the impact of shadowing on NLOS VLC resulting in reduced received optical power for the ceiling transmitter coverage and D2D communications.

Based on the results published in [J1-J6], goals G1 and G2, listed in Section 3, were fulfilled.

The results attained in this thesis open a number of directions for future research. I would like to pursue the investigation of VLC systems using experimental campaigns rather than numerical simulations as a postdoc at Czech Technical University in Prague. However, theoretical analysis is a necessary step before measurements are taken. Despite the fact that m-CAP for VLC has been implemented recently, significant results have already been reported. However, more investigation needs to be performed. For instance, the computational complexity of the m-CAP system still remains an open issue which limits the m-CAP scheme implementation on FPGAs to build a real time VLC link. We have already started to work on a method to decrease the system complexity with our research partners at University College London and Northumbria University. Another option is to increase the measured transmission speeds of m-CAP VLC using equalization techniques to demonstrate high data rate links (i.e., hundreds of Mb/s and higher) competitive with recent OFDM-based VLC systems. To optimize m-CAP performance further, I propose a number of other research areas, such as investigating PAPR, optimization of bit- and power-loading techniques, or a comparison of existing modulation formats utilized in VLC.

The field of VLC channel modeling is widely covered by a number of publications

mainly considering the LOS type of communication. NLOS-based VLC is the focus of few publications and deserves a greater research effort. I believe that including characteristics of real components, such as LEDs radiation patterns, wavelength characteristics of indoor materials and wavelength response of detectors, will bring more accurate results closer to real VLC systems. The evaluation of different modulation scheme performances in VLC channel modeling, including D2D communications, is another important topic which I would like to cover in my future research.

Last but not least, I wish to keep and even deepen the collaboration with our colleagues from University College London and Northumbria University which began at the start of my doctoral studies.

References

[1] Z. Ghassemlooy, L. N. Alves, S. Zvanovec, and M. A. Khalighi, Visible Light Communications: Theory and Applications, CRC Press, Boca Raton, 2017.

[2] Cisco Visual Networking Index: Global Mobile Data Traffic Forecast Update, 2016-2021 White Paper, 2017.

[3] Y. Tanaka, S. Haruyama, and M. Nakagawa, "Wireless optical transmissions with white colored LED for wireless home links," *11th IEEE International Symposium on Personal, Indoor and Mobile Radio Communications (PIMRC)*, London, 2000, pp. 1325-1329.

[4] Y. Tanaka, T. Komine, S. Haruyama, and M. Nakagawa, "Indoor visible communication utilizing plural white LEDs as lighting," *12th IEEE International Symposium on Personal, Indoor and Mobile Radio Communications (PIMRC)*, San Diego, 2001, pp. 81-85.

[5] T. Komine and M. Nakagawa, "Integrated system of white LED visible-light communication and power-line communication," *13th IEEE International Symposium on Personal, Indoor and Mobile Radio Communications (PIMRC)*, Lisbon, 2002, pp. 1762-1766.

[6] T. Komine and M. Nakagawa, "Fundamental analysis for visible-light communication system using LED lights," in *IEEE Transactions on Consumer Electronics*, vol. 50, no. 1, pp. 100-107, 2004.

[7] S. Rajagopal, R. D. Roberts, and L. Sang-Kyu, "IEEE 802.15.7 visible light communication: modulation schemes and dimming support," in *IEEE Communications Magazine*, vol. 50, no. 3, pp. 72-82, 2012.

[8] Y. Wang, L. Tao, X. Huang, J. Shi, and N. Chi, "8-Gb/s RGBY LED-Based WDM VLC System Employing High-Order CAP Modulation and Hybrid Post Equalizer," in *IEEE Photonics Journal*, vol. 7, no. 6, pp. 1-7, 2015.

[9] G. Cossu, W. Ali, R. Corsini, and E. Ciaramella, "Gigabit-class optical wireless communication system at indoor distances (1.5 - 4 m)," in *Optics Express*, vol. 23, no.12, pp. 15700-15705, 2015.

[10] X. Huang, S. Chen, Z. Wang, J. Shi, Y. Wang, J. Xiao, and N. Chi, "2.0-Gb/s Visible Light Link Based on Adaptive Bit Allocation OFDM of a Single Phosphorescent White LED," in *IEEE Photonics Journal*, vol. 7, no. 5, pp. 1-8, 2015.

[11] Z. Ghassemlooy, W. Popoola, and S. Rajbhandari, Optical Wireless Communications: System and Channel Modelling with MATLAB, CRC Press, Boca Raton, 2013.

[12] J. K. Kim and E. F. Schubert, "Transcending the replacement paradigm of solid-state lighting," in *Optics Express*, vol. 16, no. 26, pp. 21835-21842, 2008.

[13] B. Lin, Z. Ghassemlooy, C. Lin, X. Tang, Y. Li, and S. Zhang, "An Indoor Visible Light Positioning System Based on Optical Camera Communications," in *IEEE Photonics Technology Letters*, vol. 29, no. 7, pp. 579-582, 2017.

[14] T. Q. Wang, Y. A. Sekercioglu, A. Neild, and J. Armstrong, "Position Accuracy of Time-of-Arrival Based Ranging Using Visible Light With Application in Indoor Localization Systems," in *Journal of Lightwave Technology*, vol. 31, no. 20, pp. 3302-3308, 2013.

[15] J. Armstrong, Y. Sekercioglu, and A. Neild, "Visible light positioning: a roadmap for international standardization," in *IEEE Communications Magazine*, vol. 51, no. 12, pp. 68-73, 2013.

[16] I. Takai, S. Ito, K. Yasutomi, K. Kagawa, M. Andoh, and S. Kawahito, "LED and CMOS Image Sensor Based Optical Wireless Communication System for Automotive Applications," in *IEEE Photonics Journal*, vol. 5, no. 5, 2013.

[17] Y. Shun-Hsiang, O. Shih, T. Hsin-Mu, N. Wisitpongphan, and R. Roberts, "Smart automotive lighting for vehicle safety," in *IEEE Communications Magazine*, vol. 51, no. 12, pp. 50-59, 2013.

[18] S. Arnon, "Optimised optical wireless car-to-traffic-light communication," in *Transactions on Emerging Telecommunications Technologies*, vol. 25, no. 6, pp. 660-665, 2014.

[19] P. Luo, Z. Ghassemlooy, H. L. Minh, E. Bentley, A. Burton, and X. Tang, "Performance analysis of a car-to-car visible light communication system," in *Applied Optics*, vol. 54, no. 7, pp. 1696-1706, 2015.

[20] H. Haas, "Visible light communication," *Optical Fiber Communications Conference and Exhibition (OFC)*, Los Angeles, 2015, pp. 1-72.

[21] T. Yokotani, "Application and technical issues on Internet of Things," *10th International Conference on Optical Internet (COIN)*, Yokohama, 2012, pp. 67-68.

[22] C. Shih-Hao, "A Visible Light Communication Link Protection Mechanism for Smart Factory," *IEEE 29th International Conference on Advanced Information Networking and Applications Workshops (WAINA)*, Gwangiu, 2015, pp. 733-737.

[23] G. Corbellini, K. Aksit, S. Schmid, S. Mangold, and T. Gross, "Connecting networks of toys and smartphones with visible light communication," in *IEEE Communications Magazine*, vol. 52, no. 7, pp. 72-78, 2014.

[24] N. O. Tippenhauer, D. Giustiniano, and S. Mangold, "Toys communicating with LEDs: Enabling toy cars interaction," *IEEE Consumer Communications and Networking Conference (CCNC)*, Las Vegas, 2012, pp. 48-49.

[25] G. Cossu, R. Corsini, A. M. Khalid, S. Balestrino, A. Coppelli, A. Caiti, and E. Ciaramella, "Experimental demonstration of high speed underwater visible light communications," *2013 2nd International Workshop on Optical Wireless Communications (IWOW)*, Newcastle upon Tyne, 2013, pp. 11-15.

[26] C. Wang, H. Y. Yu, and Y. J. Zhu, "A Long Distance Underwater Visible Light Communication System With Single Photon Avalanche Diode," in *IEEE Photonics Journal*, vol. 8, no. 5, pp. 1-11, 2016.

[27] D. Krichene, M. Sliti, W. Abdallah, and N. Boudriga, "An aeronautical visible light communication system to enable in-flight connectivity," *2015 17th International Conference on Transparent Optical Networks (ICTON)*, Budapest, 2015, pp. 1-6.

[28] D. R. Dhatchayeny, A. Sewaiwar, S. V. Tiwari, and Y. H. Chung, "Experimental Biomedical EEG Signal Transmission Using VLC," in *IEEE Sensors Journal*, vol. 15, no. 10, pp. 5386-5387, 2015.

[29] B. Bangerter, S. Talwar, R. Arefi, and K. Stewart, "Networks and devices for the 5G era," in *IEEE Communications Magazine*, vol. 52, no. 2, pp. 90-96, 2014.

[30] S. Wu, H. Wang, and C. H. Youn, "Visible light communications for 5G wireless networking systems: from fixed to mobile communications," in *IEEE Network*, vol. 28, no. 6, pp. 41-45, 2014.

[31] International Organization for Standardization (ISO), ISO/TC 274: Light and lighting, Lighting of work places − Part 1: Indoor (ISO 8995-2002), Geneva, 2002.

[32] H. Le Minh, D. O'Brien, G. Faulkner, L. Zeng, K. Lee, D. Jung, Y. Oh, and E. T. Won, "100-Mb/s NRZ Visible Light Communications Using a Postequalized White LED," in *IEEE Photonics Technology Letters*, vol. 21, no. 15, pp. 1063-1065, 2009.

[33] P. A. Haigh, Z. Ghassemlooy, S. Rajbhandari, I. Papakonstantinou, and W. Popoola, "Visible Light Communications: 170 Mb/s Using an Artificial Neural Network Equalizer in a Low Bandwidth White Light Configuration," in *Journal of Lightwave Technology*, vol. 32, no. 9, pp. 1807-1813, 2014.

[34] R. X. G. Ferreira *et al.*, "High Bandwidth GaN-Based Micro-LEDs for Multi-Gb/s Visible Light Communications," in *IEEE Photonics Technology Letters*, vol. 28, no. 19, pp. 2023-2026, 2016.

[35] S. Rajbhandari *et al.*, "High-Speed Integrated Visible Light Communication System: Device Constraints and Design Considerations," in *IEEE Journal on Selected Areas in Communications*, vol. 33, no. 9, pp. 1750-1757, 2015.

[36] A. Buckley, Organic light-emitting diodes (OLEDs): Materials, devices and applications, Woodhead Publishing Limited, Cambridge, 2013.

[37] I. A. Barlow, T. Kreouzis, and D. G. Lidzey, "High-speed electroluminescence modulation of a conjugated-polymer light emitting diode," *Applied Physics Letters*, vol. 94, nol. 24, pp. 243301-24303, 2009.

[38] Z. Ghassemlooy, "Investigation of the baseline wander effect on indoor optical wireless system employing digital pulse interval modulation [optical wireless communications]," in *IET Communications*, vol. 2, no. 1, pp. 53-60, 2008.

[39] P. A. Haigh, Z. Ghassemlooy, S. Rajbhandari, and I. Papakonstantinou, "Visible light communications using organic light emitting diodes," in *IEEE Communications Magazine*, vol. 51, no. 8, pp. 148-154, 2013.

[40] P. A. Haigh, Z. Ghassemlooy, H. Le Minh, S. Rajbhandari, F. Arca, S. F. Tedde, O. Hayden, and I. Papakonstantinou, "Exploiting Equalization Techniques for Improving Data Rates in Organic Optoelectronic Devices for Visible Light Communications,"in *Journal of Lightwave Technology*, vol. 30, no. 19, pp. 3081-3088, 2012.

[41] P. A. Haigh, Z. Ghassemlooy, and I. Papakonstantinou, "1.4-Mb/s White Organic LED Transmission System Using Discrete Multitone Modulation," in *IEEE Photonics Technology Letters*, vol. 25, no. 6, pp. 615-618, 2013.

[42] P. A. Haigh, Z. Ghassemlooy, I. Papakonstantinou, and H. Le Minh, "2.7 Mb/s With a 93-kHz White Organic Light Emitting Diode and Real Time ANN Equalizer," in *IEEE Photonics Technology Letters*, vol. 25, no. 17, pp. 1687-1690, 2013.

[43] P. A. Haigh, F. Bausi, Z. Ghassemlooy, I. Papakonstantinou, H. Le Minh, C. Flechon, and F. Cacialli, "Visible light communications: real time 10 Mb/s link with a low bandwidth polymer light-emitting diode," in *Optics Express*, vol. 22, no. 3, pp. 2830-2838, 2014.

[44] S. T. Le, T. Kanesan, F. Bausi, P. A. Haigh, S. Rajbhandari, Z. Ghassemlooy, I. Papakonstantinou, W. O. Popoola, A. Burton, H. Le Minh, F. Cacialli, and A. D. Ellis, "10 Mb/s visible light transmission system using a polymer light-emitting diode with orthogonal frequency division multiplexing," in *Optics Letters*, vol. 39, no. 13, pp. 3876-3879, 2014.

[45] P. A. Haigh, F. Bausi, T. Kanesan, S. T. Le, S. Rajbhandari, Z. Ghassemlooy, I. Papakonstantinou, W. O. Popoola, A. Burton, H. Le Minh, A. D. Ellis, and F. Cacialli, "A 20-Mb/s VLC Link With a Polymer LED and a Multilayer Perceptron Equalizer," in *IEEE Photonics Technology Letters*, vol. 26, no. 19, pp. 1975-1978, 2014.

[46] P. A. Haigh, F. Bausi, H. Minh, I. Papakonstantinou, W. Popoola, A. Burton, and F. Cacialli, "Wavelength-Multiplexed Polymer LEDs: Towards 55 Mb/s Organic Visible Light Communications," in *IEEE Journal on Selected Areas in Communications*, vol. 33, no. 9, pp. 1819-1828, 2015.

[47] H. Chen, Z. Xu, Q. Gao, and S. Li, "A 51.6 Mbps Experimental VLC System Using A Monochromic Organic LED," in *IEEE Photonics Journal*, vol. PP, no. 99, pp. 1-1.

[48] S. Reineke, F. Lindner, G. Schwartz, N. Seidler, K. Walzer, B. Lussem, and K. Leo, "White organic light-emitting diodes with fluorescent tube efficiency," in *Nature*, vol. 459, pp. 234-238, 2009.

[49] J. R. Barry, J. M. Kahn, W. J. Krause, E. A. Lee, and D. G. Messerschmitt, "Simulation of multipath impulse response for indoor wireless optical channels," in *IEEE Journal on Selected Areas in Communications*, vol. 11, no. 3, pp. 367-379, 1993.

[50] K. Lee, H. Park, and J. R. Barry, "Indoor Channel Characteristics for Visible Light Communications," in *IEEE Communications Letters*, vol. 15, no. 2, pp. 217-219, 2011.

[51] F. J. Lopez-Hernandez, R. Perez-Jimenez, and A. Santamaria, "Monte Carlo calculation of impulse response on diffuse IR wireless indoor channels," in *Electronics Letters*, vol. 34, no. 12, pp. 1260-1262, 1998.

[52] F. J. Lopez-Hernandez, R. Perez-Jimenez, and A. Santamaria, "Modified Monte Carlo scheme for high-efficiency simulation of the impulse response on diffuse IR wireless indoor channels," in *Electronics Letters*, vol. 34, no. 19, pp. 1819-1820, 1998.

[53] F. Miramirkhani, O. Narmanlioglu, M. Uysal, and E. Panayirci, "A Mobile Channel Model for VLC and Application to Adaptive System Design," in *IEEE Communications Letters*, vol. 21, no. 5, pp. 1035-1038, 2017.

[54] R. M. Gagliardi and S. Karp, Optical Communications, 2nd Edition, John Wiley & Sons, New York, 1995.

[55] S. Zvanovec, P. Chvojka, P. A. Haigh, and Z. Ghasemlooy, "Visible light communications towards 5G," in *Radioengineering*, vol. 24, no. 1, 2015.

[56] Z. Ghassemlooy, P. A. Haigh, F. Arca, S. F. Tedde, O. Hayden, I. Papakonstantinou, and S. Rajbhandari, "Visible light communications: 3.75 Mbits/s data rate with a 160 kHz bandwidth organic photodetector and artificial neural network equalization [Invited]," in *Photonics Research*, vol. 1, no. 2, pp. 65-68, 2013.

[57] P. A. Haigh, Z. Ghassemlooy, I. Papakonstantinou, F. Arca, S. F. Tedde, O. Hayden, and E. Leitgeb, "A 1-Mb/s Visible Light Communications Link With Low Bandwidth Organic Components," in *IEEE Photonics Technology Letters*, vol. 26, no. 13, pp. 1295-1298, 2014.

[58] S. Rajbhandari, J. D. McKendry, J. Hernsdorf, H. Chun, G. Faulkner, H. Haas, I. M. Watson, D. O'Brien, and M. D. Dawson, "A review of gallium nitride LEDs for multi-gigabit-per-second visible light data communications", in *Semiconductor Science and Technology*, vol. 32, no. 2, 2017.

[59] H. Le Minh, D. O'Brien, G. Faulkner, L. Zeng, K. Lee, D. Jung, Y. Oh, and E. T. Won, "100-Mb/s NRZ Visible Light Communications Using a Postequalized White LED," in *IEEE Photonics Technology Letters*, vol. 21, no. 15, pp. 1063-1065, 2009.

[60] J. Vucic, Ch. Kotke, S. Nerreter, K. Habel, A. Buttner, K.-D. Langer, and J. W. Walewski, "230 Mbit/s via a wireless visible-light link based on OOK modulation of phosphorescent white LEDs," *2010 Conference on Optical Fiber Communication and National Fiber Optic Engineers Conference (OFC/NFOEC)*, San Diego, 2010, pp. 1-3.

[61] N. Fujimoto and H. Mochizuki, "614 Mbit/s OOK-based transmission by the duobinary technique using a single commercially available visible LED for high-speed visible light communications," *2012 38th European Conference and Exhibition on Optical Communications (ECOC)*, Amsterdam, 2012, pp. 1-3.

[62] H. Li, X. Chen, J. Guo, and H. Chen, "A 550 Mbit/s real-time visible light communication system based on phosphorescent white light LED for practical high-speed low-complexity application," in *Optics Express*, vol. 22, pp. 27203-27213, 2014.

[63] J. Choi, E. Cho, Z. Ghassemlooy, S. Kim, and C. G. Lee, "Visible light communications employing PPM and PWM formats for simultaneous data transmission and dimming," in *Optical and Quantum Electronics*, vol. 47, no. 3, pp. 561-574, 2015.

[64] K. Lee and H. Park, "Modulations for Visible Light Communications With Dimming Control," in *IEEE Photonics Technology Letters*, vol. 23, no. 16, pp. 1136-1138, 2011.

[65] B. Bai, Z. Xu, and Y. Fan, "Joint LED dimming and high capacity visible light communication by overlapping PPM," *The 19th Annual Wireless and Optical Communications Conference (WOCC)*, Shanghai, 2010, pp. 1-5.

[66] C. Xi, A. Mirvakili, and V. J. Koomson, "A Visible Light Communication System Demonstration Based on 16-Level Pulse Amplitude Modulation of an LED Array," *2012 Symposium on Photonics and Optoelectronics (SOPO)*, Shanghai, 2012, pp. 1-4.

[67] I. N. Osahon, E. Pikasis, S. Rajbhandari, and W. O. Popoola, "Hybrid POF/VLC link with M-PAM and MLP equaliser," *2017 IEEE International Conference on Communications (ICC)*, Paris, France, 2017, pp. 1-6.

[68] D. J. F. Barros, S. K. Wilson, and J. M. Kahn, "Comparison of Orthogonal Frequency-Division Multiplexing and Pulse-Amplitude Modulation in Indoor Optical Wireless Links," in *IEEE Transactions on Communications*, vol. 60, no. 1, pp. 153-163, 2012.

[69] X. Li *et al.*, "Wireless Visible Light Communications Employing Feed-Forward Pre-Equalization and PAM-4 Modulation," in *Journal of Lightwave Technology*, vol. 34, no. 8, pp. 2049-2055, 2016.

[70] J. F. Li, Z. T. Huang, R. Q. Zhang, F. X. Zeng, M. Jiang, and Y. F. Ji, "Superposed pulse amplitude modulation for visible light communication," in *Optics Express*, vol. 21, pp, 31006-31011, 2013.

[71] D. Bykhovsky and S. Arnon, "An Experimental Comparison of Different Bit-and-Power-Allocation Algorithms for DCO-OFDM," in *Journal of Lightwave Technology*, vol. 32, no. 8, pp. 1559-1564, 2014.

[72] J. Armstrong, "OFDM for Optical Communications," in *Journal of Lightwave Technology*, vol. 27, no. 3, pp. 189-204, 2009.

[73] S. Dimitrov, S. Sinanovic, and H. Haas, "Signal Shaping and Modulation for Optical Wireless Communication," in *Journal of Lightwave Technology*, vol. 30, no. 9, pp. 1319-1328, 2012.

[74] D. Tsonev, S. Sinanovic, and H. Haas, "Complete Modeling of Nonlinear Distortion in OFDM-Based Optical Wireless Communication," in *Journal of Lightwave Technology*, vol. 31, no. 18, pp. 3064-3076, 2013.

[75] N. Fernando, Y. Hong, and E. Viterbo, "Flip-OFDM for optical wireless communications," *2011 IEEE Information Theory Workshop (ITW)*, Paraty, 2011, pp. 5-9.

[76] J. Armstrong and A. J. Lowery, "Power efficient optical OFDM," in *Electronics Letters*, vol. 42, no. 6, pp. 370-372, 2006.

[77] A. H. Azhar and D. O'Brien, "Experimental comparisons of optical OFDM approaches in visible light communications," *2013 IEEE Globecom Workshops (GC Wkshps)*, Atlanta, 2013, pp. 1076-1080.

[78] Z. Yu, R. J. Baxley, and G. T. Zhou, "Achievable data rate analysis of clipped FLIP-OFDM in optical wireless communication," *2012 IEEE Globecom Workshops (GC Wkshps)*, Anaheim, 2012, pp. 1203-1207.

[79] S. Dimitrov and H. Haas, "Information Rate of OFDM-Based Optical Wireless Communication Systems With Nonlinear Distortion," in *Journal of Lightwave Technology*, vol. 31, no. 6, pp. 918-929, 2013.

[80] J. Armstrong and B. J. C. Schmidt, "Comparison of Asymmetrically Clipped Optical OFDM and DC-Biased Optical OFDM in AWGN," in *IEEE Communications Letters*, vol. 12, no. 5, pp. 343-345, 2008.

[81] J. Armstrong, B. J. C. Schmidt, D. Kalra, H. A. Suraweera, and A. J. Lowery, "SPC07-4: Performance of Asymmetrically Clipped Optical OFDM in AWGN for an Intensity Modulated Direct Detection System," *IEEE Globecom 2006*, San Francisco, 2006, pp. 1-5.

[82] W. O. Popoola, Z. Ghassemlooy, and B. G. Stewart, "Pilot-Assisted PAPR Reduction Technique for Optical OFDM Communication Systems," in *Journal of Lightwave Technology*, vol. 32, no. 7, pp. 1374-1382, 2014.

[83] V. Guerra, C. Suarez-Rodriguez, O. El-Asmar, J. Rabadan, and R. Perez-Jimenez, "Pulse width modulated optical OFDM," *2015 IEEE International Conference on Communication Workshop (ICCW)*, London, 2015, pp. 1333-1337.

[84] W. Kang and S. Hranilovic, "Power reduction techniques for multiple-subcarrier modulated diffuse wireless optical channels," in *IEEE Transactions on Communications*, vol. 56, no. 2, pp. 279-288, 2008.

[85] G. Cossu, A. M. Khalid, P. Choudhury, R. Corsini, and E. Ciaramella, "3.4 Gbit/s visible optical wireless transmission based on RGB LED," in *Optics Express*, vol. 20, no. 26, pp. B501-B506, 2012.

[86] H. Chun *et al.*, "LED Based Wavelength Division Multiplexed 10 Gb/s Visible Light Communications," in *Journal of Lightwave Technology*, vol. 34, no. 13, pp. 3047-3052, 2016.

[87] G. Cossu, A. M. Khalid, P. Choudhury, R. Corsini, and E. Ciaramella, "2.1 Gbit/s Visible Optical Wireless Transmission," *2012 European Conference and Exhibition on Optical Communication (ECOC)*, Amsterdam, 2012.

[88] X. Huang, J. Shi, J. Li, Y. Wang, and N. Chi, "A Gb/s VLC Transmission Using Hardware Preequalization Circuit," in *IEEE Photonics Technology Letters*, vol. 27, no. 18, pp. 1915-1918, 2015.

[89] F. M. Wu, C. T. Lin, C. C. Wei, C. W. Chen, H. T. Huang, and C. H. Ho, "1.1-Gb/s White-LED-Based Visible Light Communication Employing Carrier-Less Amplitude and Phase Modulation," in *IEEE Photonics Technology Letters*, vol. 24, no. 19, pp. 1730-1732, 2012.

[90] Y. Wang, L. Tao, X. Huang, J. Shi, and N. Chi, "Enhanced Performance of a High-Speed WDM CAP64 VLC System Employing Volterra Series-Based Nonlinear Equalizer," in *IEEE Photonics Journal*, vol. 7, no. 3, pp. 1-7, 2015.

[91] F.-M. Wu, C.-T. Lin, C.-C. Wei, C.-W. Chen, Z.-Y. Chen, and H.-T. Huang, "3.22-Gb/s WDM visible light communication of a single RGB LED employing carrier-less amplitude and phase modulation," *2013 Optical Fiber Communication Conference and Exposition and the National Fiber Optic Engineers Conference (OFC/NFOEC)*, Anaheim, 2013, pp. 1-3.

[92] F. M. Wu, C. T. Lin, C. C. Wei, C. W. Chen, Z. Y. Chen, H. T. Huang, and S. Chi, "Performance Comparison of OFDM Signal and CAP Signal Over High Capacity RGB-LED-Based WDM Visible Light Communication," in *IEEE Photonics Journal*, vol. 5, no. 4, 2013.

[93] J. Zhang, J. Yu, F. Li, N. Chi, Z. Dong, and X. Li, "11 × 5 × 9.3Gb/s WDM-CAP-PON based on optical single-side band multi-level multi-band carrier-less amplitude and phase modulation with direct detection," in *Optics Express*, vol. 21, no. 16, pp. 18842-18848, 2013.

[94] M. I. Olmedo, T. Zuo, J. B. Jensen, Q. Zhong, X. Xu, S. Popov, and I. T. Monroy, "Multiband Carrierless Amplitude Phase Modulation for High Capacity Optical Data Links," in *Journal of Lightwave Technology*, vol. 32, no. 4, pp. 798-804, 2014.

[95] J. Grubor, S. C. J. Lee, K.-D. Langer, T. Koonen, and J. W. Walewski, "Wireless High-Speed Data Transmission with Phosphorescent White-Light LEDs," *33rd European Conference and Exhibition of Optical Communication (ECOC)*, Berlin, 2007.

[96] A. M. Khalid, G. Cossu, R. Corsini, P. Choudhury, and E. Ciaramella, "1-Gb/s Transmission Over a Phosphorescent White LED by Using Rate-Adaptive Discrete Multitone Modulation," in *IEEE Photonics Journal*, vol. 4, no. 5, pp. 1465-1473, 2012.

[97] W. O. Popoola and H. Haas, "Demonstration of the Merit and Limitation of Generalised Space Shift Keying for Indoor Visible Light Communications," in *Journal of Lightwave Technology*, vol. 32, no. 10, pp. 1960-1965, 2014.

[98] G. Stepniak, M. Schuppert, and C. A. Bunge, "Advanced Modulation Formats in Phosphorous LED VLC Links and the Impact of Blue Filtering," in *Journal of Lightwave Technology*, vol. 33, no. 21, pp. 4413-4423, 2015.

[99] J.-Y. Sung, C.-W. Chow, and C.-H. Yeh, "Is blue optical filter necessary in high speed phosphor-based white light LED visible light communications?," in *Optics Express*, vol. 22, no. 17, pp. 20646-20651, 2014.

[100] H. Le Minh, D. O'Brien, G. Faulkner, L. Zeng, K. Lee, D. Jung, and Y. Oh, "High-Speed Visible Light Communications Using Multiple-Resonant Equalization," in *IEEE Photonics Technology Letters*, vol. 20, no. 14, pp. 1243-1245, 2008.

[101] H. Li, X. Chen, J. Guo, D. Tang, B. Huang, and H. Chen, "200 Mb/s visible optical wireless transmission based on NRZ-OOK modulation of phosphorescent white LED and a pre-emphasis circuit," in *Chinese Optics Letters*, vol. 12, no. 10, 2014.

[102] H. Li, X. Chen, J. Guo, and H. Chen, "A 550 Mbit/s real-time visible light communication system based on phosphorescent white light LED for practical high-speed low-complexity application," in *Optics Express*, vol. 22, no. 22, pp. 27203-27213, 2014.

[103] H. Li, X. Chen, J. Guo, Z. Gao, and H. Chen, "An analog modulator for 460 MB/S visible light data transmission based on OOK-NRS modulation," in *IEEE Wireless Communications*, vol. 22, no. 2, pp. 68-73, 2015.

[104] H. Li, X. Chen, B. Huang, D. Tang, and H. Chen, "High Bandwidth Visible Light Communications Based on a Post-Equalization Circuit," in *IEEE Photonics Technology Letters*, vol. 26, no. 2, pp. 119-122, 2014.

[105] H. Li, Y. Zhang, X. Chen, C. Wu, J. Guo, Z. Gao, W. Pei, and H. Chen, "682Mbit/s phosphorescent white LED visible light communications utilizing analog equalized 16QAM-OFDM modulation without blue filter," in *Optics Communications*, vol. 354, pp. 107-111, 2015.

[106] S. Randel, F. Breyer, S. C. J. Lee, and J. W. Walewski, "Advanced Modulation Schemes for Short-Range Optical Communications," in *IEEE Journal of Selected Topics in Quantum Electronics*, vol. 16, no. 5, pp. 1280-1289, 2010.

[107] S. Rajbhandari, P. A. Haigh, Z. Ghassemlooy, and W. Popoola, "Wavelet-Neural Network VLC Receiver in the Presence of Artificial Light Interference," in *IEEE Photonics Technology Letters*, vol. 25, no. 15, pp. 1424-1427, 2013.

[108] G. Stepniak, L. Maksymiuk, and J. Siuzdak, "1.1 GBIT/S white lighting LED-based visible light link with pulse amplitude modulation and Volterra DFE equalization," in *Microwave and Optical Technology Letters*, vol. 57, no. 7, pp. 1620-1622, 2015.

[109] Y. Wang and N. Chi, "Demonstration of High-Speed 2 $\times$ 2 Non-Imaging MIMO Nyquist Single Carrier Visible Light Communication With Frequency Domain Equalization," in *Journal of Lightwave Technology*, vol. 32, no. 11, pp. 2087-2093, 2014.

[110] Y. Wang, X. Huang, J. Zhang, Y. Wang, and N. Chi, "Enhanced performance of visible light communication employing 512-QAM N-SC-FDE and DD-LMS," in *Optics Express*, vol. 22, no. 13, pp. 15328-15334, 2014.

[111] Y. Wang, R. Li, Y. Wang, and Z. Zhang, "3.25-Gbps visible light communication system based on single carrier frequency domain equalization utilizing an RGB LED," *2014 Optical Fiber Communications Conference and Exhibition (OFC)*, San Francisco, 2014, pp. 1-3.

[112] D. O'Brien *et al.*, "High-Speed Optical Wireless Demonstrators: Conclusions and Future Directions," in *Journal of Lightwave Technology*, vol. 30, no. 13, pp. 2181-2187, 2012.

[113] Z. Chen, D. Tsonev, and H. Haas, "Improving SINR in indoor cellular visible light communication networks," *2014 IEEE International Conference on Communications (ICC)*, Sydney, 2014, pp. 3383-3388.

[114] A. Yang, Y. Wu, M. Kavehrad, and G. Ni, "Grouped modulation scheme for led array module in a visible light communication system," in *IEEE Wireless Communications*, vol. 22, no. 2, pp. 24-28, 2015.

[115] M. S. A. Mossaad and S. Hranilovic, "Practical OFDM signalling for visible light communications using spatial summation," *2014 27th Biennial Symposium on Communications (QBSC)*, Kingston, 2014, pp. 5-9.

[116] B. Yu, H. Zhang, L. Wei, and J. Song, "Subcarrier Grouping OFDM for Visible-Light Communication Systems," in *IEEE Photonics Journal*, vol. 7, no. 5, pp. 1-12, 2015.

[117] M. Di Renzo, H. Haas, A. Ghrayeb, S. Sugiura, and L. Hanzo, "Spatial Modulation for Generalized MIMO: Challenges, Opportunities, and Implementation," in *Proceedings of the IEEE*, vol. 102, no. 1, pp. 56-103, 2014.

[118] R. Mesleh, H. Elgala, and H. Haas, "Optical Spatial Modulation," in *IEEE/OSA Journal of Optical Communications and Networking*, vol. 3, no. 3, pp. 234-244, 2011.

[119] T. Fath and H. Haas, "Performance Comparison of MIMO Techniques for Optical Wireless Communications in Indoor Environments," in *IEEE Transactions on Communications*, vol. 61, no. 2, pp. 733-742, 2013.

[120] K. Cai and M. Jiang, "SM/SPPM Aided Multiuser Precoded Visible Light Communication Systems," in *IEEE Photonics Journal*, vol. 8, no. 2, pp. 1-9, 2016.

[121] M. Ijaz *et al.*, "Experimental proof-of-concept of optical spatial modulation OFDM using micro LEDs," *2015 IEEE International Conference on Communication Workshop (ICCW)*, London, 2015, pp. 1338-1343.

[122] W. O. Popoola, E. Poves, and H. Haas, "Error Performance of Generalised Space Shift Keying for Indoor Visible Light Communications," in *IEEE Transactions on Communications*, vol. 61, no. 5, pp. 1968-1976, 2013.

[123] A. Burton, H. Le Minh, Z. Ghassemlooy, E. Bentley, and C. Botella, "Experimental Demonstration of 50-Mb/s Visible Light Communications Using 4×4 MIMO," in *IEEE Photonics Technology Letters*, vol. 26, no. 9, pp. 945-948, 2014.

[124] S. Zhang, S. Watson, J. J. D. McKendry, D. Massoubre, A. Cogman, E. Gu, R. K. Henderson, A. E. Kelly, and M. D. Dawson, "1.5 Gbit/s Multi-Channel Visible Light Communications Using CMOS-Controlled GaN-Based LEDs," in *Journal of Lightwave Technology*, vol. 31, no. 8, pp. 1211-1216, 2013.

[125] K. D. Dambul, D. C. O'Brien, and G. Faulkner, "Indoor Optical Wireless MIMO System With an Imaging Receiver," in *IEEE Photonics Technology Letters*, vol. 23, no. 2, pp. 97-99, 2011.

[126] P. A. Haigh, Z. Ghassemlooy, I. Papakonstantinou, F. Tedde, S. F. Tedde, O. Hayden, and S. Rajbhandari , "A MIMO-ANN system for increasing data rates in organic visible light communications systems," *2013 IEEE International Conference on Communications (ICC)*, Budapest, 2013, pp. 5322-5327.

[127] J. Vucic, C. Kottke, K. Habel, and K.-D. Langer, "803 Mbit/s visible light WDM link based on DMT modulation of a single RGB LED luminary," *2011 Optical Fiber Communication Conference and Exposition and the National Fiber Optic Engineers Conference (OFC)*, Los Angeles, 2011, pp. 1-3.

[128] H. Q. Nguyen, J.-H. Choi, M. Kang, Z. Ghassemlooy, D. H. Kim, S.-K. Lim, T.-G. Kang, and C. G. Lee, "A MATLAB-based simulation program for indoor visible light communication system," *2010 7th International Symposium on Communication Systems, Networks & Digital Signal Processing (CSNDSP)*, Newcastle upon Tyne, 2010, pp. 537-541.

[129] C. R. Lomba, R. T. Valadas, and A. M. de Oliveira Duarte, "Efficient simulation of the impulse response of the indoor wireless optical channel," in *International Journal of Communication Systems*, vol. 13, no. 7-8, pp. 537-549, 2000.

[130] M. I. S. Chowdhury, W. Zhang, and M. Kavehrad, "Combined Deterministic and Modified Monte Carlo Method for Calculating Impulse Responses of Indoor Optical Wireless Channels," in *Journal of Lightwave Technology*, vol. 32, no. 18, pp. 3132-3148, 2014.

[131] A. Behlouli, P. Combeau, and L. Aveneau, "MCMC Methods for Realistic Indoor Wireless Optical Channels Simulation," in *Journal of Lightwave Technology*, vol. 35, no. 9, pp. 1575-1587, 2017.

[132] F. Miramirkhani and M. Uysal, "Channel Modeling and Characterization for Visible Light Communications," in *IEEE Photonics Journal*, vol. 7, no. 6, pp. 1-16, 2015.

[133] S. Rajbhandari, Z. Ghassemlooy, and M. Angelova, "Bit error performance of diffuse indoor optical wireless channel pulse position modulation system employing artificial neural networks for channel equalisation," in *IET Optoelectronics*, vol. 3, no. 4, pp. 169-179, 2009.

[134] J. B. Carruthers and J. M. Kahn, "Modeling of nondirected wireless infrared channels," in *IEEE Transactions on Communications*, vol. 45, no. 10, pp. 1260-1268, 1997.

[135] J. M. Kahn, and J. R. Barry, "Wireless infrared communications," in *Proceedings of the IEEE*, vol. 85, no. 2, pp. 265-298, 1997.

[136] J. B. Carruthers and P. Kannan, "Iterative site-based modeling for wireless infrared channels," in *IEEE Transactions on Antennas and Propagation*, vol. 50, no. 5, pp. 759-765, 2002.

[137] M. Zhang, Y. Zhang, X. Yuan, and J. Zhang, "Mathematic models for a ray tracing method and its applications in wireless optical communications," in *Optics Express*, vol. 18, no. 17, pp. 18431-18437, 2010.

[138] O. Bouchet, H. Sizun, C. Boisrobert, F. de Fornel, and P.-N. Favennec, Free-space Optics: Propagation and Communication, ISTE, Newport Beach, 2006.

[139] D. Wu, Z. Ghassemlooy, H. Le Minh, S. Rajbhandari, and M. A. Khalighi, "Optimisation of Lambertian order for indoor non-directed optical wireless communication," *2012 1st IEEE International Conference on Communications in China Workshops (ICCC)*, Bejing, 2012, pp. 43-48.

[140] H. Hashemi, G. Yun, M. Kavehrad, F. Behbahani, and P. A. Galko, "Indoor propagation measurements at infrared frequencies for wireless local area networks applications," in *IEEE Transactions on Vehicular Technology*, vol. 43, no. 3, pp. 562-576, 1994.

[141] F. R. Gfeller and U. Bapst, "Wireless in-house data communication via diffuse infrared radiation," in *Proceedings of the IEEE*, vol. 67, no. 11, pp. 1474-1486, 1979.

[142] V. Jungnickel, V. Pohl, S. Nonnig, and C. von Helmolt, "A physical model of the wireless infrared communication channel," in *IEEE Journal on Selected Areas in Communications*, vol. 20, no. 3, pp. 631-640, 2002.

[143] J. M. Kahn, W. J. Krause, and J. B. Carruthers, "Experimental characterization of non-directed indoor infrared channels," in *IEEE Transactions on Communications*, vol. 43, no. 234, pp. 1613-1623, 1995.

[144] W. Gu, M. Aminikashani, P. Deng, and M. Kavehrad, "Impact of multipath reflections on the performance of indoor visible light positioning systems," in *Journal of Lightwave Technology*, vol. 34, no. 10, pp. 2578-2587 2016.

[145] Z. Chen, D. Tsonev, and H. Haas, "Improving SINR in indoor cellular visible light communication networks," *2014 IEEE International Conference on Communications (ICC)*, Sydney, 2014, pp. 3383-3388.

[146] C. Chen, D. Basnayaka, and H. Haas, "Non-line-of-sight channel impulse response characterisation in visible light communications," *2016 IEEE International Conference on Communications (ICC)*, Kuala Lumpur, 2016, pp. 1-6.

List of Author's Publications Related to the Doctoral Thesis

All authors contributed equally unless otherwise stated.

Papers in Peer-Reviewed Journals with Impact Factor:

[J1] P. A. Haigh, S. T. Le, S. Zvanovec, Z. Ghassemlooy, P. Luo, T. Xu, P. Chvojka, T. Kanesan, E. Giacoumidis, P. Canyelles-Pericas, H. Le Minh, W. Popoola, S. Rajbhandari, I. Papakonstantinou and I. Darwazeh, "Multi-band carrier-less amplitude and phase modulation for bandlimited visible light communications systems," in *IEEE Wireless Communications*, vol. 22, no. 2, pp. 46-53, 2015.

[J2] P. A. Haigh, A. Burton, K. Werfli, H. Le Minh, E. Bentley, P. Chvojka, W. O. Popoola, I. Papakonstantinou and S. Zvanovec, "A Multi-CAP Visible-Light Communications System With 4.85-b/s/Hz Spectral Efficiency," in *IEEE Journal on Selected Areas in Communications*, vol. 33, no. 9, pp. 1771-1779, 2015.

[J3] P. Chvojka, K. Werfli, S. Zvanovec, P. A. Haigh, V. Hubata Vacek, P. Dvorak, P. Pesek and Z. Ghassemlooy, "On the m-CAP Performance with Different Pulse Shaping Filters Parameters for Visible Light Communications," in *IEEE Photonics Journal*, vol. 9, no. 5, pp. 1-12, 2017.

[J4] P. Chvojka, S. Zvanovec, P. A. Haigh and Z. Ghassemlooy, "Channel Characteristics of Visible Light Communications Within Dynamic Indoor Environment," in *Journal of Lightwave Technology*, vol. 33, no. 9, pp. 1719-1725, 2015.

[J5] P. Chvojka, S. Vitek, S. Zvanovec, Z. Ghassemlooy and S. Rajbhandari, "Analyses of non-line of sight visible light communications," in *Optical Engineering*, *submitted*.

[J6] S. Zvanovec, P. Chvojka, P. A. Haigh, Z. Ghassemlooy, "Visible Light Communications towards 5G", in *Radioengineering*, vol. 24, no. 1, p. 1-9, 2015.

[J7] K. Werfli, P. Chvojka, Z. Ghassemlooy, N. B. Hassan, S. Zvanovec, A. Burton, P. A. Haigh, M. R. Bhatnagar, "Experimental Demonstration of High-Speed 4×4 Imaging Multi-CAP MIMO Visible Light Communications," in *IEEE Journal of Lightwave Technology*, *submitted*.

[J8] P. Pesek, S. Zvanovec, P. Chvojka, Z. Ghassemlooy and M. Bhatangar, "Mobile User Connectivity in Relay-assisted Visible Light Communication," in *IEEE Photonics Journal*, *submitted*.

Papers in Conference Proceedings Listed in Web of Knowledge:

[C1] P. Chvojka, P. A. Haigh, S. Zvanovec, P. Pesek and Z. Ghassemlooy, "Evaluation of Multi-band Carrier-less Amplitude and Phase Modulation Performance for VLC under Various Pulse Shaping Filter Parameters", *Proceedings of the 13th International Joint Conference on e-Business and Telecommunications - Volume 3: OPTICS (ICETE 2016)*, Lisbon, 2016, pp. 25-31.

[C2] P. Chvojka, S. Zvanovec, K. Werfli, P. A. Haigh and Z. Ghassemlooy, "Variable m-CAP for Bandlimited Visible Light Communications," *2017 IEEE International Conference on Communications (ICC)*, Paris, 2017.

[C3] P. A. Haigh, A. Aguado, Z. Ghassemlooy, P. Chvojka, K. Werfli, S. Zvanovec, E. Ertunc and T. Kanesan, "Multi-band carrier-less amplitude and phase modulation for highly bandlimited visible light communications – Invited paper," *2015 International Conference on Wireless Communications & Signal Processing (WCSP)*, Nanjing, 2015, pp. 1-5.

[C4] P. A. Haigh, P. Chvojka, S. Zvanovec, Z. Ghassemlooy, S. Thai Le, T. Kanesan, E. Giacoumidis, N. J. Doran, I. Papakonstantinou and I. Darwazeh, "Experimental verification of visible light communications based on multi-band CAP modulation," *2015 Optical Fiber Communications Conference and Exhibition (OFC)*, Los Angeles, CA, 2015, pp. 1-3.

[C5] K. Werfli, P. A. Haigh, Z. Ghassemlooy, P. Chvojka, S. Zvanovec, S. Rajbhandari and S. Long, "Multi-band carrier-less amplitude and phase modulation with decision feedback equalization for bandlimited VLC systems," *2015 4th International Workshop on Optical Wireless Communications (IWOW)*, Istanbul, 2015, pp. 6-10.

[C6] P. Chvojka, P. Dvorak, P. Pesek, S. Zvanovec, P. A. Haigh and Z. Ghassemlooy, "Characterization of the organic LED based visible light communications," *2016 10th International Symposium on Communication Systems, Networks and Digital Signal Processing (CSNDSP)*, Prague, 2016, pp. 1-4.

[C7] P. Chvojka, K. Werfli, P. A. Haigh, S. Zvanovec, Z. Ghassemlooy and M. Bhatnagar, "Multi-band Carrier-less Amplitude and Phase Modulation for VLC: An Overview," *First South American Colloquium on Visible Light Communications (SACVLC) 2017, accepted.*

Chapters in Books:

[B1] S. Zvanovec, P. Zak, P. Chvojka, P. A. Haigh and Z. Ghassemlooy, "Visible Light Communications based on Street Lightings," in *Visible Light Communications: Theory and Applications*, Z. Ghassemlooy, L. Nero Alves, S. Zvanovec and M. Ali Khalighi, CRC Press, Boca Raton, 2017.

Citations in Web of Knowledge and Scopus:

Journal Paper [J1]:

[J1.C1] X. Lu, K. Wang, L. Qiao, W. Zhou, Y. Wang and N. Chi, "Nonlinear Compensation of Multi-CAP VLC System Employing Clustering Algorithm Based Perception Decision," in *IEEE Photonics Journal*, vol. 9, no. 5, pp. 1-9, 2017.

[J1.C2] N. Chi, J. Q. Zhao and Z. X. Wang, "Bandwidth-efficient visible light communication system based on faster-than-Nyquist pre-coded CAP modulation," in *Chinese Optics Letters*, vol. 15, no. 8, 2017.

[J1.C3] N. Stevens and L. De Strycker, "Single Edge Position Modulation as a Dimming Technique for Visible Light Communications," in *Journal of Lightwave Technology*, vol. 34, no. 23, pp. 5554-5560, 2016.

[J1.C4] J. Dang, Z. Zhang, L. Wu and Lin Guo, "DC and non-DC biased optical filter bank multicarrier communication for IM/DD channel," *2016 IEEE International Conference on Communications Workshops (ICC)*, Kuala Lumpur, 2016, pp. 423-429.

[J1.C5] T. Chen, L. Liu, Z. Zheng, J. Song, K. Wu and W. Hu, "Fisheye-lens-based space division multiplexing system for visible light communications," in *EURASIP Journal on Wireless Communications and Networking*, vol. 237, 2015.

Journal Paper [J2]:

[J2.C1] J.-T. Wu, C.-W. Chow, Y. Liu, C.-W. Hu and C.-H. Y, "Performance enhancement technique of visible light communications using passive photovoltaic cell," in *Optics Communications*, vol. 392, pp. 119-122, 2017.

[J2.C2] S. Rajbhandari, J. D. McKendry, J. Hernsdorf, H. Chun, G. Faulkner, H. Haas, I. M. Watson, D. O'Brien, and M. D. Dawson, "A review of gallium nitride LEDs for multi-gigabit-per-second visible light data communications", in *Semiconductor Science and Technology*, vol. 32, no. 2, 2017.

[J2.C3] T. Song, K. Wang, J. Ma and A. Nirmalathas, "Experimental demonstration of optical wireless personal area communication system supporting multiple users," *2016 Optical Fiber Communications Conference and Exhibition (OFC)*, Anaheim, 2016, pp. 1-3.

[J2.C4] L. Sun, J. Du and Z. He, "Multiband Three-Dimensional Carrierless Amplitude Phase Modulation for Short Reach Optical Communications," in *Journal of Lightwave Technology*, vol. 34, no. 13, pp. 3103-3109, 2016.

Journal Paper [J4]:

[J4.C1] B.-W. Kim and S.-Y. Jung, "Channel capacity of the distributed MIMO relay in visible light communication systems," in *Photonic Network Communications*, vol. 34, no. 2, pp. 298-305, 2017.

[J4.C2] Q. N. Pham, V. P. Rachim, J. An and W.-Y. Chung, "Ambient Light Rejection Using a Novel Average Voltage Tracking in Visible Light Communication System," in *Applied Sciences*, vol. 7, no. 7, 2017.

[J4.C3] F. Miramirkhani, O. Narmanlioglu, M. Uysal and E. Panayirci, "A Mobile Channel Model for VLC and Application to Adaptive System Design," in *IEEE Communications Letters*, vol. 21, no. 5, pp. 1035-1038, 2017.

[J4.C4] A. Behlouli, P. Combeau and L. Aveneau, "MCMC Methods for Realistic Indoor Wireless Optical Channels Simulation," in *Journal of Lightwave Technology*, vol. 35, no. 9, pp. 1575-1587, 2017.

[J4.C5] C.-Y. Wang, L. Wang and X.-F. Chi, "Location-adaptive transmission for indoor visible light communication," in *Optoelectronics Letters*, vol. 12, no. 1, pp. 69-73, 2016.

[J4.C6] C. Yan, Y. Xu, J. Shen and J. Chen, "A combination of VLC and WiFi based indoor wireless access network and its handover strategy," *2016 IEEE International Conference on Ubiquitous Wireless Broadband (ICUWB)*, Nanjing, 2016, pp. 1-4.

[J4.C7] C. Chen, D. Basnayaka and H. Haas, "Non-line-of-sight channel impulse response characterisation in visible light communications," *2016 IEEE International Conference on Communications (ICC)*, Kuala Lumpur, 2016, pp. 1-6.

[J4.C8] L. Kong, W. Xu, H. Zhang, C. Zhao and X. You, "R-OFDM for RGBA-LED-Based Visible Light Communication With Illumination Constraints," in *Journal of Lightwave Technology*, vol. 34, no. 23, pp. 5412-5422, 2016.

[J4.C9] S. H. Chang and C. Y. Lin, "A Visible Light Communication Positioning Mechanism in Industrial Logistics Management," *2016 30th International Conference on Advanced Information Networking and Applications Workshops (WAINA)*, Crans-Montana, 2016, pp. 878-882.

[J4.C10] C. Le Bas, S. Sahuguede, A. Julien-Vergonjanne, A. Behlouli, P. Combeau and L. Aveneau, "Human body impact on mobile visible light communication link," *2016 10th International Symposium on Communication Systems, Networks and Digital Signal Processing (CSNDSP)*, Prague, 2016, pp. 1-6.

[J4.C11] C. Ley-Bosch, I. Alonso-Gonzales, D. Sanchez-Rodriguez and C. Ramirez-Casanas, "Evaluation of the Effects of Hidden Node Problems in IEEE 802.15.7 Uplink Performance," in *Sensors*, vol. 16, no. 2, 2016.

[J4.C12] J. Jiang, Y. Huo, F. Jin, P. Zhang, Z. Wang, Z. Xu, H. Haas and L. Hanzo, "Video Streaming in the Multiuser Indoor Visible Light Downlink," in *IEEE Access*, vol. 3, pp. 2959-2986, 2015.

[J4.C13] C. Le Bas, S. Sahuguede, A. Julien-Vergonjanne, A. Behlouli, P. Combeau and L. Aveneau, "Impact of receiver orientation and position on Visible Light Communication link performance," *2015 4th International Workshop on Optical Wireless Communications (IWOW)*, Istanbul, 2015, pp. 1-5.

[J4.C14] F. Duvnjak, J. Ozegovic and A. Kristic, "Heterogeneous Wi-Fi and VLC (RF-optical) wireless access architecture," *2015 23rd International Conference on Software, Telecommunications and Computer Networks (SoftCOM)*, Split, 2015, pp. 310-314.

[J4.C15] S. Vikramaditya Tiwari, A. Sewaiwar, and Y. H. Chung, "Optical bidirectional beacon based visible light communications," in *Optics Express*, vol. 23, no. 20, pp. 26551-26564, 2015.

[J4.C16] B. Yu, H. Zhang, L. Wei and J. Song, "Subcarrier Grouping OFDM for Visible-Light Communication Systems," in *IEEE Photonics Journal*, vol. 7, no. 5, pp. 1-12, 2015.

Journal Paper [J6]:

[J6.C1] A. Assefa, P. Chen, X. Long Ho and J. D. White, "On the potential of solid state LED strips utilizing an organic color converter for non-line of sight visible light communication," in *Optics Express*, vol. 25, no. 20, pp. 24242-24250, 2017.

[J6.C2] Y. Dong, M. Shi, X. Yang, P. Zeng, J. Gong, S. Zheng, M. Zhang, R. Liang, Q. Ou, N. Chi and S. Zhang, "Nanopatterned luminescent concentrators for visible light communications," in *Optics Express*, vol. 25, no. 18, pp. 21926-21934, 2017.

[J6.C3] D. S. Sundar, A. S. Raja, C. Sanjeeviraja and D. Jeyakumar, "High Temperature Processable Flexible Polymer Films," in *International Journal of Nanoscience*, vol. 16, no. 3, 2017.

[J6.C4] T. T. Son, H. B. Hung, H. Le-Minh, N. Aslam and P. Canyelles-Pericas, "Chaos-based physical layer security model for IEEE 802.15.7 visible light communications," *2017 Seventh International Conference on Information Science and Technology (ICIST)*, Da Nang, 2017, pp. 85-90.

[J6.C5] M. Kafafy, Y. Fahmy, M. Abdallah and M. Khairy, "Power Efficient Downlink Resource Allocation for Hybrid RF/VLC Wireless Networks," *2017 IEEE Wireless Communications and Networking Conference (WCNC)*, San Francisco, 2017, pp. 1-6.

[J6.C6] J. Green, H. Perez-Olivas, S. Martinez-Diaz, J. Garcia-Marquez, C. Dominguez-Gonzales, R. Santiago-Montero, H. Guan, M. Rozenblat and S Topsu, "VLC-beacon detection with an under-sampled ambient light sensor," in *Optics Communications*, vol. 397, pp. 122-128, 2017.

[J6.C7] J. Sabino, G. Figueira and P. Andre, "Wavefront spatial-phase modulation in visible light communications," in *Microwave and Optical Technology Letters*, vol. 59, no. 7, pp. 1538-1541, 2017.

[J6.C8] M. T. Van, N. V. Tuan, T. T. Son, H. Le Minh and A. Burton, "Weighted k-nearest neighbour model for indoor VLC positioning," in *IET Communications*, vol. 11, no. 6, pp. 864-871, 2017.

[J6.C9] S. Rajbhandari, J. D. McKendry, J. Hernsdorf, H. Chun, G. Faulkner, H. Haas, I. M. Watson, D. O'Brien, and M. D. Dawson, "A review of gallium nitride LEDs for multi-gigabit-per-second visible light data communications", in *Semiconductor Science and Technology*, vol. 32, no. 2, 2017.

[J6.C10] M. Kashef, M. Ismail, M. Abdallah, K. A. Qaraqe and E. Serpedin, "Energy Efficient Resource Allocation for Mixed RF/VLC Heterogeneous Wireless Networks," in *IEEE Journal on Selected Areas in Communications*, vol. 34, no. 4, pp. 883-893, 2016.

List of Author's Publications Non-Related to the Doctoral Thesis

All authors contributed equally unless otherwise stated.

Paper in Conference Proceedings Listed in Web of Knowledge:

[C8] P. Chvojka, J. Bohata, J. Libich, S. Zvanovec and J. Perez, "Laboratory and outdoor availability and spatial coherence tests of wireless optical links," *2013 2nd International Workshop on Optical Wireless Communications (IWOW)*, Newcastle upon Tyne, 2013, pp. 109-112.

[C9] E. Pikasis, S. Karabetsos, T. Nikas, P. Chvojka, A. Nassiopoulos and D. Syvridis, "Comparison of CAP and DFT-spread DMT for high speed transmission over 50m SI-POF," *2016 10th International Symposium on Communication Systems, Networks and Digital Signal Processing (CSNDSP)*, Prague, 2016, pp. 1-5.

[C10] M. Komanec, T. Nemecek, D. Suslov, P. Chvojka, S. Zvanovec and R. Ahmad, "Thulium Pulsed Laser for Nonlinear Applications in Specialty Optical Fibers: Design and Experimental Verification," *2017 2nd International Conference on Automation, Cognitive Science, Optics, Micro Electro–Mechanical System, and Information Technology (ICACOMIT)*, *accepted*.

Petr Chvojka

chvojka.petr@gmail.com

Born:
4th August 1987
Most, Czech Republic

Web profiles:
https://www.researchgate.net/profile/Petr_Chvojka2
https://elmag.org/profile-main/161
https://cz.linkedin.com/in/petrchvojka

Work Experience

June 2013 – present
Czech Technical University in Prague, Faculty of Electrical Engineering, Department of Electromagnetic Field
(fel.cvut.cz, elmag.org)
Position: Researcher
| research in the field of visible light communications (VLC) and optical fibre communications
| PR and web administration of the study programme Electronics and communication and of the Department of Electromagnetic Field
| publications: author/co-author of 8 journal papers, 10 conference papers, 1 book chapter, more than 30 citations
| reviews of journal and conference papers
| local organizing committee member at CSNDSP16 conference in Prague

April 2012 – May 2013
ZZ Servis (zzservis.cz) / **AIRS** (airs.cz)
Position: Junior Electro Designer
| technical drawings of electrical networks for control systems for industrial technologies, the industrial production process improvement, analysis of existing control system and its documentations (EPLAN, AutoCAD)

November 2011 – April 2012
Miracle Network (miracle.cz)
Position: RMA technician
| costumer technical support service for microwave technologies and products, control and coordination of the whole repair process

Projects (as a researcher)

January 2017 – present
Wideband Optical Source Based on Soft-glass Fibers (TACR TA04010220)
| design and experimental development of thulium pulsed laser

January 2017 – present
Combined Radio Frequency and Visible Light Bands for Device-to-Device communication (GACR 17-17538S)
| VLC channel modeling for indoor environments

January 2014 – December 2016
Safety of optical transport network and development of optical components for energy grid and energy transport systems (TACR TA03020439)
| analysis and processing of measured data

June 2013 – May 2015
Research of ambient influences on novel broadband optical wireless systems (COST LD 12058)
| VLC channel modeling for indoor environments

Education

2013 – 2018 (expected defense date)
Czech Technical University in Prague, Faculty of Electrical Engineering
Postgraduate study in Radioelectronics
Dissertation thesis: Visible Light Communications for Indoor Applications

2007 – 2013
Czech Technical University in Prague, Faculty of Electrical Engineering
Master's Degree in Wireless Communications
Diploma thesis: Laboratory Research of Diversity of Wireless Optical Links (awarded diploma thesis)

International Visits

Northumbria University, Newcastle upon Tyne, UK
February 2014 – May 2014
Leader: Prof. Zabih Ghassemlooy

Ben-Gurion University of the Negev, Beersheba, Israel
September 2013
Leader: Prof. Shlomi Arnon